IMPACT OF CLIMATE-RESPONSIVE CONTROLS AND LAND USAGE ON REGIONAL CLIMATE AND AIR QUALITY

A Dissertation
Presented to
The Academic Faculty

by

Marcus Alexander Trail

In Partial Fulfillment
of the Requirements for the Degree
Doctor of Philosophy in the
School of Civil and Environmental Engineering

Georgia Institute of Technology
May, 2014

IMPACT OF CLIMATE-RESPONSIVE CONTROLS AND LAND USAGE ON REGIONAL CLIMATE AND AIR QUALITY

Approved by:

Dr. M. Armistead Russell, Advisor
School of Civil and Environmental Engineering
Georgia Institute of Technology

Dr. Michael H. Bergin
School of Civil and Environmental Engineering
Georgia Institute of Technology

Dr. James Mulholland
School of Civil and Environmental Engineering
Georgia Institute of Technology

Dr. Brian Stone
School of City and Regional Planning
Georgia Institute of Technology

Dr. Athanasios Nenes
School of Earth & Atmospheric Sciences
Georgia Institute of Technology

Date Approved: March 28th, 2014

To Quinn,

ACKNOWLEDGEMENTS

I would like to express my utmost appreciation to my advisor Dr. Armistead Russell. You have been an incredible mentor and I am privileged to have researched in your group. My experience working in your group will surely be unforgettable and priceless. I would like to thank my committee members as well, Dr. Athanasios Nenes, Dr. Brian Stone, Dr. James Mulholland, and Dr. Michael Bergin for serving on my PhD committee and all of the assistance and guidance you have offered along the way. I would like to offer a special thanks to Dr. Yongtao Hu, without whom I would never have learned to work with the tools used in this research. In addition, Dr. Alexandra Tsimpidi has graciously provided guidance for me and her involvement in this research has been invaluable. I especially want to thank the members of the Russell group for all the support, constructive criticism, and friendships you all have offered over the years. I would also like to those who funded this project, including the U.S. EPA, Phillips 66 and NASA.

Finally, I would like to thank my friends and family that have been incredibly supportive and encouraging. To my mom and dad, for your encouragement all the way and for all of the support you have given me, thank you. To my roommates during grad school, Haynes and Andrew, thank you. And most of all, to my wife Quinn, for thinking it's cool that I will have a PhD and for being my best friend, thank you.

TABLE OF CONTENTS

Page

LIST OF TABLES

Page

LIST OF FIGURES

Page

SUMMARY

Regional air quality impacts public health, visibility and ecosystem health, and is significantly affected by changes in climate, land use and pollutant emissions. Predictions of regional air quality responses to such changes can help inform policy makers in the development of effective approaches to both reduce greenhouse gases and improve air quality. However, major sources of uncertainty exist in predicting future air quality including limitations in the tools used to project future emissions, land use changes and uncertainties associated with predicting future climate. Recently, technical advances in downscaling global climate simulations to regional scales, and the development of bottom-up operational tools used to forecast emissions have enhanced our ability to account for the complex interactions between population, socio-economical development, technological change, and federal and regional environmental policies.

The overarching direction of this research is to provide information as to which global change-related control choices and forest management and utilization practices are most effective for both mitigating climate change and improving regional air quality. The primary objectives of this work are to assess and compare how climate-responsive control choices will affect regional air quality and to assess how forest and cropland management and utilization practices will impact future regional climate and air quality. Through this work, the sensitivities associated with climate change and the predicted impacts of climate-responsive control choices and land use changes on air quality were quantified. Ideally, this work will provide focused information for policy makers on the

impact of climate change/global change on strategies to meet air quality policy goals in the future, including providing results for direct use in decision support analyses.

The response of air pollutant concentrations and sensitivities are simulated using a chemical transport model with inputs of emissions and meteorology. Meteorological inputs were downscaled from a Global Circulation Model (GCM) to the regional scale using a regional climate model. The emissions inputs are prepared for the chemical transport model (CTM) using possible future emissions inventory estimates calculated using an energy system cost optimization model. The energy system model selects from available technologies to provide the least-cost path which satisfies specified demands of the residential, commercial, industrial, and transportation sectors for regionally based energy services and serves as a useful tool to identify the key technologies that will be needed to meet greenhouse gas or criteria air pollutant related policies and objectives.

While there are uncertainties in current and future emissions estimates, and uncertainties in climate change, this work shows that emissions sensitivities can be used to determine the major sources of O_3 and $PM_{2.5}$ and the current modeling platform can be used to isolate the effects of climate on air quality. Further, the energy system cost optimization models can be used to develop a range of alternative policy based emissions scenarios to address the uncertainties associated with estimating future emissions. Our results show that emissions reductions strategies will continue to play a vital role in improving air quality over the U.S., especially in regions where climate change threatens to degrade O_3 and PM air quality. The results also show that CO_2 emission reduction policies can have mixed positive and negative impacts on air quality. However, additional costs will be necessary due to climate change because deeper emission

reductions will be required to compensate for a warmer climate, even if current efforts are predicted to show improvement.

In assessing the impact of forest and cropland management on regional climate and air quality, this study shows the importance in understanding the uncertainty associated with vegetation parameters. For example, energy flux to and from the Earth's surface, and therefore climate, is sensitive to the stomatal resistance of various plant types. Also, air quality is sensitive to various parameters used in calculating biogenic emissions and deposition, such as leaf area index and emission factors which also have associated uncertainties. The results of this study show that regional climate and O_3 and aerosol concentrations are highly sensitive to reforestation and cropland conversion in the Southeast and these land use changes should be considered in air quality management plans.

CHAPTER 1

INTRODUCTION

Air pollution has been shown to have adverse ecosystem and human health effects, and future global changes in climate, emissions, land use and other factors are expected to impact air pollution [*Jacob and Winner*, 2009; *Liao et al.*, 2006c; *Pope et al.*, 1995; *Schwartz et al.*, 1994; *Weaver et al.*, 2009]. Recently, the World Health Organization (WHO) characterized air pollution as a class 1 carcinogen and the Global Burden of Disease study [*Lim et al.*, 2012] found exposure to ambient particulate matter (PM) and ozone (O_3) as major contributors to premature death. The same Global Burden of Disease Study finds that over 3 million deaths and nearly 80 million disability-adjusted life-years were attributable to ambient particulate matter and ozone pollution in 2010 and that ambient particulate matter pollution ranked ninth among risk factors ranked by their attributable burden of disease [*Lim et al.*, 2012].

In response to the health and ecological problems associated with air pollution, legislation around the world has been developed to restrict the emissions of precursors of air pollution and to set standards for ambient concentrations of pollutants. In the United States, the Clean Air Act (CAA) was established to improve U.S. air quality. The national ambient air quality standards (NAAQS) for 8-hour average O_3 and 24-hour average $PM_{2.5}$, set by the Environmental Protection Agency (EPA) of United States, are 75 parts per billion (ppb) and 35 μg m^{-3} respectively (http://www.epa.gov/air/criteria.html) while the annual $PM_{2.5}$ standard is currently 12 μg

m^{-3}. Increasingly, scientific research has focused on understanding the impact of policy on air quality.

Air quality is significantly affected by changes in climate, pollutant emissions and land use [*Weaver et al.*, 2009]. Predictions of regional air quality responses to such changes can help inform policy makers in the development of effective approaches to both reduce greenhouse gases and improve air quality. There is a consensus among most studies that future climate change, alone, would lead to an increase in O_3 concentrations over significant regions of the U.S. due to increased temperatures, surface insolation, stagnation, and biogenic VOC emissions [*Mickley et al.*, 2004; *Weaver et al.*, 2009]. Potential impacts of climate on $PM_{2.5}$ over the U.S. are more variable and likely small [*Jacob and Winner*, 2009]. Anthropogenic emissions are expected to change in the future due to changes in energy demand, technology and policy. Policies designed to mitigate climate change will not only reduce greenhouse gases but also impact emissions of precursors of PM and O_3. Land use and land cover changes (LULCC) affect air pollution as well as global and regional climate and are expected to change due to natural and human activity. In particular, the southeastern U.S. underwent intense land use and land cover changes beginning in the 1700's [*Chen et al.*, 2006b; *Pacala et al.*, 2001; *Prestemon and Abt*, 2002; *Steyaert and Knox*, 2008; *Wear and Greis*, 2002] and changes are expected to continue given the growing demand to develop forest-to-fuel technologies. Physical parameters of certain crops and forests such as albedo, stomatal resistance and surface roughness affect climate by altering the land-atmosphere energy transfer [*Pielke et al.*, 1998] while land cover changes also effect the deposition of O_3 and $PM_{2.5}$ by altering the surface area and roughness for dry deposition of pollutants.

Changes in stomatal activity also effect the deposition of O_3 and other gases. Various vegetative species also emit volatile organic compounds (VOCs), precursors for ozone and secondary organic aerosol (SOA), and nitric oxide (NO), which becomes a precursor for ozone, at different rates [*Henze et al.*, 2008; *Houweling et al.*, 1998; *Liao et al.*, 2007a; *Racherla and Adams*, 2006; *Wang et al.*, 1998].

The overarching direction of this research is to provide information as to which global change-related control choices and forest management and utilization practices are most effective for both mitigating climate change and improving regional air quality. The primary objectives of this work are to assess and compare how climate-responsive control choices will affect regional air quality and to assess how forest and cropland management and utilization practices will impact future regional climate and air quality. Through this work, the sensitivities associated with climate change and the predicted impacts of climate-responsive control choices and land use changes on air quality were quantified. Ideally, this work will provide focused information for policy makers on the impact of climate change/global change on strategies to meet air quality policy goals in the future, including providing results for direct use in decision support analyses.

The response of air pollutant concentrations and sensitivities are simulated using a eularian grid-based chemical transport model (CTM) with inputs of emissions and meteorology. Meteorological inputs were downscaled from a Global Circulation Model (GCM) to the regional scale using a regional climate model. Anthropogenic emissions inputs are prepared for the CTM using possible future emissions inventory estimates calculated using an energy system cost optimization model. The energy system model selects from available technologies to provide the least-cost path which satisfies specified

demands of the residential, commercial, industrial, and transportation sectors for regionally based energy services and serves as a useful tool to identify the key technologies that will be needed to meet greenhouse gas or criteria air pollutant related policies and objectives.

This work shows that emissions sensitivities can be used to determine the major sources impacting O_3 and $PM_{2.5}$ and the current modeling platform can be used to isolate the effects of climate on air quality. Further, the energy system cost optimization models can be used to develop a range of alternative policy based emissions scenarios to address the uncertainties associated with estimating future emissions. The results of this dissertation show that emissions reductions strategies will continue to play a vital role in improving air quality over the U.S., especially in regions where climate change threatens to degrade O_3 and PM air quality. The results also show that CO_2 emission reduction policies can have mixed positive and negative impacts on air quality. However, meeting air quality goals will require additional costs due to climate change because deeper emission reductions will be required to compensate for a warmer climate, even if current efforts are predicted to show improvement. This study also shows the importance in understanding the uncertainties associated with vegetation parameters. For example, energy flux to and from the Earth's surface, which is a major driver of climate, is sensitive to the stomatal resistance of various plant types. Also, air quality is sensitive to various parameters used in calculating biogenic emissions and deposition, such as leaf area index and emission factors. A brief description of the objectives for each chapter is given below.

Chapter 2: Downscaling a global climate model to simulate climate change of the U.S. and the implication on regional and urban air quality

We use spectral nudging with the Weather Research Forecast (WRF) model to downscale NASA earth system Goddard Institute for Space Studies (GISS) model E2 results during the years 2006 to 2010 and 2048 to 2052 over the continental United States in order to compare the resulting meteorological fields from the air quality perspective during the four seasons of five-year historic and future climatological periods. GISS results are used as initial and boundary conditions by the WRF regional climate model (RCM) to produce hourly meteorological fields. The downscaling technique and choice of physics parameterizations used are evaluated by comparing them with *in situ* observations. This study investigates changes of similar regional climate conditions down to a 12km by 12km resolution, as well as the effect of evolving climate conditions on the air quality at major U.S. cities.

Chapter 3: Sensitivity of air quality to potential changes in climate and emissions in the United States and major cities

Simulated present and future air quality is compared for the years 2006-2010 and 2048-2052 over the contiguous United States (CONUS) using the Community Multi-scale Air Quality (CMAQ) model. Regionally downscaled present and future climate results are developed using GISS and the WRF model. Present and future emissions are estimated using MARKAL 9R model. O_3 and $PM_{2.5}$ sensitivities to precursor emissions for the years 2010 and 2050 are calculated using CMAQ-DDM (Direct Decoupled

Method). Results from a Climate Penalty (CP) scenario isolate the impact of climate change on air quality.

Chapter 4: Impacts of potential policies designed to reduce CO_2 emissions and climate change on United States regional air quality

Impacts of emissions changes from four potential CO_2 emission reduction policies on regional air quality in 2050 are analyzed in the United States using the community multi-scale air quality model (CMAQ). Future meteorology was downscaled from a GCM to the regional scale using the WRF model. We use emissions growth factors from MARKAL-9R to develop 2050 emissions inventories for two climate tax policy scenarios, a combined transportation and energy sector policy scenario and a biomass energy policy scenario and compare air pollutant concentrations to the reference case.

Chapter 5: Potential impact of land use change on future regional climate in the Southeastern U.S.: reforestation and crop land conversion

The impacts of land use/land cover change (LULCC) on regional climate in the southeastern U.S. are studied by downscaling the NASA GISS global climate model E to the regional scale using a spectral nudging technique with the WRF model. Climate-relevant meteorological fields are compared for two southeastern U.S. LULCC scenarios to the current land use/cover for four seasons of the year 2050. Processes leading to this response are investigated and sensitivity analyses conducted. A sensitivity analysis provides information on which parameters have the largest impact on regional climate. Implications of LULCC on air quality are discussed.

Chapter 6: Reforestation and crop land conversion impacts on future regional air quality in the Southeastern U.S.

Possible future $PM_{2.5}$ and O_3 air quality for two LULCC scenarios are compared to a reference case scenario for the year 2050. Changes in air quality driven by changes in climate, deposition and emissions relating to the LULCC are investigated using CMAQ. Climate and deposition (CD) sensitivity simulation results are provided for the two alternative LULCC scenarios to isolate the impact of changing climate and deposition on $PM_{2.5}$ and O_3 air quality. Inputs to CMAQ were prepared for a loblolly pine reforestation scenario, a cropland conversion scenario, and the current land cover (reference) scenario and include the regionally downscaled future climate results by WRF from chapter 5 and emissions processed using the Sparse Matrix Operator Kernel Emissions (SMOKE) model. Energy related anthropogenic emissions inventories developed and described in chapter 3 are used.

Chapter 7: Summary of Conclusions and Future Research

A summary of the key conclusions of this dissertation is presented and potential future research directions are discussed.

1.1 References

Chen, H., et al. (2006), Effect of land-cover change on terrestrial carbon dynamics in the southern United States, *J. Environ. Qual.*, *35*(4), 1533-1547, doi:10.2134/jeq2005.0198.

Henze, D. K., et al. (2008), Global modeling of secondary organic aerosol formation from aromatic hydrocarbons: high- vs. low-yield pathways, *Atmospheric Chemistry and Physics*, *8*(9), 2405-2420

Houweling, S., et al. (1998), The impact of nonmethane hydrocarbon compounds on tropospheric photochemistry, *Journal of Geophysical Research-Atmospheres*, *103*(D9), 10673-10696, doi:10.1029/97jd03582.

Jacob, D. J., and D. A. Winner (2009), Effect of climate change on air quality, *Atmospheric Environment*, *43*(1), 51-63, doi:10.1016/j.atmosenv.2008.09.051.

Liao, H., et al. (2007), Biogenic secondary organic aerosol over the United States: Comparison of climatological simulations with observations, *Journal of Geophysical Research-Atmospheres*, *112*(D6), 19, doi:D06201 10.1029/2006jd007813.

Liao, K. J., et al. (2006), Impact of Future Climate Change on Regional Air Quality in the U.S, paper presented at Environmental Science & Health Symposium, Atlanta, GA.

Lim, S. S., et al. (2012), A comparative risk assessment of burden of disease and injury attributable to 67 risk factors and risk factor clusters in 21 regions, 1990-2010: a systematic analysis for the Global Burden of Disease Study 2010 (vol 380, pg 2224, 2012), *Lancet*, *381*(9874), 1276-1276

Mickley, L. J., et al. (2004), Effects of future climate change on regional air pollution episodes in the United States, *Geophysical Research Letters*, *31*(24), 4, doi:L24103 10.1029/2004gl021216.

Pacala, S. W., et al. (2001), Consistent land- and atmosphere-based US carbon sink estimates, *Science*, *292*(5525), 2316-2320, doi:10.1126/science.1057320.

Pielke, R. A., et al. (1998), Interactions between the atmosphere and terrestrial ecosystems: influence on weather and climate, *Glob. Change Biol.*, *4*(5), 461-475, doi:10.1046/j.1365-2486.1998.t01-1-00176.x.

Pope, C. A., et al. (1995), Review of epidemiological evidence of health-effects of particulate air-pollution, *Inhal. Toxicol.*, *7*(1), 1-18, doi:10.3109/08958379509014267.

Prestemon, J. P., and R. C. Abt (2002), The Southern timber market to 2040, *Journal of Forestry*, *100*(7), 16-22

Racherla, P. N., and P. J. Adams (2006), Sensitivity of global tropospheric ozone and fine particulate matter concentrations to climate change, *Journal of Geophysical Research-Atmospheres*, *111*(D24), 11, doi:D24103 10.1029/2005jd006939.

Schwartz, J., et al. (1994), Accute effects of summer air-pollution on respiratory symptom reporting in children, *Am. J. Respir. Crit. Care Med.*, *150*(5), 1234-1242

Steyaert, L. T., and R. G. Knox (2008), Reconstructed historical land cover and biophysical parameters for studies of land-atmosphere interactions within the

eastern United States, *Journal of Geophysical Research-Atmospheres*, *113*(D2), 27, doi:D02101 10.1029/2006jd008277.

Wang, Y. H., et al. (1998), Global simulation of tropospheric O-3-NOx-hydrocarbon chemistry 2. Model evaluation and global ozone budget, *Journal of Geophysical Research-Atmospheres*, *103*(D9), 10727-10755, doi:10.1029/98jd00157.

Wear, D. N., and J. G. Greis (2002), Southern Forest Resource Assessment - Summary of findings, *Journal of Forestry*, *100*(7), 6-14

Weaver, C. P., et al. (2009), A preliminary synthesis of modeled climate change impacts on US regional ozone concentrations, *Bulletin of the American Meteorological Society*, *90*(12), 1843-1863, doi:10.1175/2009bams2568.1.

CHAPTER 2

DOWNSCALING A GLOBAL CLIMATE MODEL TO SIMULATE CLIMATE CHANGE OVER THE U.S. AND THE IMPLICATION ON REGIONAL AND URBAN AIR QUALITY[1]

Abstract

Climate change can exacerbate future regional air pollution events by making conditions more favorable to form high levels of ozone. In this study, we use spectral nudging with WRF to downscale NASA earth system GISS model E2 results during the years 2006 to 2010 and 2048 to 2052 over the continental United States in order to compare the resulting meteorological fields from the air quality perspective during the four seasons of five-year historic and future climatological periods. GISS results are used as initial and boundary conditions by the WRF RCM to produce hourly meteorological fields. The downscaling technique and choice of physics parameterizations used are evaluated by comparing them with *in situ* observations. This study investigates changes of similar regional climate conditions down to a 12km by 12km resolution, as well as the effect of evolving climate conditions on the air quality at major U.S. cities. The high resolution simulations produce somewhat different results than the coarse resolution simulations in some regions. Also, through the analysis of the meteorological variables that most strongly influence air quality, we find consistent changes in regional climate that would enhance ozone levels in four regions of the U.S. during fall (Western U.S.,

[1] A modified version of this chapter has been published in (2013) Downscaling a global climate model to simulate climate change impacts on US regional and urban air quality, *Geosci. Model Dev.*, *6*, 1429-1445, doi:10.5194/gmd-6-1429-2013.

Texas, Northeastern, and Southeastern U.S), one region during summer (Texas), and one region where changes potentially would lead to better air quality during spring (Northeast). Changes in regional climate that would enhance ozone levels are increased temperatures and stagnation along with decreased precipitation and ventilation. We also find that daily peak temperatures tend to increase in most major cities in the U.S., which would increase the risk of health problems associated with heat stress. Future work will address a more comprehensive assessment of emissions and chemistry involved in the formation and removal of air pollutants.

2.1 Introduction

Changes in climate, emissions, population, technologies, and land-use can impact air quality in a variety of ways. Studies suggest that climate change can exacerbate future regional air pollution events (e.g.,[*Liao et al.*, 2006a; *Mickley et al.*, 2004; *Stevenson et al.*, 2006; *Weaver et al.*, 2009]) by making conditions more favorable to form high levels of ozone, e.g., by increasing temperature and biogenic emissions and decreasing ventilation. Increased temperatures affect air quality by affecting reaction rates and gas solubility in water droplets [*EPA*, 1989]. Pollutant dispersion and removal are affected by large-scale circulation patterns and precipitation, while cloud-cover frequency and duration impacts photolytic activity, which in turn affects reaction rate coefficients and conversion of gases to aerosols. Stagnation event frequency and duration affects the mixing of polluted air with air above the boundary layer. To simulate regional air quality dynamics, results from global models are downscaled using dynamical downscaling. The starting point of dynamical downscaling is typically a set of coarse-resolution large-scale

meteorological fields (either from a General Circulation Model, GCM, or from global reanalysis data), which are used to provide the initial, and lateral and surface boundary conditions to a regional climate model (RCM). Typically the RCM simulation does not feedback into the GCM, but adds regional detail in response to finer scale forcing (e.g., topography, land use/land cover) as it interacts with the larger-scale atmospheric circulation [*Giorgi*, 2006]. In this study, we address the benefits of downscaling using an RCM when analyzing the implications of climate change on air quality and health, especially in urban areas.

Recently, climate modeling efforts have shifted their focus from analyzing mean values of climate variables (e.g. temperature and precipitation) to extreme values, variability, and shifts in the frequency of climate patterns that are more relevant for air quality. Jacob and Winner [*Jacob and Winner*, 2009] compiled results from a number of studies on climate change and air pollution, and summarized that increases in regional stagnation consistently increases ozone and particulate matter (PM) concentrations. They show that positive temperature perturbations consistently increase ozone while they can sometimes decrease PM concentrations and that positive perturbations in mixing depth, wind speed, cloud cover, and precipitation all decrease ozone and PM concentrations to varying degrees. Mickley et al. [*Mickley et al.*, 2004] applied the Goddard Institute for Space Studies (GISS) GCM 2' [*Rind and Lerner*, 1996; *Rind et al.*, 1999] with implemented carbon monoxide (CO) and black carbon (BC) tracers to simulate the impact of climate change on air quality in the U.S. They found that increased severity of future pollutant episodes in the Northeast and Midwest during the summer was due to a decrease in frequency of surface cyclone tracking in southern Canada.

Dawson et al. [2008] developed a global-regional climate-air pollution modeling system (GRE-CAPS) by coupling GISS II GCM, MM5 regional meteorological model, and the PMCAMx regional CTM. This system was intended to enable studies of the effects of changes in climate, intercontinental transport, and emissions on regional and urban air quality. Leung and Gustafson [2005] applied a similar approach to assess the potential effects of climate change in the United States. They developed meteorological fields by downscaling the NASA GISS GCM simulations using an MM5-based RCM [*Grell*, 1994]. Their analyses were based on changes in surface air temperature and downward solar radiation, precipitation frequency, stagnation events, and ventilation. They defined a time to be stagnant when for four consecutive days the following criteria are met: a) the 10m wind speed is less than 4 m s^{-1} b) the 500 mb wind speed is less than 13 m s^{-1} at 7:00 am LST, and c) the total rainfall is less than 0.001 cm for the 4 day period [*Korshover and Angell*, 1982]. They also compared the daily average number of unvented hours, which are hours when the product of the mean wind speed within the boundary layer and the boundary layer height is less than 6000 m^2 s^{-1} [*Pielke et al.*, 1991]. In Tagaris et al. [2007], meteorological inputs to the Community Multi-scale Air Quality (CMAQ) Chemistry/Transport Model (CTM) were developed using the meteorological fields of Leung and Gustafson [2005] to investigate the potential impacts of global climate change and emissions on regional air quality using CMAQ [*Byun and Schere*, 2006]. Similarly, Nolte et al. [2008] investigated the impact of climate change on future air quality in the United States by dynamically downscaling outputs from the GISS GCM with the MM5 RCM and predicted an increase in O3 over Texas and large portions of the Southeast using CMAQ model.

These studies have illustrated the value of using the regional downscaling approach in order to better understand the impact of climate change on regional air quality. With the strong dependence on localized flow patterns, air quality models benefit from the higher-resolution wind, temperature, precipitation, and boundary layer structures produced by a RCM [*Leung and Gustafson*, 2005]. Weaver, et al. [*Weaver et al.*, 2009] stresses that the science of coupling global climate and regional air quality models is still at a young state and that there are particular questions as to which climate metrics and statistics are most relevant to air quality and how sensitive simulation results are to downscaling methodologies.

In our previous recent work [*Liu et al.*, 2012] we examined the performance of two nudging techniques, grid and spectral nudging, by downscaling NCEP/NCAR data using the Weather Research and Forecasting (WRF) Model and identified benefits of spectral nudging at producing small scale features while preserving the large scale forcings. Following these findings, in this study, we use spectral nudging to downscale the NASA earth system GISS modelE2 results during the years 2006 to 2010 and 2048 to 2052 over the continental United States (CONUS) in order to compare the resulting meteorological fields from the air quality perspective during the four seasons of five-year historic and future climatological periods. GISS results are used as initial and boundary conditions by the WRF RCM to produce hourly meteorological fields. The downscaling technique and choice of physics parameterizations used are evaluated by comparing them with *in situ* observations. This study investigates changes of similar regional climate conditions down to a 12km by 12km resolution, as well as the implications of evolving climate conditions on the air quality at major U.S. cities.

2.2 Approach

In this study a regional climate model is used to downscale a global climate model to develop meteorological fields for the present and future. Each component of the modeling system is described below along with the downscaling and evaluation methods used.

2.2.1 Model Description

Global Model: Lateral boundary and initial conditions for the regional forecast modeling are taken from the GISS ModelE2. The model has a horizontal resolution of 2°×2.5° latitude by longitude. The vertical discretization has 40 layers and follows a sigma coordinate up to 150 hPa, with constant pressure layers between 150 and 0.1 hPa. The surface is split into four types: open water (including lakes, rivers and oceans), ice-covered water (including lake ice and sea ice), ground (including bare soil and vegetated regions) and glaciers.

Simulations are carried out for the calendar years 2006-2010 and 2048-2052, driven by future atmospheric conditions over the 21st century and follow the scenario development process for IPCC AR5. The specific scenario used for this study is the "Representative Concentration Pathway" (RCP) 4.5 [*Lamarque et al.*, 2011; *Moss et al.*, 2010], that is a scenario of decadal global emissions of greenhouse gases, short-lived species, and land-use-land-cover which produces an anthropogenic radiative forcing at 4.5 W m^{-2} (approximately 650 ppm CO_2-equivalent) in the year 2100. The detailed characteristics of this scenario are enumerated in Moss et al. [2010]. The atmosphere/terrestrial biosphere-only version of the GISS modelE2 was driven by sea-ice

and sea-surface temperature conditions calculated by the coupled earth system model version that is submitted to the CMIP5 archive. The model spinup time was 3 years, starting either from 2003 or 2045, which is sufficient for the dynamic equilibration of the model's climate and chemically active tracers. SST and sea-ice boundary conditions vary both seasonally and interannually, GHG concentrations change annually, and emissions change annually by linearly interpolating the decadal CMIP5 emission datasets. Six-hourly instantaneous outputs of physical parameters were produced for regional downscaling by WRF (section 2.2). 6-hourly instantaneous outputs of gaseous and aerosol tracer concentrations were also produced, but were not used for downscaling.

***Regional Model*:** The regional climate model used is the non-hydrostatic Weather Research and Forecasting (WRF) Model [*Skamarock and Klemp*, 2008] version 3.4. The simulation domain covers the CONUS and portions of southern Canada and northern Mexico and is centered at 40°N and 97°W with dimensions of 164×138 horizontal grids cells with a grid-spacing of 36 km. It contains 35 vertical levels, with the top pressure of 50hPa. The configuration of physics schemes is as follows: the long-wave Rapid Radiative Transfer Model (RRTM) [*Mlawer et al.*, 1997] and Dudhia scheme [*Dudhia*, 1989] are used for longwave and shortwave radiation respectively; the Yonsei University (YSU) [*Hong et al.*, 2006] scheme is used for the planetary boundary layer; the Noah scheme [*Ek et al.*, 2003] is used for land surface model (LSM); a revised version of Kain-Fritsch scheme [*Kain and Fritsch*, 1993] is used to represent the effects of both deep and shallow cumulus clouds; Lin *et al.* [*Lin et al.*, 1983] is chosen for cloud microphysics.

2.2.2 Dynamical Downscale of global results

The GISS ModelE2 fields include temperature, relative humidity, horizontal wind velocities, soil temperature and moisture at different soil depths, sea surface temperature, surface pressure, ice fraction and snow water equivalent. The WRF Preprocessing System (WPS), which reads in this global data and interpolates it to the WRF grid points, does not process GISS data directly. Therefore, an interface program was developed to link the GISS output with WPS. 3D variables, such as wind and temperature, are interpolated to 21 fixed pressure levels; the lowest level of these 3D variables and surface level properties were vertically interpolated to produce 2-m temperature, 2-m humidity, and 10-m wind fields. The soil-related variables were also interpolated to the depths defined from the LSM.

Global model results are used as initial and boundary conditions for the regional climate simulations. Spectral nudging with a wave number of 3 in both zonal and meridional directions is used, i.e. all waves with wave numbers greater than 3 are filtered [*Liu et al.*, 2012]; no nudging is conducted for shorter waves to provide similarity with the large scale GCM simulation but allow small scale features to freely develop [*Liu et al.*, 2012]. Spectral nudging is applied to temperature, horizontal winds, and geopotential heights. Only horizontal winds are nudged at all vertical levels, while no nudging is conducted for other variables within the planetary boundary layer (PBL). The nudging coefficient for all variables was set to 3×10^{-4} s^{-1} [*Stauffer and Seaman*, 1990]. During the simulation, nudging is conducted every 6 h, consistent with the frequency of the GISS data.

2.3 Model Application and Evaluation

WRF is applied here using a nested grid approach. The modeling domain uses a Lambert Conformal Projection centered at 40ºN, 97ºW with true latitudes of 33ºN and 45ºN. The outer domain uses a 36-km horizontal grid spacing that covers the entire continental US as well as portions of Canada and Mexico (5940×5004 km). Two innermost domains cover 984×1020 km, and, 948×948 km regions with 12–km horizontal grid spacing and focusing on the Northeast and Southeast U.S. respectively (Figure 2-1). The periods modeled are 2006 through 2010 (historic) and 2048 to 2052 (future). The simulated coarse-grid hourly meteorology is used as initial and boundary conditions for the finer grids.

Observations are used to evaluate the ability of GISS-WRF to reproduce the long-term yearly climatic means, and the meteorological fields that strongly impact air quality. The model performance is evaluated by using statistical measures. This is a common analysis that is proposed by Emery and Tai [*Emery*, 2001] and has been adopted by the meteorological modeling community. Statistics such as mean bias (MB), mean absolute gross error (MAGE) and root mean square error (RMSE) are calculated:

$$MAGE = \frac{1}{N}\sum_{i=1}^{N}\left|P_i - O_i\right| \quad (1) \qquad MB = \frac{1}{N}\sum_{i=1}^{N}\left(P_i - O_i\right) \quad (2)$$

$$RMSE = \sqrt{\frac{1}{N}\sum_{i=1}^{N}\left(P_i - O_i\right)^2} \quad (3)$$

where P_i is the predicted value of the tested parameter (i.e. temperature), O_i is the corresponding observed value, and N is the total number of the predictions used for the

comparison. MAGE gives an estimation of the overall discrepancy between predictions and observations, while MB is sensitive to systematic errors. The root mean square error (RMSE) incorporates both the variance of the prediction and its bias. Additional details for the above evaluation metrics can be found in Yu et al. [*Yu et al.*, 2006] The observations used for the statistical analysis are TDL (Techniques Development Laboratory) data from the Research Data Archive (RDA) (http://dss.ucar.edu in dataset number ds472.0), which is maintained by the Computational and Information Systems Laboratory (CISL) at the National Center for Atmospheric Research (NCAR). These are hourly surface observations for wind speed, wind direction, and temperature during the four seasons over a five-year period (2006-2010). In the statistical analysis, the continental US domain has been divided in 4 sub regions, the West (W), the Midwest (MW), the South (S) and the Northeast (NE) USA (Figure 2-1).

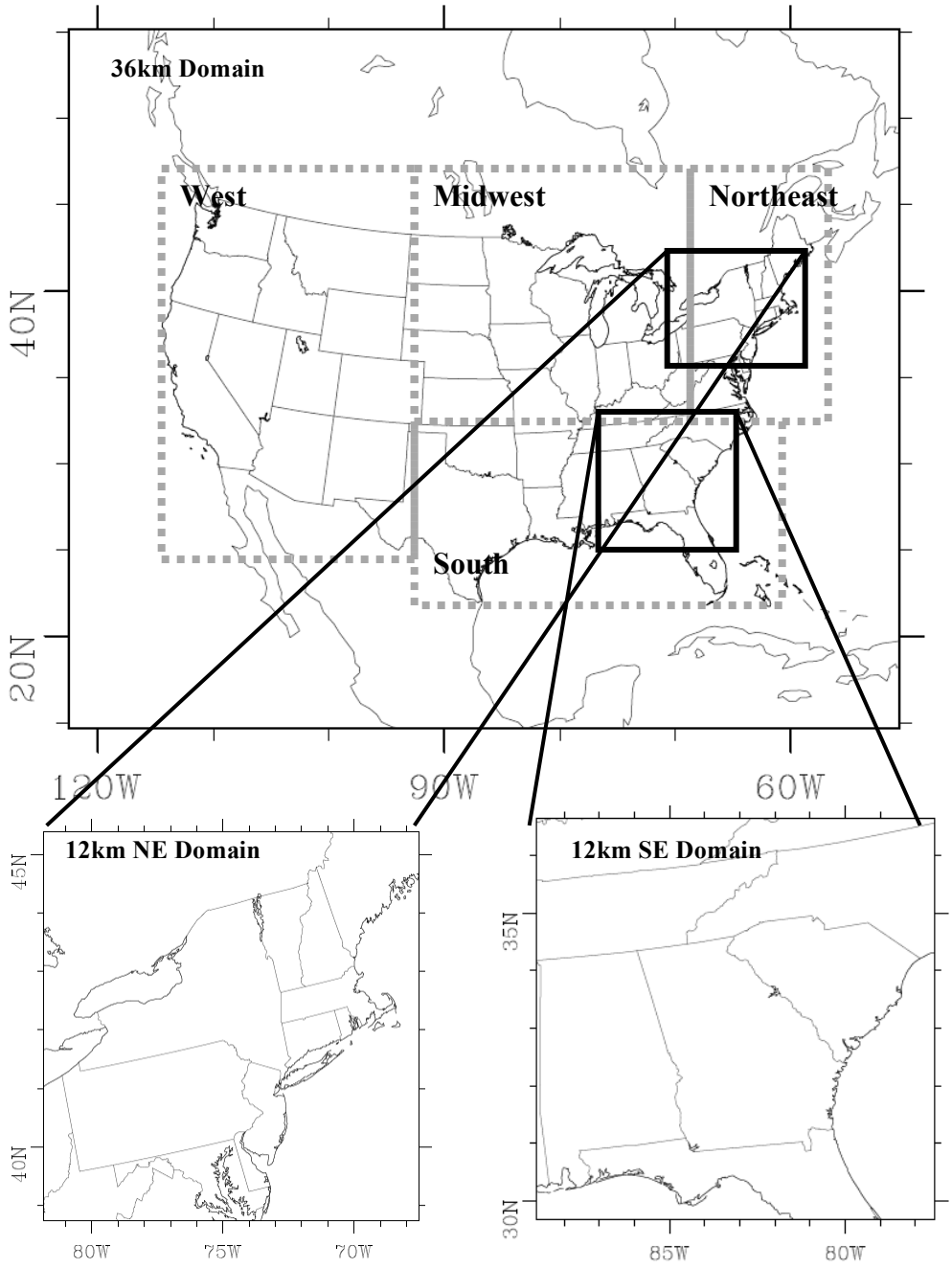

Figure 2-1 Modeling domains with horizontal grid-spacing resolutions of 36-km and 12-km Northeast (NE) and Southeast (SE). The dashed boxes indicate the four regions where model evaluation was conducted.

2.4 Results

Table 2-1 summarizes the comparison of the GISS-WRF modeling system simulations for wind speed and direction against TDL hourly surface observations during the four seasons of a five year period (2006-2010) over four regions of the continental USA: the West, the Midwest, the South, and the Northeast. Overall the model predictions agree well with observations with the MB over the total domain ranging between -0.1 m s^{-1} (during summer) 0.2 m s^{-1} (during spring). Model performance is better during summer with RMSE as a low as 2.2 m s^{-1} over the South and worst during winter with RMSE over the West up to 3.9 m s^{-1}. Wind speed is better predicted over South (with MAGE ranging from 1.7 m s^{-1} to 2.2 m s^{-1}) while wind direction is better predicted over Northeast (with MAGE ranging from 72 deg. to 78 deg.). Table 2-2 summarizes the comparison of the GISS-WRF modeling system predictions for temperature against observational data during the four seasons over the continental USA. Compared to observations, the model tends to under predict temperature during winter (MB up to -7.5 K), spring (MB up to -2.7 K), and summer (MB up to -1.9 K over West) but over predict temperature during fall (MB up to 2.9 K). The low temperature bias over the Western U.S. corresponds to low biases in the GISS fields. Model performance is better over the Southern U.S., especially during summer (RMSE = 3.5 K).

Table 2-1 GISS-WRF modeling system performance for wind speed (spd) and direction (dir) against TDL observations for U.S. regions and seasons (observed – OBS, predicted – PRD, mean bias – MB, mean absolute gross error – MAGE, root mean square error – RMSE)

	West				**Midwest**				**South**				**Northeast**				**Total Domain**			
Wind Speed & Direction	**Winter**	**Fall**	**Spring**	**Summer**	**Winter**	**Fall**	**Spring**	**Summer**	**Winter**	**Fall**	**Spring**	**Summer**	**Winter**	**Fall**	**Spring**	**Summer**	**Winter**	**Fall**	**Spring**	**Summer**
Spd Mean OBS (m s^{-1})	4.3	3.9	4.6	4.0	4.7	4.6	4.8	3.7	4.4	3.8	4.4	3.6	4.4	4.4	4.1	3.4	4.4	4.3	4.5	3.6
Spd Mean PRD (m s^{-1})	5.1	4.0	4.5	3.6	4.3	4.5	5.0	3.5	3.7	4.2	4.2	3.5	4.1	3.6	5.0	3.5	4.4	4.4	4.7	3.5
Spd MB (m s^{-1})	0.8	0.1	-0.1	-0.4	-0.4	-0.2	0.3	-0.1	-0.7	0.2	-0.2	-0.1	-0.3	-0.8	1.0	0.2	-0.0	0.1	0.2	-0.1
Spd MAGE (m s^{-1})	3.0	2.3	2.5	1.9	2.3	2.6	2.6	1.4	2.1	2.2	2.2	1.7	2.5	2.5	2.4	1.7	2.6	2.5	2.5	1.9
Spd RMSE (m s^{-1})	3.9	3.0	3.3	2.5	3.0	3.2	3.2	2.3	2.7	2.8	2.8	2.2	3.4	3.4	3.2	2.4	3.4	3.3	3.2	2.4
Dir Mean OBS (degrees)	213	256	264	248	231	242	179	219	223	183	168	145	209	218	192	216	248	265	192	214
Dir Mean PRD (degrees)	213	221	245	262	220	212	229	167	219	111	156	172	240	246	198	193	254	238	233	200
Dir MB (degrees)	5.6	-4.7	-1.0	3.8	0.3	-2.3	-5.2	1.9	-4.5	-1.8	4.6	6.5	8.2	0.9	1.1	4.1	2.2	-2.3	-1.7	2.2
Dir MAGE (degrees)	78	77	73	72	91	86	86	81	89	80	81	68	83	80	85	216	86	82	82	76

Table 2-2 GISS-WRF modeling system performance for temperature against TDL observations for U.S. regions and seasons (observed – OBS, predicted – PRD, mean bias – MB, mean absolute gross error – MAGE, root mean square error – RMSE)

	West				**Midwest**				**South**				**Northeast**				**Total Domain**			
Temperature	**Winter**	**Fall**	**Spring**	**Summer**	**Winter**	**Fall**	**Spring**	**Summer**	**Winter**	**Fall**	**Spring**	**Summer**	**Winter**	**Fall**	**Spring**	**Summer**	**Winter**	**Fall**	**Spring**	**Summer**
Mean OBS (K)	278	285	286	298	274	279	286	297	285	290	294	301	276	283	285	297	276	282	287	297
Mean PRD (K)	273	286	281	293	264	286	284	296	280	292	292	301	267	285	284	295	269	285	284	295
MB (K)	-4.7	1.1	-4.7	-4.2	-10	6.8	-1.9	-1.4	-4.5	2.4	-2.7	-0.2	-9.7	2.2	-1.4	-2.0	-7.5	2.9	-2.7	-1.9
MAGE (K)	6.7	4.7	5.9	5.4	11	7.5	5.8	3.7	7.4	5.3	4.7	2.7	11	5.2	4.7	3.2	9.2	5.7	5.4	3.8
RMSE (K)	9.1	5.9	7.8	6.7	14	8.8	7.1	4.6	9.6	6.6	6.0	3.5	13	6.4	6.0	4.1	12	7.1	6.8	5.0

2.4.1 Temperature

The 5 year mean of the modeled 2-meter air temperature across the simulation domain for the future is 1 K warmer than that of the historical simulation (284 and 285 K respectively) (Figure 2-2). Consistent with other studies [*Leung and Gustafson*, 2005; *Liao et al.*, 2007b; *Nolte et al.*, 2008; *Tagaris et al.*, 2007; *Woo et al.*, 2008] most of the warming, between 3 and 4 K, occurs over the western states (California, Nevada, Arizona, Texas, and Utah) and over western Canada (Figure 2-2a) and the results of a t-test suggest that the warming in this region is statistically significant (p-value < 0.05). Significant warming mainly occurs over these regions during the winter and spring months, where average surface temperature change reaches 4 degrees in western states, especially in and around Nevada (p-value < 0.05). Since temperatures are low during the winter and spring, warming during these seasons may not lead to increased concentrations of secondary pollutants such as O_3 and secondary PM, but warming could lead to decreased emissions of PM from heating processes such as wood burning (e.g., from wood stoves). The GCM simulations predict a similar warming pattern during the winter and spring, but only up to 3 degrees K (Figure A-1). During the summer months, Texas and northeastern Canada experience a warming of 2 and 4 degrees respectively, although the GCM predicts up to one degree more warming over western Texas and the p-value associated with the downscaled temperature changes over western Texas is between 0.05 and 0.10. An average warming of 3 degrees occurs over the Midwest (p-value <0.05) and a warming of around 2 degrees also occurs over most of Texas and Eastern U.S. (the p-value is between 0.05 and 0.15 which is not significant) during the

fall. The eastern U.S. states, on the other hand, are cooler during the winter and spring months with the southeastern states and Texas cooling up to just less than 2 degrees, however the cooling here is not statistically significant (p-value greater than 0.05).

The smaller, more highly resolved 12km domain over the Northeast simulates similar magnitudes of temperature change to the 36 km domain. The root mean square difference of the future temperature change between the 36 km and 12 km domains is very small (less than 0.004 K); indicating the similarity between the two simulations. The standard deviations of the simulated temperature changes in the Northeast for the 12 km (standard deviation of 0.25 K) and 36 km (0.24 K) domains show that the fine resolution simulation introduces slightly more variability than the coarse resolution domain, especially during the winter (0.49 K for the 36km and 0.52 K for 12 km) and spring (0.27 K for 36 km and 0.29 K for 12km). The Northeast sees cooling of less than 1 degree during the spring and warming of up to 2 degrees during the summer (Figure 2-2b). During fall, large warming between 2-3 degrees is simulated over much of New York State. Over the Southeastern 12km domain, similar warming occurs as the 36 km domain, ranging between 1 and 3 degrees during the summer and fall with the greatest warming occurring during the fall over North Carolina and Tennessee (Figure 2-2c).

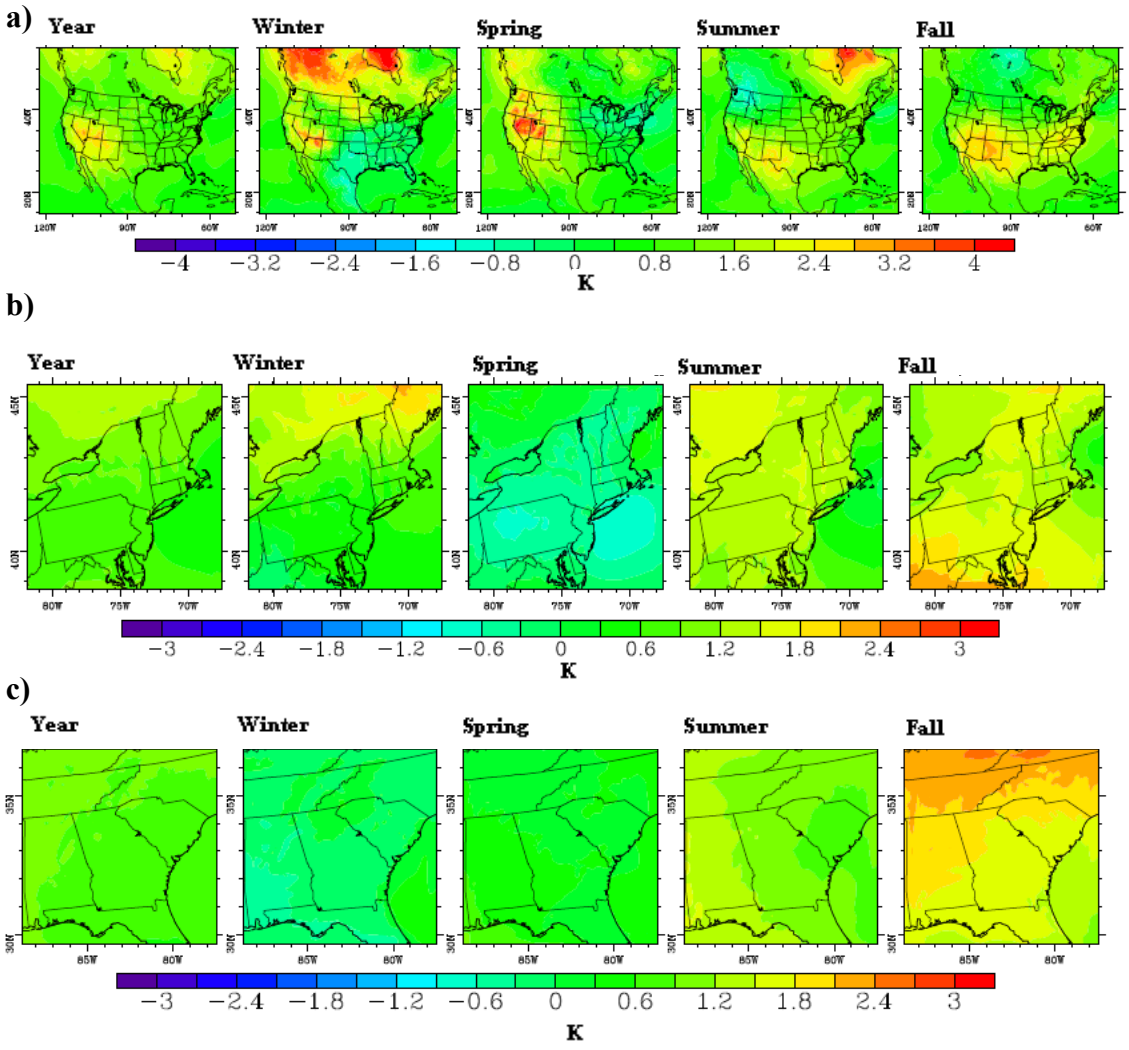

Figure 2-2 Predicted average yearly and seasonal 2-m atmospheric temperature change (2048 to 2052 minus 2006 to 2010) for **(a)** the 36x36 km resolution modeling domain, **(b)** the 12x12 km resolution sub-domain over Northeast and **(c)** the 12x12 km resolution sub-domain over Southeast.

2.4.2 Insolation and Precipitation

A change in downward solar radiation at the surface, or insolation, is an indicator of changes in cloudiness. For this reason, spatial distributions of the change in insolation at the surface are similar in structure to average daily precipitation, but not identical. Spatial distributions of surface temperature and insolation changes have similar structures in some cases. Weaver et al. (2009) explain that these meteorological conditions can have either competing or reinforcing effects on air quality. When temperature and insolation change in the same direction, O_3 concentrations tend to change in the same corresponding direction, whereas temperature and insolation varying in opposite directions correspond with mixed changes in O_3.

Decreases in daily mean precipitation are found over the Pacific coast where some regions receive 2 mm less rain per day (or 30 % less rain), on average, and some decreases were simulated over the Southeastern region (Figure 2-3a). Reduced rain along the Pacific coast occurs mostly during the winter, as a major portion of Western U.S. sees greater than a 2 mm per day decrease. Correspondingly, insolation over the Pacific coast increases during the winter by up to 15 W/m^2 (**Figure 2-4**a). The Southeast experiences a similar magnitude of drying, but mainly during the fall. Both the 36 and the 12km simulations over the Southeast predicted greater than 2 mm less rain per day during the fall, which is also consistent with insolation changes in the region (increase of up to 10 W/m^2). Interestingly, the high-resolution simulation predicts that the Southeast receives up to 2mm per day more rain during the summer, which is not apparent in the 36 km domain. The 36 and 12 km resolution simulations over the Northeast on the other hand, predict more rain over most of Vermont, New Hampshire and Maine during the summer,

while most of Connecticut and New York receive less rain (Figure 2-3b). The precipitation trend in the Northeast reverses during the fall when Connecticut and New York receive more rain and the states farther north are dryer. There is a decrease in insolation of 5-15 W/m^2 during the spring and fall and an increase during the fall of 10 - 20 W/m^2 over the Northeast (**Figure 2-4**b). Correspondingly, the temperature only decreases slightly during spring, while it increases during summer. However, contrary to the insolation trend, the temperature in the Northeast sees large increases during fall.

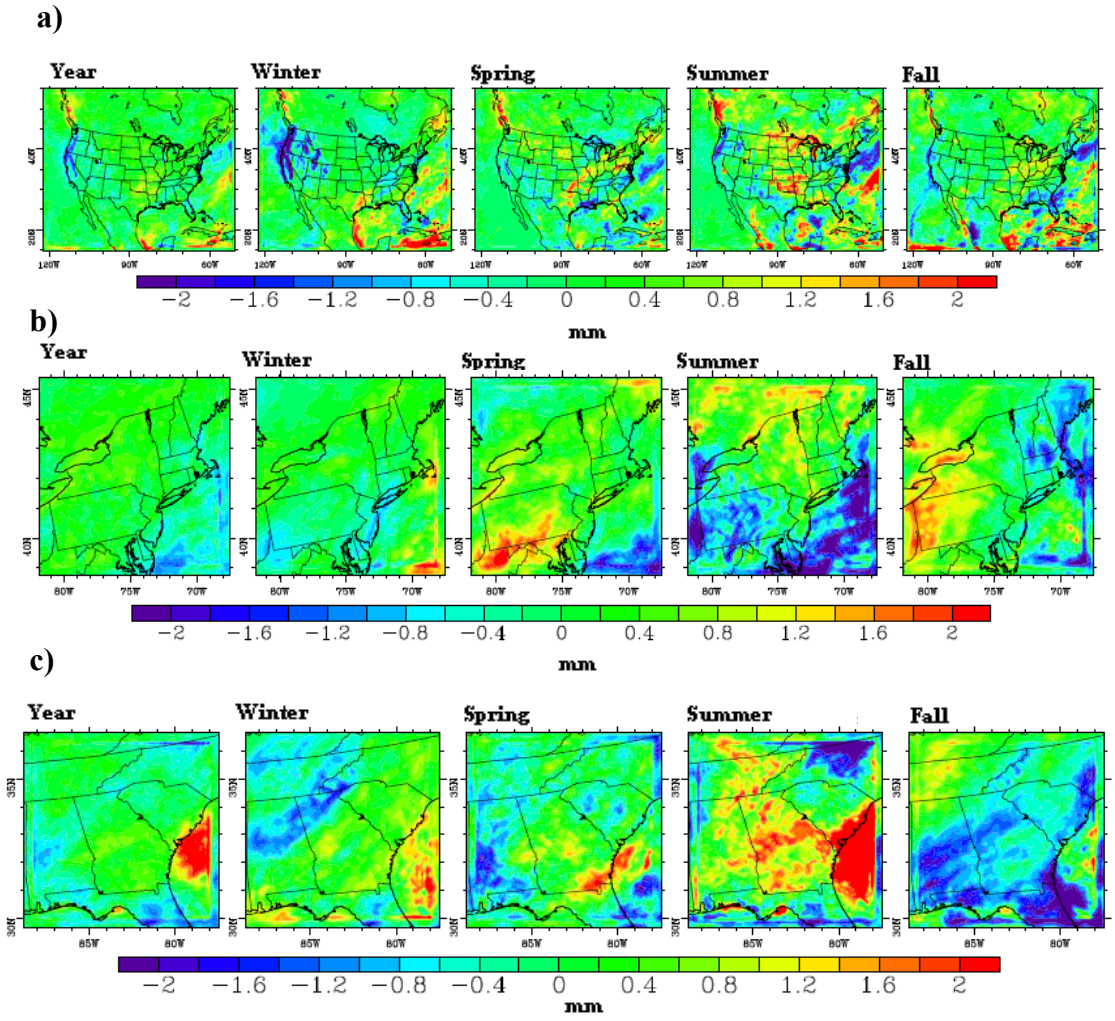

Figure 2-3 Predicted average yearly and seasonal precipitation (mm day-1) change (2048 to 2052 minus 2006 to 2010) for **(a)** the 36x36 km resolution modeling domain, **(b)** the 12x12 km resolution sub-domain over the Northeast and **(c)** the 12x12 km resolution sub-domain over Southeast.

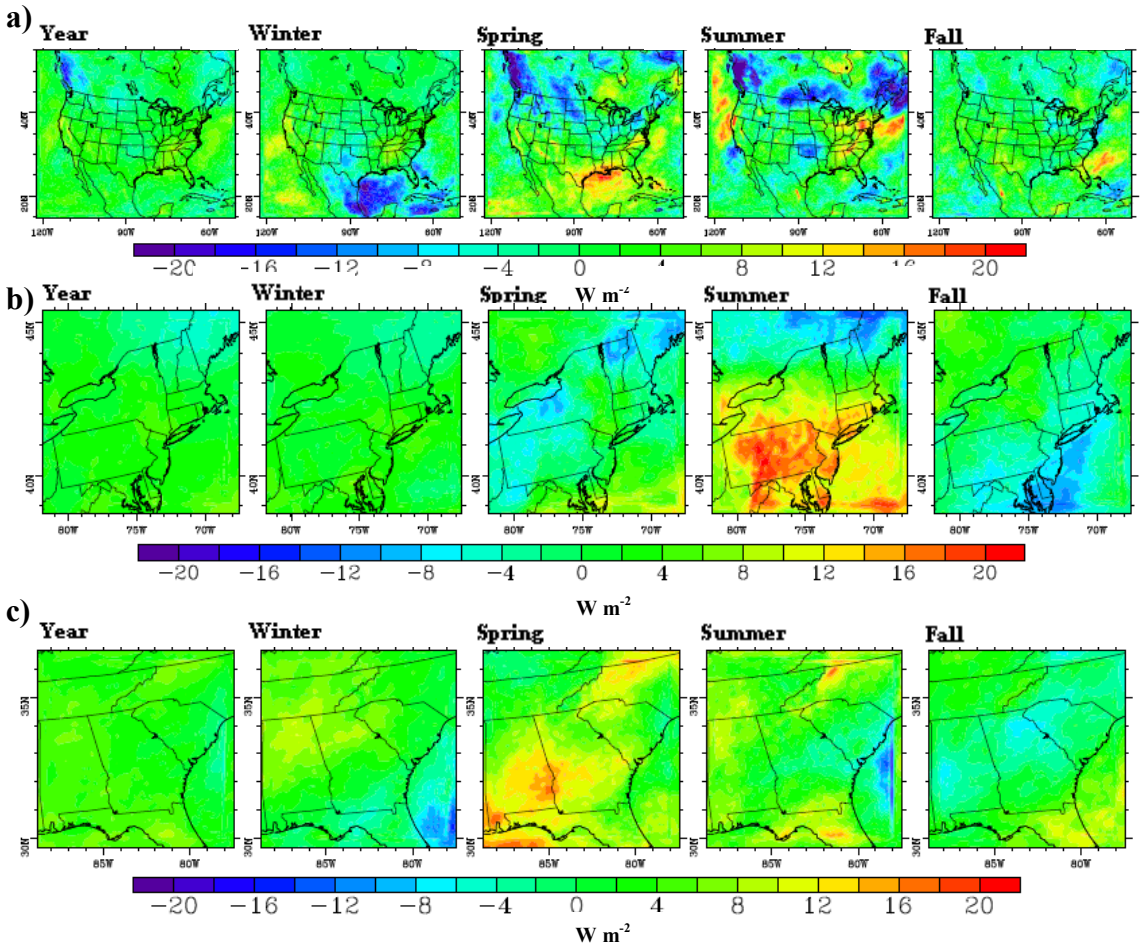

Figure 2-4 Predicted average yearly and seasonal downward short wave radiative flux at the surface (W m^{-2}) change (2048 to 2052 minus 2006 to 2010) for **(a)** the 36x36 km resolution modeling domain, **(b)** the 12x12 km resolution sub-domain over Northeast and **(c)** the 12x12 km resolution sub-domain over Southeast.

2.4.3 Stagnation events

Stagnation events occur when wind speeds are low and little precipitation occurs over an extended period. A stagnation event is defined as at least four consecutive days when the following criteria are met: a) the 10m wind speed is less than 4 m s^{-1} b) the 500 mb wind speed is less than 13 m s^{-1} at 7:00 am LST, and c) the total rainfall is less than 0.001 cm for the 4 day period [*Korshover and Angell*, 1982]. Since transport and deposition of pollutants is decreased during a stagnation period these events promote poor air quality. The number of stagnation days was compared to the National Centers for Environmental Prediction – North American Regional Reanalysis data (NCEP-NARR) for the year 2010. Results generally compare well, though with very similar regional spatial patterns. Low biases were found over Mexico and over the Western U.S. during the summer and fall. Stagnation is biased high in Texas during the summer (Figure A-2). During the winter and spring months, the spatial distribution of the number of stagnation days per season does not change significantly over the U.S. (Figure 2-5a). Over southern Texas, the number of stagnation days during fall increases in some small areas by 10 to 15 days per season, which correlates with the increase in temperature in the region. Large portions of this region already see over 30 days of stagnation per season. Stagnation decreases over Texas during the summer. Over most of the Southeast stagnation days also decrease by up to 10 days per season corresponding to the increase in precipitation (Figure 2-5c), which is large, compared to the average number of stagnation days during the summer of the historic simulation (between 15 and 30).

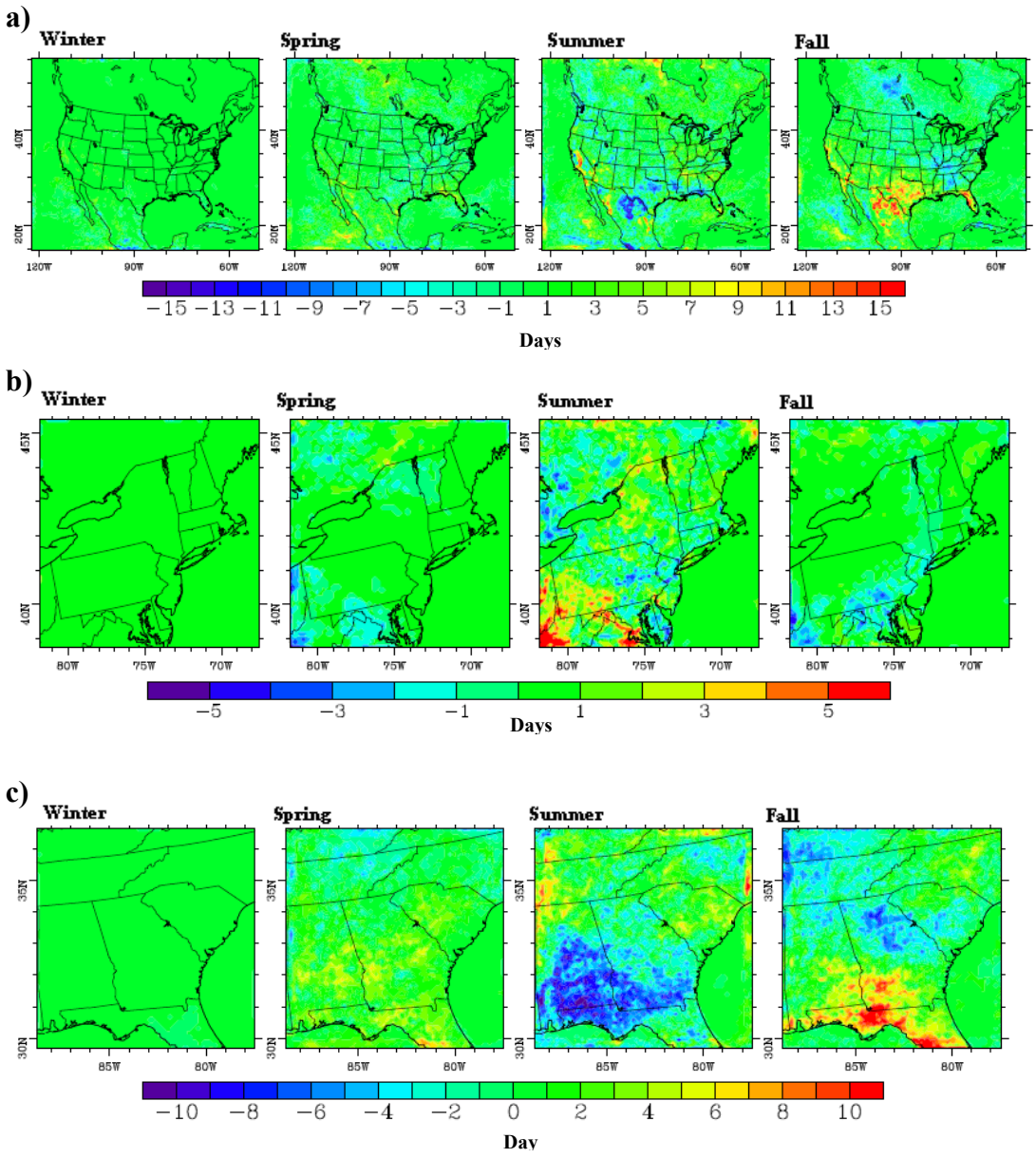

Figure 2-5 Predicted total seasonal change in the number of stagnation days (days per season) (2048 to 2052 minus 2006 to 2010) for **(a)** the 36x36 km resolution modeling domain, **(b)** the 12x12 km resolution sub-domain over the Northeast and **(c)** the 12x12 km resolution sub-domain over Southeast.

While the 36km domain shows little change in stagnation in the Northeast, the high resolution simulation shows stagnation increases of up to 5 days per season during the summer over parts of the Northeast which is large compared to the average 5 to 10 stagnation days per season that occur in this region (Figure 2-5b). Increased summertime stagnation in the 12km Northeast domain corresponds to precipitation decreases in the same domain. During fall, a large increase (over 15 days) in the number of stagnation days is found along the Gulf coast and the California coast. Along the coast of California during fall, the increase in stagnation days leads to increased concentrations of pollutants, reinforcing the negative impact that increased temperature and insolation have on air quality in the area. Similarly, the decreased precipitation along the Gulf coast may reinforce higher concentrations of pollutants due to increased stagnation in the area.

2.4.4 Ventilation

The ventilation coefficient, which is defined as the product of the mean wind speed within the boundary layer and the boundary layer height [*Pielke et al.*, 1991], reflects how well pollutants can be mixed and transported within the boundary layer. Ventilation is adversely impacted by stagnation, which is driven by the persistence of certain large-scale circulation patters, but also takes into account smaller scale meteorological conditions. An unvented hour is an hour during which the ventilation coefficient is less than 6000 m^2 s^{-1} [*Pielke et al.*, 1991]. Seasonal mean ventilation coefficients were compared with NCEP-NARR data, and similar spatial and seasonal patterns were found. There was a low bias in the Western U.S. while the Northeast and the Southeast compare well with reanalysis data (Figure A-3). During summer, Texas

has on average 1 to 2 more unvented hours per day in the future compared to the present which tends to increase pollutant concentrations, further amplifying the increased concentrations of O_3 and some secondary PM (with the exception of volatile PM such as ammonium nitrate) due to increased temperatures in the region (Figure 2-6a). The 12km simulation shows that the coast of Georgia and the Carolinas also see 1 to 2 more unvented hours per day during the summer, while the 36km shows less dramatic changes over the Southeast. Summertime differences between the two domains occur, in part, due to differences in the resolutions of the land use data since southeast Georgia and South Carolina are scattered with pine forest and cropland and these two land use categories affect surface energy fluxes and PBL height differently, which in turn affects the ventilation in the region. During fall, an increase of 1 to 2 unvented hours per day is found over much of the Northeast and Southeast. The higher resolution domains show similar trends, although with more spatial variability. In the Northeast, the combined higher temperatures and less ventilation would lead to higher concentration of pollutants, while the decrease in insolation would reduce secondary pollutants such as O_3 and secondary PM (Figure 2-6b). Unvented hours over most of Minnesota increase during spring by over 3 hours per day; however, none of the other variables examined here show either a reinforcing or competing effect on air quality.

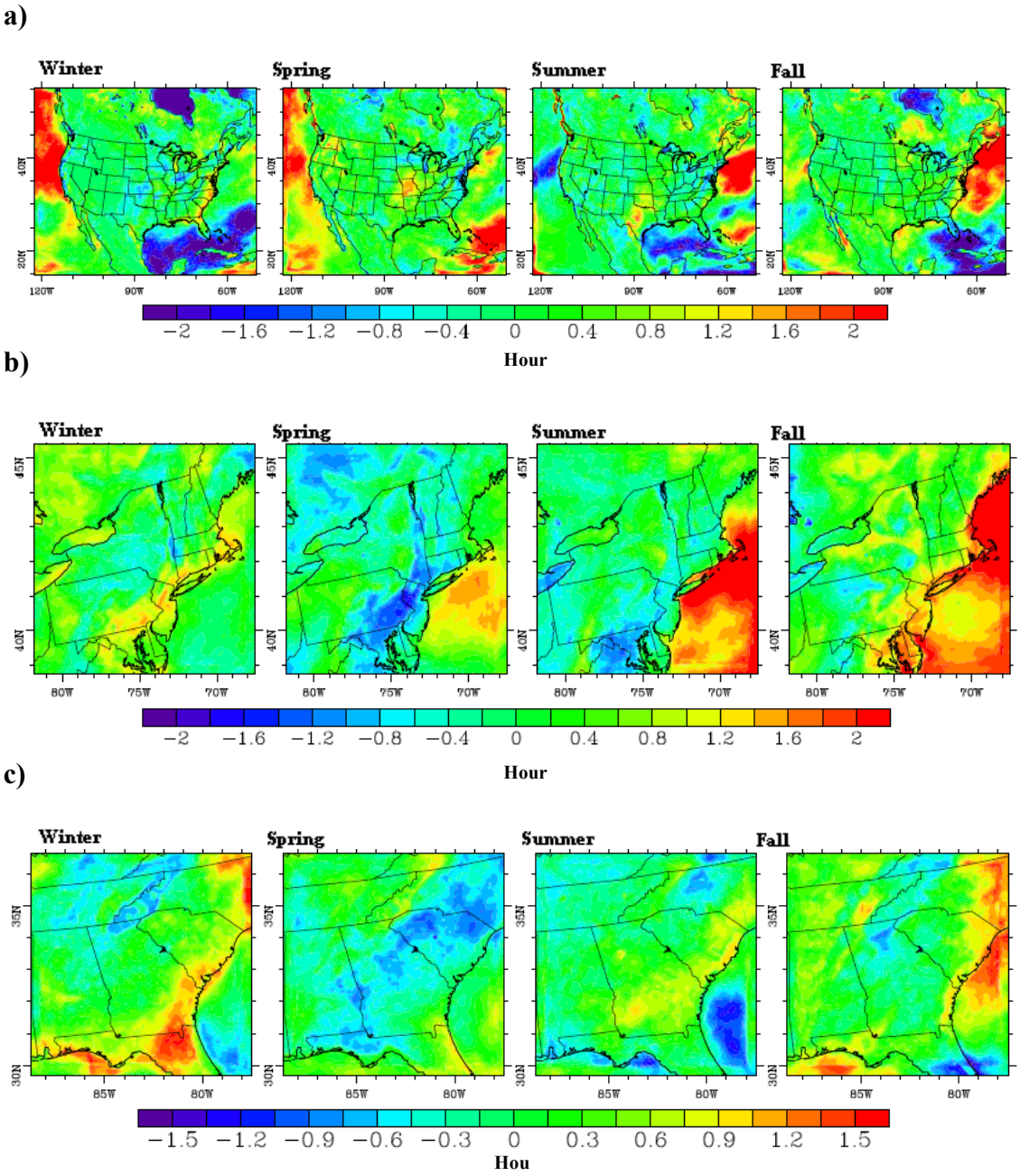

Figure 2-6 Predicted total seasonal change in average unvented hours (hours per day) (2048 to 2052 minus 2006 to 2010) for **(a)** the 36x36 km resolution modeling domain, **(b)** the 12x12 km resolution sub-domain over the Northeast and **(c)** the 12x12 km resolution sub-domain over Southeast.

2.4.5 Regional climate and urban centers

Since a large and growing fraction of the nation's population is located in dense urban areas, it is important to examine the change in air quality related climate variables over some major U.S. cities. The expected response to climate change differs among various different regions of the U.S. Here we focus on 5 geographically unique, densely populated cities that are representative of the different regions of the U.S.: Atlanta, Los Angeles, Philadelphia, Phoenix, and Seattle. Further, land use changes may exacerbate meteorological changes in cities. Philadelphia and Phoenix are chosen here, rather than more populated cities such as New York and Houston, because future studies are planned to address the impact of land use changes on regional climate in those cities. Extremes in meteorological variables are important because there are adverse health effects associated temperature extremes as well as with short term exposure to poor air quality. Air pollution is highly variable in time and temperature extremes can impact pollutant concentrations [*McMichael et al.*, 2006]. Cumulative distribution function (CDF) plots show the percentage of hourly temperature and daily precipitation that exceed a given value in major U.S. cities for each simulation year (**Figure 2-7**). The hourly temperatures within any given percentile range tend to shift a few degrees warmer in the future, except for the lower 20^{th} percentile range in Atlanta and Philadelphia and the upper 90^{th} percentile range in Seattle. Most warming in Seattle occurs at the lower 75^{th} percentile range, where high O_3 concentrations are not likely, which reflects the increase in temperature mentioned earlier during the winter in the Pacific Northwest. This can also decrease emissions related to domestic heating, including PM from wood burning. The cumulative distribution of the maximum daily temperature in Seattle follows a

similar trend, as the hourly CDF in the lower range and temperature are nearly the same in the 60th to 90th percentile range (Figure 2-8). The upper 95th percentile in daily maximum temperatures in Seattle are actually around a degree cooler in the future, decreasing the chance of high ozone during hot days (**Table 2-3**).

Table 2-3 The average present (2006-2009) and future (2048-2052) upper 95th percentile in daily maximum temperatures for Atlanta, Los Angeles, Philadelphia, Phoenix and Seattle

95th Percentile	2006-2010 Average (K)	2048-2052 Average (K)
Atlanta 36km	302	304
Atlanta 12km	303	305
Los Angeles	302	305
Philadelphia 36km	301	304
Philadelphia 12km	303	305
Phoenix	306	309
Seattle	299	298

Los Angeles and Phoenix have similar hourly temperature and maximum temperature CDF structures and shifts from present to future. These cities are warmed by 1 to 3 degrees regardless of the percentile range. Lin et al. (2001) have developed estimates of the probability that the maximum daily 8-hr average O_3 will exceed 80 ppb given the maximum daily temperature in a given region (including Los Angeles, the Southeast, and the Northeast). Given that the upper 95th percentile in daily maximum temperatures in Phoenix increases from around 306 K to 309 K, the probability that O_3 will exceed 80 ppb on these days increases. Similarly, a shift in the upper 95th percentile in daily maximum temperatures in Los Angeles, from around 302 K to 305 K, also increases the

probability of high O_3. The coolest days in Atlanta and Philadelphia are similar to, if not cooler than the future simulations, reflecting the cooling that occurs during the winter and spring in the surrounding regions. While very little, if any, warming occurs in the lower 50th percentile of daily maximum temperature, the upper 95th percentile maximum temperatures in Philadelphia and Atlanta increase from around 301 K to 304 K and 302 K to about 304 K respectively, with a corresponding increase in probability of high O_3 concentrations on those hot days. The 12 km simulations produce similar, but not identical, cumulative distribution of total hourly temperatures and maximum temperatures in Atlanta and Philadelphia (**Figure 2-9**). The 12 km domains show a shift in daily maximum temperature at the upper 95th percentile of 303 to 305 K in both Philadelphia and Atlanta, implying a higher probability of high ozone on those days than would be derived from the coarse resolution. The hottest days in Philadelphia are simulated by the future 12km domain, where temperatures reach 310 K. Maximum temperatures and high O_3 probability in New York exhibit similar changes to that of Philadelphia. Temperature distributions in Chicago were also analyzed, however the only difference from present to future is a shift in the upper 95th percentile from 300 to 301 K while the distribution below the 90th percentile does not change.

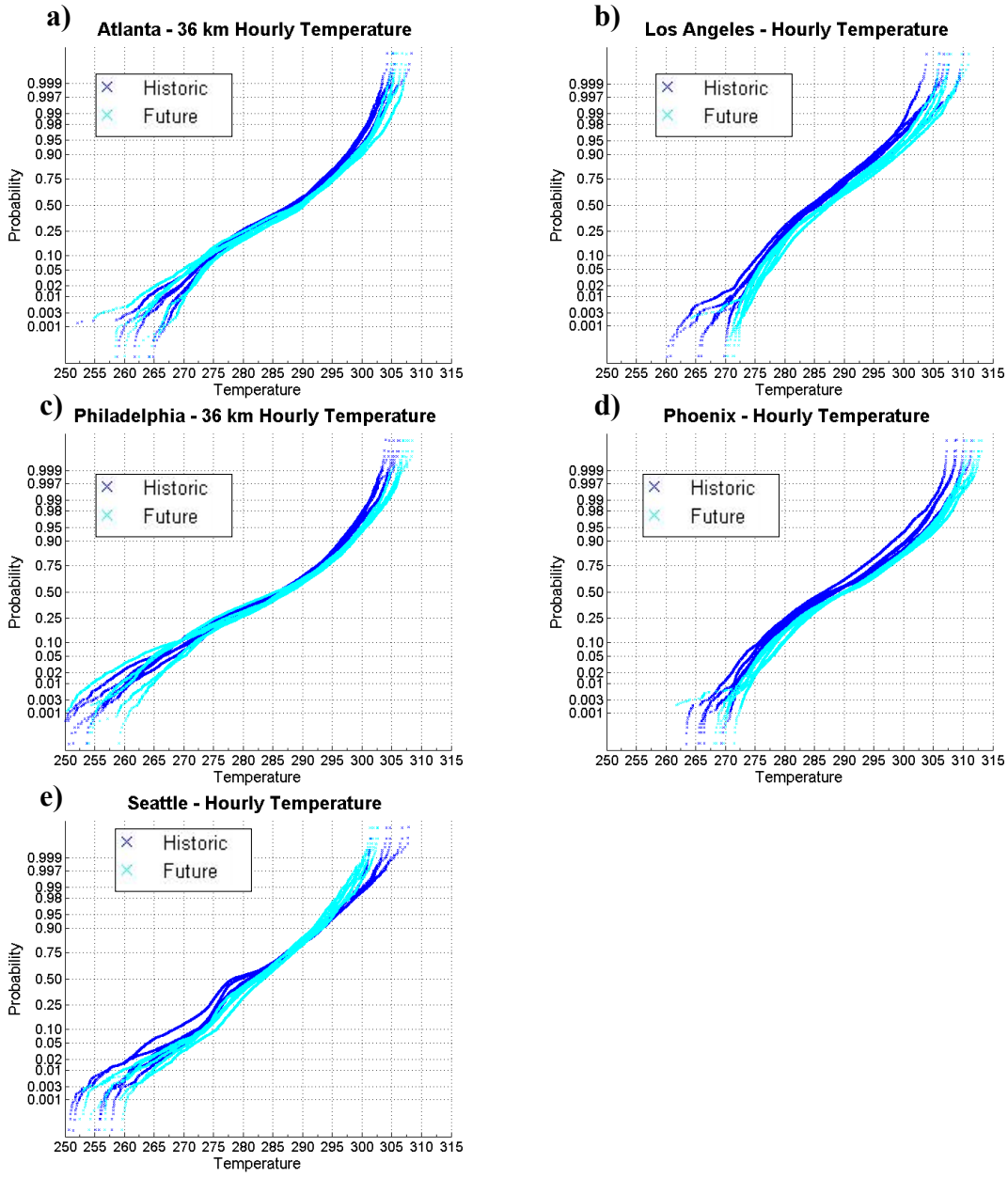

Figure 2-7 Empirically determined cumulative distribution of 36 km historic (2006-2010) and future (2048-2050) hourly temperatures (K) at major U.S. cities: **a)** Atlanta **b**) Los Angeles **c)** Philadelphia **d)** Phoenix and **e)** Seattle

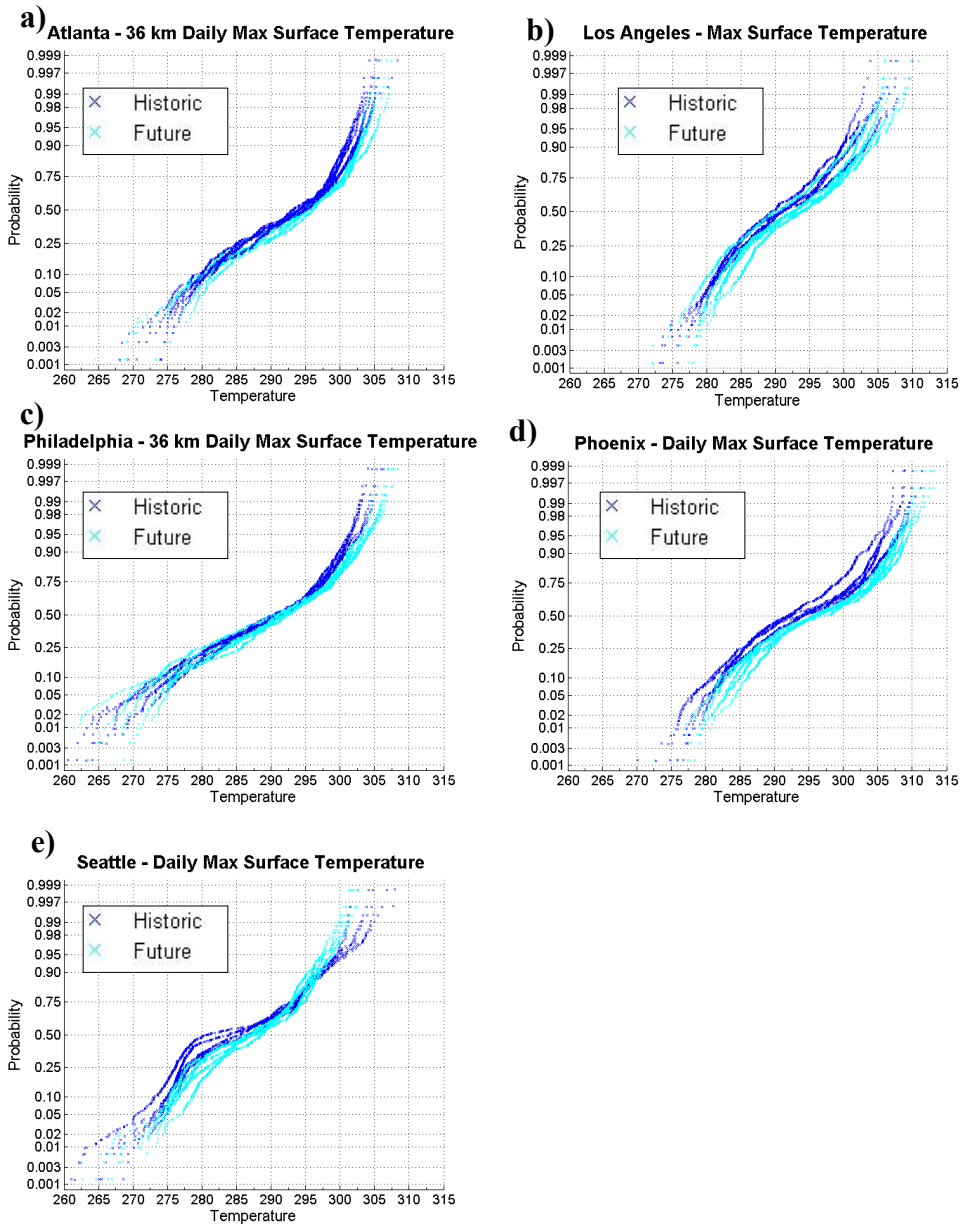

Figure 2-8 Empirically determined cumulative distribution of 36 km historic (2006-2010) and future (2048-2050) maximum daily 1-hr average temperature (K) at major U.S. cities: **a)** Atlanta **b)** Los Angeles **c)** Philadelphia **d)** Phoenix and **e)** Seattle

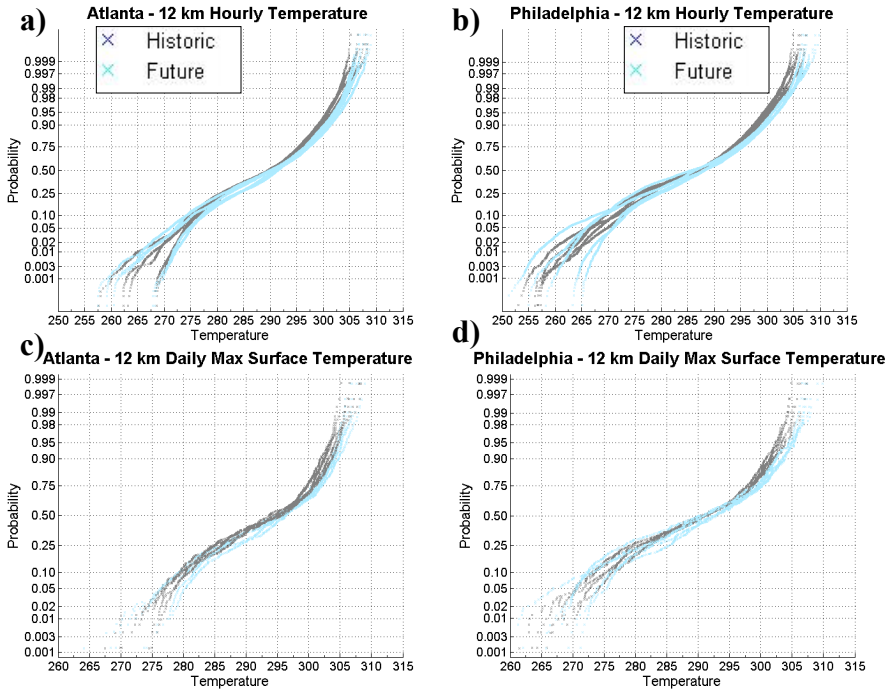

Figure 2-9 Empirically determined cumulative distribution of 12 km historic (2006-2010) and future (2048-2050) hourly temperature (K) **a)** Atlanta, **b)** Philadelphia and maximum daily 1-hr average temperature at **c)** Atlanta, **d)** Philadelphia

Rain can improve air quality, and although the seasonal mean precipitation has already been examined, it is important to also understand how the frequency and distribution of rainfall can shift over time. Rainfall frequency shifts are especially important in cities, where frequent light rains will clean the air more than infrequent heavy rains. The most notable change in daily precipitation distribution occurs in Los Angeles, where the driest year is simulated in the future and the wettest year is simulated in the historic simulations (**Error! Reference source not found.**). Seattle does not seem to receive more or less rain in the future but does have a more consistent distribution of daily rainfall from year to year in the future. The precipitation distributions of the remaining cities do not appear to be affected. Precipitation distributions produced from

the 12 km simulations over Atlanta and Philadelphia are similar to the coarse simulation (Figure A-4).

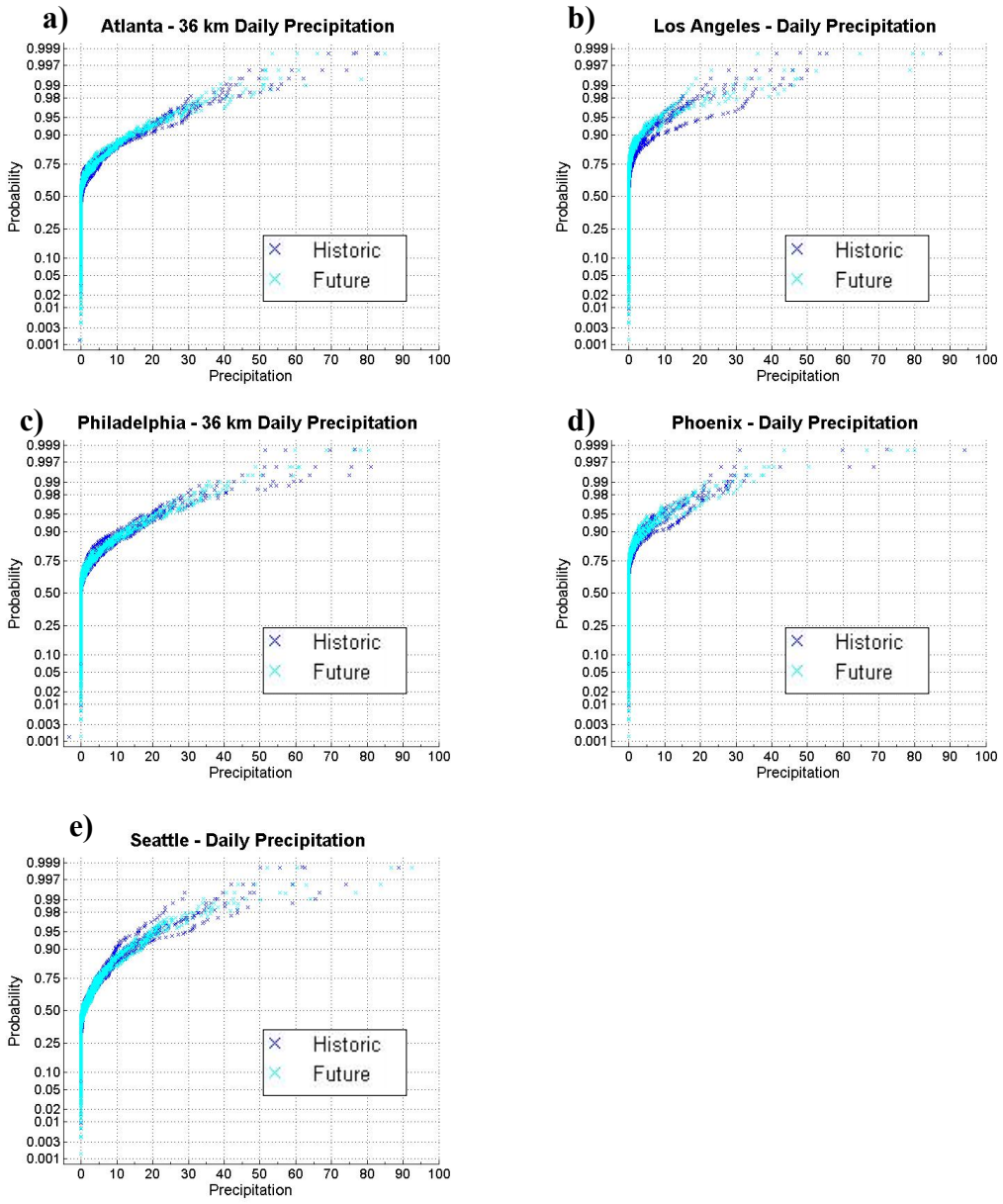

Figure 2-10 Cumulative distribution of 36 km historic (dark) and future (light) daily precipitation (mm) at major U.S. cities: **a)** Atlanta **b)** Los Angeles **c)** Philadelphia **d)** Phoenix and **e)** Seattle

2.5 Conclusions

The high resolution simulations produce somewhat different results than the coarse resolution simulations in some regions. Also, through the analysis of the meteorological variables that most strongly influence air quality, we find consistent changes in regional climate that would enhance ozone levels in four regions of the U.S. during fall (Western U.S., Texas, Northeastern, and Southeastern U.S), one region during summer (Texas), and one region where changes potentially would lead to better air quality during spring (Northeast).

During summer and fall, all air quality indicators, with the exception of insolation and precipitation, suggest an increase in air pollutant concentrations, including increased production of secondary PM and O_3, in most of Texas. Consistent with Leung and Gustafson [*Leung and Gustafson*, 2005], when comparing 2048-2052 to 2006-2010, we find warmer temperatures (2 - 3 K),), less ventilation (1 – 2 hours per day) and more stagnation (10 – 15 days per season) during summer in Texas and the same for fall, though slightly less intense.

The West Coast is marked by warmer temperatures (ranging from 1 – 4 K), slightly less rainfall (less than 1 mm per day), and more stagnation (10 – 15 days) during fall, while there is no significant change in ventilation and insolation. Similarly during fall, the Southeast shows little change in ventilation and stagnation but is warmer (2 – 3 K), dryer (up to 2 mm per day in some areas) and with slightly higher insolation (5 - 10 W/m^2). Also, the shift in the distribution of maximum daily temperatures in Atlanta increases the probability of high O_3 concentrations for days when the maximum temperature is in the 95^{th} percentile.

The Northeast is also warmer during fall (2 – 3 K) and less ventilated (1 – 2 hours per day) but increased rainfall (up to 2 mm per day) and decreased insolation (~5 W/m^2) compete for better air quality. Regardless, as in Atlanta, the shift in the distribution of maximum daily temperature in New York and Philadelphia increases the probability of high O_3 concentrations (0.06 - 0.12) for days when the maximum temperature is in the 95^{th} percentile. During spring, however, increased rain (1 – 2 mm per day), more ventilation (~ 1 hour per day) and decreased temperatures (~1 K) could promote better air quality in the Northeast.

While climate conditions strongly impact air quality, emissions and chemistry also play a vital and complex role in the formation and removal of atmospheric pollutants. A more comprehensive assessment of emissions and chemistry will be addressed in the future.

2.6 References

Byun, D., and K. Schere (2006), Review of the Governing Equations, Computational Algorithms, and Other Components of the Models-3 Community Multiscale Air Quality (CMAQ) Modeling System, *Applied Mechanics Reviews*, *59*(2), 51-77

Dawson, J. P., et al. (2008), Simulating present-day and future air quality as climate changes: Model evaluation, *Atmospheric Environment*, *42*(19), 4551-4566, doi:10.1016/j.atmosenv.2008.01.058.

Dudhia, J. (1989), Numerical study of convection observed during the winter monsoon experiment using a mesoscale two-dimensional model, *J. Atmos. Sci.*, *46*(20), 3077-3107

Ek, M. B., et al. (2003), Implementation of Noah land surface model advances in the National Centers for Environmental Prediction operational mesoscale Eta model, *Journal of Geophysical Research-Atmospheres*, *108*(D22), 16, doi:8851 10.1029/2002jd003296.

Emery, C., Edward Tai (2001), Meteorological Modeling and Performance Evaluation of hte September 13-20, 1999 Ozone Episode, in *Prepared for the Texas Near Non-*

Attainment Areas through the Alamo Area Council of Governments, by ENVIRON International Corp, edited, Navato, CA.

EPA, U. S. (1989), The potential effects of global climate change on the United States, *EPA*, *EPA-230-05-89-050*, 457

Giorgi, F. (2006), Regional climate modeling: Status and perspectives, *J. Phys. IV*, *139*, 101-118, doi:10.1051/jp4:2006139008.

Grell, G. A., Dudhia, J., Stauffer, D. R. A (1994), A description of the fifth generation Penn State/NCAR mesoscale model (MM5), *National Center for Atmospheric Research: Boulder, CO*

Hong, S. Y., et al. (2006), A new vertical diffusion package with an explicit treatment of entrainment processes, *Mon. Weather Rev.*, *134*(9), 2318-2341

Jacob, D. J., and D. A. Winner (2009), Effect of climate change on air quality, *Atmospheric Environment*, *43*(1), 51-63, doi:10.1016/j.atmosenv.2008.09.051.

Kain, J. S., and J. M. Fritsch (1993), Convective parameterization models: The Kain–Fritsch scheme. Cumulus Convection in Numerical Models, *American Meteorological Society*, *46*, 165-170

Korshover, J., and J. K. Angell (1982), A review of air-stagnation cases in the Eastern-United-States during 1981 - Annual summary, *Monthly Weather Review*, *110*(10), 1515-1518, doi:10.1175/1520-0493(1982)110<1515:aroasc>2.0.co;2.

Lamarque, J. F., et al. (2011), Global and regional evolution of short-lived radiatively-active gases and aerosols in the Representative Concentration Pathways, *Clim. Change*, *109*(1-2), 191-212, doi:10.1007/s10584-011-0155-0.

Leung, L. R., and W. I. Gustafson (2005), Potential regional climate change and implications to US air quality, *Geophysical Research Letters*, *32*(16), 4, doi:L16711 10.1029/2005gl022911.

Liao, H., et al. (2006), Role of climate change in global predictions of future tropospheric ozone and aerosols, *Journal of Geophysical Research-Atmospheres*, *111*(D12), 18, doi:D12304 10.1029/2005jd006852.

Liao, K. J., et al. (2007), Sensitivities of ozone and fine particulate matter formation to emissions under the impact of potential future climate change, *Environmental Science & Technology*, *41*(24), 8355-8361

Lin, Y. L., et al. (1983), Bulk parameterization of the snow field in a cloud model, *Journal of Climate and Applied Meteorology*, *22*(6), 1065-1092, doi:10.1175/1520-0450(1983)022<1065:bpotsf>2.0.co;2.

Liu, P., et al. (2012), Differences between downscaling with spectral and grid nudging using WRF, *Atmospheric Chemistry and Physics*, *12*(8), 3601-3610, doi:10.5194/acp-12-3601-2012.

McMichael, A. J., et al. (2006), Climate change and human health: present and future risks, *Lancet*, *367*(9513), 859-869, doi:10.1016/s0140-6736(06)68079-3.

Mickley, L. J., et al. (2004), Effects of future climate change on regional air pollution episodes in the United States, *Geophysical Research Letters*, *31*(24), 4, doi:L24103 10.1029/2004gl021216.

Mlawer, E. J., et al. (1997), Radiative transfer for inhomogeneous atmospheres: RRTM, a validated correlated-k model for the longwave, *Journal of Geophysical Research-Atmospheres*, *102*(D14), 16663-16682, doi:10.1029/97jd00237.

Moss, R. H., et al. (2010), The next generation of scenarios for climate change research and assessment, *Nature*, *463*(7282), 747-756, doi:10.1038/nature08823.

Nolte, C. G., et al. (2008), Linking global to regional models to assess future climate impacts on surface ozone levels in the United States, *Journal of Geophysical Research-Atmospheres*, *113*(D14), D14307, doi:10.1029/2007JD008497.

Pielke, R. A., et al. (1991), A procedure to estimate worst-case air-quality in complex terrain, *Environ. Int.*, *17*(6), 559-574, doi:10.1016/0160-4120(91)90168-p.

Rind, D., and J. Lerner (1996), Use of on-line tracers as a diagnostic tool in general circulation model development .1. Horizontal and vertical transport in the troposphere, *Journal of Geophysical Research-Atmospheres*, *101*(D7), 12667-12683, doi:10.1029/96jd00551.

Rind, D., et al. (1999), Use of on-line tracers as a diagnostic tool in general circulation model development 2. Transport between the troposphere and stratosphere, *Journal of Geophysical Research-Atmospheres*, *104*(D8), 9151-9167, doi:10.1029/1999jd900006.

Skamarock, W. C., and J. B. Klemp (2008), A time-split nonhydrostatic atmospheric model for weather research and forecasting applications, *Journal of Computational Physics*, *227*(7), 3465-3485, doi:10.1016/j.jcp.2007.01.037.

Stauffer, D. R., and N. L. Seaman (1990), Use of a 4-dimensional data assimilation in a limeted-area mesoscale model .1. Experiments with synoptic-scale data, *Monthly Weather Review*, *118*(6), 1250-1277, doi:10.1175/1520-0493(1990)118<1250:uofdda>2.0.co;2.

Stevenson, D. S., et al. (2006), Multimodel ensemble simulations of present-day and near-future tropospheric ozone, *Journal of Geophysical Research-Atmospheres*, *111*(D8), D08301, doi:10.1029/2005JD006338

Tagaris, E., et al. (2007), Impacts of global climate change and emissions on regional ozone and fine particulate matter concentrations over the United States, *Journal of Geophysical Research-Atmospheres*, *112*(D14), D14312, doi:10.1029/2006JD008262.

Weaver, C. P., et al. (2009), A preliminary synthesis of modeled climate change impacts on US regional ozone concentrations, *Bulletin of the American Meteorological Society*, *90*(12), 1843-1863, doi:10.1175/2009bams2568.1.

Woo, J. H., et al. (2008), Development of North American Emission Inventories for Air Quality Modeling under Climate Change, *Journal of the Air & Waste Management Association*, *58*(11), 1483-1494, doi:10.3155/1047-3289.58.11.1483.

Yu, S. C., et al. (2006), New unbiased symmetric metrics for evaluation of air quality models, *Atmos. Sci. Lett.*, *7*(1), 26-34, doi:10.1002/asl.125.

CHAPTER 3

SENSITIVITY OF AIR QUALITY TO POTENTIAL CHANGES IN CLIMATE AND EMISSIONS IN THE UNITED STATES AND MAJOR CITIES[2]

Abstract

Simulated present (2006-2010) and future (2048-2052) air quality are compared over the contiguous United States (CONUS) using the Community Multi-scale Air Quality (CMAQ) model. Regionally downscaled present and future climate results are developed using GISS and the Weather Research Forecasting (WRF) model. Present and future emissions are estimated using MARKAL 9R model. O_3 and $PM_{2.5}$ sensitivities to precursor emissions for the years 2010 and 2050 are calculated using CMAQ-DDM (Direct Decoupled Method). We find major improvements in future U.S. air quality including generally decreased MDA8 O_3 (maximum daily 8-hr average O_3) mixing ratios and $PM_{2.5}$ concentrations and reduced frequency of NAAQS O_3 standard exceedances in most major U.S. cities. The Eastern and Pacific U.S. experience the largest reductions in summertime seasonal average MDA8 (up to 12 ppb) with localized decreases in the 4th highest MDA8 of the year, decreasing by up to 25 ppb. Results from a Climate Penalty (CP) scenario isolate the impact of climate change on air quality and show that future climate change tends to increase O_3 mixing ratios in some regions of the U.S., with climate change causing increases of over 10 ppb in the annual 4th highest MDA8 in Los Angeles. Seasonal average $PM_{2.5}$ decreases (2 to 4 μg m^{-3}) over the Eastern U.S. are

[2] A modified version of this chapter is under review as Sensitivity of air quality to potential future climate change and emissions in the United States and major cities, *Atmospheric Environment*

accounted for by decreases in sulfate and nitrate concentrations resulting from reduced mobile and point source emissions of NO_X and SO_X.

3.1 Introduction

Regional air quality impacts public health [*Ito et al.*, 2005; *Lim et al.*, 2012; *Murray et al.*, 2013; *Zhou et al.*, 2011], visibility and ecosystem health [*Likens et al.*, 1996; *Mauzerall and Wang*, 2001], and is significantly affected by changes in climate, land use and pollutant emissions [*Weaver et al.*, 2009]. Predictions of regional air quality responses to such changes can help inform policy makers in the development of effective approaches to both reduce greenhouse gases and improve air quality. However, major sources of uncertainty exist in predicting future air quality including limitations in the tools used to project future emissions, land use changes and uncertainties associated with predicting future climate. Recently, technical advances in downscaling global climate simulations to regional scales, and, the development of bottom-up operational tools used to forecast emissions have enhanced our ability to account for the complex interactions between population, socio-economical development, technological change, and federal and regional environmental policies [*Fishbone et al.*, 1980; *Liu et al.*, 2012]. In this chapter, we address the potential impacts of changing climate and emissions on regional $PM_{2.5}$ and O_3 levels in the U.S., focusing on major cities, by applying recent downscaling and emissions projection techniques to inputs of a chemical transport model [*Fishbone et al.*, 1980; *Liu et al.*, 2012].

There is a consensus among most studies that future climate change, alone, would lead to an increase in O_3 concentrations over significant regions of the U.S. due to

increased temperatures, surface insolation, stagnation, and biogenic VOC emissions [*Mickley et al.*, 2004; *Weaver et al.*, 2009]. Potential impacts of climate on $PM_{2.5}$ over the U.S. are more variable and likely small [*Jacob and Winner*, 2009]. Recent scientific efforts include investigating the effect of projected emissions changes on future air quality [*Brown et al.*, 2013; *Fann et al.*, 2013; *Liao et al.*, 2007b; *Nolte et al.*, 2008; *Tagaris et al.*, 2007]. Tagaris et al. [2007] used the Community Multiscale Air Quality (CMAQ) model with inputs of downscaled future climate [*Leung and Gustafson*, 2005] and emissions projected to the near future (2020) using the Clean Air Interstate Rule (CAIR) emissions inventory and to the more distant future (2050) using the Integrated Model to Assess the Global Environment (IMAGE). They find reductions of maximum daily 8-hr average (MDA8) O_3 mixing ratios over most of the U.S. and reductions in sulfate, nitrate and ammonium concentrations in aerosols, causing organic carbon to be the most abundant species in aerosols in 2050. Liao et al. [2007] expanded on the work of Tagaris et al. [2007] by calculating the present and future sensitivities of O_3 and particulate matter to emissions using CMAQ-DDM (Direct Decoupled Method). Nolte et al. [2008] also use the CMAQ model with inputs of downscaled future climate from Leung and Gustafson [2005] and emissions projected from the 2001 National Emissions Inventory (NEI) according to the Asian Pacific Integrated Model (AIM) to compare recent (1999-2003) and future (2048-2052) O_3 levels over the U.S. This study predicted that decreases in O_3 precursor emissions lead to decreased MDA8 O_3 mixing ratios over large regions of the U.S. despite the tendency for future climate to increase MDA8 levels. Fann et al. [2013] use the Comprehensive Air Quality Model with Extensions (CAMx) photochemical model to estimate recent and future health burdens of air pollution

attributable to U.S. anthropogenic emissions sectors. They projected the 2005 NEI to 2016 and found marked decreases in the health burdens associated with electricity generating units (EGU) and mobile sources due to the implementation of current emissions regulations. Some recent studies have investigated the feedbacks of changing aerosol concentrations to climate on a global scale [*Leibensperger et al.*, 2012a; b; *Ramanathan et al.*, 2001; *Shindell et al.*, 2012]. These studies agree that changes in global scale radiative forcing from aerosols can significantly impact global climate. However, Leibensperger et al. [2012] conclude that climate change associated with changes in aerosol radiative forcing from U.S. emissions has already been realized and that future decreases in U.S. emissions will only have a small impact on future climate change associated with aerosols. In light of this research, the present study focuses on the impact of changing emissions and climate on air pollutants in the U.S. and does not consider global scale feedbacks of future aerosol concentrations on climate.

This study takes advantage of recent technological advances in climate and emission-prediction modeling to simulate the response of future regional air quality in the U.S. to changes in climate and emissions. We employ several methods to improve upon the methods presented in Tagaris et al. [2007] and Liao et al. [2007]. We use spectral nudging to downscale global climate simulations [*Liu et al.*, 2012; *Trail*, 2013]. We also use detailed emissions projections from the MARKAL 9R (MARKet ALlocation 9 Region) model [*Fishbone et al.*, 1980], and use the Direct Decoupled Method (DDM) to calculate sensitivities of pollutants to precursor emissions. Liu et al. [2012] identified the benefit of using spectral nudging to downscale global meteorology in that using spectral nudging maintains the small-scale meteorological features driven by local topography

while preserving large-scale forcings. The MARKAL energy system model responds to prescribed demand for regionally based energy services (in this case, energy required to meet the associated energy service demands of the residential, commercial, industrial and transportation sectors) and selects from available technologies to select the least-cost path which satisfies the specified demands. MARKAL is a flexible modelling framework that considers mid-to-long-term technology choices that aim to reshape an energy system to meet specific environmental (or other) goals. The model also allows the implications of specific policy options to be examined and compared.

In the present study, we use the CMAQ model to compare present and simulated future air quality for the years 2006-2010 and 2048-2052 over the contiguous United States. Inputs to CMAQ include the regionally downscaled present and future climate results developed using GISS and the Weather Research Forecasting (WRF) model from Trail et al. [2013], as well as, emissions processed using the Sparse Matrix Operator Kernel Emissions (SMOKE) model [*CEP*, 2003]. Emissions inventories are projected to future year levels using the MARKAL 9R model. We also use CMAQ-DDM to calculate O_3 and $PM_{2.5}$ sensitivities to precursor emissions for the years 2010 and 2050. Results from a Climate Penalty (CP) scenario are also presented here in order to isolate the impact of climate change on air quality for comparison to past studies (e.g.; Weaver et al. [2009] and Nolte et al. [2008]). Present $PM_{2.5}$ and O_3 simulated concentrations are evaluated using *in situ* measurements. We also investigate and discuss the impacts of climate and emissions changes on air quality in major U.S. cities.

3.2 Model Approach

Air pollutant concentrations and sensitivities are simulated using a chemical transport model with inputs from emissions and meteorological models. Meteorological inputs were downscaled from a Global Circulation Model (GCM) to the regional scale using a regional climate model as described in Trail et al. [2013]. The components of the modeling system are described below along with an evaluation of the chemical transport model.

3.2.1 Global Climate

The Goddard Institute for Space Studies (GISS) ModelE2 is used to provide base global scale meteorological fields which are used as initial and boundary conditions to the regional climate model [*Schmidt et al.*, 2013]. As used, the model has a Cartesian grid point formulation with horizontal resolution of $2^o \times 2.5^o$ latitude by longitude. The vertical discretization has 40 layers and follows a sigma coordinate up to 150 hPa and constant pressure layers between 150 and 0.1 hPa. Simulations are carried out for years 2006-2010, and, 2048-2052 with a 3 year spin-up time, are driven by future atmospheric conditions over the 21st century and follow the scenario development process for IPCC AR5. The "Representative Concentration Pathway" (RCP) 4.5 [*Lamarque et al.*, 2011; *Moss et al.*, 2010] is used for this study, which is a scenario of decadal global emissions of greenhouse gases, short-lived species, and land-use-land-cover producing a 4.5 W m^{-2} anthropogenic radiative forcing (corresponding to 650 ppm CO_2-equivalent) in the year 2100 [*Moss et al.*, 2010]. Outputs of physical parameters were produced at 6-hr intervals for regional downscaling by WRF (section 2.2).

3.2.2 Regional Climate

The regional climate model used is the non-hydrostatic Weather Research and Forecasting (WRF) Model [*Skamarock and Klemp*, 2008] version 3.4. Simulations were carried out for years 2006-2010 and 2048-2052 with a 10 day spin-up time period. The model domain covers the CONUS and portions of southern Canada and northern Mexico and is centered at 40°N and 97°W with dimensions of 164×138 horizontal grids cells with a grid-spacing of 36 km. It contains 35 vertical levels, with the top pressure of 50hPa. The model scheme configuration is as follows: the long-wave Rapid Radiative Transfer Model (RRTM) [*Mlawer et al.*, 1997] and Dudhia scheme [*Dudhia*, 1989] are used for longwave and shortwave radiation respectively; the Yonsei University (YSU) [*Hong et al.*, 2006] scheme is used for the planetary boundary layer; the Noah scheme [*Ek et al.*, 2003] is used for the land surface model (LSM); a revised version of the Kain-Fritsch scheme [*Kain and Fritsch*, 1993] is used to represent the effects of both deep and shallow cumulus clouds; and Lin *et al.* [1983] is chosen for cloud microphysics. Spectral nudging is applied to temperature, horizontal winds, and geopotential heights with a wave number of 3 in both zonal and meridional directions at 6 hour intervals [*Liu et al.*, 2012]. Only horizontal winds are nudged at all vertical levels, while no nudging is conducted for other variables within the planetary boundary layer (PBL). The ability of GISS-WRF to reproduce the long-term yearly climatic means and the meteorological fields that strongly impact air quality are evaluated in Trail et al. (2013) and are summarized in Table B-1 and B-2. Trail et al. [2013] found that the distribution of model predictions agree well with observations when conducted for 2010.

3.2.3 Emissions

Hourly, gridded and speciated emissions are generated for input to CMAQ using the Sparse Matrix Operator Kernel Emissions (SMOKE V3) model [*CEP*, 2003] based on the 2005 National Emissions Inventory (NEI) and ancillary data which include temporal, spatial and chemical allocation of emissions according to source category. Spatial surrogates (e.g., population and landuse distributions) are used to allocate the NEI's county-level emissions to the modeling gridded domain. The Biogenic Emissions Inventory System (BEIS) and Biogenic Emissions Landcover Database 3.0 (BELD3) are used here to compute hourly emissions from U.S. vegetation. The resulting inventory consists of pollutants emitted from area, mobile, point, fire, ocean, biogenic, agricultural and other sources. NEI 2005 energy related emissions are projected to the years 2010 and 2050 using factors calculated by the EPA MARKAL 9R model. MARKAL 9R [*Fishbone et al.*, 1980] models the energy system of the nine Census Divisions of the U.S. and estimates future energy dynamics. Future emissions projections were calculated assuming the implementation of the following policies: Clean Air Act Title IV (Acid Rain Program) SO_2 and NO_X requirements, Clean Air Interstate Rule (CAIR), Utility Mercury and Air Toxics Standards (MATS), aggregated state Renewable Portfolio Standards (RPS) by region, Federal Corporate Average Fuel Economy (CAFE) standards as modeled in AEO 2012, Tier 2 light duty vehicle tailpipe emission standards and heavy duty vehicle fuel and engine rules. Non-energy related emissions were projected according to the Intergovernmental Panel on Climate Change Special Report on Emissions Scenarios [IPCC SRES], using the A1B scenario [*Woo et al.*, 2008].

3.2.3 Air Quality

The Community Multiscale Air Quality Model (CMAQ 4.7.1) [*Foley et al.*, 2001] is used to simulate the transformation and fate of air pollutants for the present (2006-2010) and future years (2048-2052) and for a climate penalty scenario (CP). The climate penalty scenario uses future emissions and present climate as inputs to determine the sensitivity of future air quality to the simulated climate change. Gas-phase chemistry is modeled using the SAPRC-99 [*Carter*, 2000] chemical mechanism. The modeling domain uses a Lambert Conformal Projection centered at 40ºN, 97ºW with true latitudes of 33ºN and 45ºN (**Figure 3-1**). The domain uses a 36-km horizontal grid-spacing that covers the entire continental US as well as portions of Canada and Mexico (5328×4032 km) with thirteen vertical layers extending ~15.9 km above ground, with 7 layers below 1 km and the first layer is 18 m thick. Present and future dynamic boundary conditions are derived from the GISS global simulation. The default CMAQ initial conditions are used here and a spin-up period of 10 days is used to minimize the influence of initial conditions.

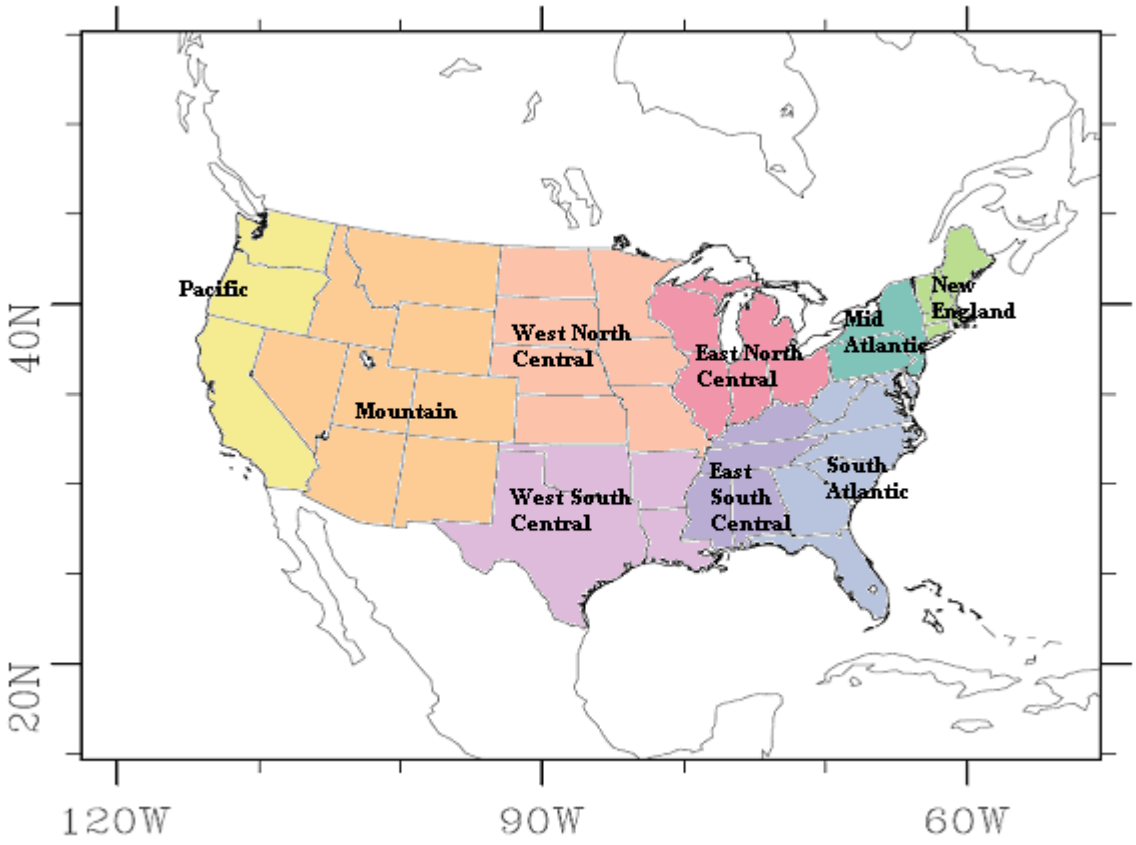

Figure 3-1 CMAQ modeling domain with EPA US 9 census regions used in the MARKAL 9R modeling

Pollutant sensitivities, $S_{ij}^{(1)}$, to perturbations in an input parameter (e.g. emission rate, initial condition or boundary condition) are calculated in CMAQ using the Decoupled Direct Method in Three Dimensions DDM-3D:

$$S_{ij}^{(1)} = P_j \frac{\partial C_i}{\partial P_j} \quad (1)$$

where C_i is the ambient concentration of species i, and P_j is the unperturbed "base case" emissions rate of source j. The sensitivities, S_{ij}, are computed for all modeled species over space and time. In CMAQ, DDM-3D uses the same numerical algorithms and

operator splitting processes as for calculating concentrations [*Napelenok et al.*, 2006; *Yang et al.*, 1997]. DDM-3D has been successfully integrated into CMAQ and updated to include algorithms for computing particulate matter (PM) sensitivity coefficients. First-order sensitivities are typically accurate for up to 30% perturbations in input parameters [*Dunker et al.*, 2002]. Our focus is on calculating the sensitivities of ambient O_3 and PM, $S_{ij}^{(1)}$, to total emissions of NO_X, SO_2, and VOCs and emissions from mobile, point, and biogenic sources.

3.3 Model Evaluation

Cumulative distributions functions (CDFs) of observed and modeled $PM_{2.5}$ (during 1 January to 31 December, 2010) and maximum daily 8-hr O_3 (MDA8; during 1 May to 30 September, 2010) concentration at observational cites are compared for each of the 9 U.S. census regions (Figures B-1 and B-2). The modeled air quality was not evaluated by comparing observed and modeled pollutant concentrations coupled in space and time because the simulations were driven using boundary conditions from a global climate model rather than reanalysis data. Comparison using CDFs, on the other hand, evaluates the models ability to capture distributions of pollutant concentrations and enables the evaluation of concentrations of pollutants at the upper and lower tails of the distributions. Simulated pollutant concentrations used in for the evaluation were simulated using 2010 emissions and meteorology (sections 2.1-2.3). Observed ambient 2010 O_3 and $PM_{2.5}$ concentrations were downloaded from the Environmental Protection Agency (EPA) Air Quality System (AQS) website (www.epa.gov/ttn/airs/airsaqs/detaildata/downloadaqsdata.htm).

In each of the 9 U.S. census regions, modeled MDA8 mixing ratios show good agreement with observations (Figure B-1). The Mid-Atlantic and Mountain regions modeled MDA8 agrees best with observations when MDA8 exceeds 60 ppb while modeled MDA8 is biased high at the lower end of the distribution. Modeled MDA8 mixing ratio is biased high in every region with the largest high biases occurring at the lower end of the distributions. Other studies have shown that CMAQ tends to overestimate O_3 on days when O_3 mixing ratios are low [*Nolte et al.*, 2008].

The mean bias (MB) and normalized mean bias (NMB) were also calculated using mean observed and modeled $PM_{2.5}$ and O_3 at each site where observations are available (Table B-1 and B-2) to evaluate the model configuration. The NMB (in %) and MB (in ppm or $\mu g\ m^{-3}$) are sensitive to systematic errors [*Yu et al.*, 2006]. Overall the simulated O_3 and $PM_{2.5}$ surface concentrations show good agreement with observed concentrations (Tables B-1 and B-2). Daily max 1-hr and 8-hr O_3 are simulated best during the spring with a small positive bias (NMB<10%). Simulated 1-hr O_3 and 8-hr O_3 also show good agreement with observations during the spring. During summertime, 1-hr and 8-hr O_3 simulations show very little bias (NMB = 0.17 and 1.1 %). However, the model tends to simulate daily max 1-hr and 8-hr O_3 high (NMB = 13% and 25% respectively) during the summer.

The distributions of modeled PM2.5 show overall good agreement with observations in the 9 U.S. regions (Figure B-2). The model tends to underestimate $PM_{2.5}$ concentrations at the upper 99^{th} percent of the distributions. The Mountain region shows a large underestimation of $PM_{2.5}$ in the upper 90^{th} percentile of the distribution. Mean bias and normalized mean biases were also calculated for mean $PM_{2.5}$ modeled and

observed concentrations for four seasons (Table B-2). The model tends to be biased low for 24-hr $PM_{2.5}$ during winter, spring and summer with the greatest bias occurring during the summer (NMB = -39%). The bias is smaller during winter and spring (NMB = -21% and -23%, respectively) and is the least during the fall (NMB = -1%).

3.4 Results

The overall emissions rates of CO, NO_X and VOC decrease from 2010 levels over all nine regions of the U.S. by 2050 (Table 3-1 and Table 3-2). Emissions of SO_2 decrease in most regions except East North Central and South Atlantic while primary $PM_{2.5}$ emissions increase in the Mid and South Atlantic regions and decrease over the rest of the U.S. Mobile sector emission decreases account for most of the total decreased CO, NO_X, VOC and $PM_{2.5}$ emissions. Increased emissions of SO_2 and $PM_{2.5}$ in some regions are attributed to increased emissions from point sources such as power plants and refineries. Emissions of SO_2 from area sources, on the other hand, experience slight reductions.

Table 3-1 Present day anthropogenic emission rates of NO_X, VOC, SO_2 and primary $PM_{2.5}$ emitted by area, point and mobile sources from each of the 9 U.S. census tracks. The last four columns are the total anthropogenic emissions from each census track and the bottom row shows the total emissions of each pollutant over the entire U.S.

2010	Area [tons/yr *10^3]				Point [tons/yr *10^3]				Mobile [tons/yr *10^3]				Total Anthropogenic [tons/yr*10^3]			
Census Track	NO_X	VOC	SO_2	$PM_{2.5}$	NO_X	VOC	SO_2	$PM_{2.5}$	NO_X	VOC	SO_2	$PM_{2.5}$	NO_X	VOC	SO_2	$PM_{2.5}$
New England	87	174	63	100	75	19	141	9	2970	952	12	27	3134	1145	216	135
Mid Atlantic	274	322	215	87	407	62	1100	82	7034	2478	37	68	7721	2862	1352	238
East North Central	475	409	317	141	1099	233	2544	145	12505	3750	64	90	14092	4392	2926	377
West North Central	474	240	462	198	606	121	972	56	6266	1837	28	44	7357	2198	1462	299
South Atlantic	436	1065	347	368	898	224	2228	162	15131	4468	78	129	16476	5757	2653	660
East South Central	281	328	182	125	593	213	1092	77	6260	1590	28	41	7137	2131	1302	244
West South Central	883	526	391	209	906	308	1206	105	10700	2551	44	70	12497	3385	1642	385
Mountain	455	1296	221	325	491	78	351	45	5940	1571	28	43	6890	2945	600	414
Pacific	458	703	188	337	197	86	103	39	8233	2355	19	237	8900	3145	310	614
Total	3824	5064	2385	1891	5271	1345	9737	720	75040	21551	339	749	84204	27960	12463	3366

Table 3-2 Percent change (future minus present divided by present) in annual emission rates of NO_X, VOC, SO_2 and primary $PM_{2.5}$ emitted by area, point and mobile sources from each of the 9 U.S. census tracks.

Change (2050-2010)	Area [%]				Point [%]				Mobile [%]				Total Anthropogenic [%]			
Census Track	NO_X	VOC	SO_2	$PM_{2.5}$	NO_X	VOC	SO_2	$PM_{2.5}$	NO_X	VOC	SO_2	$PM_{2.5}$	NO_X	VOC	SO_2	$PM_{2.5}$
New England	-6.13	-19.18	-20.77	-26.54	-11.32	-1.05	-25.74	-0.43	-77.99	-58.89	-14.28	-21.94	-74.35	-51.88	-23.64	-23.86
Mid Atlantic	-7.04	7.25	-13.61	7.96	-4.82	0.12	-8.43	44.75	-79.06	-65.22	-22.55	-35.48	-72.52	-55.66	-9.64	8.31
East North Central	-3.74	1.57	-2.06	-0.63	-15.22	-0.33	22.09	21.81	-76.56	-60.44	-20.34	-29.99	-69.26	-51.47	18.54	1.02
West North Central	-1.27	3.13	-0.69	0.14	-5.56	0.93	-2.50	-2.60	-74.28	-57.31	-13.15	-25.23	-63.81	-47.51	-2.14	-4.09
South Atlantic	5.07	0.35	3.12	-2.43	-1.80	-0.07	10.44	83.71	-75.21	-50.85	17.12	-8.54	-69.03	-39.40	9.67	17.45
East South Central	-0.76	2.56	-1.91	3.41	-0.46	0.17	-44.76	-0.02	-74.55	-52.67	-10.50	-16.59	-65.46	-38.87	-38.03	-1.07
West South Central	2.03	-0.41	-0.11	-0.66	-9.63	0.12	-7.24	3.86	-73.87	-44.72	13.99	-1.35	-63.80	-33.76	-4.97	0.44
Mountain	2.29	0.39	-0.49	0.73	-10.21	-0.47	-6.91	-0.32	-72.94	-43.04	26.40	-25.13	-63.46	-22.80	-3.00	-2.06
Pacific	4.46	0.29	-8.71	1.37	0.04	0.90	-5.26	2.33	-75.20	-46.83	5.15	-49.01	-69.34	-34.98	-6.74	-18.03
Total	0.53	0.41	-2.63	-1.01	-7.31	0.09	0.37	28.74	-75.40	-53.48	-0.64	-28.54	-67.63	-41.14	-0.23	-0.77

3.4.1 Surface Ozone

The National Ambient Air Quality Standards for O_3 is based on the MDA8 O_3. Currently, an area exceeds the standard if the 4th highest MDA8 of a year, averaged over three continuous years, is greater than 75 ppb. Health analyses, however, are often based upon longer term exposures (e.g., seasonally or annually averaged changes in daily 8-hr ozone), and may differ between warm and cool seasons, so the analyses here presents both 4th highest ozone responses, as well as seasonal responses in the MDA8. Seasonal averages of daily MDA8 (SA-MDA8) decrease over most of the U.S during spring (Mar - May), summer (Jun - Aug) and fall (Sep - Nov) (Figure 3-2). The largest average SA-MDA8 decreases of 6 - 12 ppb occur over the Eastern U.S. and along the Pacific Coast during summer. Average SA-MDA8 also decrease by up to 4 ppb over the Eastern U.S. during spring while increases of up to 3 ppb are simulated over New England and East North Central regions during fall. In part, this is due to decreases in NO_X emissions that can lead to increases in ozone on less photochemically active days. A map of the 4th highest MDA8, averaged over all five present years, shows regions of California, Arizona, and much of the Eastern U.S. with NAAQS exceedances (Figure 3-3a). In the future simulation, the 4th highest MDA8 decreases by 15 to 20 ppb in the regions with greatest present day 4th highest MDA8 (Figure 3-3c).

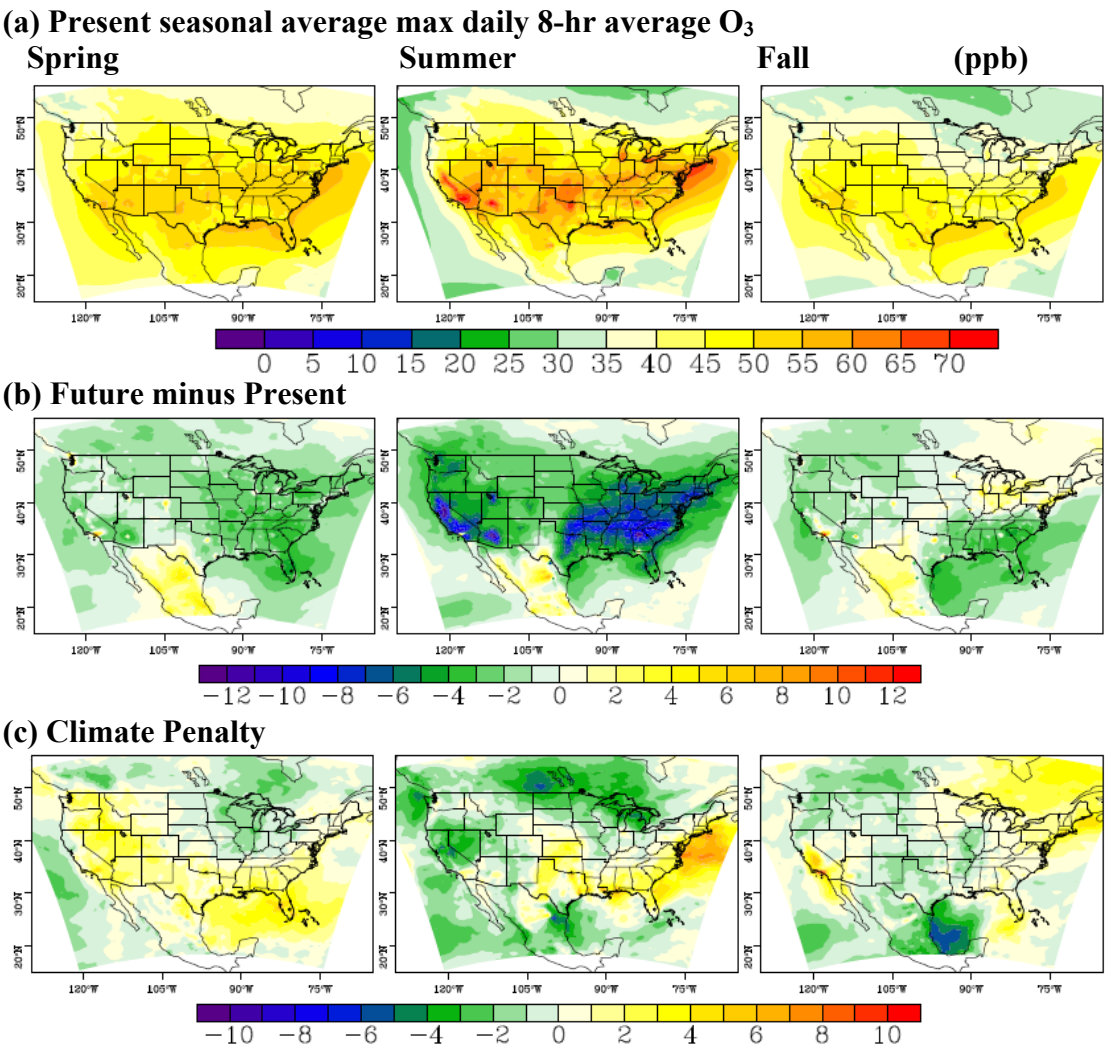

Figure 3-2 (a) Average present SA-MDA8 (ppb), **(b)** change in SA-MDA8 (future minus present) and **(c)** change in SA-MDA8 for the CP scenario (SA-MDA8 simulated using 2050 climate and 2050 emissions minus SA-MDA8 simulated using 2010 climate and 2050 emissions)

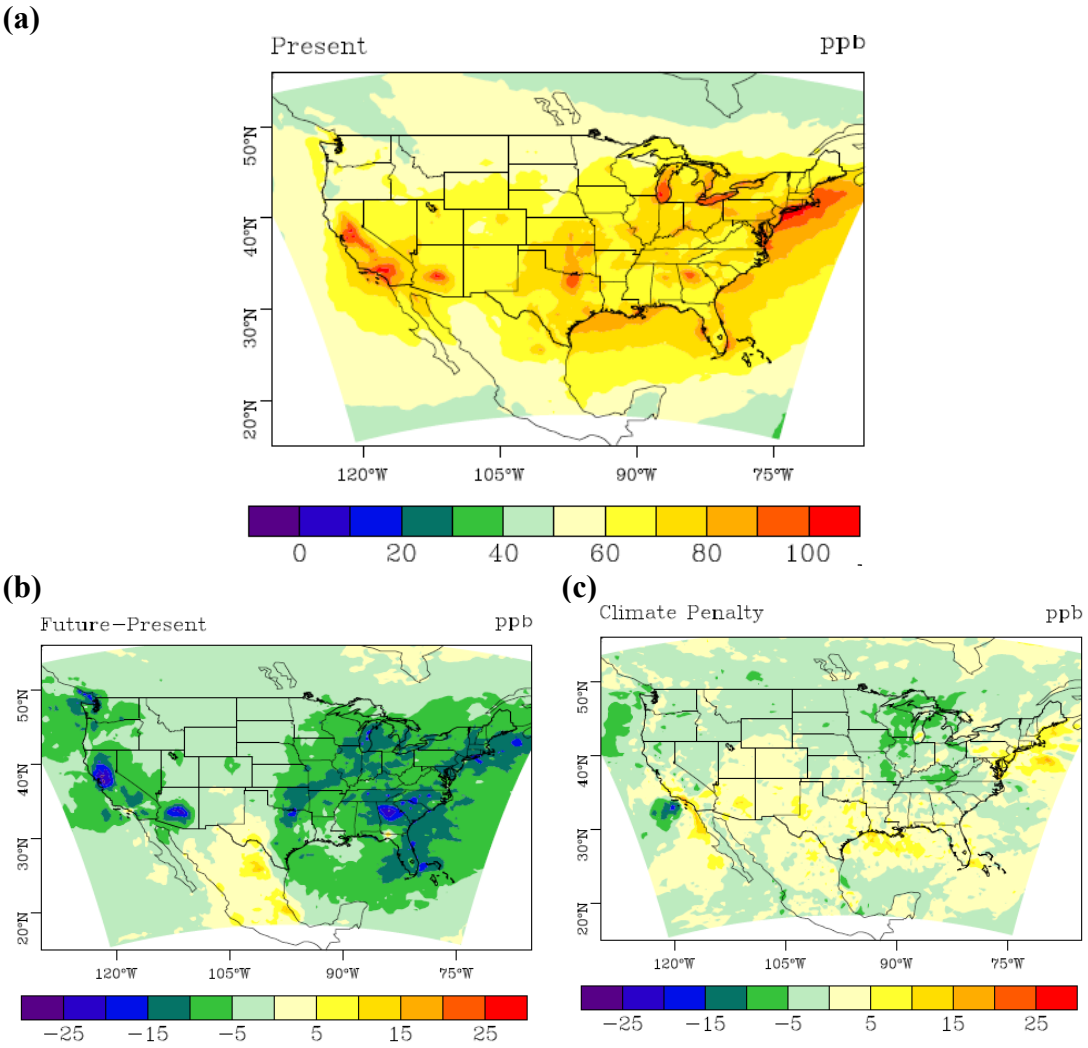

Figure 3-3 (a) Average of 5 years (2006-2010) 4th Highest MDA8 (ppb)of each year **(b)** Average difference of 4th highest yearly MDA8 (5 future years minus 5 present years) and **(c)** difference in 4th highest MDA8 for the Climate Penalty scenario (4th highest MDA8 using 2050 climate minus 4th highest MDA8 using 2010 climate)

The climate penalty (CP) simulation isolates the sensitivity of future air quality to climate change from the emission changes by simulating air quality using future emission rates and present climate (Figure 3-2c). The CP results indicate a climate induced increase in SA-MDA8 mixing ratio of up to 3 ppb in West, South Central, South Atlantic, Mid Atlantic, and New England regions during the summer. Climate also induces

increases up to 10 ppb in the 4th highest MDA8 of the year over southern California, the southern Mountain region, Texas, and some portions of the South and Mid-Atlantic regions (Figure 3-3c). Increased MDA8 in the CP scenario means that efforts directed at improving O_3 air quality will be less effective with climate change than without. Using the same two 5-year meteorological datasets as in this study, Trail et al. [2013] examined the changes in meteorological trends related to air quality and predicted increased O_3 mixing ratio in Texas during the summer and in most of the U.S. during fall. Similarly, Leung and Gustafson [2005] used downscaled meteorology and predicted worsening air quality over Texas during summer due to increased temperature and stagnation and Nolte et al. [2008] confirmed their results. The CP simulation results also show increased MDA8 mixing ratio during the spring over most of the U.S. except West North Central U.S. and increases during fall in Pacific and Eastern regions which indicates that the O_3 season is extending into spring and fall (Figure 3-2c). Climate change causes an increase in the 4th highest MDA8 of up to 10 ppb in Texas, the Mountain region, the Southern Pacific region and in the Mid-Atlantic (Figure 3-4c). The largest increases in 4th highest MDA8 occur over Los Angeles, with increases exceeding 10ppb.

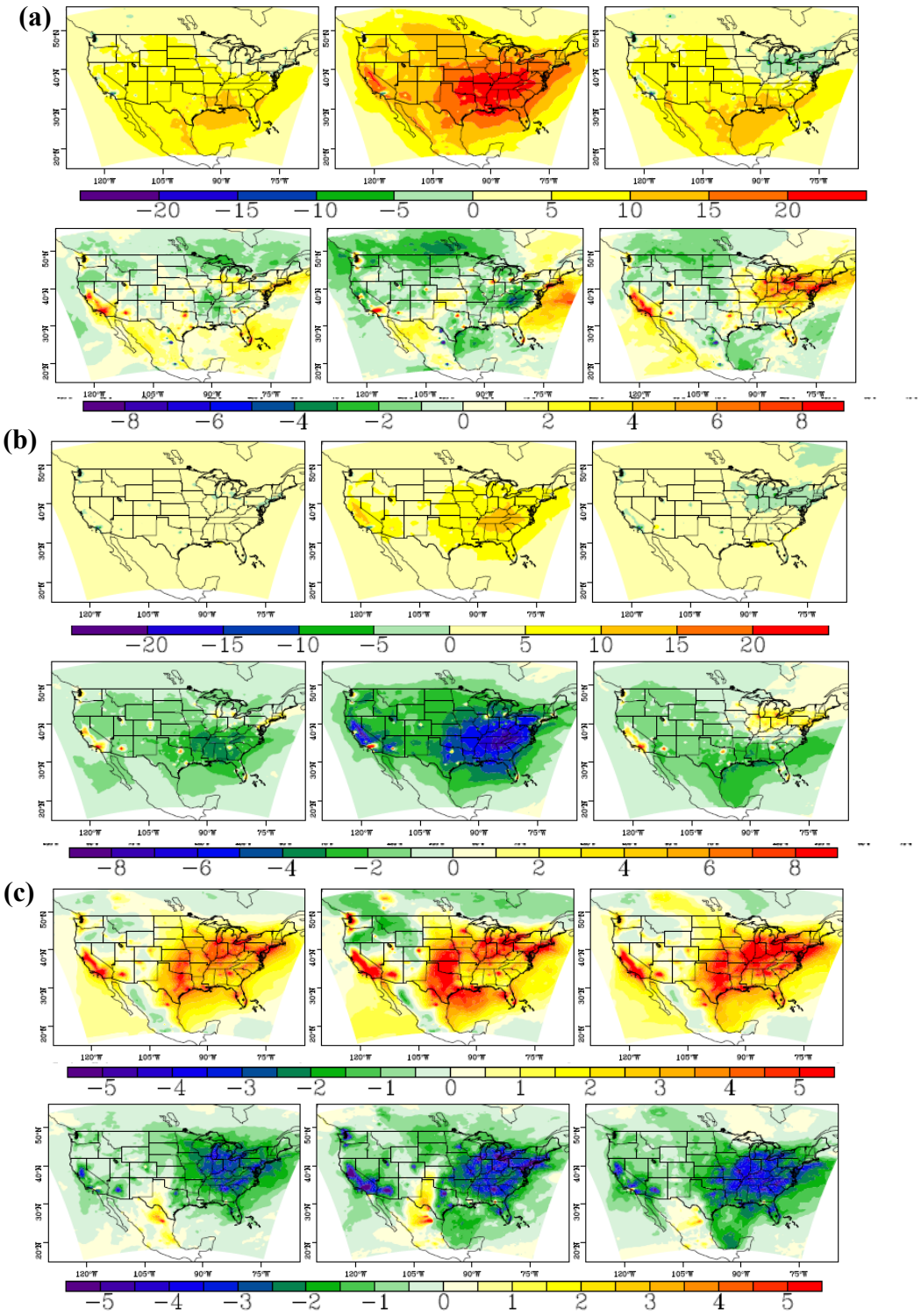

Figure 3-4 (a) Average present SA-MDA8 sensitivity to total NO_X emissions (top) and sensitivity change (difference of future minus present sensitivities) (bottom), **(b)** SA-MDA8 sensitivity to mobile NO_X (top) and sensitivity change (difference of future minus present sensitivities) (bottom) and **(c)** SA-MDA8 sensitivity to total VOC emissions (top) and sensitivity change (difference of future minus present sensitivities) (bottom)

Cumulative distribution plots of urban MDA8 show changes in the frequency of extreme O_3 events and exceedances in major cities that are representative of various regions of the U.S. (Figure 3-5). The upper 95th percentile MDA8 decreases in all cities analyzed except Los Angeles. A localized increase in summertime MDA8 occurs over Los Angeles and, like the Northeast during the fall, is caused by a future decrease in O_3 titration by NO_X emissions from mobile sources (Figure 3-4). Similar localized patterns of increased MDA8 occur during the spring and fall in other urban areas. Atlanta experiences the greatest decrease in the upper 95th percentile MDA8 from 85 ppb to 68 ppb. The percentile above which MDA8 mixing ratios are greater than 75 ppb indicates the frequency of MDA8 exceedances of the current standard for a particular year. In Atlanta, the frequency of MDA8 exceedances of 75 ppb decreases from just over 10% to around 1% of the year. Future MDA8 exceeds 75 ppb 2 – 3% less of the year than present day in Chicago and 3 – 5% less of the year in New York and Philadelphia. Seattle present day MDA8 rarely exceeds the standard and no future exceedances were simulated. In Phoenix, simulated MDA8 exceeds 75 ppb up to 20% of the year while future MDA8 exceeds 75 ppb between 2 and 10%. The cumulative distribution of the CP scenario shows that future MDA8 exceedances under present day climate would be less frequent than those under the predicted future climate in all cities except Seattle and Chicago given the same level of anthropogenic emissions.

Climate penalty results indicate that future MDA8 reductions result from emissions changes. CMAQ-DDM results show that during present day summers, the SA-MDA8 sensitivity to emissions of NO_X is from 5 - 20 ppb over the U.S. with the highest sensitivities in the Eastern U.S. and along the southern Pacific region (Figure 3-4a). In

other words, a 10% reduction in NO_X emissions would result in a 0.5 to 2 ppb decrease in the annual average MDA8 in the Eastern U.S. The summertime MDA8 sensitivity to NO_X experiences little change between the present and future simulation. The MDA8 sensitivity to NO_X emissions from mobile sectors, however, decreases in the future in regions with high NO_X sensitivity with the largest decreases exceeding 8 ppb (Figure 3-4b). The decreased MDA8 sensitivity to mobile NO_X corresponds to decreases in NO_X from the mobile sector. Interestingly, New England, East North Central, and Mid-Atlantic regions are characterized by a negative present day sensitivity of average MDA8 to emissions of NO_X during fall which indicates the titration of O_3 by NO_X. Future reductions in mobile NO_X emissions in those regions leads to less titration of O_3 and therefore higher average MDA8 mixing ratios seen in the Northeast during the fall (Figure 3-4). The sensitivity of MDA8 to VOC also decreases during spring, summer and fall in Eastern and Pacific regions by up to 5 ppb between 2010 and 2050 (Figure 3-4c). Although mobile VOC emissions are reduced in the future, the sensitivity of MDA8 to mobile VOC emissions does not undergo much change in the future; rather most of the change in sensitivity occurs in the sensitivity to biogenic emissions of VOC (Figures B-3 and B-4). The change in MDA8 sensitivity to VOC is due to decreased NO_X emissions, causing these regions to become more NO_X-limited.

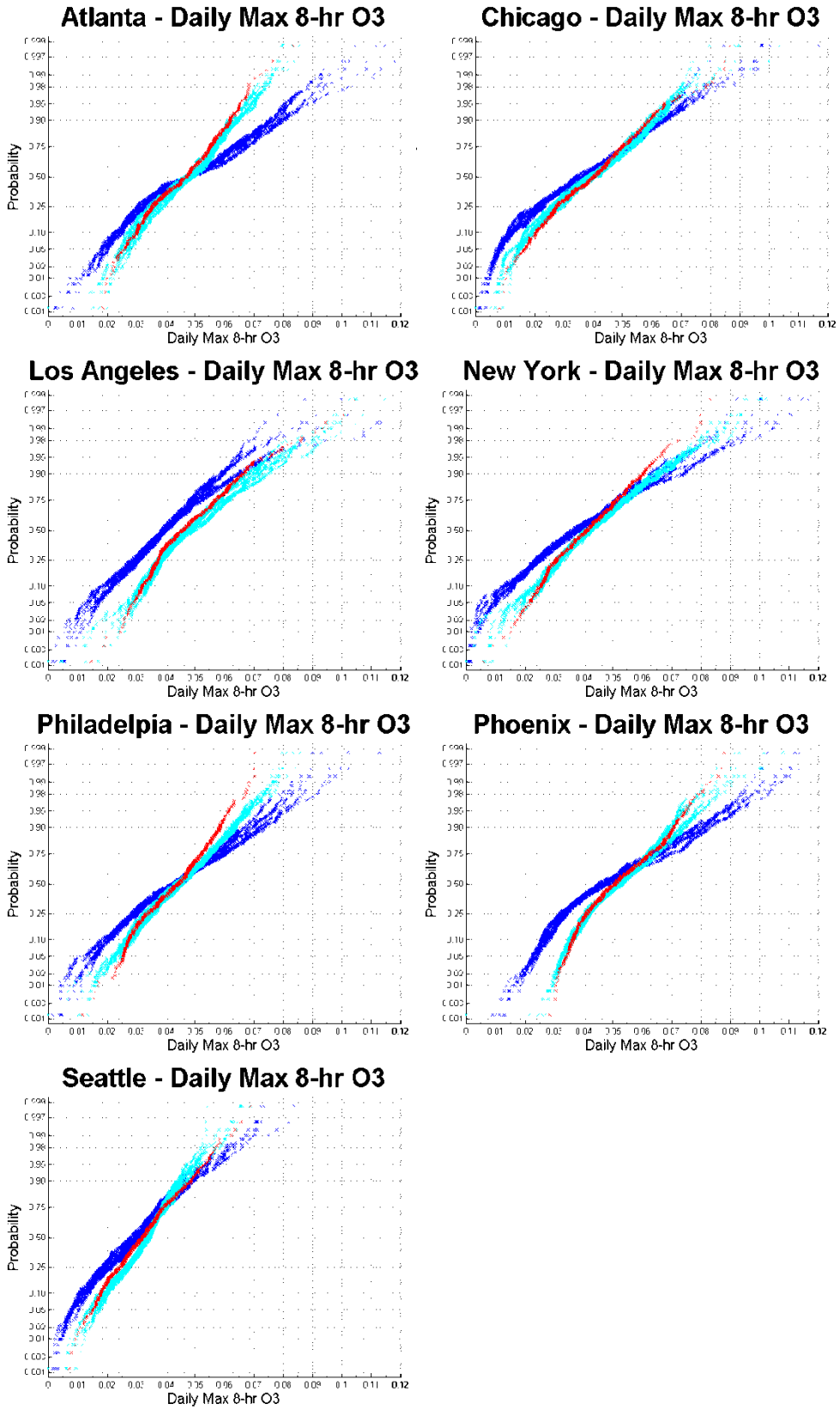

Figure 3-5 CDF plots of daily max 8 hr O3 (ppm) future (light blue) and present (dark blue) and CP scenario (2010 climate and 2050 emissions) (red)

3.4.2 Fine Particulate Matter ($PM_{2.5}$)

Understanding the response of $PM_{2.5}$ concentration and composition becomes important and complex in the face of changing climate and emissions rates. In the U.S., $PM_{2.5}$ is typically composed of sulfate (SO_4), organic matter (OM), elemental carbon (EC), nitrate (NO_3), ammonium (NH_4), and other components. $PM_{2.5}$ comes from both primary emissions and secondary production and undergoes complex chemistry and transport in the atmosphere. Total annual average $PM_{2.5}$ tends to decrease with future emissions and climate change with the greatest decreases in the Eastern U.S. ranging from 1 – 3 μg m^{-3} (Figure 3-6). During winter, $PM_{2.5}$ decreases of 1 – 3 μg m^{-3} occur in the New England and West North Central regions. Nitrate aerosol concentration decreases along with the sensitivity of $PM_{2.5}$ to emissions of NO_X (Figure 3-7b and Figure 3-8). OM and EC concentration changes show similar spatial patterns in the Northeast during winter corresponding to further decreases in $PM_{2.5}$ from regionally decreased emissions of primary $PM_{2.5}$ from mobile sources (Figure 3-7). EC decreases during the entire year over Northeastern U.S. and the Pacific region, with the exception of some localized increases, corresponding to reductions in primary PM from mobile and area sources. Sulfate aerosol increases during winter in East North Central are caused by increased emissions of SO_X from point sources in the region (Figure 3-7a and B-5).

While wintertime $PM_{2.5}$ decreases occur in the Northeastern regions, the CP simulation shows that, in the absence of reduced emissions, climate change would lead to $PM_{2.5}$ increases in the region (Figure 3-6c). Also, in Texas, wintertime $PM_{2.5}$ increases of up to 1 μg m^{-3} are caused by climate change in the region. Summertime $PM_{2.5}$ decreases of 0.5 – 2 μg m^{-3} span the Eastern U.S. and share similar spatial patterns as decreased

concentration of sulfate aerosol and reduced sensitivity of $PM_{2.5}$ to emissions of total SO_X and SO_X from point sources. Along with decreased emissions of SO_X from point sources, climate change also contributes to decreased $PM_{2.5}$ in the region except along the Atlantic Coast where increases of up to 1 µg m^{-3} develop (Figure 3-6c). Climate change also contributes to large $PM_{2.5}$ decreases during the fall over the Eastern U.S., especially over the East North Central region (up to 3.5 µg m^{-3}).

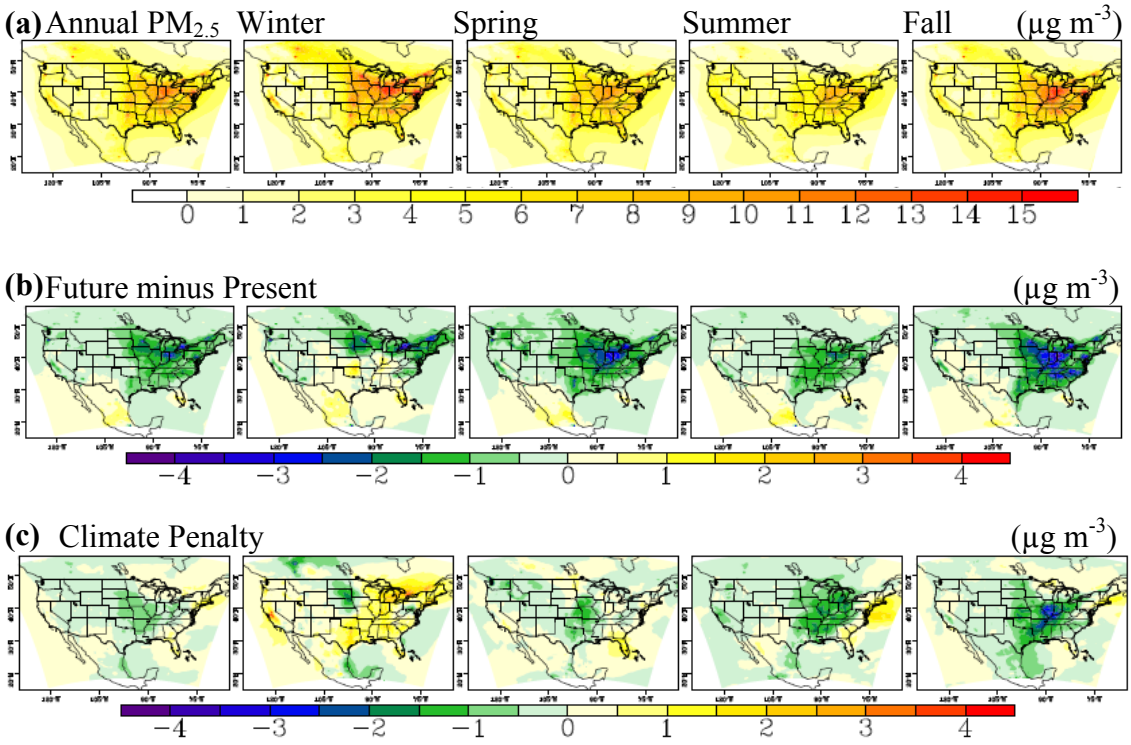

Figure 3-6 (a) Average simulated present day $PM_{2.5}$ µg m^{-3}, **(b)** change in $PM_{2.5}$ (future minus present) and **(c)** change in $PM_{2.5}$ for the CP scenario ($PM_{2.5}$ simulated using 2050 climate and 2050 emissions minus $PM_{2.5}$ simulated using 2010 climate and 2050 emissions)

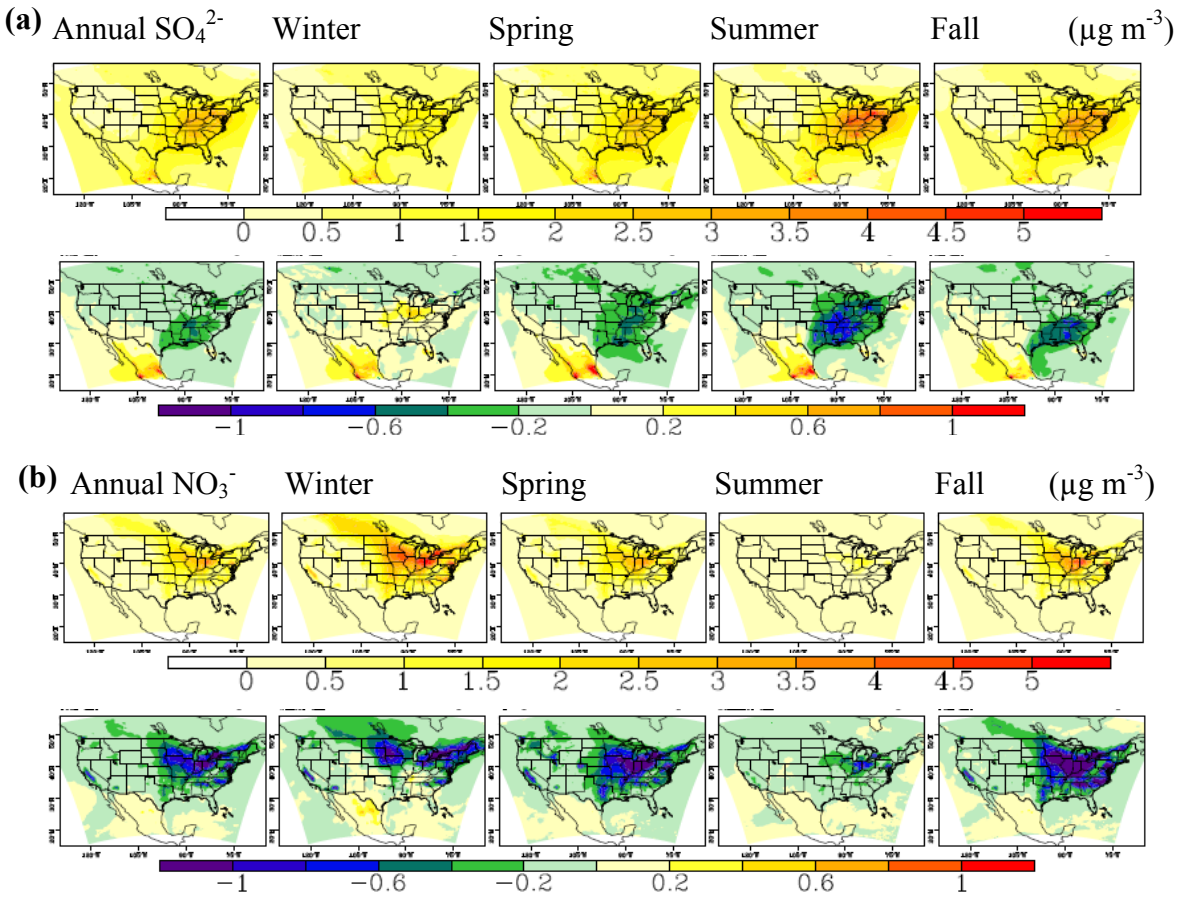

Figure 3-7 (continued on next page) Simulated present and future PM species concentrations across the U.S. **(a)** Average present day SO_4 (top) and difference (bottom; future minus present), **(b)** NO_3 (top) and difference (bottom; future minus present), **(c)** OM (top) and difference (bottom; future minus present), **(d)** EC (top) and difference (bottom; future minus present)

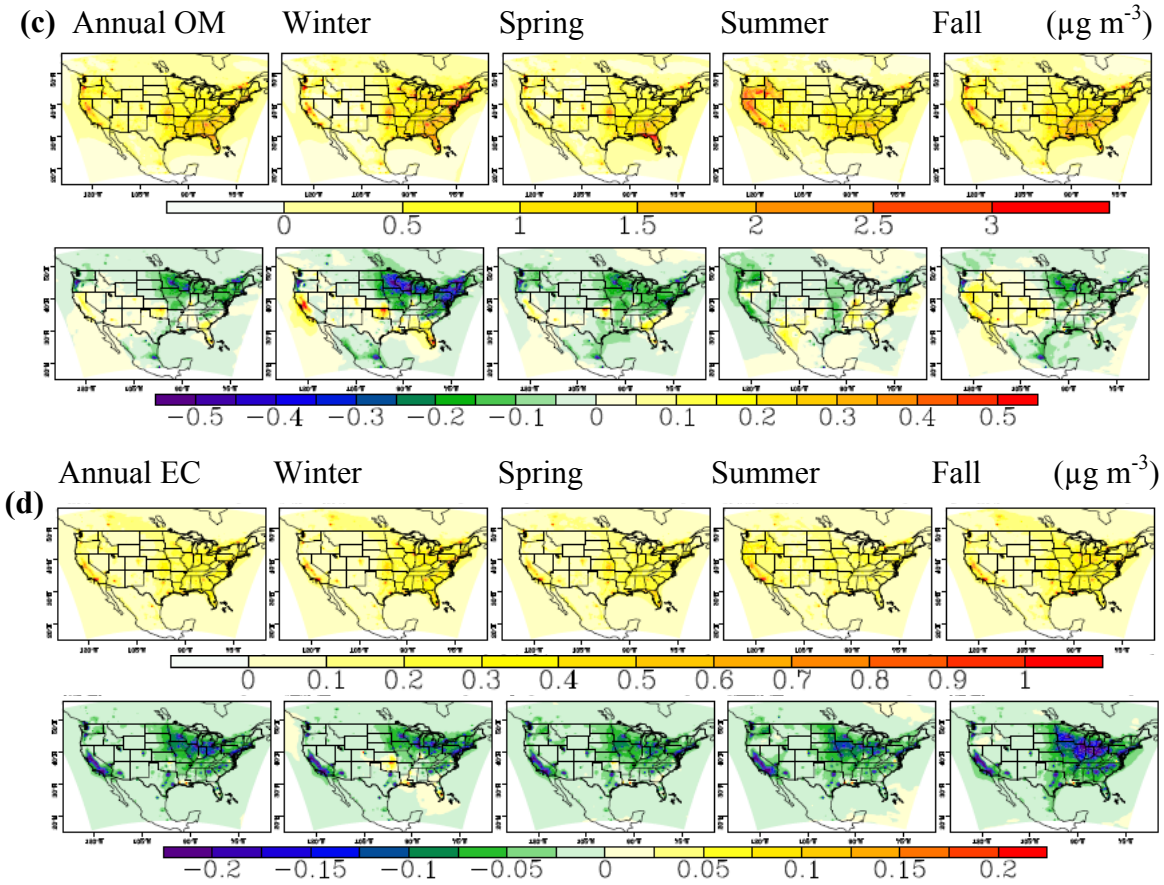

Figure 3-7 (continued from previous page) Simulated present and future PM species concentrations across the U.S. **(a)** Average present day SO_4 (top) and difference (bottom; future minus present), **(b)** NO_3 (top) and difference (bottom; future minus present), **(c)** OM (top) and difference (bottom; future minus present), **(d)** EC (top) and difference (bottom; future minus present)

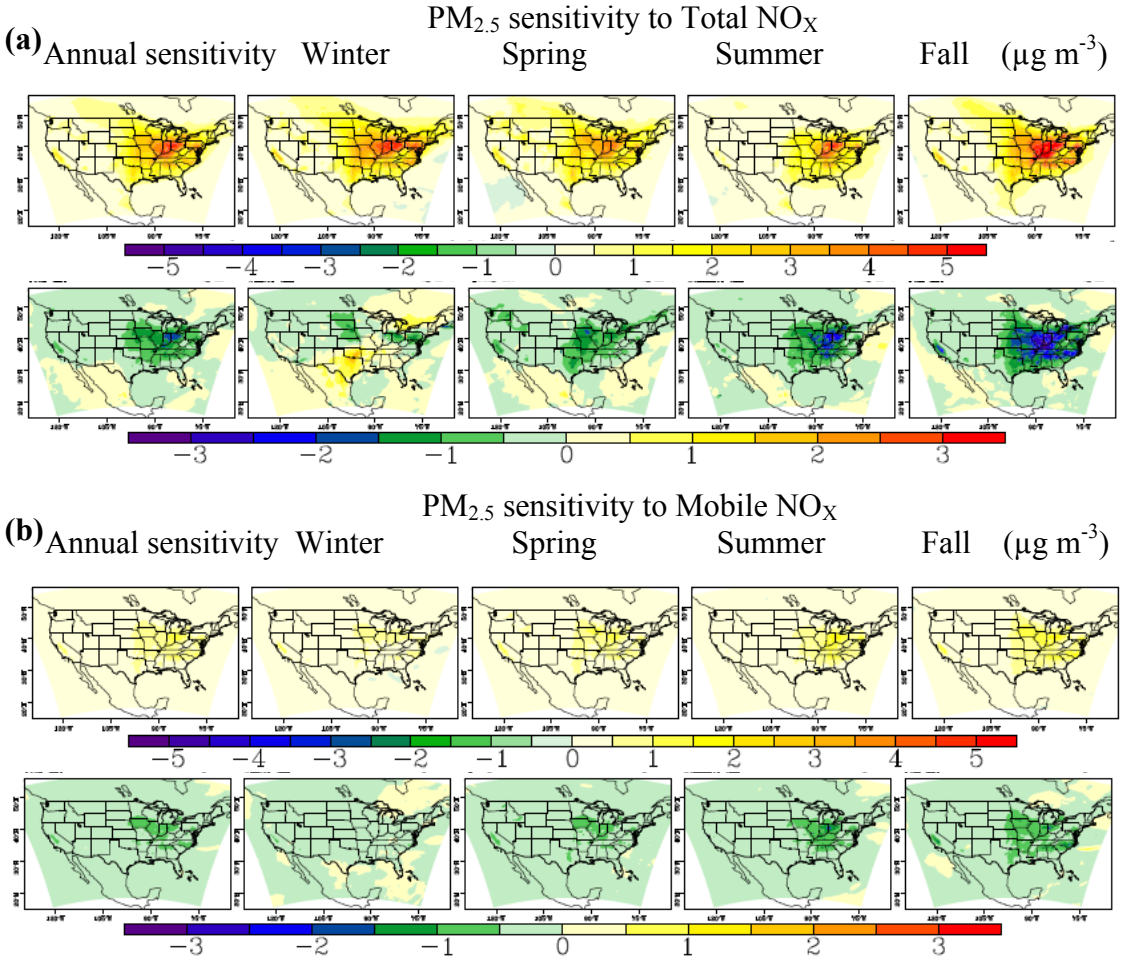

Figure 3-8 (a) Average present $PM_{2.5}$ sensitivity to total NO_X emissions (top) and difference (bottom; future minus present) and **(b)** $PM_{2.5}$ sensitivity to mobile sector NO_X (top) and difference in $PM_{2.5}$ sensitivity to mobile NO_X (bottom; future minus present)

3.5 Summary and Conclusions

In the present study, we determine the potential impact of changing climate and emissions on future ambient O_3 and $PM_{2.5}$ in the U.S. Present and future emissions were estimated using the NEI and MARKAL-9R. In comparing the impact of present and potential future climate and emissions changes on air quality, we find major improvements in future U.S. air quality including generally decreased MDA8 mixing ratios and $PM_{2.5}$ concentrations and reduced frequency of NAAQS O_3 standard exceedances in most major U.S. cities.

Reductions in mobile and point source emissions account for reduced $PM_{2.5}$ concentrations while climate change reinforces the reduced concentrations in some regions during the spring, summer and fall. However in some regions, e.g. the East Coast, emissions reductions are necessary to overcome the climate change induced increases in $PM_{2.5}$. Future decreases in MDA8 O_3 concentration are mainly attributed to decreased emissions rate of VOC and NO_X from mobile sources. Even though reductions are predicted to occur in the future from current efforts, the CP scenario of future emissions with present meteorology indicates that the extent of air quality improvement is less due to predicted climate change. In other words, present emission reduction efforts will lead to less O_3 and $PM_{2.5}$ in the future, but these efforts will be less effective with climate change than without. This means additional costs due to climate change because deeper emission reductions will be required to compensate for a warmer climate, even if current efforts are predicted to show improvement.

While most U.S. cities potentially exceed the MDA8 NAAQS standard less frequently in the future, decreased titration of O_3 by NO_X could increase the frequency of

exceedances in Los Angeles and increase spring and fall average MDA8 mixing ratio in other urban areas. However, as these cities become more NO_X-limited, further reductions in NO_X emissions in these urban environments will lead to reduced levels of O_3.

While there are uncertainties in current and future emissions estimates, and uncertainties in climate, emissions sensitivities can be used to determine the major sources of O_3 and $PM_{2.5}$ and the current modeling platform can be used to isolate the effects of climate on air quality. Further, the MARKAL 9R model can be used to develop a range of alternative policy based emissions scenarios to address the uncertainties associated with estimating future emissions. Our results further the findings of Tagaris et al. [2007], showing that emissions reductions strategies will continue to play a vital role in improving air quality over the U.S., especially in regions where climate change threatens to degrade O_3 and PM air quality. Future research will consider the impact of alternative future emissions, using the MARKAL 9R model, and land use scenarios on U.S. air quality.

3.6 References

Brown, K. E., et al. (2013), Accounting for Climate and Air Quality Damages in Future US Electricity Generation Scenarios, *Environmental Science & Technology*, *47*(7), 3065-3072, doi:10.1021/es304281g.

Carter, W. P. L. (2000), Documentation of the SAPRC-99 chemical mechanism for VOC reactivity assessment, University of California, Riverside, Riverside, CA.

CEP (2003), Sparse Matrix Operator Kernel Emissions Modeling System (SMOKE) User Manual, edited, Chapel Hill, NC.

Dudhia, J. (1989), Numerical study of convection observed during the winter monsoon experiment using a mesoscale two-dimensional model, *J. Atmos. Sci.*, *46*(20), 3077-3107

Dunker, A. M., et al. (2002), The decoupled direct method for sensitivity analysis in a three-dimensional air quality model - Implementation, accuracy, and efficiency, *Environmental Science & Technology*, *36*(13), 2965-2976

Ek, M. B., et al. (2003), Implementation of Noah land surface model advances in the

National Centers for Environmental Prediction operational mesoscale Eta model, *Journal of Geophysical Research-Atmospheres*, *108*(D22), 16, doi:8851 10.1029/2002jd003296.

Fann, N., et al. (2013), The Recent and Future Health Burden of Air Pollution Apportioned Across US Sectors, *Environmental Science & Technology*, *47*(8), 3580-3589, doi:10.1021/es304831q.

Fishbone, L. G., et al. (1980), MARKAL, a Multiperiod Linear-Programming Model for Energy-Systems Analysis Applied to the United-States, *Bulletin of the American Physical Society*, *25*(4), 494-495

Foley, K. M., et al. (2001), Incremental testing of the Community Multiscale Air Quality (CMAQ) modeling system version 4.7, *Geoscientific Model Development*, *3*(1), 205-226

Hong, S. Y., et al. (2006), A new vertical diffusion package with an explicit treatment of entrainment processes, *Mon. Weather Rev.*, *134*(9), 2318-2341

Ito, K., et al. (2005), Associations between ozone and daily mortality - Analysis and meta-analysis, *Epidemiology*, *16*(4), 446-457, doi:10.1097/01.ede.0000165821.90114.7f.

Jacob, D. J., and D. A. Winner (2009), Effect of climate change on air quality, *Atmospheric Environment*, *43*(1), 51-63, doi:10.1016/j.atmosenv.2008.09.051.

Kain, J. S., and J. M. Fritsch (1993), Convective parameterization models: The Kain–Fritsch scheme. Cumulus Convection in Numerical Models, *American Meteorological Society*, *46*, 165-170

Lamarque, J. F., et al. (2011), Global and regional evolution of short-lived radiatively-active gases and aerosols in the Representative Concentration Pathways, *Clim. Change*, *109*(1-2), 191-212, doi:10.1007/s10584-011-0155-0.

Leibensperger, E. M., et al. (2012a), Climatic effects of 1950-2050 changes in US anthropogenic aerosols - Part 2: Climate response, *Atmospheric Chemistry and Physics*, *12*(7), 3349-3362, doi:10.5194/acp-12-3349-2012.

Leibensperger, E. M., et al. (2012b), Climatic effects of 1950-2050 changes in US anthropogenic aerosols - Part 1: Aerosol trends and radiative forcing, *Atmospheric Chemistry and Physics*, *12*(7), 3333-3348, doi:10.5194/acp-12-3333-2012.

Leung, L. R., and W. I. Gustafson (2005), Potential regional climate change and implications to US air quality, *Geophysical Research Letters*, *32*(16), 4, doi:L16711 10.1029/2005gl022911.

Liao, K. J., et al. (2007), Sensitivities of ozone and fine particulate matter formation to emissions under the impact of potential future climate change, *Environmental Science & Technology*, *41*(24), 8355-8361, doi:10.1021/es070998z.

Likens, G. E., et al. (1996), Long-term effects of acid rain: Response and recovery of a forest ecosystem, *Science*, *272*(5259), 244-246, doi:10.1126/science.272.5259.244.

Lim, S. S., et al. (2012), A comparative risk assessment of burden of disease and injury attributable to 67 risk factors and risk factor clusters in 21 regions, 1990-2010: a systematic analysis for the Global Burden of Disease Study 2010 (vol 380, pg 2224, 2012), *Lancet*, *381*(9874), 1276-1276

Lin, Y. L., et al. (1983), Bulk parameterization of the snow field in a cloud model, *Journal of Climate and Applied Meteorology*, *22*(6), 1065-1092, doi:10.1175/1520-0450(1983)022<1065:bpotsf>2.0.co;2.

Liu, P., et al. (2012), Differences between downscaling with spectral and grid nudging using WRF, *Atmospheric Chemistry and Physics*, *12*(8), 3601-3610, doi:10.5194/acp-12-3601-2012.

Mauzerall, D. L., and X. P. Wang (2001), Protecting agricultural crops from the effects of tropospheric ozone exposure: Reconciling science and standard setting in the United States, Europe, and Asia, *Annu. Rev. Energ. Environ.*, *26*, 237-268, doi:10.1146/annurev.energy.26.1.237.

Mickley, L. J., et al. (2004), Effects of future climate change on regional air pollution episodes in the United States, *Geophysical Research Letters*, *31*(24), 4, doi:L24103 10.1029/2004gl021216.

Mlawer, E. J., et al. (1997), Radiative transfer for inhomogeneous atmospheres: RRTM, a validated correlated-k model for the longwave, *Journal of Geophysical Research-Atmospheres*, *102*(D14), 16663-16682, doi:10.1029/97jd00237.

Moss, R. H., et al. (2010), The next generation of scenarios for climate change research and assessment, *Nature*, *463*(7282), 747-756, doi:10.1038/nature08823.

Murray, C. J. L., et al. (2013), Disability-adjusted life years (DALYs) for 291 diseases and injuries in 21 regions, 1990-2010: a systematic analysis for the Global Burden of Disease Study 2010, *Lancet*, *380*(9859), 2197-2223

Napelenok, S., et al. (2006), Implementation of the Decoupled Direct 3D Sensitivity Analysis Method for Particulate Matter and Analysis of Pollutant Responses in the Southeastern United States, *Atmospheric Environment*, *in press*

Nolte, C. G., et al. (2008), Linking global to regional models to assess future climate impacts on surface ozone levels in the United States, *Journal of Geophysical Research-Atmospheres*, *113*(D14), D14307, doi:10.1029/2007JD008497.

Ramanathan, V., et al. (2001), Atmosphere - Aerosols, climate, and the hydrological cycle, *Science*, *294*(5549), 2119-2124, doi:10.1126/science.1064034.

Schmidt, G. A., et al. (2013), Configuration and assessment of the GISS ModelE2 contributions to the CMIP5 archive, *J. Adv. in Modeling Earth Systems, Submitted*

Shindell, D., et al. (2012), Simultaneously Mitigating Near-Term Climate Change and Improving Human Health and Food Security, *Science*, *335*(6065), 183-189, doi:10.1126/science.1210026.

Skamarock, W. C., and J. B. Klemp (2008), A time-split nonhydrostatic atmospheric model for weather research and forecasting applications, *Journal of Computational Physics*, *227*(7), 3465-3485, doi:10.1016/j.jcp.2007.01.037.

Tagaris, E., et al. (2007), Impacts of global climate change and emissions on regional ozone and fine particulate matter concentrations over the United States, *Journal of Geophysical Research-Atmospheres*, *112*(D14), D14312, doi:10.1029/2006JD008262.

Trail, M., Tsimpidi, A. P., Liu, P., Tsigaridis, K., Hu, Y., Nenes, A., and Russell, A. G. (2013), Downscaling a global climate model to simulate climate change impacts on US regional and urban air quality, *Geosci. Model Dev.*, *6*, 1429-1445, doi:10.5194/gmd-6-1429-2013.

Weaver, C. P., et al. (2009), A preliminary synthesis of modeled climate change impacts on US regional ozone concentrations, *Bulletin of the American Meteorological Society*, *90*(12), 1843-1863, doi:10.1175/2009bams2568.1.

Woo, J. H., et al. (2008), Development of North American Emission Inventories for Air Quality Modeling under Climate Change, *Journal of the Air & Waste Management Association*, *58*(11), 1483-1494, doi:10.3155/1047-3289.58.11.1483.

Yang, Y. J., et al. (1997), Fast, direct sensitivity analysis of multidimensional photochemical models, *Environmental Science & Technology*, *31*(10), 2859-2868

Yu, S. C., et al. (2006), New unbiased symmetric metrics for evaluation of air quality models, *Atmos. Sci. Lett.*, *7*(1), 26-34, doi:10.1002/asl.125.

Zhou, J. A., et al. (2011), Time-Series Analysis of Mortality Effects of Fine Particulate Matter Components in Detroit and Seattle, *Environ. Health Perspect.*, *119*(4), 461-466, doi:10.1289/ehp.1002613.

CHAPTER 4

IMPACTS OF POTENTIAL POLICIES DESIGNED TO REDUCE CO_2 EMISSIONS AND CLIMATE CHANGE ON UNITED STATES REGIONAL AIR QUALITY[3]

Abstract

Impacts of emissions changes from four potential CO_2 emission reduction policies on regional air quality in 2050 are analyzed in the United States using the community multi-scale air quality model (CMAQ). Future meteorology was downscaled from a General Circulation Model (GCM) to the regional scale using the Weather Research Forecasting (WRF) model. We use emissions growth factors from MARKAL-9R to develop 2050 emissions inventories for two climate tax policy scenarios, a combined transportation and energy sector policy scenario and a biomass energy policy scenario and a reference case and compare air pollutant concentrations. Implementation of an aggressive carbon tax leads to improvements in $PM_{2.5}$ air quality compared to the 2050 reference case due to increased incentives for facilities to install flue-gas desulfurization (FGD) and carbon capture and sequestration (CCS) technologies. However, less capital is available to install NO_X reduction technologies and O_3 increases as a result. An unaggressive carbon tax leads to worse air quality, in the form of increased $PM_{2.5}$ concentrations because there is less incentive to install FGD and CCS technologies. A policy aimed at reducing CO_2 from the transportation sector as well as electricity

[3] A modified version of this chapter is under review as Impacts of potential policies designed to reduce CO_2 emissions and climate change on United States regional air quality, *Environmental Science & Technology*

production sectors lead to reduced emissions of mobile source NO_X, thus reducing O_3 mixing ratio. Over most of the U.S., this scenario leads to reduced $PM_{2.5}$ concentrations. However, increased VOC emissions associated with fuel switching from coal to natural gas leads to increased OM and $PM_{2.5}$ in most major U.S. cities.

4.1 Introduction

Air pollution has been shown to have adverse ecosystem and human health effects, and future global changes in climate, emissions, land use and other factors are expected to impact air pollution [*Jacob and Winner*, 2009; *Liao et al.*, 2006b; *Liao et al.*, 2007b; *Schwartz et al.*, 1994; *Weaver et al.*, 2009]. Recently, the World Health Organization (WHO) characterized air pollution as a class 1 carcinogen and the Global Burden of Disease study [*Lim et al.*, 2012] found exposure to ambient particulate matter (PM) and ozone (O_3) as major contributors to premature death. In order for decision-makers to appropriately mitigate future air pollution, the impact that future global changes involving emissions, population, land-use and climate can have on air pollution should be considered. In particular, the impact of policies designed to mitigate climate change will have on air quality is of concern. A major source of uncertainty lies in predicting future emissions. However, recent modeling advances have shown potential to reduce uncertainties by accounting for complex interactions between driving forces such as population growth, socio-economical development, technology change, and federal and regional environmental policies [*Fishbone et al.*, 1980]. In this study, we assess the impact of four potential climate mitigation policies on air quality in the U.S. in a future

(2050) climate by using recent advances in climate downscaling and emissions projection approaches.

Significant effort has already been made to investigating the impact of future climate change on air pollutant concentration [*Jacob and Winner*, 2009; *Weaver et al.*, 2009]. A general consensus among studies is that future climate change can cause increased O_3 concentration in some regions of the U.S. while changes in PM will likely be small and variable. While these studies focus on air pollution changes due to climate change, some recent studies have addressed the impact of future changes in emissions as well [*Dholakia et al.*, 2013; *Liao et al.*, 2007b; *McCollum et al.*, 2013; *Mickley*, 2007; *Tagaris et al.*, 2007]. Mickley et al. [2007] use the Community Multiscale Air Quality (CMAQ) model with inputs of downscaled future climate [*Leung and Gustafson*, 2005] with anthropogenic emissions changed according to the A1B projections of the Asian Pacific Integrated Model (AIM) and find decreased O_3 over most regions of the U.S. despite the tendency for climate change to increase O_3 concentration. Mickley et al. [2007] suggest assessing alternative emissions scenarios as well as the impacts on $PM_{2.5}$ concentrations. Tagaris et al. [2007] use the same methodologies as Mickley et al. [2007] but with emissions projected to the near future (2020) using the 2020 Clean Air Interstate Rule (CAIR) emissions inventory and to the distant future (2050) using the Integrated Model to Assess the Global Environment (IMAGE). They find reduced maximum daily 8-hr average (MDA8) O_3 mixing ratios over most of the U.S. and reduced sulfate, nitrate and ammonium aerosol concentrations. Dholakia et al. [2013] use the Greenhouse Gases and Air Pollution Interactions and Synergies (GAINS) model to assess the impact of advanced control technologies and climate change mitigation on $PM_{2.5}$ in Delhi, India

and predicted that the climate change mitigation strategies would have modest impacts on reducing $PM_{2.5}$ concentrations in 2030. McCollum et al. [2012] linked the GAINS model and the Model for Energy Supply Systems And their General Environmental impact (MESSAGE), and integrated assessment model, to develop an ensemble of future global energy scenarios and predicted the impacts on human health related to air pollution. They found that decarbonization efforts can improve air quality and reduce the health impacts. They also point out that there is still a need for comparison among various modeling technologies aimed at predicting the impact of future emissions on air pollution.

In this study, we use a chemistry-transport model (CTM) to simulate air pollutant concentrations and apply recent modeling advancements to assess a suite of detailed emissions projections scenarios chosen based on their potential to mitigate climate change. In particular, we use MARKAL 9R (MARKet ALlocation 9 Region) [Rudukas et al., 2014, submitted] to develop emissions scenarios and spectral nudging to downscale global climate [*Liu et al.*, 2012; *Trail*, 2013] to a regional scale over the U.S. The benefits of using spectral nudging to downscale global climate are described in Lui et al. [2012]. The MARKAL energy system model selects from available technologies to provide the least-cost path which satisfies specified demands of the residential, commercial, industrial, and transportation sectors for regionally based energy services. The flexible modelling framework allows examination of the mid-to-long-term technology choices as well as specific policy options that shape the evolution of an energy system in meeting specific environmental or other goals. MARKAL serves as a useful tool to identify the likely technologies that will be used to meet greenhouse gas or

criteria air pollutant-related policies and objectives. Various versions of MARKAL are used in previous studies to estimate emissions for investigating air quality changes due to the implementation of policies aimed at reducing emissions of greenhouse gas (GHG) and air pollutants in Shanghai and Beijing [*Chen and Chen*, 2013; *Chen et al.*, 2006a; *Gielen and Chen*, 2001] and in developing countries such as Nepal [*Shrestha and Rajbhandari*, 2010] and Pakistan [*Farooq et al.*, 2013]. To the knowledge of the authors, this is the first study to use MARKAL to investigate the effect of CO_2 reduction strategies on air quality in the U.S.

We use CMAQ [*Foley et al.*, 2001] to analyze the impact of emissions changes from four potential climate change mitigation policies on regional air quality in 2050 in the contiguous United States and compare them to a reference case policy scenario, which accounts for current policies. We use emissions growth factors from MARKAL-9R [Rodukas et al., 2014 submitted] to develop 2050 inventory and the Sparse Matrix Operator Kernel Emissions (SMOKE) model to provide spatial and temporal variation. Future meteorology was downscaled from the Global Institute for Space Studies (GISS) ModelE2 General Circulation Model (GCM) to the regional scale using the Weather Research Forecasting (WRF) model with spectral nudging [*Liu et al.*, 2012]. Trail et al. [2013] provide a detailed description of meteorology used in the present study and compare present (2006-2010) and future (2048-2052) regional climate from an air quality perspective. Trail et al. [2013] also conducted an extensive evaluation of the 2006-2010 results using observations from the same period. In a previous study [Trail et al., 2014, submitted], we use the CMAQ model to compare present (2006-2010) and future (2048-2052) air pollutant concentrations and their sensitivities to emissions from different

sectors for the reference case emissions scenario and found decreased O_3 and $PM_{2.5}$ concentrations over most of the U.S. That paper also conducted an extensive evaluation of the 2006-2010 air quality model results using observations. In the present study, we compare air pollutant concentrations, including O_3 and $PM_{2.5}$, for two climate tax policy scenarios (CT1 and CT2), a combined transportation energy sector policy scenario (TE) and a biomass energy policy scenario (BE) to the reference case for the year 2050. We also analyze air pollutant concentrations and National Ambient Air Quality Standards (NAAQS) exceedances in major U.S. cities and provide a discussion of the implications of the results of this study.

4.2 Methods

Future air pollutant concentration responses to climate mitigation policies are simulated using a CTM with inputs of emissions from multiple policy scenarios and downscaled meteorology. Emission inputs are prepared for the CTM using and energy system cost optimization model. Components of the modeling system are described below

4.2.1 *Meteorology*

The Goddard Institute for Space Studies (GISS) ModelE2 provides the initial and boundary conditions to a regional climate model for the years 2006-2010 and 2048-2052 [*Schmidt et al.*, 2013]. The global simulation has 40 layers and follows a sigma coordinate up to 150 hPa, with constant pressure layers between 150 and 0.1 hPa with a

horizontal resolution of 2°×2.5° latitude by longitude. Simulations are carried out for the years 2006-2010 and 2048-2052 with a 3 year spin-up time, driven by future atmospheric conditions over the 21st century and follow the scenario development process for IPCC AR5. The "Representative Concentration Pathway" (RCP) 4.5 [*Lamarque et al.*, 2011; *Moss et al.*, 2010] is used for this study, that is a scenario of decadal global emissions of greenhouse gases, short-lived species, and land-use-land-cover which produces an anthropogenic radiative forcing at 4.5 W m^{-2} (approximately 650 ppm CO_2-equivalent) in the year 2100 [*Moss et al.*, 2010]. Instantaneous outputs of physical parameters were produced at 6-hr intervals for regional downscaling by WRF. The Weather Research and Forecasting (WRF) Model [*Skamarock and Klemp*, 2008] (version 3.4) is used to downscale GISS simulations for the years 2006-2010 and 2048-2052 with 10 day spinup times. The present study only uses meteorological results from the years 2010 and 2050 which were average years during those five year periods. The model domain covers the CONUS and portions of southern Canada and northern Mexico and is centered at 40°N and 97°W with 164×138 horizontal 36 x 36 km grids cells (Figure 4-1). It contains 35 vertical levels, with the top pressure of 50hPa. The model scheme configuration is as follows: the Rapid Radiative Transfer Model (RRTM) [*Mlawer et al.*, 1997] and Dudhia scheme [*Dudhia*, 1989] are used for long-wave and shortwave radiation respectively; the Yonsei University (YSU) [*Hong et al.*, 2006] scheme is used for planetary boundary layer dynamics; the Noah scheme [*Ek et al.*, 2003] is used for land surface model (LSM); a revised version of Kain-Fritsch scheme [*Kain and Fritsch*, 1993] is used to represent the effects of both deep and shallow cumulus clouds; Lin *et al.* [*Lin et al.*, 1983] is chosen for cloud microphysics. Spectral nudging of global model results is applied in

WRF to temperature, horizontal winds, and geopotential heights with a wave number of 3 in both zonal and meridional directions at 6 hour intervals [*Liu et al.*, 2012]. Only horizontal winds are nudged at all vertical levels, while no nudging is conducted for other variables within the planetary boundary layer (PBL).

The ability of GISS-WRF to reproduce long-term yearly climatic means and meteorological fields that strongly impact air quality are evaluated in Trail et al. [2013]. The GISS-WRF simulations and configuration are documented in more detail in Trail et al. [2013].

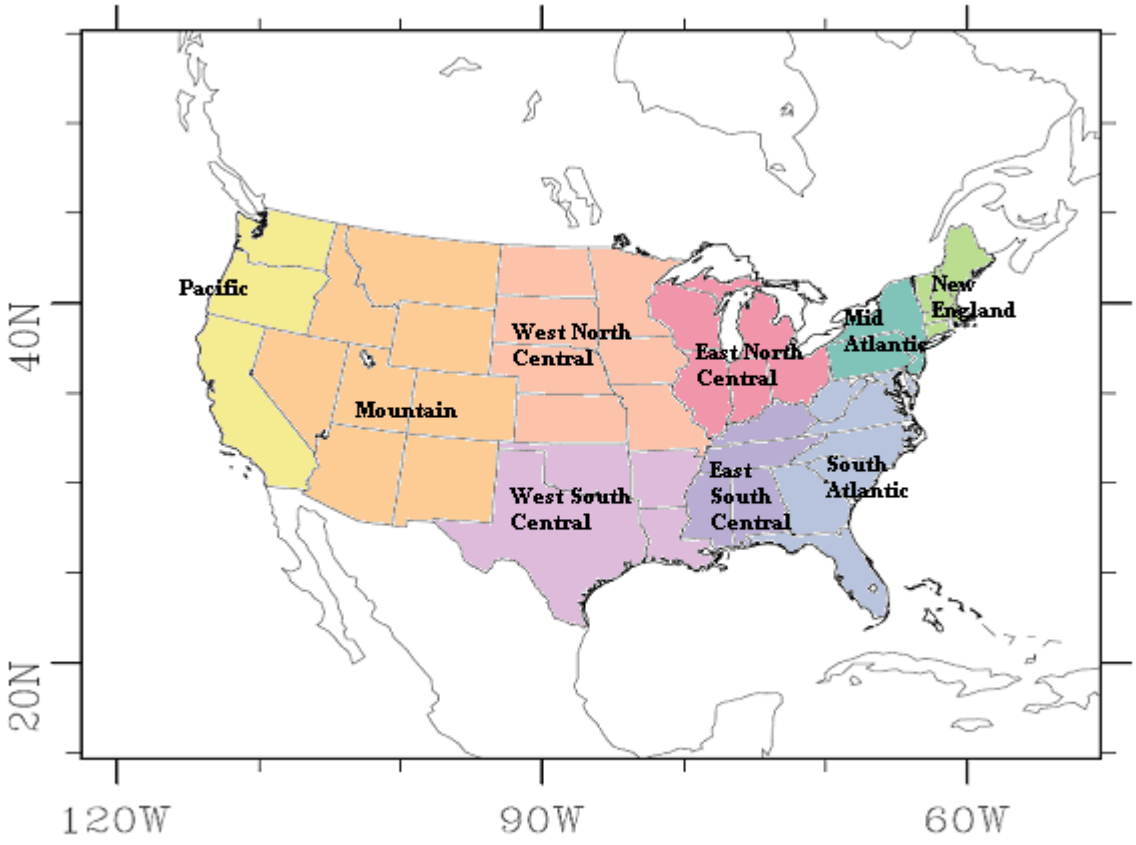

Figure 4-1 CMAQ modeling domain with EPA US 9 census regions used in the MARKAL 9R modeling

4.2.2 *Emissions*

The NEI energy related emissions are projected to the years 2010 and 2050 for a reference case and for four alternative emissions scenarios (2050 only) using projection factors calculated by the EPA MARKAL 9R [*Fishbone et al.*, 1980]. MARKAL 9R models future energy dynamics of the energy systems in the nine Census Divisions of the U.S. (Figure 4-1). The reference case emissions scenario assumes the implementation of the following policies: Clean Air Act Title IV (Acid Rain Program) SO_2 and NOx requirements, Clean Air Interstate Rule (CAIR), Utility Mercury and Air Toxics Standards (MATS), Aggregated state Renewable Portfolio Standards (RPS) by region, Federal Corporate Average Fuel Economy (CAFE) standards as modeled in AEO 2012, Tier 2 light duty vehicle tailpipe emission standards and heavy duty vehicle fuel and engine rules. Projections of non-energy related emissions were calculated according to the A1B emissions scenario developed by the Intergovernmental Panel on Climate Change Special Report on Emissions Scenarios (IPCC SRES) [*Woo et al.*, 2008].

Four alternative emissions scenarios, including two carbon tax scenarios (CT1 and CT2), a transportation scenario (TE) and a biomass scenario (BE), were developed by Rodukas et al. [2014] by assuming the implementation of various climate mitigation policies in addition to the policies assumed in the reference case (Table 4-1). The first carbon tax scenario (CT1) represents a carbon tax option with taxes beginning in 2015 at \$20 per ton CO_2 and reaching \$90 per ton in 2050, while the second carbon tax scenario (CT2) is a more aggressive option with taxes beginning in 2020 at \$50 per ton and reaching \$1,400 per ton in 2050. The combined TE scenario assumes a 70% reduction of GHG from transportation sectors and an additional cap on electricity sector emissions

rates of CO_2 at 800 lb/MWh, similar to that of new combined cycle natural gas power plants. The purpose of the additional cap on the electricity sector is to mitigate increased emissions from electric generation due to increased use of electric vehicles. Finally, the BE scenario assumes that all available biomass will be used in the energy sector. Rather than predetermining which sectors the biomass would be directed to or how the biomass would be employed, MARKAL uses cost optimization logic to determine how and where the biomass feedstocks were employed.

Table 4-1 Emissions scenario descriptions. All alternative emissions scenarios include the policies included in the reference case description

Scenario	Description
Reference Case	• Clean Air Act Title IV (Acid Rain Program) SO_2 and NOx requirements • Clean Air Interstate Rule • Utility Mercury and Air Toxics Standards (MATS) • Aggregated state Renewable Portfolio Standards (RPS) standards by region • Federal Corporate Average Fuel Economy (CAFE) standards as modeled in AEO 2012 • Tier 2 light duty vehicle tailpipe emission standards • Heavy duty vehicle fuel and engine rules
CT1	• Carbon tax of $20 per ton beginning in 2015 and increasing at a rate of 4% per year ($90 per ton in 2050)
CT2	• Carbon tax of $50 per ton beginning in 2020 and increasing at a rate of 10% per year ($1,400 per ton in 2050)
TE	• 70% reduction in GHG emissions from the transportation sector by 2050 relative to 2005 levels • Limit CO_2 emission rate from electricity sector to 800 lb/MWh (similar to that of a new combined cycle natural gas power plant)
BE	• All available biomass in the U.S. is used (includes agricultural residues, energy crops, mill residues and urban wood waste)

Temporally (hourly) and spatially (36km) resolved speciated emissions are generated for input to CMAQ using the SMOKE V3 model [*CEP*, 2003] which uses inputs of the National Emissions Inventory (NEI) 2005 inventory and ancillary data. The Biogenic Emissions Inventory System (BEIS) and the Biogenic Emissions Landcover Database 3.0 (BELD3) are used in SMOKE to compute hourly emissions from U.S. vegetation. The resulting inventory consists of pollutants emitted from area, mobile, point, fire, ocean, biogenic, and agricultural sources.

4.2.3 *Air Quality*

Simulations of the transformation and fate of air pollutants for the four alternative emissions scenarios in the year 2050 and for the present (2010) and future (2050) year reference cases are carried out using the CMAQ 4.7.1 model [*Foley et al.*, 2001]. Gas-phase chemistry is modeled using the SAPRC-99 [*Carter*, 2000] chemical mechanism. The domain covers the entire continental US as well as portions of Canada and Mexico (5328×4032 km) using a 36-km horizontal grid-spacing with thirteen vertical layers extending ~15.9 km above ground (Figure 4-1). The first layer is 18 m thick and there are 7 layers below 1 km. The modeling domain uses a Lambert Conformal Projection centered at 40ºN, 97ºW with true latitudes of 33ºN and 45ºN. The GISS global simulation provides the present and future dynamic boundary conditions. Default initial conditions of air pollutant concentrations are used here with a spin-up period of 10 days for each simulation to minimize the influence of the initial conditions.

In a previous paper, Trail et al. [submitted, 2014] compare present (2006-2010) and future (2048-2052) air quality using the same methods as in the present study for the

reference case emissions scenario. 2010 and 2050 air quality model results were found to be typical during those years. They also evaluated the simulated present day air quality with observations and found that simulated O_3 and $PM_{2.5}$ show good agreement with observations.

4.3 Results

Rudokas et al. [2014] describe the changes from the reference case of emissions rates of major air pollutants from 2010 to 2050 for the four emissions scenarios analyzed in this study. For the first carbon tax scenario, CT1, they found a 20% reduction in SO_2 emissions from combined industry and electricity sectors and little change in NO_X emissions in 2050 versus the 2050 reference case (Figure 4-2). The CT2 scenario, on the other hand, leads to a 61% decline in SO_2 emissions from the electricity sector and a 20% decline from industry sectors. However, NO_X emissions increase by 20% in the electricity sector for the CT2 scenario. The unique divergence between SO_2 and NO_X emissions in the electricity sector for the CT2 scenario is related to both the incentive to dramatically reduce carbon dioxide emissions and the sequence in which control technologies become available in the MARKAL model. In the first stage of emissions control, MARKAL either purchases a flue-gas desulfurization (FGD) process or foregoes the upgrade. If the FGD upgrade is not installed, then carbon capture and sequestration (CCS) technologies (the second stage of controls) are not available to install. Due to the stringency of the carbon tax in the CT2 scenario, there is a significant incentive to install CCS technologies in the electricity sector. This incentive was not present in the less aggressive CT1 carbon tax scenario. For the reasons mentioned above, increased demand

for CCS technologies leads to an increase in FGD installations, thus driving SO_2 emissions further down. NO_X controls represent the third stage of emission control devices in the MARKAL model. In the CT2 scenario, there is a significant decline in NO_X control investments relative to the reference case, which drives NO_X emission up. Eroded investments in NO_X controls are primarily caused by a crowding out effect as CCS technology investments are significantly ramped up to forego the costs associated with emitting carbon dioxide. In short, there are fewer dollars available for NO_X control investments after significantly increasing investments in CCS technologies. It should be noted that while NO_X emissions do increase in the electricity sector for the CT2 scenario, the power plant NO_X regulations modeled in Rudokas et al. [2014] are still binding.

SO_2 emissions in the TE scenario increase by 3% in the electricity sector and by 33% in the commercial sector but decrease in the transportation sector by 19% while NO_X emissions from the electricity sector decrease by 74%. The dramatic reduction in electric sector NOx results from the assumptions made in Rudokas et al. [2014] about the emissions rates for coal plants in the TE scenario. The MARKAL analysis assumed the emissions rates for all coal plants would conform to the standards of a new combined cycle natural gas plant after 2020. The rationale for the emissions rate assumption in the transportation scenario was to examine the implications of both a clean transportation and clean grid future because battery electric vehicles and plug-in hybrid electric vehicles are the two primary technologies deployed to meet the transportation GHG target. Therefore, the emissions characteristics of the recharging infrastructure (i.e., electricity grid) will greatly affect the implications of a low carbon transportation future. The BM scenario

leads to a 10% decrease in emissions of SO_2 from the reference case by 2050 and a slight decrease in NO_X and VOC emissions.

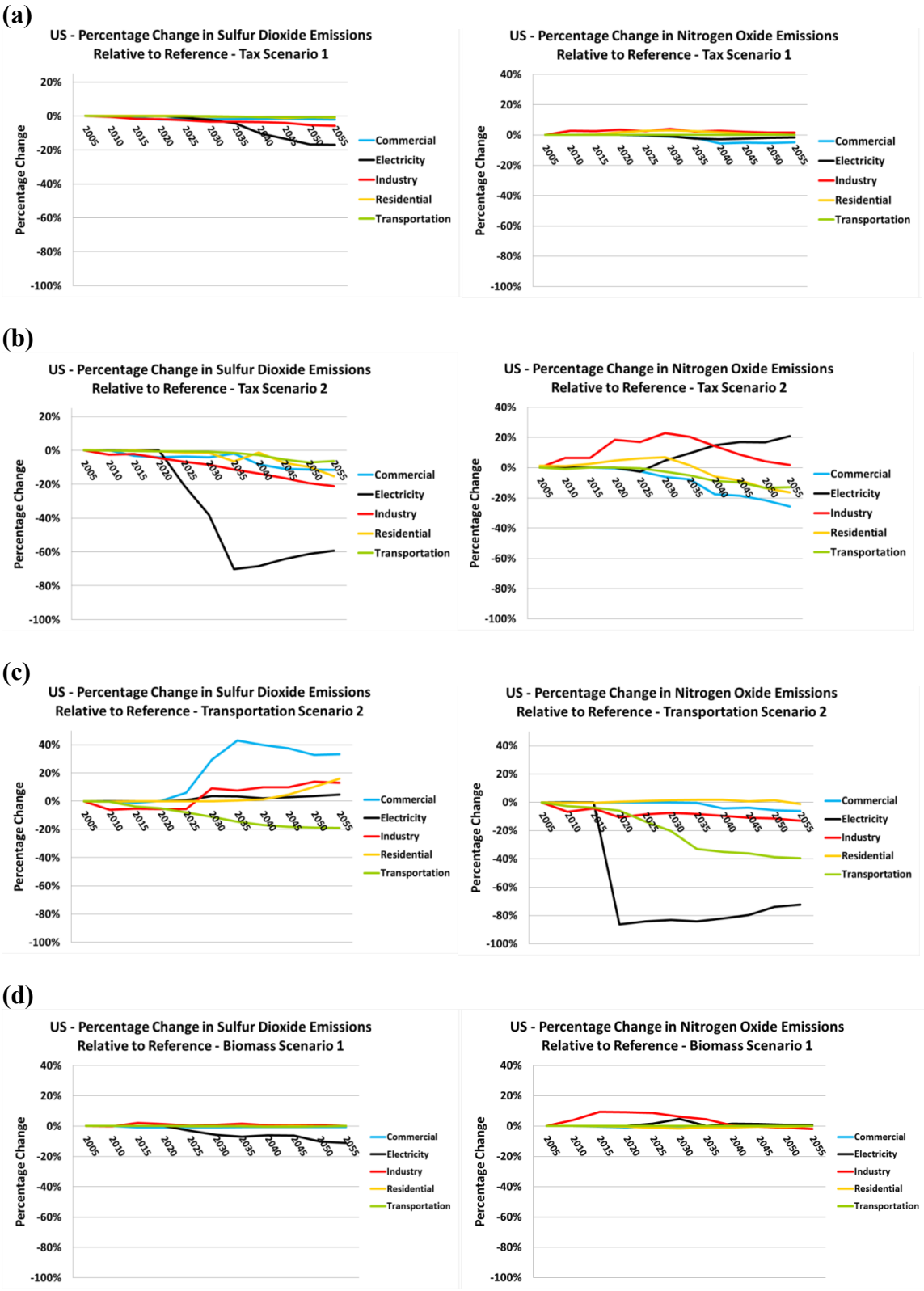

Figure 4-2 Percent change in emissions rates of SO_2 (left column) and NO_X (right) from the reference case over time (from 2005 to 2055) for the (a) CT1, (b) CT2, (c) TN, (d) and BM emissions scenarios [*Rudokas*, 2013]

4.3.1 *Ozone*

Using the reference case emissions scenario and comparing present and future air quality, Trail et al. [submitted, 2014] found that the O_3 concentration is expected to decrease in the future over much of the U.S. despite the tendency for climate change to increase O_3 mixing ratio. Decreased O_3 over time, according to Trail et al. [submitted, 2014], is mainly attributed to decreased emission rates of ozone precursors (e.g VOC, CO and NO_X) from mobile sources in response to the implementation of the CAFE standards along with further decreases in NO_X from electricity generation. A site is in non-attainment of the current NAAQS standard for O_3 if the 4th highest maximum daily 8-hr average (MDA8) O_3 mixing ratio for the year, averaged over three consecutive years, is greater than 75 ppb. In the present study we compare MDA8 mixing ratios of the four emissions scenarios to the reference case for the year 2050 and find that, of the four alternative emissions scenarios tested, the TE scenario shows the largest MDA8 decreases from the future reference case while the CT2 scenario leads to increased MDA8 and the CT1 and BE scenarios have little impact on MDA8 O_3 concentrations (Figure 4-3). During the summer, seasonal average MDA8 is up to 4 ppb greater for the CT2 scenario than the reference case over most of the Eastern U.S. and parts of the Mountain region. Increased MDA8 concentrations in the CT2 scenario is caused by higher NO_X emissions resulting from increased investments in CCS that divert investments away from NO_X controls at power plants as the carbon tax becomes more aggressive in the post-2025 timeframe [Rodukas et al., 2014, submitted]. The 4th highest MDA8 concentration for the CT2 scenario also increases from the reference case by between 2 to 6 ppb over the Eastern U.S. In the CT2 scenario, Atlanta, Chicago, New

York, Philadelphia, Los Angeles and Phoenix all experience an increase in the number of days with MDA8 concentrations exceeding the NAAQS standard of 75 ppb (Table 4-1). The CT1 scenario, on the other hand, shows only small changes in 4th highest MDA8 concentrations and number of days with exceedances in the major cities.

Decreases in NO_X emissions from the electricity and transportation sectors lead to the large decreases of MDA8 concentration in the TE scenario over much of the U.S. Seasonal average MDA8 concentration decreases over most of the U.S. by up to 5 ppb during the spring and fall and by over 10 ppb during the summer with the largest decreases occurring over the Eastern U.S. (Figure 4-3). The 4th highest MDA8 concentration also decreases by up to 20 ppb over most of the Eastern U.S. and parts of the Pacific regions (Figure 4-4). The 4th highest MDA8 of the year is lower for the TE scenario than the reference case in every city analyzed with the largest decreases occurring in Atlanta and Philadelphia of 15 ppb and 10 ppb, respectively (Table 4-2). The 4th highest MDA8 of the year in New York exceeds the NAAQS standard of 75 ppb in the reference case but the NO_X emission reductions in the TE scenario lead to decreases in 4th highest MDA8 to below the standard. In Los Angeles, decreased NO_X emissions over time in the reference case lead to a decrease in 4th highest MDA8 concentration from 110 ppb in 2010 to 94 ppb in 2050, however the number of days exceeding the standard only decreases slightly from 45 to 41 days. In the TE scenario, further reductions in NO_X emissions lead to a large reduction in the number of days exceeding the standard (from 41 to 28 days) and decrease in the 4th highest MDA8 mixing ratio (from 94 ppb to 87 ppb).

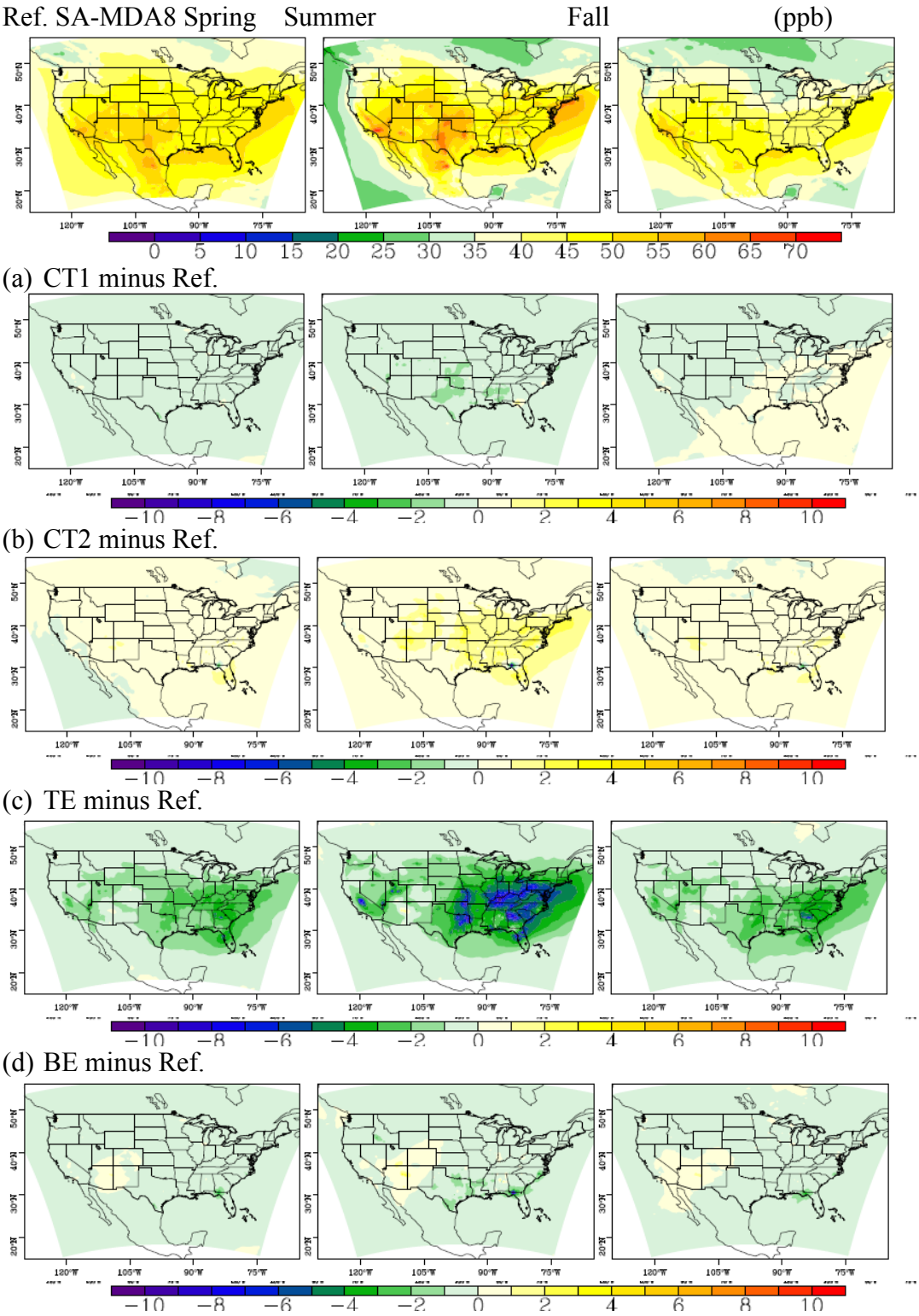

Figure 4-3 (a) Seasonal average MDA8 (ppb) for the future year (2050) reference case during spring, summer and fall and the change in seasonal average MDA8 for the **(b)** CT1 scenario (scenario minus reference), **(c)** CT2 scenario (scenario minus reference), **(d)** TN scenario (scenario minus reference) and **(e)** BM scenario (scenario minus reference)

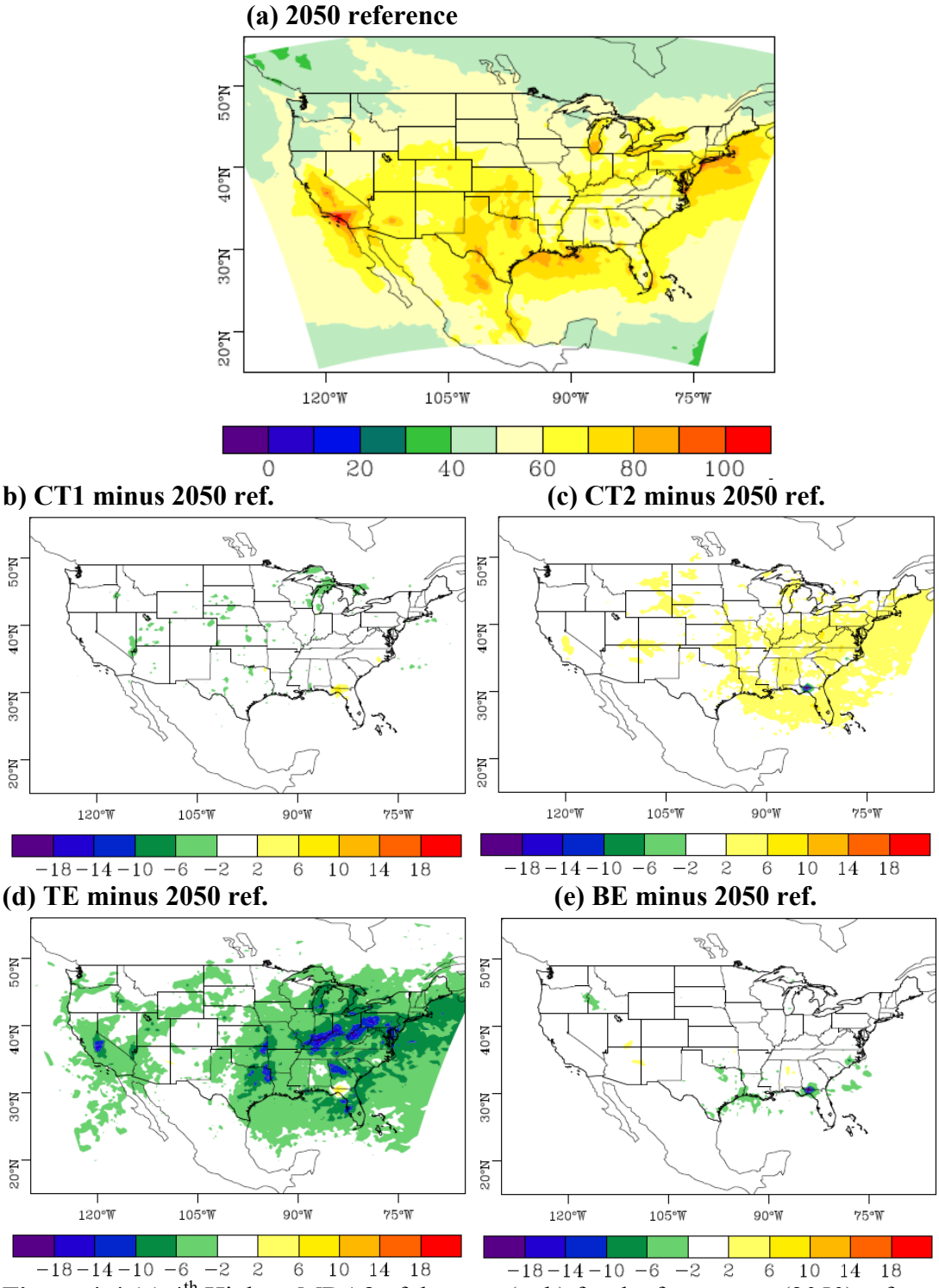

Figure 4-4 (a) 4th Highest MDA8 of the year (ppb) for the future year (2050) reference case and the change in 4th highest MDA8 for the **(b)** CT1 scenario (scenario minus reference), **(c)** CT2 scenario (scenario minus reference), **(d)** TN scenario (scenario minus reference) and **(e)** BM scenario (scenario minus reference)

Table 4-2 4th highest MDA8 (ppb) of the year and the number of days where MDA8 exceeded 75 ppb in parentheses for the present (2010) and future (2050) year reference case and for the four alternative emissions scenarios

City	2010	2050	CT1	CT2	TE	BE
Atlanta	97 (26)	74 (1)	73 (3)	75 (3)	59 (0)	74 (1)
Chicago	94 (15)	72 (1)	71 (2)	74 (2)	68 (1)	72 (1)
Los Angeles	110 (45)	94 (41)	94 (42)	94 (42)	87 (28)	94 (42)
New York	91 (16)	81 (14)	82 (12)	86 (20)	74 (3)	82 (14)
Philadelphia	80 (9)	74 (3)	74 (3)	78 (9)	64 (1)	74 (3)
Phoenix	97 (54)	89 (29)	114 (36)	89 (30)	87 (22)	86 (29)
Seattle	77 (6)	62 (0)	62 (0)	62 (0)	61 (0)	62 (0)

Table 4-3 Highest 98th % 24-hr average $PM_{2.5}$ (μg m^{-3}) of the year, mean annual $PM_{2.5}$ (μg m^{-3}) of the year and the number of days where 24-hr $PM_{2.5}$ exceeds 35 μg m^{-3} in parentheses for the present (2010) and future (2050) year reference case and for the four alternative emissions scenarios

	2010		2050		CT1		CT2		TE		BE	
City	**98th %**	**Mean**	**98th %**	**Mean**	**98th %**	**Mean**	**98th %**	**Mean**	**98th %**	**Mean**	**98th %**	**Mean**
Atlanta	19.0 (0)	10.0	22.4 (0)	9.1	20.3 (0)	9.8	18.6 (0)	8.2	20.3 (0)	9.2	22.2 (0)	10.3
Chicago	28.1 (1)	10.8	24.8 (1)	9.2	26.8 (2)	9.9	25.3 (0)	8.7	26.1 (0)	9.3	28.0 (0)	10.2
Los Angeles	20.5 (0)	9.3	18.4 (0)	8.6	20.2 (0)	9.3	19.2 (0)	9.0	19.2 (0)	8.9	20.2 (0)	9.5
New York	29.6 (3)	10.4	32.5 (3)	11.2	34.2 (6)	12.6	32.7 (4)	10.7	43.8 (15)	14.1	38.0 (12)	13.2
Philadelphia	28.4 (1)	9.6	28.5 (2)	9.4	29.2 (2)	10.1	28.2 (1)	8.4	32.7 (4)	9.4	31.3 (4)	10.6
Phoenix	15.3 (0)	7.6	10.4 (0)	6.5	11.2 (0)	6.9	9.8 (0)	6.0	9.5 (0)	5.7	10.8 (0)	6.8
Seattle	24.1 (1)	9.1	17.5 (0)	6.7	20.5 (0)	7.6	20.4 (0)	7.4	19.2 (0)	7.0	21.5 (0)	8.0

4.3.2 *Particulate Matter ($PM_{2.5}$)*

The CT2 and TE scenarios lead to further decreases in PM in the Eastern U.S. of up to 4 μg m^{-3} and 2 μg m^{-3} less than the 2050 reference case, respectively during the summer (Figure 4-5). The BE scenario tends to increase PM concentration by up to 2 μg m^{-3} over much of the U.S. during the entire year, especially in the Eastern regions while the CT1 scenario shows only small changes over the U.S. In the CT2 scenario, the scenario with the largest reductions in $PM_{2.5}$ concentration, large reductions in SO_2 emissions from the electricity sector, resulting from the carbon tax, lead to reductions in SO_4 aerosol concentration (Figure 4-5 and 4-6). Average annual sulfate aerosol concentrations in Atlanta, New York and Philadelphia are over 1 μg m^{-3} lower for the CT2 scenario compared to the reference case (Figure 4-6). Decreased sulfate aerosol accounts for lower annual average $PM_{2.5}$ concentrations in Atlanta (decrease from 9.1 to 8.2 μg m^{-3}) and Philadelphia (from 9.4 to 8.4 μg m^{-3}) and a large decrease in the 98% highest 24-hr $PM_{2.5}$ by 3.8 μg m^{-3}. Chicago and Philadelphia also experience fewer days with 24-hr average $PM_{2.5}$ in exceedance of the NAAQS 35 μg m^{-3} standard for the CT2 scenario, although the change is small and the 98% highest PM2.5 concentration increases slightly in Chicago (Table 4-3). The CT1 scenario, on the other hand, sees slight increases in annual average and peak 24-hr $PM_{2.5}$ concentration due to increased OM at every city analyzed.

In the TE scenario, the scenario with the second largest $PM_{2.5}$ decreases, decreased emissions of NO_X from the mobile sectors and electricity sectors account for lower seasonal average $PM_{2.5}$ concentration during the wintertime, since NO_X is converted to nitrate aerosol and is a major component of $PM_{2.5}$ during winter (Figure 4-5

and 4-6). The largest $PM_{2.5}$ decreases, up to 4 μg m^{-3} occurring over the Eastern U.S., results from lower SO_2 emission rates from the electricity generation sector in the Eastern regions. Lower sulfate aerosol concentrations account for decreased summertime $PM_{2.5}$ concentration in particular since sulfate is typically most abundant during summer. Annual average $PM_{2.5}$ and sulfate aerosol concentrations, on the other hand, increase by 0.4 and 0.5 μg m^{-3}, respectively, in Los Angeles and by 0.7 and 0.1 μg m^{-3} in Seattle (Figure 4-6 and Table 4-3). Increased sulfate aerosol concentrations are caused by increased SO_2 emissions from the electricity generation sector in the Pacific region resulting from increased electricity demand from electric vehicles. Although $PM_{2.5}$ tends to decrease on most Eastern U.S. regions, annual average $PM_{2.5}$ and the 98th percent 24-hr $PM_{2.5}$ increases in most urban areas except Atlanta and Phoenix (Table 4-3). In particular, the 98th percent 24-hr $PM_{2.5}$ in New York increases from 32.5 to 43.8 μg m^{-3} and New York sees 12 more days with $PM_{2.5}$ in exceedance of the 35 μg m^{-3} NAAQS standard. The increased urban $PM_{2.5}$ in New York corresponds to increased urban OM concentration, which more than doubles in annual average concentration, from 2.3 to 5.0 μg m^{-3} (Figure 6), and increased urban elemental carbon (EC) concentrations. Light-duty vehicles fuel consumption shifts from gasoline to electric and diesel in the TE scenario, resulting in increased emissions of primary $PM_{2.5}$, OC, and EC from diesel vehicles. Increased emissions of primary OM and $PM_{2.5}$ aerosol from diesel vehicles also leads to increased annual $PM_{2.5}$ concentrations of up to 2 μg m^{-3} over Portland, Dallas, Houston, Austin, Minneapolis and San Francisco (Figure 4-5 and C-1).

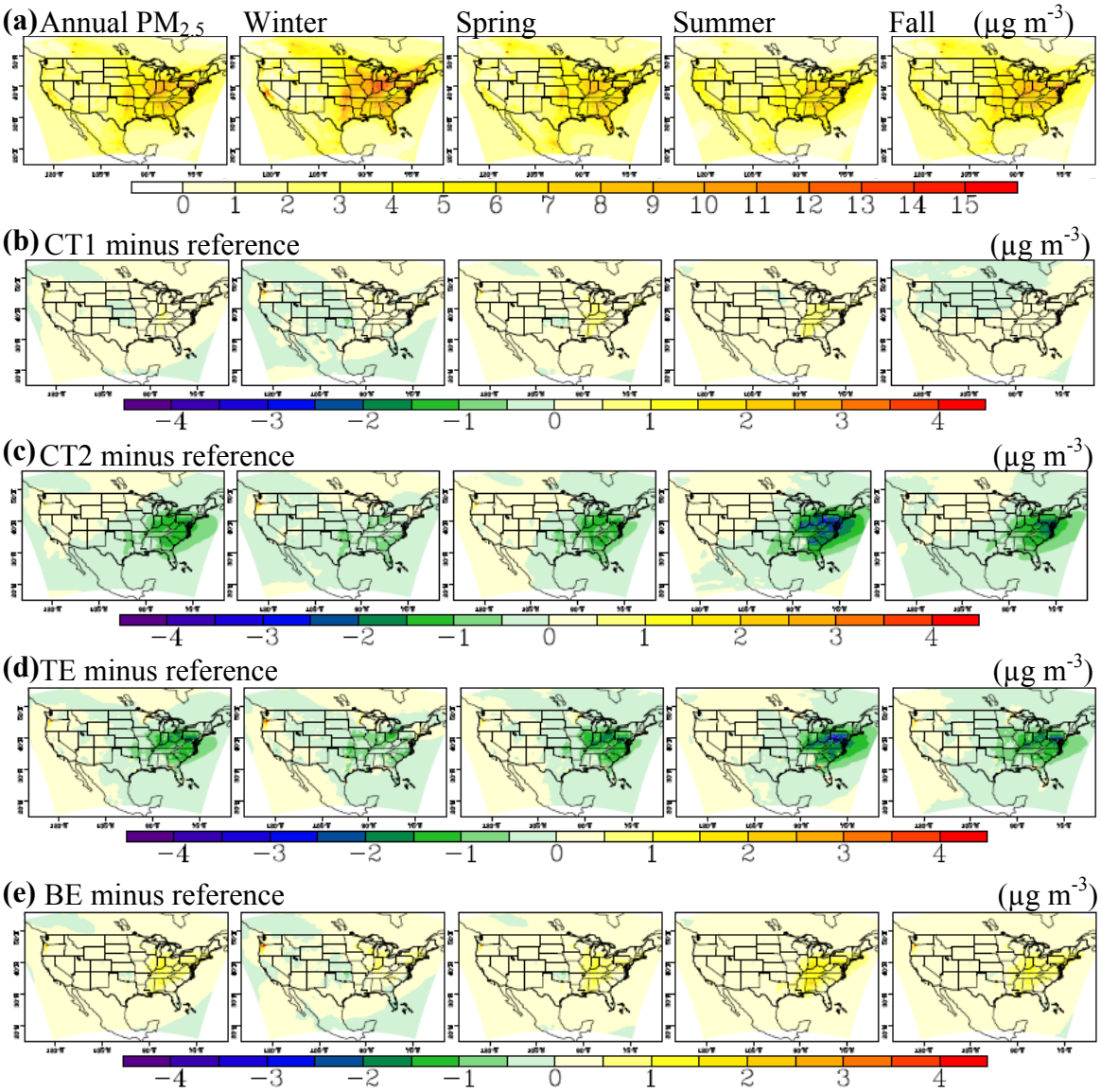

Figure 4-5 (a) Annual and seasonal average PM2.5 concentrations (µg m-^{3}) for the future year (2050) reference case and the change in PM2.5 concentration for the **(b)** CT1 scenario (scenario minus reference), **(c)** CT2 scenario (scenario minus reference), **(d)** TN scenario (scenario minus reference) and **(e)** BM scenario (scenario minus reference)

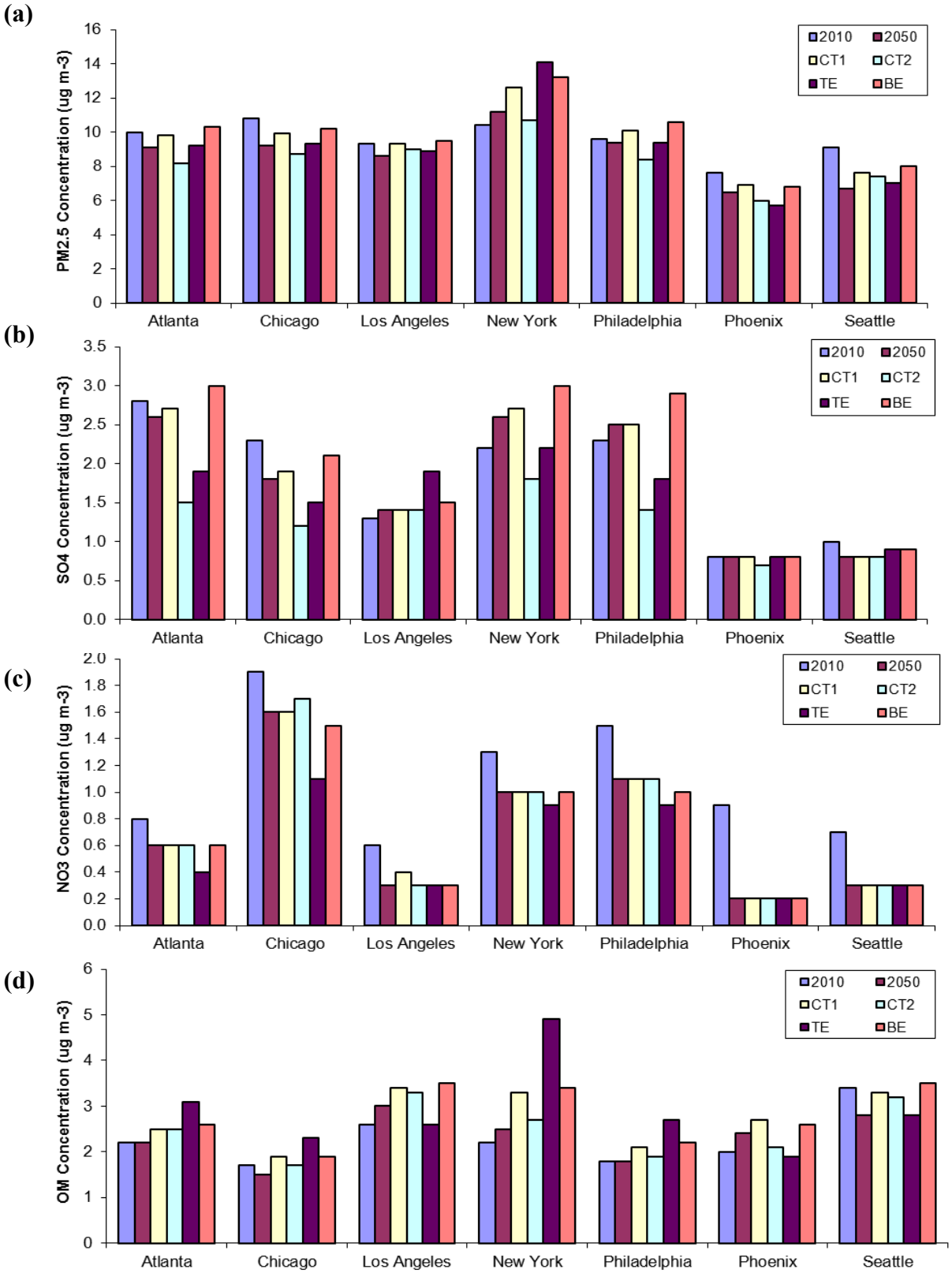

Figure 4-6 Annual average concentrations of $PM_{2.5}$ and its component species in major U.S. cities for the present and future year reference case and for each alternative emissions scenario: **(a)** total $PM_{2.5}$ **(b)** SO_4 **(c)** NO_3 and **(d)** OM

In the BE scenario, increases in annual $PM_{2.5}$ concentration are seen over the Eastern U.S. of 1 - 2 μg m^{-3} relative to the reference case (Figure 4-5). Urban areas tend to see the largest increases in $PM_{2.5}$ with New York seeing an increase in 98th percent 24-hr average $PM_{2.5}$ from 32.5 to 38.0 μg m^{-3} and exceeding the NAAQS standard 9 more days than the reference case scenario (Table 4-3). Sulfate aerosol and OM are the main components of $PM_{2.5}$ that increase in urban areas in the BE scenario due to increased SO_2 and VOC emissions (Figure 4-6).

4.4 Discussion

In simulating the effect of CO_2 emission reduction policies on air quality in the U.S., we find two potential policies (CT1 and BE) which can lead to worse air quality, in the form of increased $PM_{2.5}$ concentrations, compared to the 2050 reference case and two policies which lead to improvements compared to the 2050 reference case (CT2 and TE). The implementation of a relatively aggressive carbon taxes can lead to improvements in $PM_{2.5}$ air quality compared to the 2050 reference case due to the increased incentives to install flue-gas desulfurization (FGD) process technologies and carbon capture and sequestration (CCS) technologies. However, there is an air quality trade-off because less capital is available to install NO_X reduction technologies and O_3 increases as a result. Relatively unaggressive carbon taxes, on the other hand, may lead to worse air quality, in the form of increased $PM_{2.5}$ concentrations because there is less incentive to install FGD and CCS technologies.

A policy aimed at reducing CO_2 from the transportation sector as well as electricity production sectors lead to reduced emissions of mobile source NO_X, thus

reducing O_3 mixing ratio. Over most of the U.S., this scenario leads to reduced $PM_{2.5}$ concentrations. However, increased primary $PM_{2.5}$, OC and EC emissions associated with fuel switching from gasoline to diesel leads to increased annual ambient $PM_{2.5}$ in most major U.S. cities, making it more difficult for those cities to reach attainment of the NAAQS. In other words, in order for the transportation and energy sector policy to be effective at improving air quality in major cities further measures should be taken to reduce primary $PM_{2.5}$ emissions from diesel vehicles.

The use of the MARKAL 9R model in conjunction with a chemical transport model is proven here to be a useful tool in developing a range of alternative policy based emissions scenarios which can be used to provide information to policy makers as well as to address the uncertainties associated with estimating future emissions. As discussed in the introduction, O_3 and $PM_{2.5}$ have been shown to negatively impact human health, ecological health, and the economy to different degrees and in different ways. Therefore, in order to determine the overall benefit or harm of these emissions scenarios, future research could include further investigation into the overall health and economic impacts of the emissions scenarios.

4.5 References

Carter, W. P. L. (2000), Documentation of the SAPRC-99 chemical mechanism for VOC reactivity assessment, University of California, Riverside, Riverside, CA.

CEP (2003), Sparse Matrix Operator Kernel Emissions Modeling System (SMOKE) User Manual, edited, Chapel Hill, NC.

Chen, C. C., and Y. T. Chen (2013), Energy recovery or material recovery for MSW treatments?, *Resour. Conserv. Recycl.*, *74*, 37-44, doi:10.1016/j.resconrec.2013.02.003.

Chen, C. H., et al. (2006), Reductions in emissions of local air pollutants and co-benefits of Chinese energy policy: a Shanghai case study, *Energy Policy*, *34*(6), 754-762, doi:10.1016/j.enpol.2004.07.007.

Dholakia, H. H., et al. (2013), Impact of current policies on future air quality and health outcomes in Delhi, India, *Atmospheric Environment*, *75*, 241-248, doi:10.1016/j.atmosenv.2013.04.052.

Dudhia, J. (1989), Numerical study of convection observed during the winter monsoon experiment using a mesoscale two-dimensional model, *J. Atmos. Sci.*, *46*(20), 3077-3107

Ek, M. B., et al. (2003), Implementation of Noah land surface model advances in the National Centers for Environmental Prediction operational mesoscale Eta model, *Journal of Geophysical Research-Atmospheres*, *108*(D22), 16, doi:8851 10.1029/2002jd003296.

Farooq, M. K., et al. (2013), Energy, environmental and economic effects of Renewable Portfolio Standards (RPS) in a Developing Country, *Energy Policy*, *62*, 989-1001, doi:10.1016/j.enpol.2013.07.098.

Fishbone, L. G., et al. (1980), MARKAL, a Multiperiod Linear-Programming Model for Energy-Systems Analysis Applied to the United-States, *Bulletin of the American Physical Society*, *25*(4), 494-495

Foley, K. M., et al. (2001), Incremental testing of the Community Multiscale Air Quality (CMAQ) modeling system version 4.7, *Geoscientific Model Development*, *3*(1), 205-226

Gielen, D., and C. H. Chen (2001), The CO2 emission reduction benefits of Chinese energy policies and environmental policies: A case study for Shanghai, period 1995-2020, *Ecol. Econ.*, *39*(2), 257-270, doi:10.1016/s0921-8009(01)00206-3.

Hong, S. Y., et al. (2006), A new vertical diffusion package with an explicit treatment of entrainment processes, *Mon. Weather Rev.*, *134*(9), 2318-2341

Jacob, D. J., and D. A. Winner (2009), Effect of climate change on air quality, *Atmospheric Environment*, *43*(1), 51-63, doi:10.1016/j.atmosenv.2008.09.051.

Kain, J. S., and J. M. Fritsch (1993), Convective parameterization models: The Kain–Fritsch scheme. Cumulus Convection in Numerical Models, *American Meteorological Society*, *46*, 165-170

Lamarque, J. F., et al. (2011), Global and regional evolution of short-lived radiatively-active gases and aerosols in the Representative Concentration Pathways, *Clim. Change*, *109*(1-2), 191-212, doi:10.1007/s10584-011-0155-0.

Leung, L. R., and W. I. Gustafson (2005), Potential regional climate change and implications to US air quality, *Geophysical Research Letters*, *32*(16), 4, doi:L16711 10.1029/2005gl022911.

Liao, K. J., et al. (2006), Impact of Climate Change on Sulfur and Nitrogen Deposition in the U.S, paper presented at 86th AMS Annual Meeting, Atlanta, GA.

Liao, K. J., et al. (2007), Sensitivities of ozone and fine particulate matter formation to emissions under the impact of potential future climate change, *Environmental Science & Technology*, *41*(24), 8355-8361, doi:10.1021/es070998z.

Lim, S. S., et al. (2012), A comparative risk assessment of burden of disease and injury attributable to 67 risk factors and risk factor clusters in 21 regions, 1990-2010: a systematic analysis for the Global Burden of Disease Study 2010 (vol 380, pg 2224, 2012), *Lancet*, *381*(9874), 1276-1276

Lin, Y. L., et al. (1983), Bulk parameterization of the snow field in a cloud model, *Journal of Climate and Applied Meteorology*, *22*(6), 1065-1092, doi:10.1175/1520-0450(1983)022<1065:bpotsf>2.0.co;2.

Liu, P., et al. (2012), Differences between downscaling with spectral and grid nudging using WRF, *Atmospheric Chemistry and Physics*, *12*(8), 3601-3610, doi:10.5194/acp-12-3601-2012.

McCollum, D. L., et al. (2013), Climate policies can help resolve energy security and air pollution challenges, *Clim. Change*, *119*(2), 479-494, doi:10.1007/s10584-013-0710-y.

Mickley, L. J. (2007), A future short of breath? Possible effects of climate change on smog, *Environment*, *49*(6), 34-43

Mlawer, E. J., et al. (1997), Radiative transfer for inhomogeneous atmospheres: RRTM, a validated correlated-k model for the longwave, *Journal of Geophysical Research-Atmospheres*, *102*(D14), 16663-16682, doi:10.1029/97jd00237.

Moss, R. H., et al. (2010), The next generation of scenarios for climate change research and assessment, *Nature*, *463*(7282), 747-756, doi:10.1038/nature08823.

Rudokas, J. (2013), Regional Air Quality Management Aspects of Global Change:Impact of Climate Mitigation Options on Regional Air Emissions, In Review

Schmidt, G. A., et al. (2013), Configuration and assessment of the GISS ModelE2 contributions to the CMIP5 archive, *J. Adv. in Modeling Earth Systems, Submitted*

Schwartz, J., et al. (1994), Accute effects of summer air-pollution on respiratory symptom reporting in children, *Am. J. Respir. Crit. Care Med.*, *150*(5), 1234-1242

Shrestha, R. M., and S. Rajbhandari (2010), Energy and environmental implications of carbon emission reduction targets: Case of Kathmandu Valley, Nepal, *Energy Policy*, *38*(9), 4818-4827, doi:10.1016/j.enpol.2009.11.088.

Skamarock, W. C., and J. B. Klemp (2008), A time-split nonhydrostatic atmospheric model for weather research and forecasting applications, *Journal of Computational Physics*, *227*(7), 3465-3485, doi:10.1016/j.jcp.2007.01.037.

Tagaris, E., et al. (2007), Impacts of global climate change and emissions on regional ozone and fine particulate matter concentrations over the United States, *Journal of Geophysical Research-Atmospheres*, *112*(D14), D14312, doi:10.1029/2006JD008262.

Trail, M., Tsimpidi, A. P., Liu, P., Tsigaridis, K., Hu, Y., Nenes, A., and Russell, A. G. (2013), Downscaling a global climate model to simulate climate change impacts on US regional and urban air quality, *Geosci. Model Dev.*, *6*, 1429-1445, doi:10.5194/gmd-6-1429-2013.

Weaver, C. P., et al. (2009), A preliminary synthesis of modeled climate change impacts on US regional ozone concentrations, *Bulletin of the American Meteorological Society*, *90*(12), 1843-1863, doi:10.1175/2009bams2568.1.

Woo, J. H., et al. (2008), Development of North American Emission Inventories for Air Quality Modeling under Climate Change, *Journal of the Air & Waste Management Association*, *58*(11), 1483-1494, doi:10.3155/1047-3289.58.11.1483.

CHAPTER 5

POTENTIAL IMPACT OF LAND USE CHANGE ON FUTURE REGIONAL CLIMATE IN THE SOUTHEASTERN U.S.: REFORESTATION AND CROP LAND CONVERSION[4]

Abstract

The impact of future land use and land cover changes (LULCC) on regional and global climate is one of the most challenging aspects of understanding anthropogenic climate change. We study the impacts of LULCC on regional climate in the southeastern U.S. by downscaling the NASA Goddard Institute for Space Studies (GISS) global climate model E to the regional scale using a spectral nudging technique with the Weather Research and Forecasting (WRF) Model. Climate-relevant meteorological fields are compared for two Future southeastern U.S. LULCC scenarios to the current land use/cover for four seasons of the year 2050. In this work it is shown that pine reforestation of cropland in the southeastern U.S. tends to warm surface air by up to 0.5 K while replacing forested land with cropland tends to cool the surface air by 0.5 K. Processes leading to this response are investigated and sensitivity analyses conducted. The sensitivity analysis shows that results are most sensitive to changes in albedo and the stomatal resistance. Evaporative cooling of croplands also plays an important role in regional climate. Implications of LULCC on air quality are discussed. Summertime warming associated with pine reforestation of croplands could increase the production of

[4] A modified version of this chapter has been published in (2013) Potential impact of land use change on future regional climate in the Southeastern U.S.: Reforestation and crop land conversion, *Journal of Geophysical Research: Atmospheres*, *Early View*, doi:10.1002/2013JD020356.

some secondary pollutants while a higher boundary layer will decrease pollutant concentrations; wintertime warming may decrease emissions from biomass burning from wood stoves.

5.1 Introduction

Humans have changed the global environment for centuries and our impact has intensified over recent decades due to increased population and intensification of industrial activity. A considerable forcing for global change is land use and land cover changes (LULCC). The impact of future LULCC on atmospheric temperatures and global climate is of growing interest as it can impact human and ecosystem health. Increased importance has been given to the study of LULCC impact on climate at a regional level rather than studying the changes in the global mean radiative forcing because "it is the regional responses, not a global average, that produce drought, floods, and other societally important climate impacts" [*Mahmood et al.*, 2010]. The National Research Council (NRC) recently reported that "Improving societally relevant projections of regional climate impacts will require a better understanding of the magnitudes of regional forcings and the associated climate responses" [*NRC*, 2005]. The NRC includes LULCC as an area that has an impact on climate which is highly variable by region.

Beginning in the 1700s and continuing through the 19th century, the southeastern U.S. underwent intense land use and land cover changes [*Chen et al.*, 2006b; *Pacala et al.*, 2001; *Prestemon and Abt*, 2002; *Steyaert and Knox*, 2008; *Wear and Greis*, 2002]. The South experienced forest clearing from the 1700s up to the 1930s, a trend which has

been reversed in the past few decades with the growth of the timber industry [*Wear and Greis*, 2002]. Even though there has been significant reforestation since 1930, the 214 million acres of currently forested land in the South only constitutes 60 % of the forested land that existed in 1630 [*Wear and Greis*, 2002]. The Southeast now produces 60% of the nation's timber products [*Prestemon and Abt*, 2002] and in the past 30 years, pine plantations have rapidly increased (from 2 million acres in 1953 to more than 30 million acres in 1999) [*Conner and Hartsell*, 2002.]. These trends are slated to continue given the growing demand to develop forest-to-fuel technologies, as well as to increase wood products-related industries. While changes in mobile source fuels may lead to improvements in global climate (or decreases in the projected warming trend) [*Bull*, 1996; *Leiby and Rubin*, 2003], the implications of LULCC with regard to climate change are less understood [*Akhtar et al.*, 2008; *IPCC*, 2007; *Jihee et al.*, 2008; *Skamarock et al.*, 2005; *Stooksbury*, 2008].

Climate impacts of global- and regional-scale LULCC have been studied using both observations and models [*Beltran-Przekurat et al.*, 2012; *Cai and Kalnay*, 2004; *Chase et al.*, 2000; *Christy et al.*, 2006; *Davin and de Noblet-Ducoudre*, 2010; *Fall et al.*, 2010b; *Kalnay and Cai*, 2003; *Lawrence and Chase*, 2010; *Nunez et al.*, 2008; *Pielke et al.*, 2011]. Global LULCC studies have shown that afforestation at high latitudes typically tends to warm the atmosphere while afforestation at equatorial latitudes tends to cool. The effects of afforestation at mid-latitudes however are highly uncertain. Bala et al. [*Bala et al.*, 2007] used the Lawrence Livermore National Laboratory INCCA (Integrated Climate and Carbon) model [*Bala et al.*, 2005; *Thompson et al.*, 2004] to simulate the interactions within the climate system including those from LULCC. They

found that while the decrease in carbon uptake due to global deforestation would have a warming effect, the biophysical (albedo) changes would induce cooling that would overwhelm the warming associated with carbon in most areas of the globe, particularly in Northern high latitudes. Fall et al.[2010] used observation minus reanalysis (OMR) methods to estimate the impacts of historical land cover changes on temperature trends in North America. Fall et al. determined in their study that historical warming trends can be explained on the basis of LULCC and that climate models should include LULCC along with the typical greenhouse-gas driven radiative forcings. Arora and Montenegro [2011] also simulate future global warming in their study to investigate the impacts of potential realistic LULCC scenarios, rather than extreme cases such as complete deforestation, on climate, where they conclude that any global cooling associated with realistic afforestation is not large enough to take the place of global greenhouse-gas emissions reductions.

More recent global LULCC studies have analyzed the impacts of biophysical changes that impact radiative processes (albedo) as well as those that impact nonradiative processes, such as partitioning of sensible and latent heat transfer [*Davin and de Noblet-Ducoudre*, 2010; *Lawrence and Chase*, 2010]. Davin et al. [2010] used the Institut Pierre-Simon (IPSL) climate model [*Marti*, 2005] to investigate the climate impacts of individual biophysical parameters associated with LULCC. The study reveals the significance of changes in evaporation and surface roughness as well as albedo on climate. Similarly, Lawrence et al. [2010] use the Community Climate System Model [*Lawrence and Chase*, 2007] to show that, in some afforested regions, nonradiative processes like evapotranspiration can have a cooling effect that overwhelms warming

associated with decreased albedo. Beltran-Przekurat et al. [2012] also focused on analyzing the effects of changes in heat flux partitioning, surface roughness and albedo on temperature but concentrated over a region in South America. They found that changes in regional climate are correlated with changes in diurnal heat flux partitioning.

In this chapter, we use the spectral nudging technique for dynamic downscaling of global model results to the regional scale and compare resulting climate relevant meteorological fields of two southeastern U.S. LULCC scenarios and a base case scenario for four seasons of the year 2050. The downscaling technique used is a type 4 as discussed by [*Castro et al.*, 2005]. In our previous work [*Liu et al.*, 2012] we examined the performance of two nudging techniques, grid and spectral nudging, by downscaling NCEP/NCAR data using the Weather Research and Forecasting (WRF) Model and showed that spectral nudging can outperform grid nudging at the small scale while preserving the large scale features. We also compare future versus present day downscaled meteorological fields in previous work [*Trail*, 2013] using spectral nudging to downscale the NASA Goddard Institute for Space Studies (GISS) global climate model E results during the years 2006 to 2010 and 2048 to 2052 over the continental United States and predicted an average warming of 1-3 °C during the summer and fall in the southeastern U.S. In this study, we use the same approach to simulate meteorological fields for the year 2050 for current day LULCC, a reforested Southeast scenario, and an increased cropland scenario. The role of specific processes and parameters are investigated. We also discuss some of the implications of LULCC on regional air quality. The downscaling technique and choice of physics parameterizations used were

evaluated in Trail et al [2013] by comparing them with in situ observations for the present year.

5.2 Model Approach

5.2.1 *Global Model*

Lateral boundary and initial conditions for the regional forecast modeling are taken from the GISS ModelE2 [*Schmidt*, 2013]. The model has a horizontal resolution of 2°×2.5° latitude by longitude. The model has 40 layers which follow a sigma coordinate up to 150 hPa, with constant pressure layers between 150 and 0.1 hPa. Simulations are carried out for the calendar years 2006-2010 and 2048-2052 with a 3 year spinup time for each period, driven by possible future atmospheric conditions over the 21st century and follow the scenario development process for IPCC AR5. This study uses the "Representative Concentration Pathway" (RCP) 4.5 scenario [*Lamarque et al.*, 2011; *Moss et al.*, 2010] where global emissions of greenhouse gases, short-lived species, and land-use-land-cover produce an anthropogenic radiative forcing at 4.5 W m^{-2} (approximately 650 ppm CO_2-equivalent) in the year 2100 [2010]. Physical and chemical parameters were produced at 6-hour intervals for regional downscaling by WRF (section 2.2). Further details of the global simulations can be found in Trail et al. [2013].

5.2.2 *Regional Model*

The Weather Research and Forecasting (WRF) Model [*Skamarock and Klemp*, 2008] version 3.4 is used as the regional simulation model. The modeling domain

includes the contiguous United States (CONUS) and southern Canada and northern Mexico. The domain is centered at 40°N and 97°W with dimensions of 164×138 horizontal grids cells (5940×5004 km) with 36-km horizontal grid-spacing and the top level at 50hPa (~15.9 km above ground) (**Figure 5-1**). Planetary boundary layer dynamics are simulated using the Yonsei University (YSU) [*Hong et al.*, 2006] scheme; the Noah scheme [*Ek et al.*, 2003] is used for land surface model (LSM). The long-wave Rapid Radiative Transfer Model (RRTM) [*Mlawer et al.*, 1997] and Dudhia scheme [*Dudhia*, 1989] are used for longwave and shortwave radiation respectively. A revised version of the Kain-Fritsch scheme [*Kain J. S.*, 1993] is used to represent the effects of both deep and shallow cumulus clouds while cloud microphysics are simulated based on Lin *et al.* [1983].

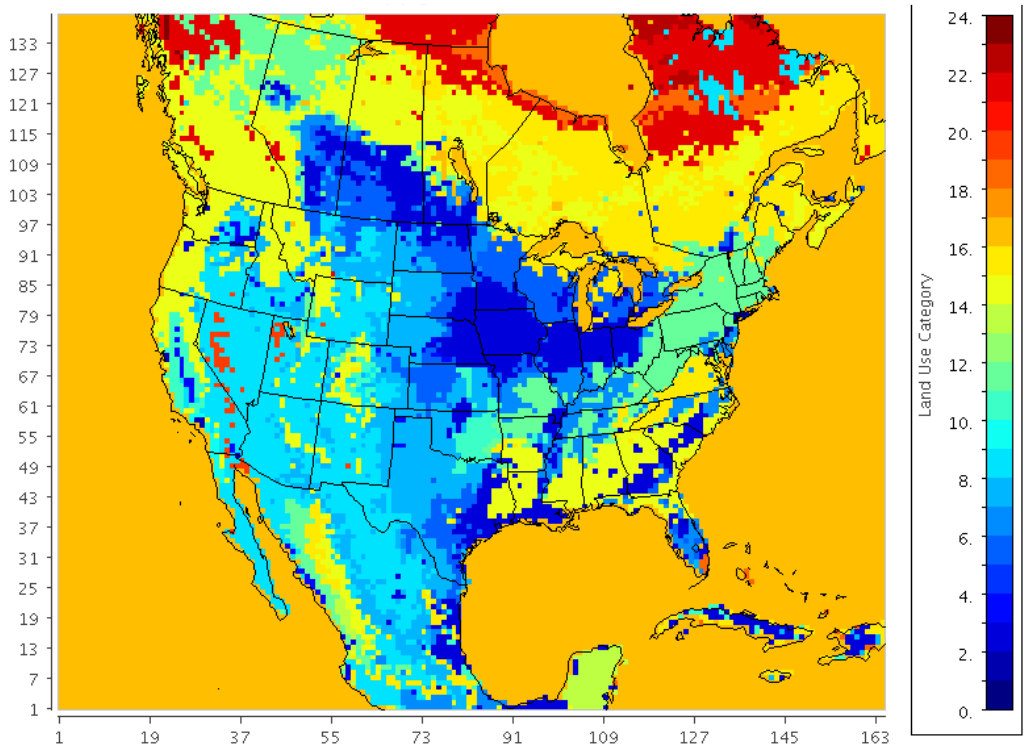

Figure 5-1 Original dominant land use map of the base case simulation. The area of the tested LULCC scenarios is also shown (red dashed box). Land use category numbers from legend correspond to categories in **Table 5-1**.

Key parameters used by WRF associated with LULCC that impact climate include albedo, stomatal resistance (RS), leaf area index (LAI), and surface roughness (Z^0) [*Pielke et al.*, 1998]. Albedo is the fraction of solar energy reflected. Stomatal resistance refers to the leaf's resistance to release moisture into the atmosphere, affecting whether energy is released as sensible or latent heat. Leaf area index is defined as the one-sided green leaf area per unit ground surface area (LAI = leaf area / ground area, m^2/m^2). The LAI and stomatal resistance are used by the Noah scheme to calculate transpiration via the Jarvis mechanism which also takes into account water availability, photosynthetically active radiation (PAR), and CO_2 concentration. Surface roughness is a parameter used to calculate the turbulent diffusion of energy and represents the height

of the land cover, and affects whether energy is transferred to the atmosphere as sensible or latent heat. Here, the MM5 Monin-Obukhov surface layer scheme in WRF uses the surface roughness to calculate latent and sensible heat flux via standard similarity functions.

In the USGS 24-category landuse dataset, the standard data currently used for WRF simulations, the Southeast is primarily made up of evergreen needleleaf forest, dryland cropland and pasture, deciduous broadleaf forest, and mixtures of these. Two southeastern LULCC scenarios and a base scenario were simulated in this study (Figure 5-2): one in which all types of current cropland are replaced by evergreen needleleaf ("SE_for"), and one in which all types of forest or forest mixture are replaced by dryland cropland and pasture ("SE_crop"). Evergreen needleleaf forest is chosen due to its commercial use in the timber industry. Typically, loblolly pine is used for tree farms and reforestation for commercial use. However, it should be noted that other common tree types can be used for reforestation, which would lead to different results than presented in this chapter. Evergreen needleleaf forest in the USGS dataset is a combination of the various species of evergreen needleleaf trees and does not differentiate loblolly and slash pine from other species, which may have different physiological characteristics. Loblolly and slash pine make up the majority of the species of pine in the Southeast. Dryland cropland and pasture in the USGS dataset includes semi-irrigated crops, or crops that are irrigated with overhead sprinklers, which make up most of the cropland in the Southeast. There is an irrigated cropland category but this refers to heavily irrigated crops such as rice paddies and is not prevalent in the Southeast where crops are made up of cotton, wheat, corn and others. The base case simulation will be referred to as SE_norm.

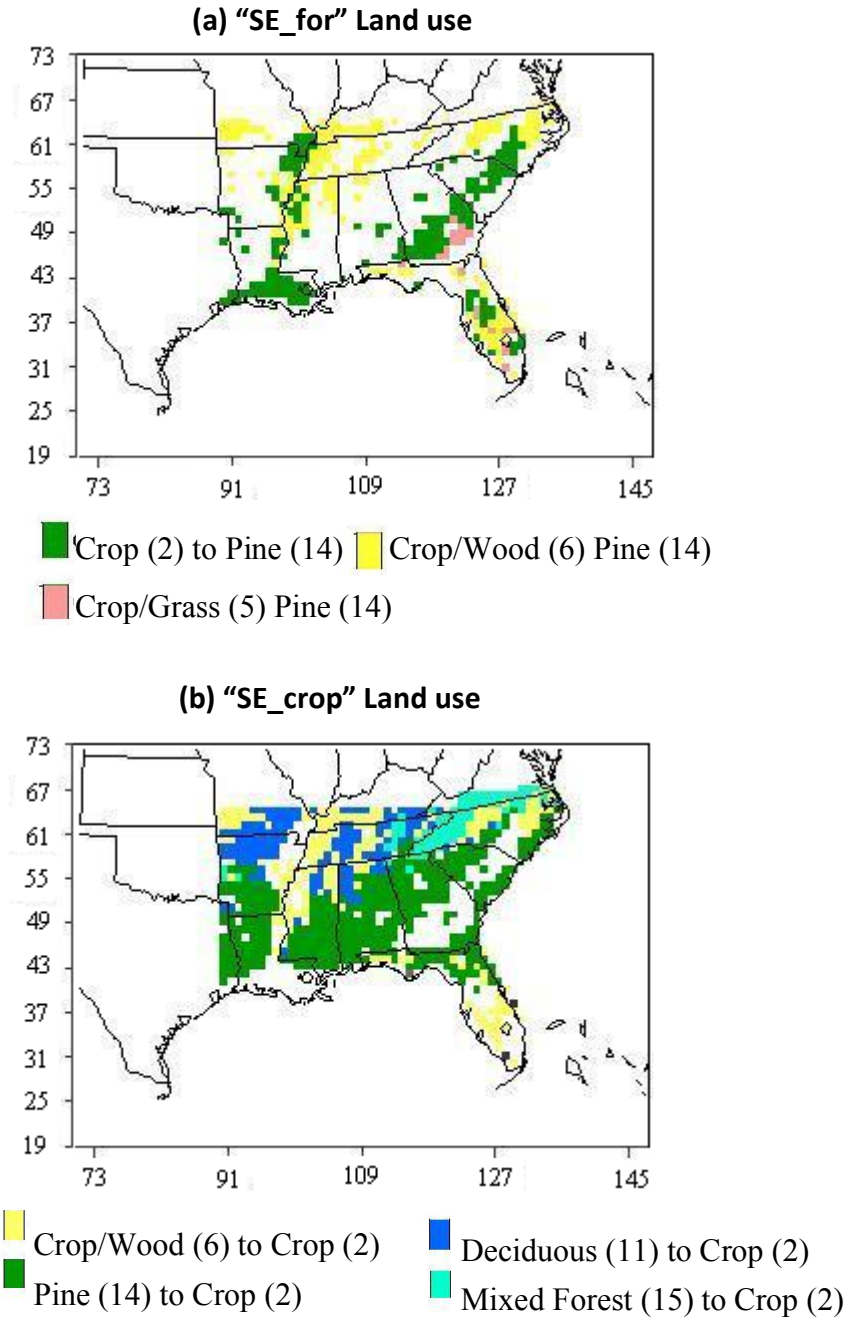

Figure 5-2 Spatial maps of the dominant land use covers that changed to pine **(a)** and crop **(b)** in the SE_for and SE_crop scenario respectively. Land use category numbers in parentheses correspond to categories in **Table** 5-1

In addition, sensitivity analyses are conducted to determine which model land use parameters have the greatest influence on regional climate, and how changes in those parameters affect results. We calculated the sensitivity of regional meteorological variables to individual parameters including surface roughness height (Z^0), albedo, leaf area index (LAI), emissivity, and stomatal resistance (RS). Wintertime (DJF) and summertime (JJA) sensitivities to a parameter are calculated by changing the dryland/cropland parameter of interest to that of evergreen needleleaf land cover, and separately to that of deciduous broadleaf forest. Sensitivity simulations are conducted for three-month periods. Table 5-1 contains details of the vegetative parameters and Table 5-2 contains the sensitivity test parameters. The resulting seasonal mean meteorology is then compared to the base case meteorology over regions where dryland/cropland is the dominant land use.

We do not include simulated changes in atmospheric composition-induced radiative forcing due to LULCC, such as the change in greenhouse gases due to carbon uptake of crops and forests, or the changes in the direct and indirect aerosol effect associated with changes in biogenic emissions and air quality.

Table 5-1 USGS Land use categories and relevant WRF parameters [a]

	Land use Category	RS	LAIMIN (area/area)	LAIMAX (area/area)	ALBEDO MIN	ALBEDO MAX	Z0MIN (m)	Z0MAX (m)
1	'Urban and Built-Up Land'	200	1	1	0.15	0.15	0.5	0.5
2	'Dryland Cropland and Pasture'	40	1.56	5.68	0.17	0.23	0.05	0.15
3	'Irrigated Cropland and Pasture'	40	1.56	5.68	0.2	0.25	0.02	0.1
4	'Mixed Dry/Irr. Cropland and Pasture'	40	1	4.5	0.18	0.23	0.05	0.15
5	'Cropland/Grassland Mosaic'	40	2.29	4.29	0.18	0.23	0.05	0.14
6	'Cropland/Woodland Mosaic'	70	2	4	0.16	0.2	0.2	0.2
7	'Grassland'	40	0.52	2.9	0.19	0.23	0.1	0.12
8	'Shrubland'	300	0.5	3.66	0.25	0.3	0.01	0.05
9	'Mixed Shrubland/Grassland'	170	0.6	2.6	0.22	0.3	0.01	0.06
10	'Savanna'	70	0.5	3.66	0.2	0.2	0.15	0.15
11	'Deciduous Broadleaf Forest'	100	1.85	3.31	0.16	0.17	0.5	0.5
12	'Deciduous Needleleaf Forest'	150	1	5.16	0.14	0.15	0.5	0.5
13	'Evergreen Broadleaf Forest'	150	3.08	6.48	0.12	0.12	0.5	0.5
14	'Evergreen Needleleaf Forest'	125	5	6.4	0.12	0.12	0.5	0.5
15	'Mixed Forest'	125	2.8	5.5	0.17	0.25	0.2	0.5
16	'Water Bodies'	100	0.01	0.01	0.08	0.08	0.0001	0.0001
17	'Herbaceous Wetland'	40	1.5	5.65	0.14	0.14	0.2	0.2
18	'Wooded Wetland'	100	2	5.8	0.14	0.14	0.4	0.4
19	'Barren or Sparsely Vegetated'	999	0.1	0.75	0.38	0.38	0.01	0.01
20	'Herbaceous Tundra'	150	0.41	3.35	0.15	0.2	0.1	0.1
21	'Wooded Tundra'	150	0.41	3.35	0.15	0.2	0.3	0.3
22	'Mixed Tundra'	150	0.41	3.35	0.15	0.2	0.15	0.15
23	'Bare Ground Tundra'	200	0.41	3.35	0.25	0.25	0.05	0.1
24	'Snow or Ice'	999	0.01	0.01	0.55	0.7	0.001	0.001

[a]Parameters include stomatal resistance (RS), maximum and minimum leaf area index (LAIMAX, LAIMIN), maximum and minimum albedo (ALBEDOMAX, ALBEDOMIN), and maximum and minimum roughness height (Z0MAX, Z0MIN).

Table 5-2 Parameterizations used for each of the sensitivity analyses [b]

	'Dryland Cropland and Pasture' parameters						
Sensitivity Case	RS	LAIMIN (area/area)	LAIMAX (area/area)	ALBEDO MIN	ALBEDO MAX	Z0MIN (m)	Z0MAX (m)
Base	40	1.56	5.68	0.17	0.23	0.05	0.15
ALBp	40	1.56	5.68	**0.12**	**0.12**	0.05	0.15
Z^0p	40	1.56	5.68	0.17	0.23	**0.5**	**0.5**
RSp	**125**	1.56	5.68	0.17	0.23	0.05	0.15
LAIp	40	**5**	**6.4**	0.17	0.23	0.05	0.15
ALBd	40	1.56	5.68	**0.16**	**0.17**	0.05	0.15
Z^0d	40	1.56	5.68	0.17	0.23	**0.5**	**0.5**
RSd	**100**	1.56	5.68	0.17	0.23	0.05	0.15
LAId	40	**1.85**	**3.31**	0.17	0.23	0.05	0.15

[b] Parameters include minimum stomatal resistance (RS), maximum and minimum leaf area index (LAIMAX, LAIMIN), maximum and minimum albedo (ALBEDOMAX, ALBEDOMIN), and maximum and minimum roughness height (Z0MAX, Z0MIN). The name of each sensitivity case begins with the parameter that changed and ends with "p" or "d" indicating whether the new parameter is from the pine (p) or deciduous (d) land use category. The affected parameters in each case are highlighted in bold.

5.2.3 *Dynamical downscale of global results*

Spectral nudging is used with a wave number of 2 in both zonal and meridional directions to account for the large scale GCM simulation, but allow the small scale features expected from LULCC in the southeastern U.S. to freely develop [*Liu et al.*, 2012]. In other words, no nudging is conducted at wavelengths shorter than the preset value. A wavelength of 2 corresponds to about 1500 km, which is larger than the spatial scale of changes simulated here. Spectral nudging is applied to temperature, horizontal winds, and geopotential height. No nudging is conducted for variables within the planetary boundary layer (PBL), with the exception of the horizontal winds which are nudged at all vertical levels. The nudging coefficient for all nudged variables was set to

$3x10^{-4}$ s^{-1} [*Stauffer and Seaman*, 1990]. Nudging is conducted every 6 h during the simulation, consistent with the frequency of the global model data.

Trail et al. [2013] found that the model predictions agree well with observations when conducted for 2010. They show that the simulated temperature agrees best with surface observations over the southern U.S., particularly during summer. Simulated wind speed had a root mean square error (RMSE) as low as 2.2 m s^{-1} over the South. Details of the base simulation are given in chapter 2.

5.3 Results

5.3.1 *Southeast reforestation scenario ("SE_for")*

5.3.1.1 Land cover change and affected parameters

The two major LULCC occurring in the Southeast reforestation scenario are the conversion of dryland/cropland and pasture to evergreen needleleaf forest (which will be referred to as "crop" and "pine", respectively) and conversion of cropland/woodland mosaic (or "crop/wood") to pine (Figure 5-2). It is important to note that crop/wood has parameters that represent a combination of not only crop and pine, but also of deciduous broadleaf forest. There is also a small region in south Georgia where cropland/grassland mosaic is converted to pine, however this region is small compared to the other two LULCC. A large region of crop is converted to pine in southern Louisiana and continuing north along the western borders of Mississippi and Tennessee. Crop is also converted to pine in Florida and in a large region beginning in south Georgia and continuing in a streaking pattern across the eastern regions of South and North Carolina.

Crop/wood is converted to pine in the northern regions of the land cover change area including Missouri, Tennessee, and North Carolina, as well as regions in western Mississippi and some in the middle of Florida.

In this simulation the albedo of pine is 0.12 all year, meaning that, within that land use category, 12% of the incoming solar radiation is reflected away from the Earth's surface (Table 5-2). The albedo of crop, on the other hand, is higher than pine and changes from 0.17 to 0.23 depending on the time of year, with the lowest albedo occurring when crops are green and the higher when cropland appears whiter and there is increased soil exposure after harvest. Impacts of snow cover on albedo are simulated as well. Correspondingly, in regions where crop is converted to pine, the albedo change causes 10-12% less reflected solar radiation during the winter and fall and only 5-10% less during the spring and summer (Figure D-1a). The albedo of crop/wood varies from 0.16 to 0.2 depending on the time of year and the corresponding decreased albedo and seasonal change is reflected in Figure D-1a over regions where crop/wood is converted to pine.

The LAI is correlated to albedo since a higher leaf area index usually means more green area to absorb sunlight. However, the combined effect of LAI and stomatal resistance plays another important role in climate because it drives sensible and latent heat flux partitioning via transpiration. Heat flux partitioning, in turn, strongly impacts temperature and planetary boundary layer (PBL) dynamics [*Pielke et al.*, 1998]. In WRF, the RS is calculated using the Jarvis mechanism where a minimum RS is adjusted by various forcings (ie, sunlight, temperature, relative humidity, and soil moisture availability). RS for crop and pine are 40 and 125 s m^{-1} respectively. In other words,

pine trees are more resistant to releasing water and latent heat than crops. During the winter, the LAI increases by up to 4 units (leaf area per area) in regions where the land cover is converted to pine (Figure D-1b). Similar to the change in albedo, the difference in LAI decreases during the spring and more so during the summer as crops grow and produce more leaves. During summer, in regions where crop changes to pine, the difference in LAI is only slightly positive (less than 1 unit area area^{-1}), while the LAI difference is higher (up to 2.5 units area area^{-1}) in regions where crop/wood changes to pine. We see a greater difference in LAI over regions where crop/wood changes to pine during the summer because, as mentioned earlier, crop/wood includes some parameters from deciduous broadleaf forest which has a lower LAI than that of pine.

Changing surface roughness impacts turbulence within the boundary layer which affects the transfer of momentum, heat and water vapor from the Earth's surface. Increasing Z^0 causes more energy to be transferred as latent heat and less as sensible heat. However, the direct implications with regard to climate change are not very well known [*Davin and de Noblet-Ducoudre*, 2010]. The Z^0 of pine and crop/wood remain constant throughout the year at 0.5 m and 0.2 m, respectively while the Z^0 of crop (between 0.05 and 0.15 m) is smaller during the winter (Table 5-1). Again, as crops grow during the spring and summer, the difference in Z^0 decreases slightly in regions where crop is converted to pine.

5.3.1.2 Impacts on Meteorology

A heating pattern of up to 0.5 degrees occurs during the winter over most of the areas where crop and crop/wood are converted to pine (Figure 5-3a). P-values resulting

from a paired t-test show significant temperature anomalies over regions that are converted to pine (Figure D-2). The average diurnal changes in temperature over regions where crop is converted to pine show that this heating occurs during the day, while at night the temperature does not change nearly so much (Figure D-3 and D-4). The decreased albedo attributed to converting from inactive and exposed soil crop to green pine during the winter drives the heating in these regions (Figure D-1a). However, since Z^0 increases with pine reforestation, the winter heating is diminished slightly, although not overcome, by the increase in latent heat flux via evapotranspiration. Also, the daytime boundary layer height increases by 10% on average where crop is converted to pine because more of the energy flux is realized as sensible heat (Figure D-3) [*Pielke et al.*, 1998]. During the spring we see a similar heating of around 0.3 degrees mostly over regions where crop is converted to pine. We did not find significant changes in precipitation due to the LULCC perturbations.

Interesting patterns of cooling in Louisiana near the Mississippi river (up to 0.5 degrees decrease) and warming in South Carolina and southern Georgia (up to 0.5 degrees increase) over regions where crop is converted to pine occur during the summer and continue through the fall (Figure 5-3a). Changes in precipitation may explain some cooling during the summer when Louisiana receives approximately 2 mm more rain per day in the afforested scenario while net rain near the eastern coast changes little. However, during the fall there is little apparent change in precipitation over the two regions (Figure D-5). Despite little differences in precipitation, there is still an increase in soil moisture in Louisiana during both summer and fall (Figure 5-3b).

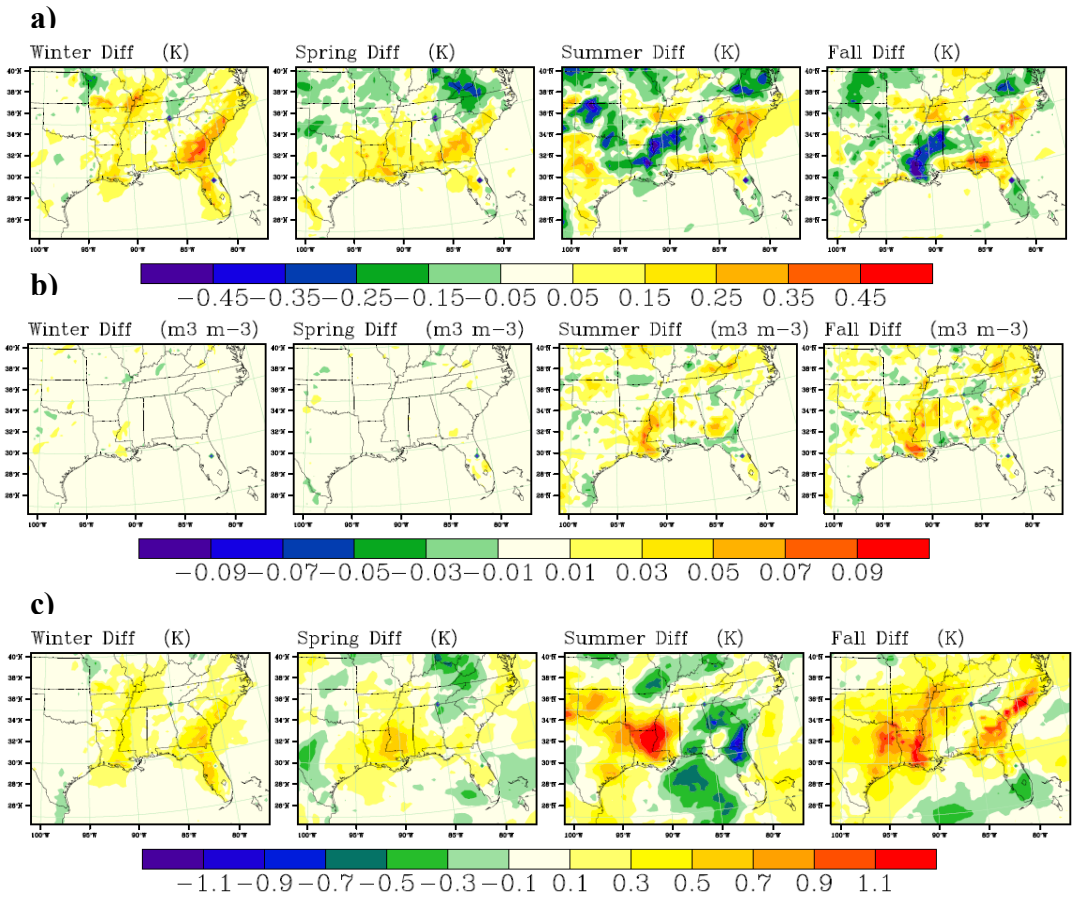

Figure 5-3 (a) Simulated temperature (b) soil moisture (c) and equivalent temperature change of SE_for minus SE_norm scenario during the four seasons of the year 2050.

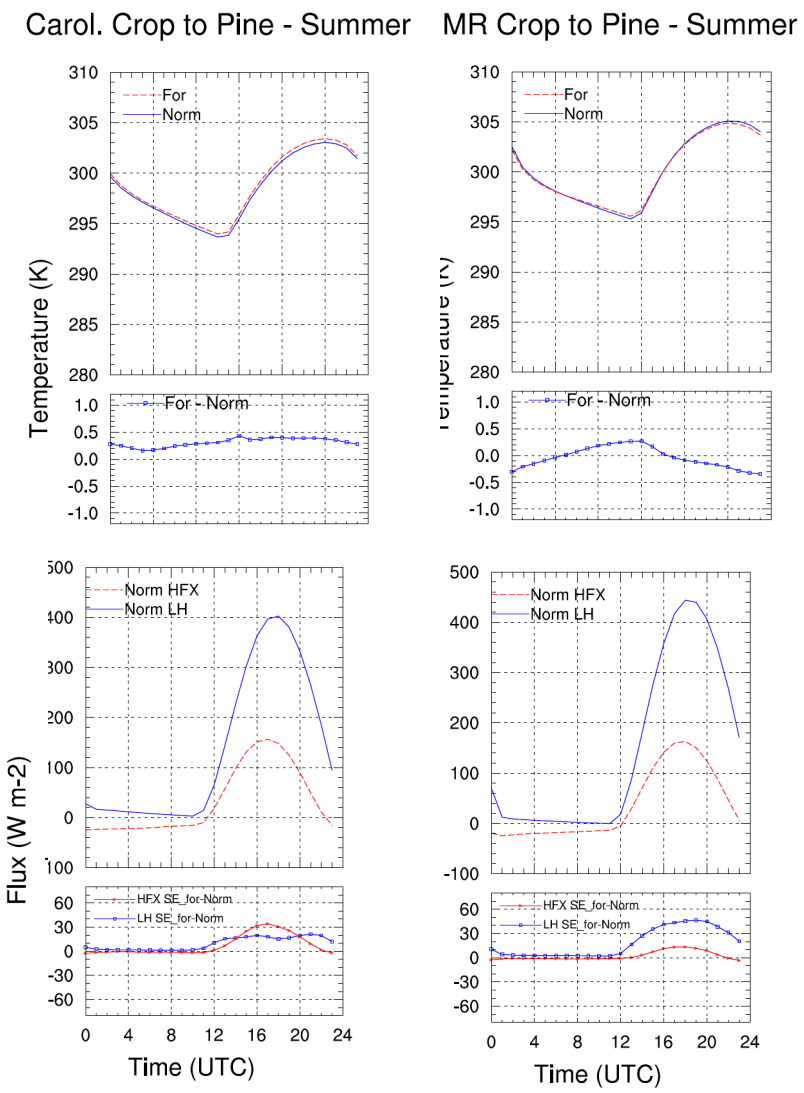

Figure 5-4 Average diurnal temperature and heat flux trends and anomalies over the grid cells where the dominant land use is converted from crop to pine and separated by the Carolinas and Mississippi river (MR) regions during summer of the year 2050. Top row: average diurnal temperature by region and season for "SE_norm" and "SE_for". Second row: average diurnal temperature anomaly by region and season ("SE_for" minus "SE_norm"). Third row: average diurnal sensible (red) and latent (blue) heat flux to the atmosphere for the "SE_norm" case. Bottom row: average diurnal sensible (red) and latent (blue) heat flux anomalies ("SE_for" minus "SE_norm")

Pine has a higher RS and over time, water is allowed to accumulate throughout the season in the soil near the Mississippi river rather than be evaporated. Correspondingly, the diurnal latent heat flux in Louisiana increases during the daytime in the summer, cooling the surface air, while in Georgia and the Carolinas the increase in latent heat flux is not as strong, leading to an increase in sensible heat flux to maintain the energy balance, causing the warming (Figure 5-4). Recent studies show that temperature changes alone do not completely characterize changes in surface air heat content because some energy is stored in moisture in the air. These studies suggest using an equivalent temperature which takes into account the latent heat energy [*Fall et al.*, 2010a]. While cooling occurs during the summer and fall over the Mississippi river, the change in equivalent temperature (Figure 5-3c) shows an increase in surface heat air content equivalent of up to a degree.

5.3.2 *Southeast cropification scenario ("SE_crop")*

5.3.2.1 Land cover change and affected parameters

There are four major LULCC that occur in the Southeast cropification scenario where the following four land covers are converted to dryland/cropland and pasture (or "crop"): evergreen needleleaf forest (or "pine" as before), cropland/woodland mosaic ("crop/wood" as before), deciduous broadleaf forest ("deciduous"), and mixed forest (Figure 5-2). The region where pine is converted to crop, the largest LULCC in this scenario, covers almost all of Louisiana, Mississippi, Alabama, Georgia, and South Carolina except where crop already existed. The pine to crop conversion also extends to southern Arkansas and northern Florida. In this scenario, crop/wood is converted to crop

in the same regions where crop/wood is converted to pine in the Southeast reforestation scenario discussed earlier. Deciduous forest is converted to crop in large regions of northern Arkansas and southern Missouri, as well as some parts of Tennessee. Some mixed forest is converted to crop in eastern Tennessee and parts of North Carolina.

In this scenario the albedo increases for all LULCC and all seasons except for regions where mixed forest is converted to crop (Figure D-6a). The most dramatic increase of albedo is in the large regions where pine is converted, due to the year round low albedo of pine. Spring and summer see a less intense increase (around 5%) in albedo when the crops emerge. Also during the spring and summer, the albedo of crop/wood, deciduous, and mixed forest are all nearly the same as that of crop (0.16 to 0.17 from Table 5-2).

The LAI decreases with the conversion of pine to crop mostly during the winter (up to 3.5 units area area^{-1}), less during the spring and fall (around 2 units area area^{-1}), and only slightly during the summer (less than 1 unit area area^{-1}) (Figure D-6b). The LAI also decreases slightly for all other LULCC during the winter. However, during the summer the LAI increases for all other LULCC with the highest increase over regions where deciduous is converted to crop (more than 2 units area area^{-1}). In this scenario, RS decreases from between 70 and 125 s m^{-1} to 40 s m^{-1}. The surface roughness decreases for all LULCC and for all seasons with the biggest decreases happening during the winter where pine and deciduous change to crop.

5.3.2.2 Impacts on Meteorology

Most regions in the Southeast are cooled with future cropification (**Figure 5-5**a) with the largest and most significant (Figure D-2; p-values < 0.05) decreases occurring during the summer over northern Mississippi and Alabama and southern Tennessee (over 0.6 degree decrease). Similarly, decreases in surface air heat content are found over most of the region of LULCC (Figure 5-5c). During the winter, average cooling during the hottest hour of the day reaches 0.5 degree over regions where pine is converted to crop (Figure D-7). Increases in albedo over regions where deciduous and pine forests are converted to crop drives the cooling during the winter, despite the warming effect that is expected from the decrease in Z^0 and latent heat flux. Also, boundary layer height during the daytime drops by an average of 100 m (more than 10% decrease) where pine changes to crop (Figure D-7), and slightly less where deciduous changes to crop, because boundary layer depth is reduced when less energy flux is realized as sensible heat [*Pielke et al.*, 1998].

In the spring and summer most cooling occurs over regions where deciduous is converted to crop (up to 0.8 degree decrease) and less cooling is seen over other LULCC regions. Cooling in converted deciduous regions is driven by increased albedo and decreased RS. Diurnal heat flux trends (Figure 5-6) show a decrease in sensible heat flux and an increase in latent heat flux, due to the combined effect of albedo change and increased evapotranspiration from combined RS and LAI change. In contrast, regions changed from pine experience less cooling because LAI and Z^0 decreases exert a warming force via latent heat flux decreases (Figure 5-6). There is also less soil moisture available for evaporation due to a decrease in RS in some regions (Figure 5-5b).

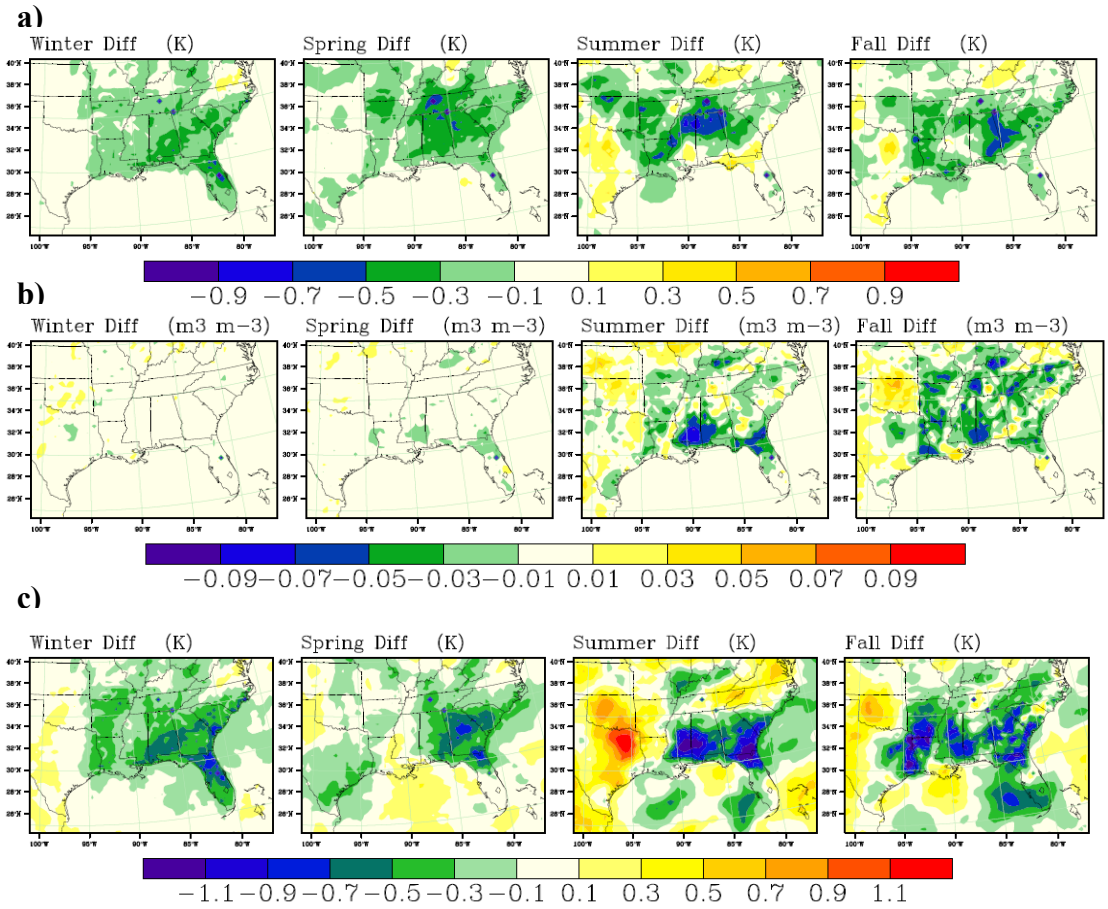

Figure 5-5 Simulated temperature **(a)** soil moisture **(b)** equivalent temperature **(c)** change of SE_crop minus SE_norm scenario during the four seasons of the year 2050.

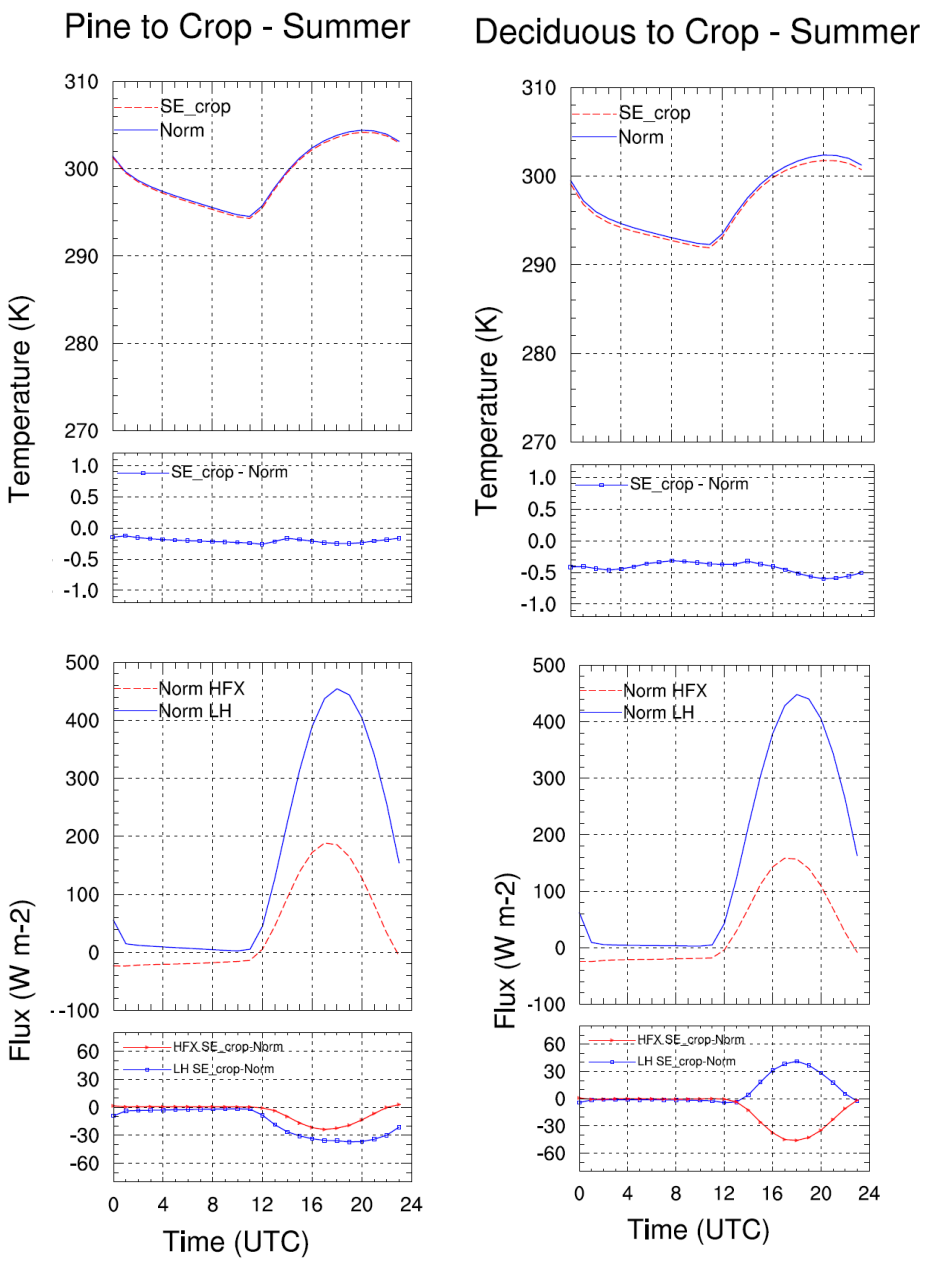

Figure 5-6 Average diurnal temperature and heat flux trends and anomalies over the grid cells where the dominant land use is converted from pine to crop (left column) and from deciduous to crop (right column) during summer of the year 2050. Top row: average diurnal temperature by season for "SE_norm" and "SE_crop". Second row: average diurnal temperature anomaly by season ("SE_crop" minus "SE_norm"). Third row: average diurnal sensible (red) and latent (blue) heat flux to the atmosphere

5.3.3 Integration of Sensitivity Analysis

Analyses were conducted to test the sensitivity of regional climate to albedo, surface roughness, leaf area index, and stomatal resistance. The sensitivity analyses indicate that surface temperatures and energy flux distributions are more sensitive to RS during the summer than all other sensitivity scenarios (Figure 5-7) with average surface temperatures increasing by 0.5 degrees during the daytime. Winter temperature and surface fluxes are not sensitive to RS since evaporation is minimal, as is the related energy flux when crops are not in season. Surface temperature and energy flux over cropland are less sensitive to increasing the cropland LAI as compared to those of pine; however when the cropland LAI is reduced to that of deciduous forest the temperature increases slightly during the summer (Figure D-8). During summer and winter, the daytime surface temperature in grids dominated by cropland increases by 0.2 degrees when crop albedo is replaced by that of pine. The sensible and latent heat fluxes also increase (Figure 5-7 and 5-8). During summer, temperatures tend to decrease due to an increased surface roughness by 0.1 degree while the latent heat is increased and the sensible heat decreased. Temperature and energy fluxes are less sensitive to Z^0 during the winter (Figure 5-8). Sensitivity analyses were also conducted using North American Regional Reanalysis (NARR) data as initial and boundary conditions. These sensitivity analyses were conducted with and without using spectral nudging and using 2010 NARR data (Figures D-9 to D-12). In the case that spectral nudging is used (Figures D-9 and D-10), the sensitivity results are nearly identical to the results using GISS fields as initial and boundary conditions.

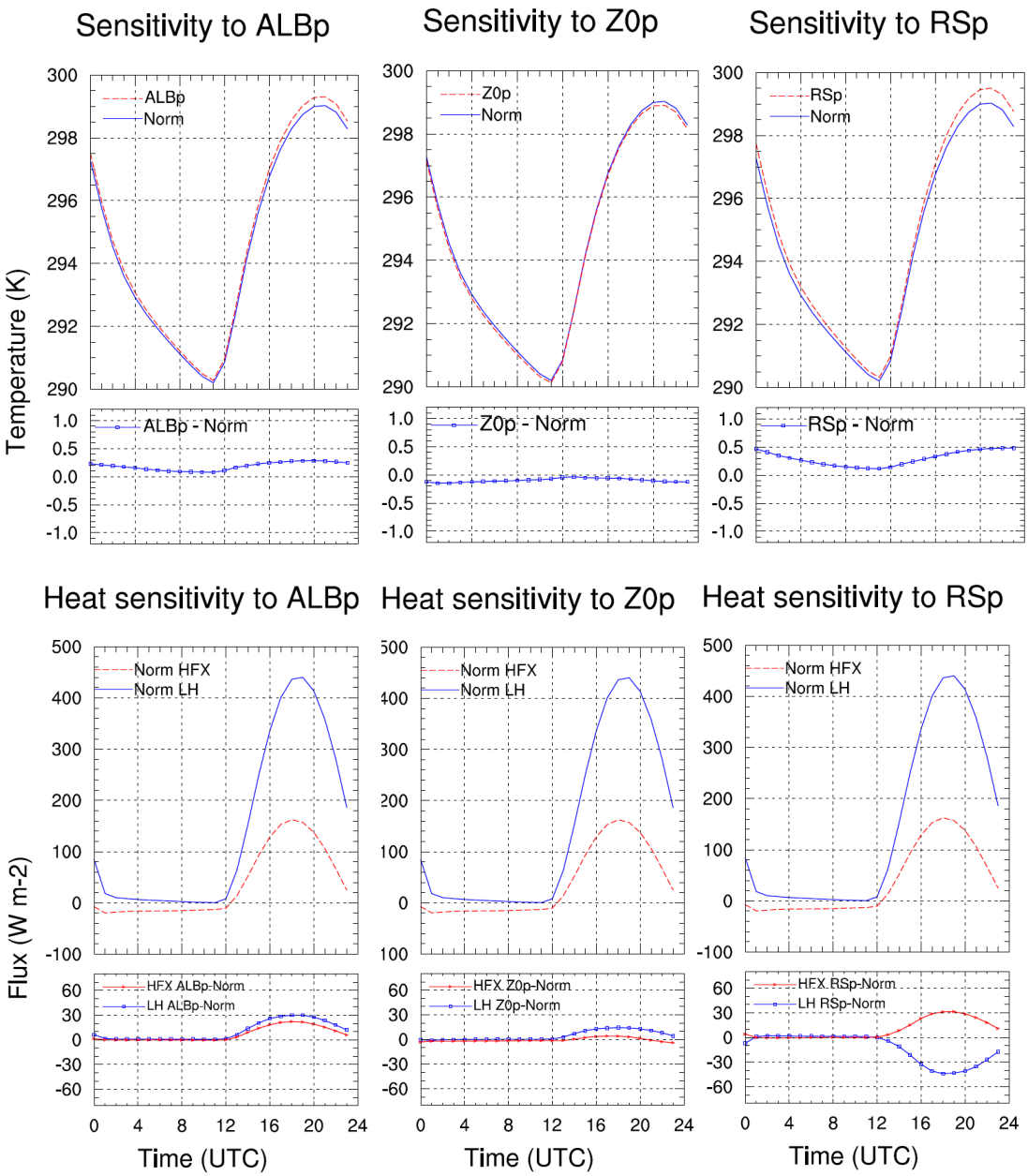

Figure 5-7 Average diurnal temperature and heat flux trends and sensitivities to pine albedo (ALBp), surface roughness (Z^0p), and stomatal resistance (RSp) over the grid cells where the dominant land use is crop during summer of the year 2050. Top row: average diurnal surface temperature of the base case (blue) and the perturbed parameter simulation (red). Second row: average diurnal surface temperature sensitivity (perturbed case minus base case). Third row: average diurnal sensible (red) and latent (blue) heat flux to the atmosphere for the base case. Bottom row: average diurnal sensible (red) and latent (blue) heat flux sensitivities (perturbed case minus base case).

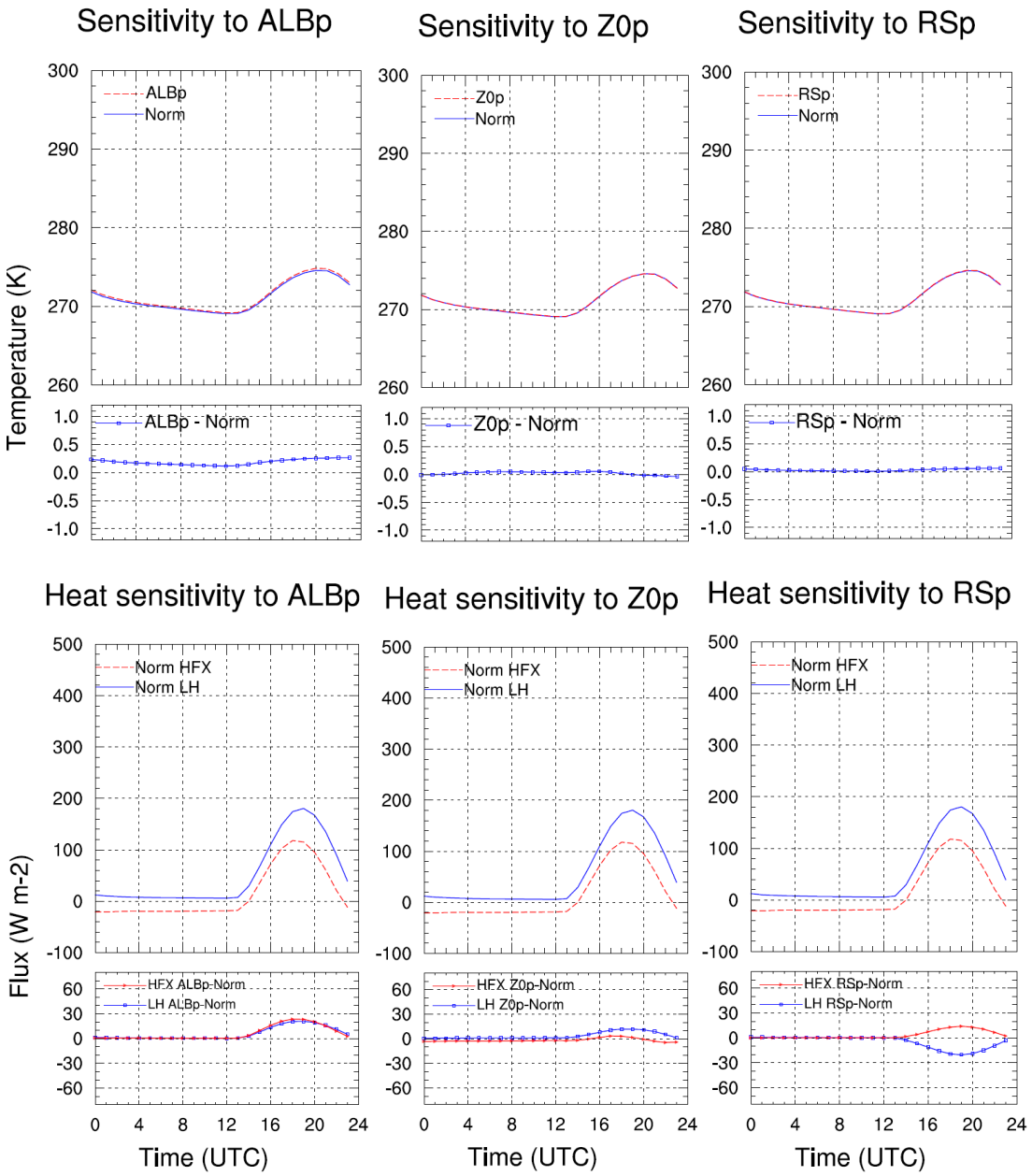

Figure 5-8 Average diurnal temperature and heat flux trends and sensitivities to pine albedo (ALBp), surface roughness (Z^0p), and stomatal resistance (RSp) over grid cells where the dominant land use is crop during winter of the year 2050. Top row: average diurnal surface temperature of the base case (blue) and the perturbed parameter simulation (red). Second row: average diurnal surface temperature sensitivity (perturbed case minus base case). Third row: average diurnal sensible (red) and latent (blue) heat flux to the atmosphere for the base case. Bottom row: average diurnal sensible (red) and latent (blue) heat flux sensitivities (perturbed case minus base case).

With no spectral nudging (Figures D-11 and D-12), we see increased sensitivity of surface temperature to albedo and stomatal resistance, while the sensitivity to surface roughness and leaf area index remain near zero.

5.4 Discussion

The simulated impacts of LULCC in the Southeast on regional climate were expected given the changes in land use parameters (eg. albedo, RS, LAI and Z^0). Reforestation of crop regions in the Southeast with pine forest tends to lead to warming primarily due to the increase of RS and decrease in albedo while the Z^0 increase may lessen the degree of warming by shifting the transfer of energy to the atmosphere from sensible to latent heat. Warming during the spring, summer and fall can enhance the production of O_3 and secondary PM while, on the other hand, the increased boundary layer height can help decrease concentrations. Warming during the winter may influence less use of wood burning stoves and therefore lead to less emission of PM [*Alfarra et al.*, 2007]. This result compares well with other studies on the impacts of reforestation on climate [*Beltran-Przekurat et al.*, 2012; *Betts*, 2000; *Betts et al.*, 2007]. However, over time, reduced transpiration from increased RS can lead to the accumulation of soil moisture in wet areas such that cooling from soil moisture evaporation overcomes the warming from albedo changes, which is the case for the afforested summer and fall in Louisiana near the Mississippi river. Lawrence and Chase [2010] found similar cooling from reforestation.

Our results suggest that cooling tends to occur when forest is replaced with crop in the Southeast, though not enough to counter the simulated warming of 1-3 °C from

green house gas increases [*Trail et al.*, 2013]. Cooling during the winter is attributed to the high albedo of cropland while during the spring and summer the decrease in RS also contributes to cooling. Also increased LAI helps cool where deciduous forests are replaced. These results agree with other studies simulating the impacts of cropification [*Beltran-Przekurat et al.*, 2012; *Davin and de Noblet-Ducoudre*, 2010] as well as looking at historical LULCC and temperature data [*Fall et al.*, 2010b]. Cooling during the winter could lead to more emissions of PM from wood burning while during the rest of the year the rate of production of O_3 and secondary PM could decrease.

While the results of the LULCC study show that reforestation of cropland with pine does not appear to be an effective method for climate mitigation in the Southeast, the sensitivity analysis shows that these results are sensitive to assumed physical parameters. Some recent studies have found significant cooling from reforestation in the Southeast [*Juang et al.*, 2007; *Murphy et al.*, 2012]. In particular, Murphy et al. suggest that the stomatal conductance of loblolly pine, the major species of pine in the Southeast, should be adjusted from the default value and this would lead to more simulated cooling in the Southeast [*Murphy et al.*, 2012]. We assumed the default value for stomatal resistance from the USGS 24-category landuse data for a combined "evergreen needleleaf" category. Thus, further investigation is needed to minimize uncertainty in the stomatal resistance and to consider the physiological differences between actual loblolly pine and the evergreen needleleaf category typically used as well as the physiological differences among the various crops present in the Southeast. Our results suggest that a reduction in the stomatal resistance of pine equivalent to the Murphy simulations would lead to a cooler surface over pine forest. Juang et al. found that in a region of North Carolina, pine

forest tend to be cooler than marginal, or abandoned, fields [*Juang et al.*, 2007]. These fields have less leaf area and lower roughness heights than cropland, and are not subject to irrigation, all of which would tend to make marginal fields warmer than cropland, and potentially warmer than pine forest, especially loblolly pine.

5.5 References

Akhtar, F., et al. (2008), Beyond the standards: Designer Air Quality in 2050, *Bulletin of the American Meteorological Society*, *89*(1), 38-38

Alfarra, M. R., et al. (2007), Identification of the mass spectral signature of organic aerosols from wood burning emissions, *Environmental Science & Technology*, *41*(16), 5770-5777, doi:10.1021/es062289b.

Bala, G., et al. (2005), Multiceutury changes to the global climate and carbon cycle: Results from a coupled climate and carbon cycle model, *Journal of Climate*, *18*(21), 4531-4544, doi:10.1175/jcli3542.1.

Bala, G., et al. (2007), Combined climate and carbon-cycle effects of large-scale deforestation, *Proc. Natl. Acad. Sci. U. S. A.*, *104*(16), 6550-6555, doi:10.1073/pnas.0608998104.

Beltran-Przekurat, A., et al. (2012), Modelling the effects of land-use/land-cover changes on the near-surface atmosphere in southern South America, *Int. J. Climatol.*, *32*(8), 1206-1225, doi:10.1002/joc.2346.

Betts, R. A. (2000), Offset of the potential carbon sink from boreal forestation by decreases in surface albedo, *Nature*, *408*(6809), 187-190, doi:10.1038/35041545.

Betts, R. A., et al. (2007), Biogeophysical effects of land use on climate: Model simulations of radiative forcing and large-scale temperature change, *Agric. For. Meteorol.*, *142*(2-4), 216-233, doi:10.1016/j.agrformet.2006.08.021.

Bull, S. R. (1996), Renewable energy transportation technologies, *Renewable Energy*, *9*(1-4), 1019-1024

Cai, M., and E. Kalnay (2004), Climate - Impact of land-use change on climate - Reply, *Nature*, *427*(6971), 214-214, doi:10.1038/427214a.

Castro, C. L., et al. (2005), Dynamical downscaling: Assessment of value retained and added using the regional atmospheric modeling system (RAMS), *Journal of*

Geophysical Research-Atmospheres, *110*(D5), 21, doi:D05108 10.1029/2004jd004721.

Chase, T. N., et al. (2000), Simulated impacts of historical land cover changes on global climate in northern winter, *Climate Dynamics*, *16*(2-3), 93-105, doi:10.1007/s003820050007.

Chen, H., et al. (2006), Effect of land-cover change on terrestrial carbon dynamics in the southern United States, *J. Environ. Qual.*, *35*(4), 1533-1547, doi:10.2134/jeq2005.0198.

Christy, J. R., et al. (2006), Methodology and results of calculating central california surface temperature trends: Evidence of human-induced climate change?, *Journal of Climate*, *19*(4), 548-563, doi:10.1175/jcli3627.1.

Conner, R. C., and A. J. Hartsell (2002.), The Southern Forest Resource Assessment: Chapter 16, Forest Area and Conditions, Department of Agriculture, Forest Service, Southern Research Station,.

Davin, E. L., and N. de Noblet-Ducoudre (2010), Climatic Impact of Global-Scale Deforestation: Radiative versus Nonradiative Processes, *Journal of Climate*, *23*(1), 97-112, doi:10.1175/2009jcli3102.1.

Dudhia, J. (1989), Numerical study of convection observed during the winter monsoon experiment using a mesoscale two-dimensional model, *J. Atmos. Sci.*, *46*(20), 3077-3107

Ek, M. B., et al. (2003), Implementation of Noah land surface model advances in the National Centers for Environmental Prediction operational mesoscale Eta model, *Journal of Geophysical Research-Atmospheres*, *108*(D22), 16, doi:8851 10.1029/2002jd003296.

Fall, S., et al. (2010a), Temperature and equivalent temperature over the United States (1979-2005), *Int. J. Climatol.*, *30*(13), 2045-2054, doi:10.1002/joc.2094.

Fall, S., et al. (2010b), Impacts of land use land cover on temperature trends over the continental United States: assessment using the North American Regional Reanalysis, *Int. J. Climatol.*, *30*(13), 1980-1993, doi:10.1002/joc.1996.

Hong, S. Y., et al. (2006), A new vertical diffusion package with an explicit treatment of entrainment processes, *Mon. Weather Rev.*, *134*(9), 2318-2341

IPCC (2007), Climate Change 2007 IPCC Fourth Assessment Report: Synthesis Report, 184 pp, IPCC, Geneva, Switzerland.

Jihee, S., et al. (2008), The Impacts of Urbanization on Emissions and Air Quality: Comparison of Four Visions of Austin, Texas, *Environmental Science & Technology*, *42*(19), 7294-7300

Juang, J. Y., et al. (2007), Separating the effects of albedo from eco-physiological changes on surface temperature along a successional chronosequence in the southeastern United States, *Geophysical Research Letters*, *34*(21), 5, doi:L21408 10.1029/2007gl031296.

Kain J. S., F. J. M. (1993), Convective parameterization models: The Kain–Fritsch scheme. Cumulus Convection in Numerical Models, *American Meteorological Society*, *46*, 165-170

Kalnay, E., and M. Cai (2003), Impact of urbanization and land-use change on climate, *Nature*, *423*(6939), 528-531, doi:10.1038/nature01675.

Lamarque, J. F., et al. (2011), Global and regional evolution of short-lived radiatively-active gases and aerosols in the Representative Concentration Pathways, *Clim. Change*, *109*(1-2), 191-212, doi:10.1007/s10584-011-0155-0.

Lawrence, P. J., and T. N. Chase (2007), Representing a new MODIS consistent land surface in the Community Land Model (CLM 3.0), *J. Geophys. Res.-Biogeosci.*, *112*(G1), 17, doi:G01023 10.1029/2006jg000168.

Lawrence, P. J., and T. N. Chase (2010), Investigating the climate impacts of global land cover change in the community climate system model, *Int. J. Climatol.*, *30*(13), 2066-2087, doi:10.1002/joc.2061.

Leiby, P. N., and J. Rubin (2003), Transitions in light-duty vehicle transportation - Alternative-fuel and hybrid vehicles and learning, in *Energy, Air Quality, and Fuels 2003*, edited, pp. 127-134.

Lin, Y. L., et al. (1983), Bulk parameterization of the snow field in a cloud model, *Journal of Climate and Applied Meteorology*, *22*(6), 1065-1092, doi:10.1175/1520-0450(1983)022<1065:bpotsf>2.0.co;2.

Liu, P., et al. (2012), Differences between downscaling with spectral and grid nudging using WRF, *Atmospheric Chemistry and Physics*, *12*(8), 3601-3610, doi:10.5194/acp-12-3601-2012.

Mahmood, R., et al. (2010), Impacts of land use/land cover change on climate and future research priorities, *Bulletin of the American Meteorological Society*, *91*(1), 37-+, doi:10.1175/2009bams2769.1.

Marti, O., and Coauthors (2005), The new IPSL climate system model: IPSL-CM4, *Note du Pole de Modelisation 26*, 86

Mlawer, E. J., et al. (1997), Radiative transfer for inhomogeneous atmospheres: RRTM, a validated correlated-k model for the longwave, *Journal of Geophysical Research-Atmospheres*, *102*(D14), 16663-16682, doi:10.1029/97jd00237.

Moss, R. H., et al. (2010), The next generation of scenarios for climate change research and assessment, *Nature*, *463*(7282), 747-756, doi:10.1038/nature08823.

Murphy, L. N., et al. (2012), Local and Remote Climate Impacts from Expansion of Woody Biomass for Bioenergy Feedstock in the Southeastern United States, *Journal of Climate*, *25*(21), 7643-7659, doi:10.1175/jcli-d-11-00535.1.

NRC (2005), Radiative Forcing of Climate Change: Expanding the Concept and Addressing Uncertainties, *National Research Council*, 208

Nunez, M. N., et al. (2008), Impact of land use and precipitation changes on surface temperature trends in Argentina, *Journal of Geophysical Research-Atmospheres*, *113*(D6), 11, doi:D06111 10.1029/2007jd008638.

Pacala, S. W., et al. (2001), Consistent land- and atmosphere-based US carbon sink estimates, *Science*, *292*(5525), 2316-2320, doi:10.1126/science.1057320.

Pielke, R. A., et al. (1998), Interactions between the atmosphere and terrestrial ecosystems: influence on weather and climate, *Glob. Change Biol.*, *4*(5), 461-475, doi:10.1046/j.1365-2486.1998.t01-1-00176.x.

Pielke, R. A., et al. (2011), Land use/land cover changes and climate: modeling analysis and observational evidence, *Wiley Interdiscip. Rev.-Clim. Chang.*, *2*(6), 828-850, doi:10.1002/wcc.144.

Prestemon, J. P., and R. C. Abt (2002), The Southern timber market to 2040, *Journal of Forestry*, *100*(7), 16-22

Schmidt, G. A., et al (2013), Configuration and assessment of the GISS ModelE2 contributions to the CMIP5 archive, *J. Adv. Modeling Earth Systems, in preparation*

Skamarock, W., et al. (2005), A Description of the Advanced Research WRF Version 2.

Skamarock, W. C., and J. B. Klemp (2008), A time-split nonhydrostatic atmospheric model for weather research and forecasting applications, *Journal of Computational Physics*, *227*(7), 3465-3485, doi:10.1016/j.jcp.2007.01.037.

Stauffer, D. R., and N. L. Seaman (1990), Use of a 4-dimensional data assimilation in a limeted-area mesoscale model .1. Experiments with synoptic-scale data, *Monthly Weather Review*, *118*(6), 1250-1277, doi:10.1175/1520-0493(1990)118<1250:uofdda>2.0.co;2.

Steyaert, L. T., and R. G. Knox (2008), Reconstructed historical land cover and biophysical parameters for studies of land-atmosphere interactions within the eastern United States, *Journal of Geophysical Research-Atmospheres*, *113*(D2), 27, doi:D02101 10.1029/2006jd008277.

Stooksbury, D. (2008), A Primer on Drought History In Georgia, in *Georgia Climate and AIr Quality Summit*, edited, Atlanta, GA.

Thompson, S. L., et al. (2004), Quantifying the effects of CO2-fertilized vegetation on future global climate and carbon dynamics, *Geophysical Research Letters*, *31*(23), 4, doi:L23211 10.1029/2004gl021239.

Trail, M., Tsimpidi, A. P., Liu, P., Tsigaridis, K., Hu, Y., Nenes, A., and Russell, A. G. (2013), Downscaling a global climate model to simulate climate change impacts on US regional and urban air quality, *Geosci. Model Dev.*, *6*, 1429-1445, doi:10.5194/gmd-6-1429-2013.

Wear, D. N., and J. G. Greis (2002), Southern Forest Resource Assessment - Summary of findings, *Journal of Forestry*, *100*(7), 6-14

CHAPTER 6

REFORESTATION AND CROP LAND CONVERSION IMPACTS ON FUTURE REGIONAL AIR QUALITY IN THE SOUTHEASTERN U.S.

Abstract

Possible future $PM_{2.5}$ and O_3 air quality for two LULCC scenarios, reforestation and cropland conversion, are compared to a reference case scenario for the year 2050 using the Community Multi-scale Air Quality (CMAQ) model. Changes in air quality driven by changes in climate, deposition and emissions relating to the LULCC scenarios are investigated. Results to a climate and deposition (CD) sensitivity simulation are provided for the two alternative LULCC scenarios to isolate the impact of changing climate and deposition on $PM_{2.5}$ and O_3 air quality. Reforestation with loblolly pine in the southeast tends to decrease the ambient O_3 mixing ratio while slightly increasing summertime $PM_{2.5}$ in the Southeastern U.S. We find that deposition and emissions changes associated with reforestation impact O_3 and $PM_{2.5}$ concentrations as much as, and in most cases more than, changes in meteorology. Conversion of forest to cropland in the Southeast, on the other hand, tends to increase O_3 and increase $PM_{2.5}$ year-round. Cropland conversion leads to increased NO_X emissions and increases in the 4^{th} highest maximum daily 8-hr O_3 (MDA8) of the year by up to 10 ppb despite the tendency for increased deposition and decreased temperature to reduce the MDA8 mixing ratio. The results of this study show that O_3 and aerosol concentrations are highly sensitive to reforestation and cropland conversion in the Southeast and these land use changes should be considered in air quality management plans.

6.1 Introduction

Land use and land cover changes (LULCC) affect air pollution, which has been linked to premature death (cite), as well as global and regional climate. The southeastern U.S. underwent intense land use and land cover changes beginning in the 1700's [*Chen et al.*, 2006b; *Pacala et al.*, 2001; *Prestemon and Abt*, 2002; *Steyaert and Knox*, 2008; *Wear and Greis*, 2002] and changes are expected to continue given the growing demand to develop forest-to-fuel technologies. Physical parameters of certain crops and forests such as albedo, stomatal resistance and surface roughness affect climate by altering the land-atmosphere energy transfer [*Pielke et al.*, 1998] while land cover changes also effect the deposition of O_3 and $PM_{2.5}$ by altering the surface area and roughness for dry deposition of pollutants. Changes in stomatal activity also effect the deposition of O_3 and other gases. Various vegetative species also emit volatile organic compounds (VOCs), precursors for ozone and secondary organic aerosol (SOA), and nitric oxide (NO), which becomes a precursor for ozone, at different rates [*Henze et al.*, 2008; *Houweling et al.*, 1998; *Liao et al.*, 2007a; *Racherla and Adams*, 2006; *Wang et al.*, 1998].

Currently, there are 214 million acres of forested land in the South. This constitutes only 60% of the forested land that existed in 1630 despite significant reforestation due to the growth of the timber industry since 1930 [*Wear and Greis*, 2002]. Around 60% of the nation's timber products are produced in the Southeast [*Prestemon and Abt*, 2002] causing pine plantations to rapidly increase in the past few decades (from 2 million acres in 1953 to more than 30 million acres in 1999) [*Conner and Hartsell*, 2002.]. The growing demand to increase wood products-related industries and to develop forest-to-fuel technologies and bio-fuels from crops will continue to alter the land cover,

and therefore the air quality, in the Southeast. Although changes in mobile source fuels may lead to decreases in the projected warming trend [*Bull*, 1996; *Leiby and Rubin*, 2003], the use of bio-energy in the future may lead to worsened PM air quality [Trail et al. 2014, submitted]. Still, the impact that LULCC associated with bio-energy demand will have on future air quality is not well understood.

Although few studies have focused on investigating the impact of vegetative LULCC on air quality in the Southeastern U.S., recent studies have addressed LULCC on a regional scale in other regions [*Jiang et al.*, 2008] and on a global scale [*Ganzeveld and Lelieveld*, 2004; *Wu et al.*, 2008]. Wu et al. [2012] found that potential global land cover changes caused by warmer climate and increased CO_2 abundance could lead to a general decrease in summertime afternoon O_3 by up to 10 ppb. They report that the O_3 decreases are driven by increased O_3 dry deposition associated with increased vegetation density. In polluted regions, such as the northeastern U.S., however, O_3 and SOA increased due to higher isoprene emissions. Ganzeveld and Lelieveld [2004] found that deforestation in the Amazon Basin could decrease global isoprene emissions and O_3 deposition. Jiang et al. [2008] use the Weather Research Forecasting model with Chemistry (WRF/CHEM) to compare current and future air quality changes associated with climate change and land use change. They report that changing climate and urban land use can increase the daily maximum 8-hr O_3 mixing ratio by up to 6.2 ppb.

In this study, we use the Community Multi-scale Air Quality (CMAQ) model to compare possible future $PM_{2.5}$ and O_3 air quality for two LULCC scenarios to a reference case scenario for the year 2050. We investigate changes in air quality driven by changes in climate, deposition and emissions relating to the LULCC. We also provide results to

climate and deposition (CD) sensitivity simulations for the two alternative LULCC scenarios to isolate the impact of changing climate and deposition on $PM_{2.5}$ and O_3 air quality. Inputs to CMAQ were prepared for a pine reforestation scenario, a cropland conversion scenario, and the current land cover (reference) scenario and include the regionally downscaled future climate results by the Weather Research Forecasting (WRF) model from Trail et al. [2013] and emissions processed using the Sparse Matrix Operator Kernel Emissions (SMOKE) model. Energy related anthropogenic emissions inventories are projected to the future year levels using MARKAL 9R [Rodukus et al, submitted]. The present study expands upon previous work [Trail et al, submitted; Trail et al., submitted] in which we used the emissions inventories projected by MARKAL 9R to investigate the impact of various climate change mitigation strategies on U.S. air quality.

6.2 Methods

6.2.1 Meteorology

We use the non-hydrostatic Weather Research and Forecasting (WRF) Model [*Skamarock and Klemp*, 2008] (version 3.4) to downscale global climate to the regional scale. Initial and boundary conditions to the WRF are derived from meteorology simulated by the Goddard Institute for Space Studies (GISS) ModelE2 [*Schmidt et al.*, 2013]. Global simulations were carried out for the years 2006-2010 and 2048-2052 with a 3 year spin-up time and instantaneous outputs of physical parameters were produced at 6-hr intervals for regional downscaling by WRF. Simulations were driven by future atmospheric conditions over the 21st century and follow the scenario development process for IPCC AR5. The "Representative Concentration Pathway" (RCP) 4.5

[*Lamarque et al.*, 2011; *Moss et al.*, 2010], where anthropogenic radiative forcing is 4.5 W m^{-2} in the year 2100 [*Moss et al.*, 2010], is used for this study. The global model domain has a horizontal resolution of 2°×2.5° latitude by longitude. The 40 layers of the global simulation follow a sigma coordinate up to 150 hPa, with constant pressure layers between 150 and 0.1 hPa.

Trail et al. [2013] simulated regional climate for the years 2006-2010 and 2048-2052 with 10 day spinup times, however the present study uses the meteorological results from the year 2050. The model domain covers the contiguous United States (CONUS) and portions of southern Canada and northern Mexico with dimensions of 164×138 horizontal grids cells and a grid-spacing of 36 km centered at 40°N and 97°W. The model domain contains 35 vertical levels, with the top pressure of 50hPa. The model scheme uses the Rapid Radiative Transfer Model (RRTM) [*Mlawer et al.*, 1997] and Dudhia scheme [*Dudhia*, 1989] for longwave and shortwave radiation respectively, the Yonsei University (YSU) [*Hong et al.*, 2006] scheme for the planetary boundary layer, the Noah scheme [*Ek et al.*, 2003] for the land surface model (LSM), a revised version of Kain-Fritsch scheme [*Kain and Fritsch*, 1993] to represent the effects of both deep and shallow cumulus clouds, and Lin *et al.* [*Lin et al.*, 1983] for modeling cloud microphysics. Spectral nudging of global model results is applied with a wave number of 2 in both zonal and meridional directions at 6 hour intervals [*Liu et al.*, 2012]. Spectral nudging is applied to horizontal winds at all vertical levels while temperature and geopotential heights are only nudged at layers above the planetary boundary layer (PBL). Trail et al. [2013] evaluated the ability of GISS-WRF to reproduce the long-term yearly climatic means and the meteorological fields.

WRF simulations use the USGS 24-category landuse dataset. In this dateset, evergreen needleleaf forest, dryland cropland and pasture, deciduous broadleaf forest, and mixtures of these are the primary land cover categories in the Southeast U.S. In this study, we use the meteorology from two southeastern LULCC scenarios and a base scenario described in Trail et al. [2013]. The reforestation scenario uses the meteorology simulated by converting all types of current cropland to evergreen needleleaf (referred to as "SE_for" in Trail et al. [2013]), and the cropland conversion scenario uses meteorology simulated by converting all types of forest or forest mixture to dryland cropland and pasture (referred to as "SE_crop" in Trail et al. [2013]). Although, in reality, loblolly and slash pine make up the majority of the pine species in the Southeast, the USGS-24 category database does not differentiate between the species. Also, most of the cropland in the Southeast is made up of crops that are irrigated with overhead sprinklers, or semi-irrigated crops which are included in the dryland cropland category of the USGS dataset. The base case meteorology, referred to as SE_norm in Trail et al. [2013], will be used for the reference case in the present study.

Trail et al. [2013] found that reforestation of crop regions in the Southeast tends to lead to warming primarily due to the increase of RS and decrease in albedo while the Z^0 increase may lessen the degree of warming by shifting the transfer of energy to the atmosphere from sensible to latent heat. Our results suggest that cooling tends to occur when forest is replaced with crop in the Southeast; though not enough to counter the simulated warming of 1-3 °C from greenhouse gas increases [*Trail et al.*, 2013]. Cooling during the winter is attributed to the high albedo of cropland while during the spring and

summer the decrease in RS also contributes to cooling. Also increased LAI helps cool where deciduous forests are replaced.

6.2.2 Emissions

The Sparse Matrix Operator Kernel Emissions (SMOKE V3) model [*CEP*, 2003] produces hourly, gridded and speciated emissions for input to CMAQ. SMOKE uses inputs of the 2005 National Emissions Inventory (NEI) and ancillary data. To project emissions to 2050 levels, energy related emissions projection factors are calculated using EPA MARKAL 9R model for the year 2050. MARKAL 9R [*Fishbone et al.*, 1980] models the energy system of the nine Census Divisions of the U.S. and estimates future energy dynamics. Implementation of the following policies were assumed in calculating the future emissions projections in MARKAL 9R: Clean Air Act Title IV (Acid Rain Program) SO_2 and NO_X requirements, Clean Air Interstate Rule (CAIR), Utility Mercury and Air Toxics Standards (MATS), Aggregated state Renewable Portfolio (RPS) standards by region, Federal Corporate Average Fuel Economy (CAFE) standards as modeled in AEO 2012, Tier 2 light duty vehicle tailpipe emission standards and heavy duty vehicle fuel and engine rules. Non-energy related emissions were projected to 2050 according to the International Panel for Climate Change (IPCC) A1B scenario [*Woo et al.*, 2008]. Trail et al. [2014, submitted] provide a summary of changes in future anthropogenic emission rates and a sensitivity assessment of their impacts on air quality.

Hourly emissions from U.S. vegetation are computed using the Biogenic Emissions Inventory System (BEIS) and the Biogenic Emissions Landcover Database 3.0 (BELD3). The resulting inventory consists of pollutants emitted from area, mobile, point,

fire, ocean, biogenic, and agricultural sources. The BELD3 database consists of 229 categories, including 17 crop types, 193 species of tree and 19 USGS categories. For every grid cell in the domain, each vegetation category is designated a percentage value corresponding to the percent of the land covered by a particular vegetation class in that grid cell. The primary tree species in the Southeast are loblolly and jack pine while crops in the Southeast are more variant by region and include tobacco, wheat, cotton, corn, soybean and others. Each vegetation type has corresponding emission factors for 34 chemical species including isoprene, carbon monoxide and nitric oxide (Table 6-1). In developing the biogenic emissions for the reforestation scenario, all crops in the Southeast domain were converted to loblolly pine since loblolly pine is commonly used in the timber industry (Figure 6-1a). Biogenic emissions for the cropland conversion scenario were developed by converting all tree species to the most common crop within a particular grid cell (Figure 6-1b). For example, if 60% of the land in a grid cell is covered by tree species, 20% is urban, 15% is corn and 5% is cotton, then the 60% of land covered by trees will be changed to corn. In this scenario, tree species are overwhelmingly converted to corn with some land being converted to cotton (Figure 6-1b and c). Biogenic emissions changes in this study do not include altered emissions from wildfires and prescribed burns related to reforestation and cropland conversion.

Table 6-1 Emission rates of Isoprene and NO for the vegetation categories that change the most in the LULCC scenarios.

	Isoprene (gC/km2 hr)	Nitric Oxide (gN/km2 hr)
Loblolly Pine	70	2
Corn	1	68
Cotton	7	45

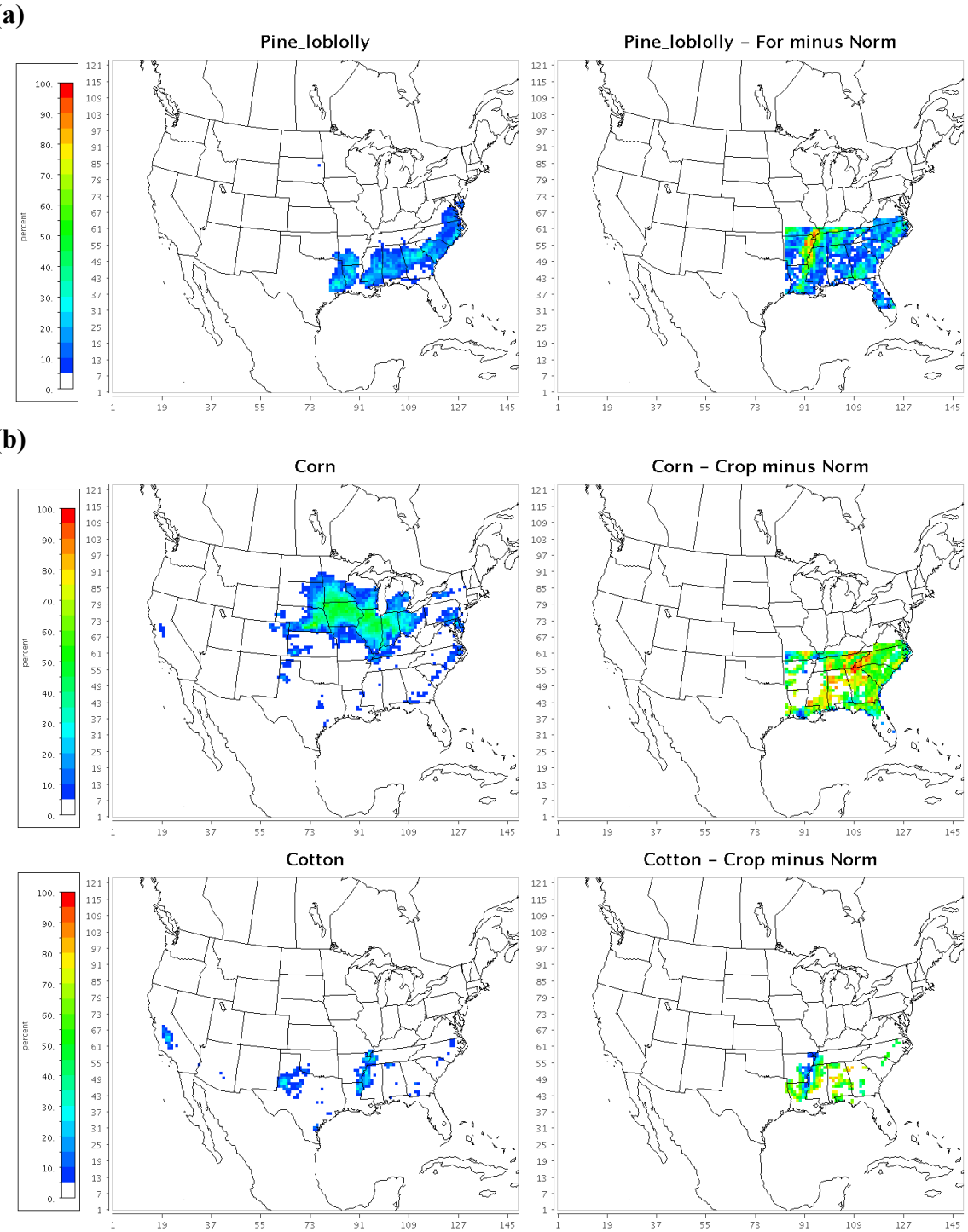

Figure 6-1 (a) Percentage of loblolly pine in the original BELD3 landuse dataset (left) and the change in loblolly pine for the reforestation scenario (right). **(b)** Percentage of corn (top) and cotton (bottom) crop in the original BELD3 dataset (left column) and the change in corn and cotton crop for the cropland conversion scenario (right column).

6.2.3 Air Quality

We use the CMAQ 4.7.1 [*Foley et al.*, 2001] to simulate the transformation and fate of air pollutants for the future (2050) reference case and for the two LULCC scenarios. A spin-up period of 10 days for each simulation minimizes the influence of the initial conditions. Gas-phase chemistry is modeled using the SAPRC-99 [*Carter*, 2000] chemical mechanism. The domain covers the entire contiguous U.S. as well as portions of Canada and Mexico (5328×4032 km). The modeling domain uses a Lambert Conformal Projection with true latitudes of 33ºN and 45ºN centered at 40ºN, 97ºW. A horizontal grid-spacing of 36-km is used with thirteen vertical layers extending ~15.9 km above ground. There are 7 layers below 1 km and the first layer is 18 m thick. Future dynamic boundary conditions are taken from the GISS global simulation while the default CMAQ initial conditions of pollutant concentrations are used here.

In addition to the two LULCC scenarios, which span the entire year 2050, a climate and deposition (CD) sensitivity case is simulated for a winter (Jan) and a summer (Jul) month to isolate the effects of altered climate and deposition associated with LULCC on ambient air pollutant concentrations. For the CD scenarios, we fix the biogenic emissions for each scenario to the reference case emissions while using the meteorology and deposition from the two LULCC scenarios.

Trail et al. [2014, submitted] provide a detailed description and evaluation of the CMAQ model set up. The CMAQ simulations were evaluated by simulating air quality over the U.S. for the year 2010 using downscaled 2010 global climate and emissions projected to the year 2010 and comparing the results to Environmental Protection Agency (EPA) Air Quality System (AQS) data. Trail et al. [2014, submitted] found that

simulated surface $PM_{2.5}$ and O_3 show good agreement with observations for the year 2010.

6.3 Results

6.3.1 Reforestation

Trail et al. [2014] compared present and future U.S. air quality and found overall decreases in O_3 and $PM_{2.5}$ during summer and small increases in $PM_{2.5}$ during winter. They compare the change in the 4th highest mean daily 8-hr average (MDA8) O_3 mixing ratio of the year, which is the metric used to determine if an area is in non-attainment according to the National Ambient Air Quality Standard (NAAQS). The current NAAQS standard is 75 ppb. In the present study, reforestation with loblolly pine leads to decreased 4th highest MDA8 of the year by up to 10 ppb from the reference case in the Southeast U.S. (Figure 6-2). Decreased 4th highest MDA8 occurs mostly over Mississippi, Alabama, Tennessee, Arkansas, and southern Kentucky while Georgia and the Carolinas experience small decreases. Reforestation of cropland leads to decreased emissions of NO_X and therefore decreased O_3 mixing ratio in NO_X limited environments (Table 6-1). However, land use changes also alter regional meteorology and deposition rates of pollutants.

The CD scenario isolates the impacts of changing meteorology and deposition from land use change to air quality by fixing the emissions to the reference case emissions for one month during the O_3 season. The summertime one-month average MDA8 decreases by up to 3 ppb in the CD scenario over the same regions where the largest decreases in 4th highest MDA8 occur near the Mississippi river (Figure 6-2). In

this region, although some localized deposition decreases are seen, reforestation mostly leads to O_3 deposition increases, leading to more efficient removal of O_3 from the atmosphere (Figure 6-2). Mixed crop/woodland is converted to pine in this region and Trail et al. [2013] predicted potential decreases in daytime temperature due to increased soil moisture and therefore increased evaporation, especially in Mississippi. They predicted that the temperature decreases in this region could lead to lower MDA8 mixing ratio. Therefore, over Arkansas, Tennessee and Kentucky, decreases in the 4th highest MDA8 are caused by decreased emissions of NO, increased deposition from reforestation of crops/woodland areas and decreased daytime temperatures.

Over the Eastern regions of Georgia and the Carolinas on the other hand, summertime one-month average MDA8 increases by up to 3 ppb in the CD scenario. Deposition of O_3 decreases due to reforestation in Georgia and the Carolinas where crop is converted to pine, contributing to the increased MDA8 over those regions (Figure 6-2). Also increased temperature over Georgia and the Carolinas predicted in Trail et al. [2013] may enhance the formation of O_3. In this region, lower NO emissions leads to reduced O_3 mixing ratio, though enhanced formation from climate and reduced removal efficiency from deposition changes would tend to increase ambient levels of O_3.

Summertime (JJA) average $PM_{2.5}$ concentration increases of around 1 $\mu g\ m^{-3}$ occur over the Southeast due to reforestation of croplands with the largest increases over the Mississippi river and in Georgia and South Carolina (Figure 6-3a). Summertime average organic matter (OM) aerosol increases by 0.35 $\mu g\ m^{-3}$ while nitrate and sulfate aerosol concentrations experience small changes (Table 6-2). In the CD scenario however, $PM_{2.5}$ and OM concentrations decrease by around 1 $\mu g\ m^{-3}$ and 0.47 $\mu g\ m^{-3}$

(Figure 6-3b). Deposition of $PM_{2.5}$ also increases in Georgia, South Carolina and southern Missouri, which would lead to decreased concentrations of $PM_{2.5}$ (Figure 6-3b), meaning that increased emissions of organic compounds from reforestation leads to higher concentrations of $PM_{2.5}$ despite the tendency for meteorology and deposition changes to decrease $PM_{2.5}$ concentration. During the winter, small decreases in seasonal average $PM_{2.5}$ concentration of up to 0.5 $\mu g\ m^{-3}$ occur over the Southeast (Figure 6-4a). The CD scenario shows similar decreased PM concentrations (Figure 6-4b) while the deposition does not change much (Figure 6-4c). Since, during wintertime, biogenic VOC emissions are low, and deposition does not change much, regional climate change from reforestation leads to the decreased $PM_{2.5}$ seen here.

Table 6-2 Concentrations of major $PM_{2.5}$ species during the winter (DJF) and summer (JJA) and for the summertime CD scenarios (Jul) for the reference case and the change in concentrations for the two LULCC scenarios (scenario minus reference case). OM is organic matter, NO_3 is nitrate aerosol and SO_4 is sulfate aerosol.

	Reference case (ug m-3)			Reforestation change (ug m-3)			Cropland Conversion change (ug m-3)		
	Win	Sum	Sum CD	Win	Sum	Sum CD	Win	Sum	Sum CD
OM	1.14	1.16	0.96	0.37	0.35	-0.47	0.00	-0.41	0.01
NO3	1.12	0.03	0.04	-0.18	-0.01	0.00	0.31	0.11	0.01
SO4	1.30	1.90	1.90	0.07	0.06	-0.08	0.10	0.67	0.01

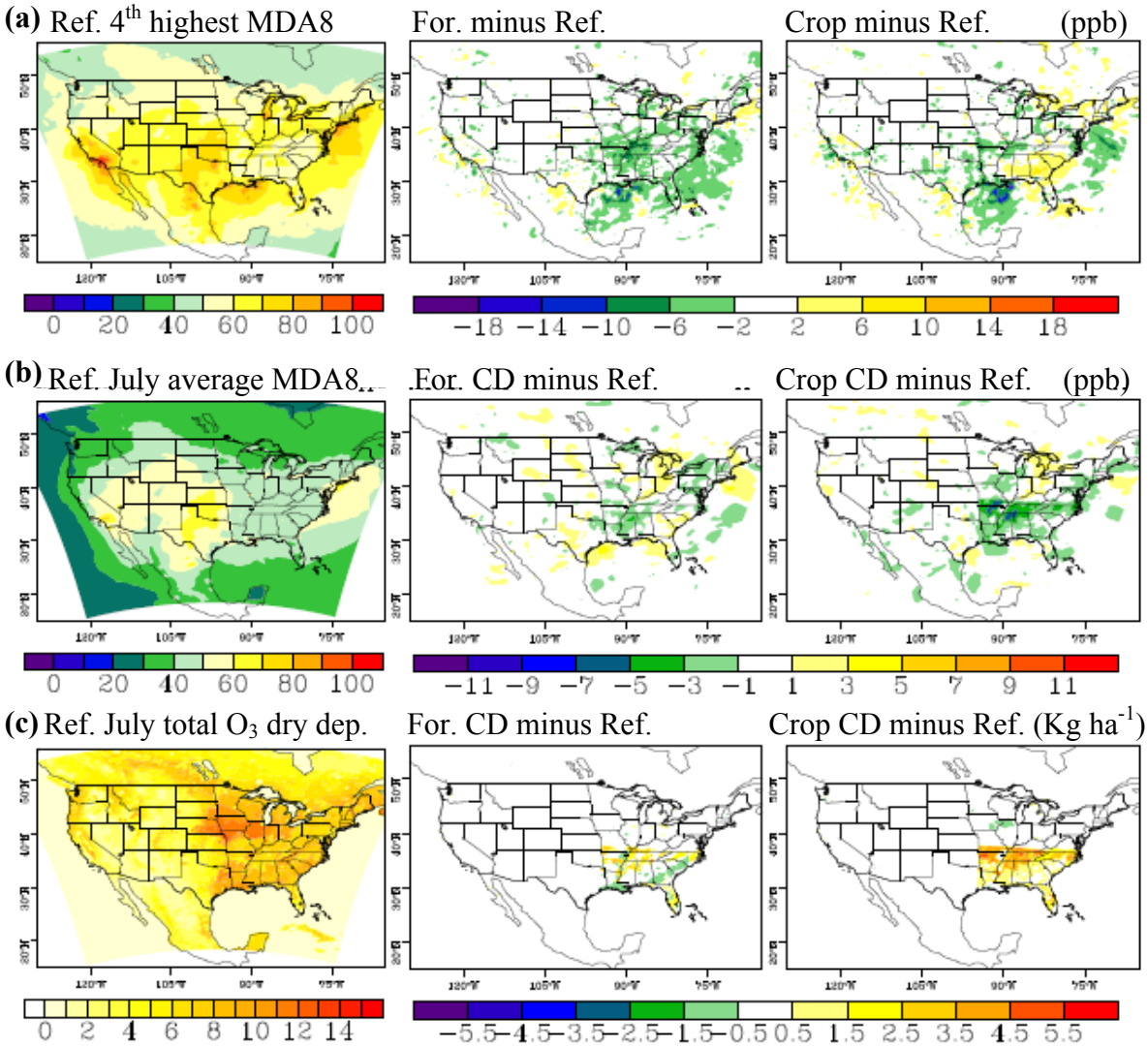

Figure 6-2 (a) 4th highest MDA8 mixing ratio of the year (left) and the difference (scenario minus reference case) in the 4th highest MDA8 for the reforestation scenario (middle) and the cropland conversion scenario (right). **(b)** MDA8 averaged over the month of July for the reference CD case (left) and the difference (scenario minus reference case) in the July average MDA8 for the reforestation scenario (middle) and the cropland conversion scenario (right). **(c)** The same as (b) but for the total deposition of O_3.

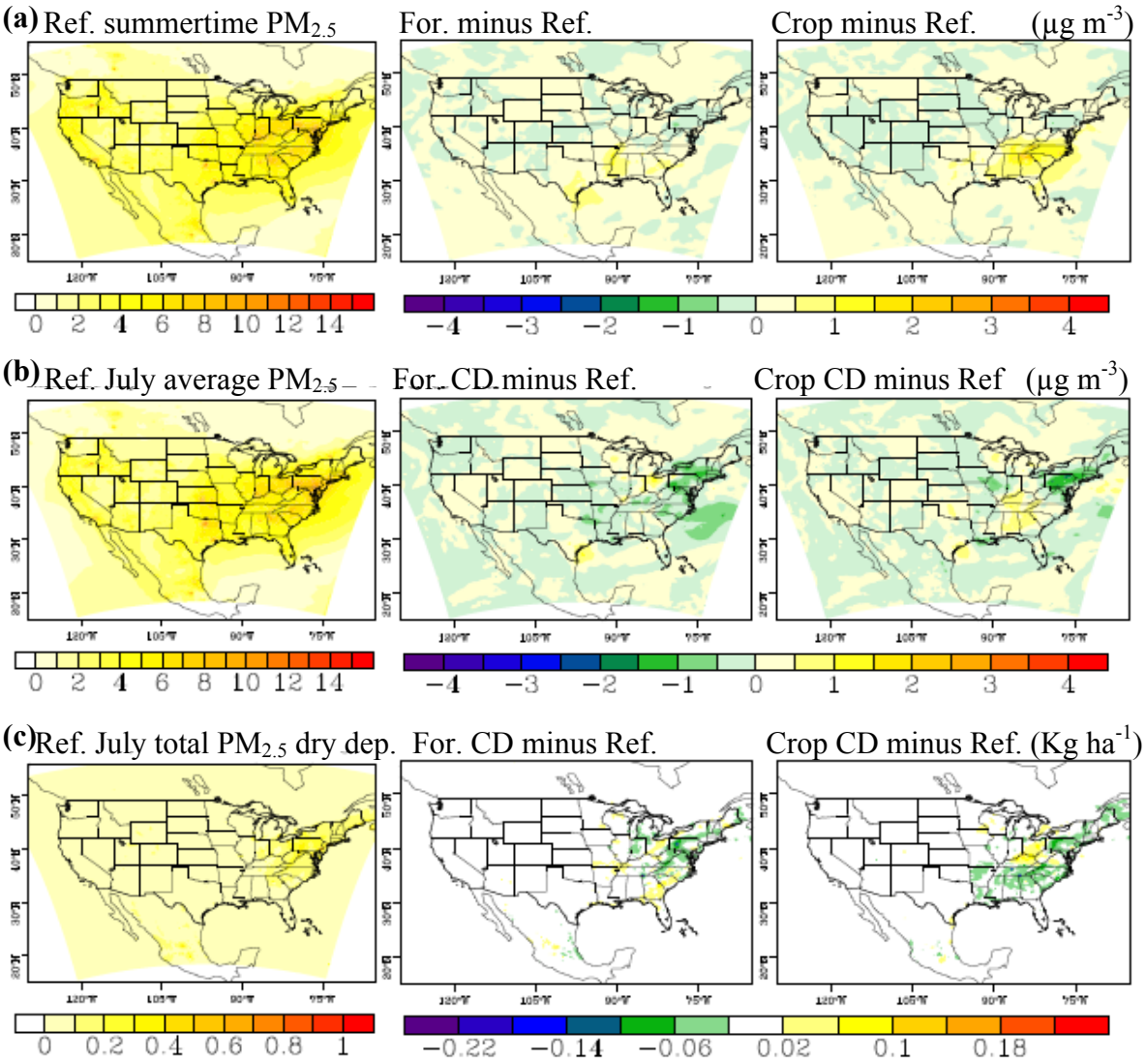

Figure 6-3 (a) Summertime (JJA) average $PM_{2.5}$ concentration for the reference case (left) and the difference (scenario minus reference case) in the summer time average $PM_{2.5}$ for the reforestation scenario (middle) and the cropland conversion scenario (right). **(b)** $PM_{2.5}$ averaged over the month of July for the reference CD case (left) and the difference (scenario minus reference case) in the July average $PM_{2.5}$ for the reforestation scenario (middle) and the cropland conversion scenario (right). **(c)** The same as (b) but for the total deposition of $PM_{2.5}$.

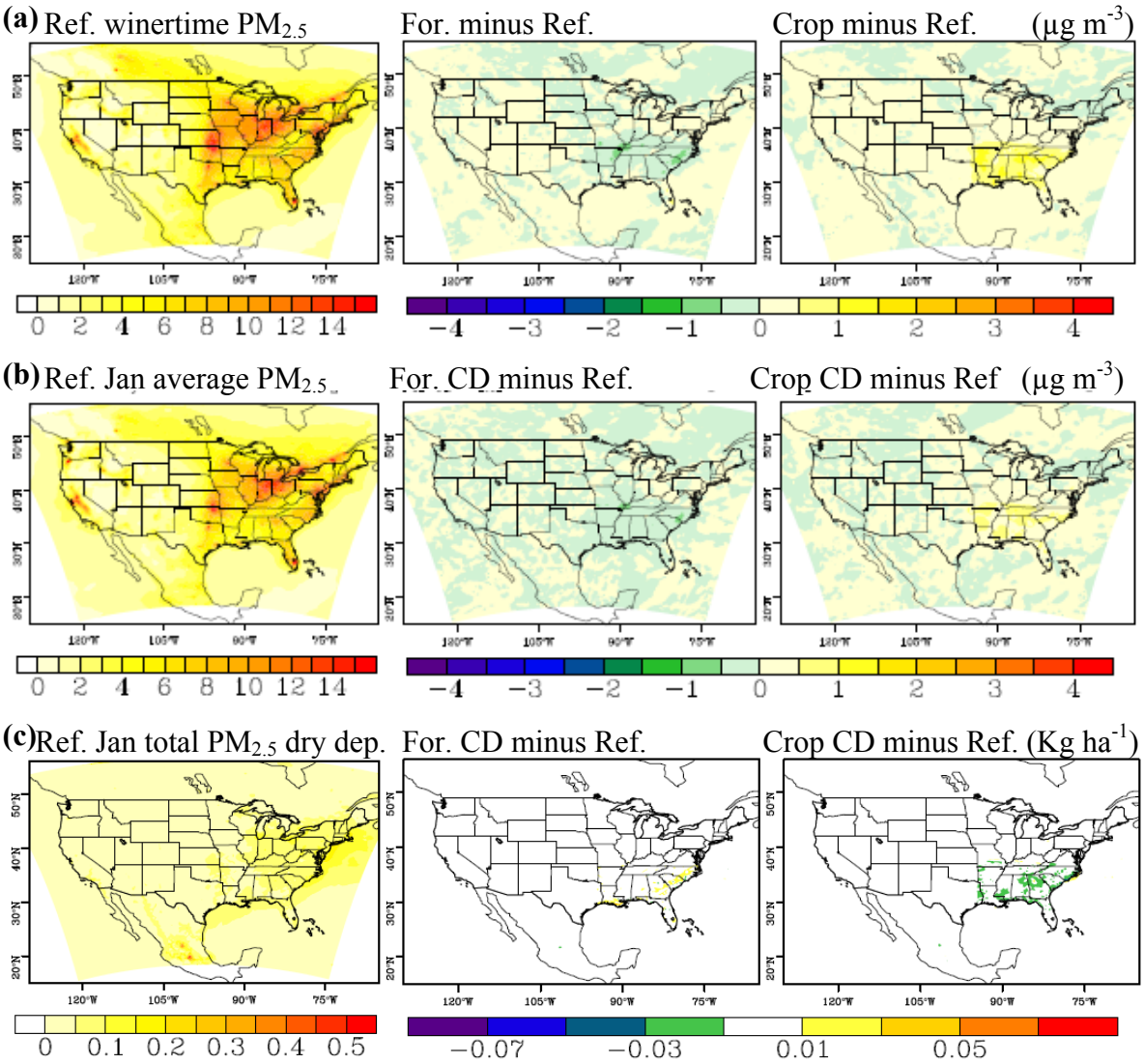

Figure 6-4 (a) Wintertime (DJF) average $PM_{2.5}$ concentration for the reference case (left) and the difference (scenario minus reference case) in the wintertime average $PM_{2.5}$ for the reforestation scenario (middle) and the cropland conversion scenario (right). **(b)** $PM_{2.5}$ averaged over the month of January for the reference CD case (left) and the difference (scenario minus reference case) in the January average $PM_{2.5}$ for the reforestation scenario (middle) and the cropland conversion scenario (right). **(c)** The same as (b) but for the total deposition of $PM_{2.5}$.

6.3.2 Cropland Conversion

Conversion of forest to cropland in the Southeast leads to increases in 4th highest MDA8 mixing ratio in Mississippi, Alabama, Georgia, and South Carolina of up to 10 ppb (Figure 6-2a). Cropland emits NO_X at a much higher rate than forest, leading to this increased production of O_3 in the atmosphere. On the other hand, decreased 4th highest MDA8 occur in Louisiana, Arkansas, Tennessee, and South Missouri by up to 6 ppb even though NO_X emissions increase. In the CD scenario, the month average MDA8 also decreases over most of the Southeastern domain with the largest decreases (up to 7 ppb) occurring over Arkansas, Tennessee, and northern Mississippi (Figure 6-2b). Increased O_3 deposition follows a similar spatial pattern as the decreased MDA8 for the CD scenario, indicating that increased deposition leads to decreased MDA8 mixing ratios in regions of crop land conversion (Figure 6-2c). Further, Trail et al. (2013) found decreased temperature due to cropland conversion, which could decrease O_3 mixing ratio.

Seasonal average $PM_{2.5}$ concentration over the Southeast domain increases by to 1.5 μg m^{-3} in the cropland conversion scenario occur during winter and summer (Figure 6-3a and 6-4a). During the summer, sulfate aerosol average over the Southeast domain increases by 0.67 μg m^{-3} while OM aerosol decreases by 0.41 μg m-3 (Table 6-2). The decreased OM results from lower emissions of organic compounds, such as isoprene, from crops than from forests (Table 6-2). Increased $PM_{2.5}$ concentration of up to 1 μg m^{-3} also occurs in the CD scenario during winter and summer (Figure 6-3b and 6-4b). Aerosol deposition decreases during the summer, because the surface roughness is reduced where forest is converted to crop, contributing to increased aerosol concentration (Figure 6-3c). Interestingly, even though land use does not change in Kentucky, West

Virginia and Ohio, increased $PM_{2.5}$ concentrations lead to deposition increases in these states. During the winter decreased deposition and increased NO emission rates lead to increased nitrate aerosol concentration of 0.31 μg m^{-3} averaged over the Southeast domain (Table 6-1 and Figure 6-4).

6.4 Summary and Conclusions

We investigated the impacts of potential reforestation and cropland conversion on future regional air quality in the Southeastern U.S. using downscaled meteorology from a general circulation model and emissions projected to 2050. We explore how altered biogenic emissions, deposition rates and meteorology associated with reforestation and cropland conversion influence ambient O_3 and $PM_{2.5}$ concentrations. Reforestation with loblolly pine tends to decrease the 4th highest MDA8 of the year while increasing summertime $PM_{2.5}$ in the Southeast. Conversion of forest to cropland, on the other hand, tends to increase the 4th highest MDA8 of the year and increase $PM_{2.5}$ year-round.

In a previous study, Trail et al. [2013] analyzed the meteorology used in the present study and predicted that changes in meteorology related to reforestation of cropland with pine leads to warming and potentially enhanced production of O_3, except over the Mississippi river where cooling occurs. In the present study however, we find that deposition and emissions changes impact O_3 and $PM_{2.5}$ concentrations as much as, and in most cases more than, changes in meteorology. For example, where Trail et al. [2013] predicted enhanced production of O_3 due to reforestation, we found little change in O_3 concentration because of decreased biogenic NO emissions. Over the Mississippi river, however, decreased temperature, increased deposition and decreased NO_X

emissions all drive down the O_3 concentration. Trail et al. [2013] also predict that conversion of forest to cropland leads to cooling and could reduce the production of O_3. However, the results of the present study show that increased NO_X emissions leads to increases in the 4th highest MDA8 of the year of up to 10 ppb despite the tendency for increased deposition and decreased temperature to reduce the MDA8 mixing ratio.

Trail et al. [2013] also note the importance in understanding the uncertainty associated with vegetation parameters when simulating the impact of agricultural changes on regional climate due to the regional climate sensitivity to parameters such as the stomatal resistance. In the present study, air pollution concentrations are sensitive to the parameters used in calculating biogenic emissions and deposition, such as leaf area index and emission factors. The results of this study further the findings of studies aimed at understanding strategies to improve future air quality by showing that O_3 and aerosol concentrations are highly sensitive to reforestation and cropland conversion in the Southeast and these land use changes should be considered in air quality management plans.

6.5 References

Bull, S. R. (1996), Renewable energy transportation technologies, *Renewable Energy*, *9*(1-4), 1019-1024

Carter, W. P. L. (2000), Documentation of the SAPRC-99 chemical mechanism for VOC reactivity assessment, University of California, Riverside, Riverside, CA.

CEP (2003), Sparse Matrix Operator Kernel Emissions Modeling System (SMOKE) User Manual, edited, Chapel Hill, NC.

Chen, H., et al. (2006), Effect of land-cover change on terrestrial carbon dynamics in the southern United States, *J. Environ. Qual.*, *35*(4), 1533-1547, doi:10.2134/jeq2005.0198.

Conner, R. C., and A. J. Hartsell (2002.), The Southern Forest Resource Assessment: Chapter 16, Forest Area and Conditions, Department of Agriculture, Forest Service, Southern Research Station,.

Dudhia, J. (1989), Numerical study of convection observed during the winter monsoon experiment using a mesoscale two-dimensional model, *J. Atmos. Sci.*, *46*(20), 3077-3107

Ek, M. B., et al. (2003), Implementation of Noah land surface model advances in the National Centers for Environmental Prediction operational mesoscale Eta model, *Journal of Geophysical Research-Atmospheres*, *108*(D22), 16, doi:8851 10.1029/2002jd003296.

Fishbone, L. G., et al. (1980), MARKAL, a Multiperiod Linear-Programming Model for Energy-Systems Analysis Applied to the United-States, *Bulletin of the American Physical Society*, *25*(4), 494-495

Foley, K. M., et al. (2001), Incremental testing of the Community Multiscale Air Quality (CMAQ) modeling system version 4.7, *Geoscientific Model Development*, *3*(1), 205-226

Ganzeveld, L., and J. Lelieveld (2004), Impact of Amazonian deforestation on atmospheric chemistry, *Geophysical Research Letters*, *31*(6), 5, doi:L06105 10.1029/2003gl019205.

Henze, D. K., et al. (2008), Global modeling of secondary organic aerosol formation from aromatic hydrocarbons: high- vs. low-yield pathways, *Atmospheric Chemistry and Physics*, *8*(9), 2405-2420

Hong, S. Y., et al. (2006), A new vertical diffusion package with an explicit treatment of entrainment processes, *Mon. Weather Rev.*, *134*(9), 2318-2341

Houweling, S., et al. (1998), The impact of nonmethane hydrocarbon compounds on tropospheric photochemistry, *Journal of Geophysical Research-Atmospheres*, *103*(D9), 10673-10696, doi:10.1029/97jd03582.

Jiang, X. Y., et al. (2008), Predicted impacts of climate and land use change on surface ozone in the Houston, Texas, area, *Journal of Geophysical Research-Atmospheres*, *113*(D20), 16, doi:D20312 10.1029/2008jd009820.

Kain, J. S., and J. M. Fritsch (1993), Convective parameterization models: The Kain–Fritsch scheme. Cumulus Convection in Numerical Models, *American Meteorological Society*, *46*, 165-170

Lamarque, J. F., et al. (2011), Global and regional evolution of short-lived radiatively-active gases and aerosols in the Representative Concentration Pathways, *Clim. Change*, *109*(1-2), 191-212, doi:10.1007/s10584-011-0155-0.

Leiby, P. N., and J. Rubin (2003), Transitions in light-duty vehicle transportation - Alternative-fuel and hybrid vehicles and learning, in *Energy, Air Quality, and Fuels 2003*, edited, pp. 127-134.

Liao, H., et al. (2007), Biogenic secondary organic aerosol over the United States: Comparison of climatological simulations with observations, *Journal of Geophysical Research-Atmospheres*, *112*(D6), 19, doi:D06201 10.1029/2006jd007813.

Lin, Y. L., et al. (1983), Bulk parameterization of the snow field in a cloud model, *Journal of Climate and Applied Meteorology*, *22*(6), 1065-1092, doi:10.1175/1520-0450(1983)022<1065:bpotsf>2.0.co;2.

Liu, P., et al. (2012), Differences between downscaling with spectral and grid nudging using WRF, *Atmospheric Chemistry and Physics*, *12*(8), 3601-3610, doi:10.5194/acp-12-3601-2012.

Mlawer, E. J., et al. (1997), Radiative transfer for inhomogeneous atmospheres: RRTM, a validated correlated-k model for the longwave, *Journal of Geophysical Research-Atmospheres*, *102*(D14), 16663-16682, doi:10.1029/97jd00237.

Moss, R. H., et al. (2010), The next generation of scenarios for climate change research and assessment, *Nature*, *463*(7282), 747-756, doi:10.1038/nature08823.

Pacala, S. W., et al. (2001), Consistent land- and atmosphere-based US carbon sink estimates, *Science*, *292*(5525), 2316-2320, doi:10.1126/science.1057320.

Pielke, R. A., et al. (1998), Interactions between the atmosphere and terrestrial ecosystems: influence on weather and climate, *Glob. Change Biol.*, *4*(5), 461-475, doi:10.1046/j.1365-2486.1998.t01-1-00176.x.

Prestemon, J. P., and R. C. Abt (2002), The Southern timber market to 2040, *Journal of Forestry*, *100*(7), 16-22

Racherla, P. N., and P. J. Adams (2006), Sensitivity of global tropospheric ozone and fine particulate matter concentrations to climate change, *Journal of Geophysical Research-Atmospheres*, *111*(D24), 11, doi:D24103 10.1029/2005jd006939.

Schmidt, G. A., et al. (2013), Configuration and assessment of the GISS ModelE2 contributions to the CMIP5 archive, *J. Adv. in Modeling Earth Systems, Submitted*

Skamarock, W. C., and J. B. Klemp (2008), A time-split nonhydrostatic atmospheric model for weather research and forecasting applications, *Journal of Computational Physics*, *227*(7), 3465-3485, doi:10.1016/j.jcp.2007.01.037.

Steyaert, L. T., and R. G. Knox (2008), Reconstructed historical land cover and biophysical parameters for studies of land-atmosphere interactions within the

eastern United States, *Journal of Geophysical Research-Atmospheres*, *113*(D2), 27, doi:D02101 10.1029/2006jd008277.

Wang, Y. H., et al. (1998), Global simulation of tropospheric O-3-NOx-hydrocarbon chemistry 2. Model evaluation and global ozone budget, *Journal of Geophysical Research-Atmospheres*, *103*(D9), 10727-10755, doi:10.1029/98jd00157.

Wear, D. N., and J. G. Greis (2002), Southern Forest Resource Assessment - Summary of findings, *Journal of Forestry*, *100*(7), 6-14

Woo, J. H., et al. (2008), Development of North American Emission Inventories for Air Quality Modeling under Climate Change, *Journal of the Air & Waste Management Association*, *58*(11), 1483-1494, doi:10.3155/1047-3289.58.11.1483.

Wu, S. L., et al. (2008), Effects of 2000-2050 global change on ozone air quality in the United States, *Journal of Geophysical Research-Atmospheres*, *113*(D6)

CHAPTER 7

SUMMARY OF CONCLUSIONS AND FUTURE RESEARCH

7.1 Summary of Conclusions

The research presented in this dissertation aims to provide information to policy makers by estimating impacts of a changing climate, implementation of CO_2 emission reduction policies, and LULCC on future ambient O_3 and $PM_{2.5}$ in the U.S. Present and future global climate were downscaled to the regional scale and emissions were estimated and projected using the NEI and MARKAL-9R. The downscaling methods described in chapter 2 produce somewhat different results than the coarse resolution global simulations in some regions due to the introduction of finer scale geographical data. In comparing the impact of present and potential future climate and emissions changes on air quality, emissions from a reference case policy scenario leads to major improvements in future U.S. air quality compared to present air quality, including generally decreased MDA8 mixing ratios and $PM_{2.5}$ concentrations and reduced frequency of NAAQS O_3 standard exceedances in most major U.S. cities. The results presented in chapter 4 show that aggressive carbon tax policies may further improve $PM_{2.5}$ air quality while CO_2 reduction policies aimed at the transportation and electricity generation sectors lead to improved O_3 air quality but potentially higher $PM_{2.5}$ concentrations in some major U.S. cities.

Without the implementation of any carbon regulation, future reductions in mobile and point source emissions account for reduced annual $PM_{2.5}$ concentrations while climate change reinforces the reduced concentrations in some regions. Future decreases

in MDA8 mixing ratio are mainly attributed to decreased emissions rate of VOC and NO_X from mobile sources. Even though reductions of pollutant concentrations are predicted to occur in the future from current efforts, the climate penalty scenario of future emissions with present meteorology indicates that the extent of air quality improvement is less due to predicted climate change. In other words, present emission reduction efforts will lead to less O_3 and $PM_{2.5}$ in the future, but these efforts will be less effective with climate change than without. This means additional costs due to climate change because deeper emission reductions will be required to compensate for a warmer climate, even if current efforts are predicted to show improvement.

In simulating the effect of CO_2 emission reduction policies on air quality in the U.S., the results in chapter 4 show that the implementation of a relatively aggressive carbon taxes can lead to improvements in $PM_{2.5}$ air quality compared to the 2050 reference case due to the increased incentives to install flue-gas desulfurization (FGD) process technologies and carbon capture and sequestration (CCS) technologies. However, there is an air quality trade-off because less capital is available to install NO_X reduction technologies and O_3 increases as a result. Relatively unaggressive carbon taxes, on the other hand, may lead to worse air quality, in the form of increased $PM_{2.5}$ concentrations because there is less incentive to install FGD and CCS technologies. A policy aimed at reducing CO_2 from the transportation sector as well as electricity production sectors lead to reduced emissions of mobile source NO_X, thus reducing O_3 mixing ratio. Over most of the U.S., this scenario leads to reduced $PM_{2.5}$ concentrations. However, increased primary $PM_{2.5}$ emissions associated with fuel switching from gasoline to diesel leads to increased OM, EC and $PM_{2.5}$ in most major U.S. cities.

While there are uncertainties in current and future emissions estimates, and uncertainties in climate, emissions sensitivities can be used to determine the major sources of O_3 and $PM_{2.5}$ and the current modeling platform can be used to isolate the effects of climate on air quality. Further, the MARKAL 9R model is shown here to be a useful tool in developing a range of alternative policy based emissions scenarios to address the uncertainties associated with estimating future emissions.

Reforestation and cropland conversion impacts on regional climate were expected given the changes in land use parameters (eg. albedo, RS, LAI and Z^0) while the impacts on air quality were less obvious. Reforestation of crop regions with pine forest in the Southeast tends to lead to warming primarily due to the increase of RS and decrease in albedo while the Z^0 increase may lessen the degree of warming by shifting the transfer of energy to the atmosphere from sensible to latent heat. However, pine reforestation tends to decrease the 4th highest MDA8 of the year while slightly increasing summertime $PM_{2.5}$ in the Southeast due to deposition and emissions changes.

On the other hand, cooling tends to occur when forest is replaced with crop in the Southeast, though not enough to counter the simulated warming of 1-3 °C from greenhouse gas increases (chapter 2). Cooling during the winter is attributed to the high albedo of cropland while during the spring and summer the decrease in RS also contributes to cooling. However, conversion of forest to cropland leads to reduced air quality in the form of increased the 4th highest MDA8 of the year and increased $PM_{2.5}$ year-round.

The sensitivity analysis of the LULCC studies shows that the climate and air quality results are sensitive to assumed physical parameters, which are uncertain and vary

by species and region. Murphy et al. [2012], suggest that the stomatal conductance of loblolly pine, the major species of pine in the Southeast, should be adjusted from the default value and this would lead to more simulated cooling in the Southeast. Air pollution concentrations are sensitive to the parameters used in calculating biogenic emissions and deposition, such as leaf area index and emission factors. The results of this study further the findings of studies aimed at understanding strategies to improve future air quality by showing that O_3 and aerosol concentrations are highly sensitive to reforestation and cropland conversion in the Southeast and these land use changes should be considered in air quality management plans.

7.2 Future research directions

7.2.1 *Economic and health analysis of CO_2 emission reduction strategies*

The results presented in this dissertation focus on the impacts of changes in policy and land cover on regional climate and ambient concentrations of air pollutants while largely ignoring their implications to the U.S. economy. This research also lacks an objective analysis of policy and land cover change impact on human health. Through the use of recent advances in operational systems used to model the economy of energy and climate policies, and, the health impacts of changes in air pollution, it may be possible to quantify the effect of future policy and LULCC on the U.S. economy and on human health.

There are two types of modeling approaches used in energy-economic literature to estimate the relationship among policy, economy, and emissions, namely bottom-up and top-down models. Future year emissions used for air quality modeling here in chapters 3,

4 and 6 are estimated using the bottom-up model, MARKAL 9R. Bottom-up approaches differentiate technologies from each other by their anticipated cost and bring in a large amount of energy system detail, allowing for the evaluation of a wide range of policy assumptions. However, bottom-up approaches lack the ability to model Macro-economic feedbacks into the system. Top-Down approaches are typically used by economists and are able to capture Macro-economic feedbacks but lack energy system detail. Recently, hybrid approaches, such as MARKAL-macro combine bottom-up and top-down models and provide detailed energy system data and economic feedbacks and have been used to estimate the effect that air pollution and climate mitigation policies could have on imports, exports, and U.S. gross domestic product (GDP) [*Sarica and Tyner*, 2013].

Human health impacts of O_3 and $PM_{2.5}$ pollution have been extensively studied and a variety of models have been developed to estimate health implications of changes in air pollution. The EPA developed an air pollution related health model, BenMAP, which calculates changes in premature mortality and other health responses using inputs of pollutant concentrations, population and concentration-response functions. A number of the studies mentioned in this dissertation have used BenMAP to estimate the effect of changing air quality on human health [*Tagaris et al.*, 2008].

7.2.2 *Apply a Monte Carlo approach to estimating future emissions*

The greatest uncertainty associated with the results presented in this dissertation likely lies in estimating future emissions. Although future climate predictions are uncertain, hind-casts of climate models like the one used here and described in chapter 2 have shown that these climate models can be fairly accurate. More importantly, in

chapter 3, the sensitivity analysis shows that future air pollutant concentrations are more sensitive to changing emissions than to climate change. In developing the emissions used here, one realization of a reference case emission scenario was created and in chapter 4 single realizations of each policy scenario were created. Rather than using single realizations of emissions, a Monte Carlo based approach could minimize the uncertainties of these scenarios. A recent study uses a Monte Carlo based approach to assess future energy use in a carbon constrained future [*Vithayasrichareon and MacGill*, 2013]. The tool used in Vithayasrichareon et al. [2012] incorporates probability distributions for estimated fossil-fuel costs, carbon prices, plant investment costs, and demand.

7.2.3 *Integrating agricultural and energy systems to investigate impacts of increased biofuel utilization in the Southeastern U.S.*

Currently, the Southeastern U.S. produces 60% of the nation's timber products [*Prestemon and Abt*, 2002] and in the past 30 years, pine plantations have rapidly increased (from 2 million acres in 1953 to more than 30 million acres in 1999) [*Conner and Hartsell*, 2002.]. These trends are slated to continue given the growing demand to develop forest-to-fuel technologies, as well as to increase wood products-related industries. Chapter 4 shows that using all available biomass in the U.S. to produce energy potentially leads to worse air quality while Chapters 5 and 6 show some mixed improved and decreased air quality due to LULCC in the Southeast. The integration of agricultural and energy system models may provide more information on the combined effect of LULCC and energy policies relating to biofuels in the Southeast.

In a recent study [*Elobeid et al.*, 2013], the integration of the MARKAL energy system model with an agricultural macro-economic model, Iowa State University's Center for Agricultural and Rural Development (CARD) U.S. agricultural markets model, is used to estimate "shifts in farming practices, average productivity, and costs of production, as well as the environmental consequences of farmers' decisions resulting from the expansion of biomass feedstock production" [*Elobeid et al.*, 2013]. A similar approach may further the findings of this dissertation by capturing the interactions among biomass energy systems and LULCC associated with the energy demand and cost. The resulting LULCC would provide a basis for simulating regional climate change and deposition changes in the Southeast.

7.2.4 *Global analysis of LULCC impacts on climate and air quality*

The LULCC analyses discussed in chapters 5 and 6 focus on the Southeastern U.S. in order to address the burden that increasing biomass energy demand places on land cover. In the developing regions of the world, LULCC is occurring rapidly and on large scales because of great food and space increases required to meet the demands of increasing population in the regions. Efforts are currently focused on improving the emissions estimates of reactive nitrogen species from crops and livestock farming [*Aneja et al.*, 2012] and biogenic VOC [*Geron et al.*, 2006] in regions of rapid anthropogenic LULCC. The integrated agricultural and energy systems mentioned above used on a global scale may provide important information on how changes in land cover in one area of the globe impacts the rest of the globe. A global scale approach can capture the effects

of changes in imports and exports among countries and the resulting changes in economies where a regional based approach does not.

7.2.5 *Flux measurements for evaluation of model parameters*

Chapters 5 and 6 highlight the importance of reducing uncertainty in parameters which most strongly influence the biophysical feedback of LULCC impacting climate and air quality. Increasingly, efforts are focusing on improving our understanding of the interaction between vegetation and the atmosphere by measuring fluxes of latent heat [*Murphy et al.*, 2012] and organic compounds [*Geron et al.*, 2006] from various plant species. In conducting latent heat flux measurements and optimizing their model parameters to correlate to observations, Murphy et al. [2012] found large increases in the latent heat flux of loblolly pine compared to the default model parameters (Figure 7-1). Using the Murphy et al. [2012] approach to update the vegetative properties, especially the stomatal resistance, in WRF may add to the results of this dissertation. A similar approach could be used to validate the deposition of O_3 on various vegetative species.

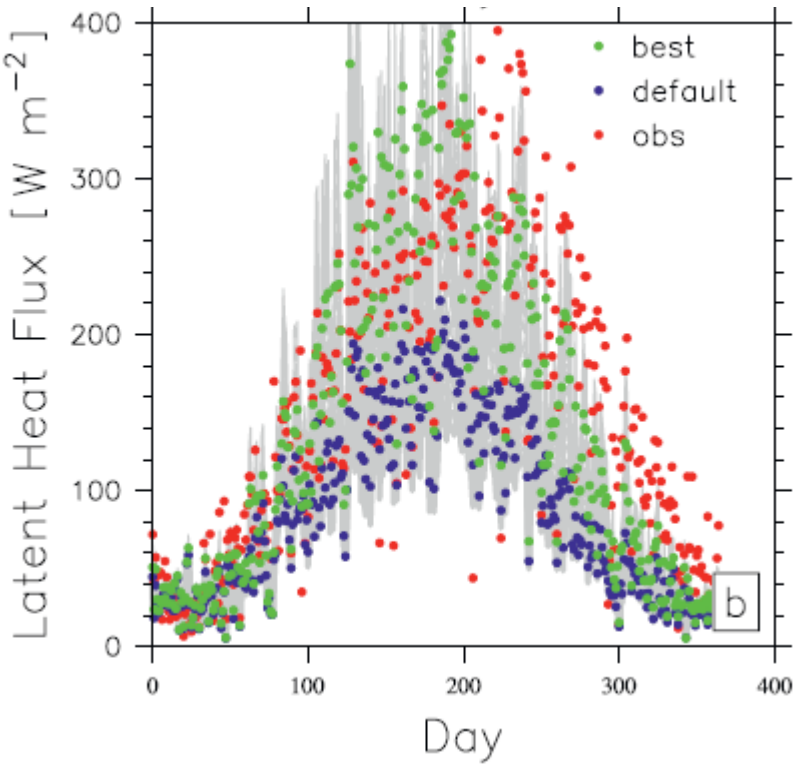

Figure 7-1 The average daytime (1000-1600 LT) latent heat flux (W m-2) averaged over the period 2003-05. Individual ensemble members are shown in gray, the observations are shown in red, a run with default CLM parameters is shown in blue, and the best ensemble member predicted from the Bayesian inversion method is shown in green (cite)

7.3 References

Aneja, V. P., et al. (2012), Reactive nitrogen emissions from crop and livestock farming in India, *Atmospheric Environment*, *47*, 92-103, doi:10.1016/j.atmosenv.2011.11.026.

Conner, R. C., and A. J. Hartsell (2002.), The Southern Forest Resource Assessment: Chapter 16, Forest Area and Conditions, Department of Agriculture, Forest Service, Southern Research Station,.

Elobeid, A., et al. (2013), Integration of agricultural and energy system models for biofuel assessment, *Environ. Modell. Softw.*, *48*, 1-16, doi:10.1016/j.envsoft.2013.05.007.

Geron, C., et al. (2006), Volatile organic compounds from vegetation in southern Yunnan Province, China: Emission rates and some potential regional implications, *Atmospheric Environment*, *40*(10), 1759-1773, doi:10.1016/j.atmosenv.2005.11.022.

Murphy, L. N., et al. (2012), Local and Remote Climate Impacts from Expansion of Woody Biomass for Bioenergy Feedstock in the Southeastern United States, *Journal of Climate*, *25*(21), 7643-7659, doi:10.1175/jcli-d-11-00535.1.

Prestemon, J. P., and R. C. Abt (2002), The Southern timber market to 2040, *Journal of Forestry*, *100*(7), 16-22

Sarica, K., and W. E. Tyner (2013), Alternative policy impacts on US GHG emissions and energy security: A hybrid modeling approach, *Energy Econ.*, *40*, 40-50, doi:10.1016/j.eneco.2013.06.003.

Tagaris, E., et al. (2008), Potential impact of climate change on human health caused by changes in ozone and particulate matter concentrations, *submitted*

Vithayasrichareon, P., and I. F. MacGill (2013), A Monte Carlo based decision-support tool for assessing generation portfolios in future carbon constrained electricity industries, *Energy Policy*, *41*, 374-392, doi:10.1016/j.enpol.2011.10.060.

APPENDIX A

SUPPLEMENTAL MATERIAL FOR CHAPTER 2

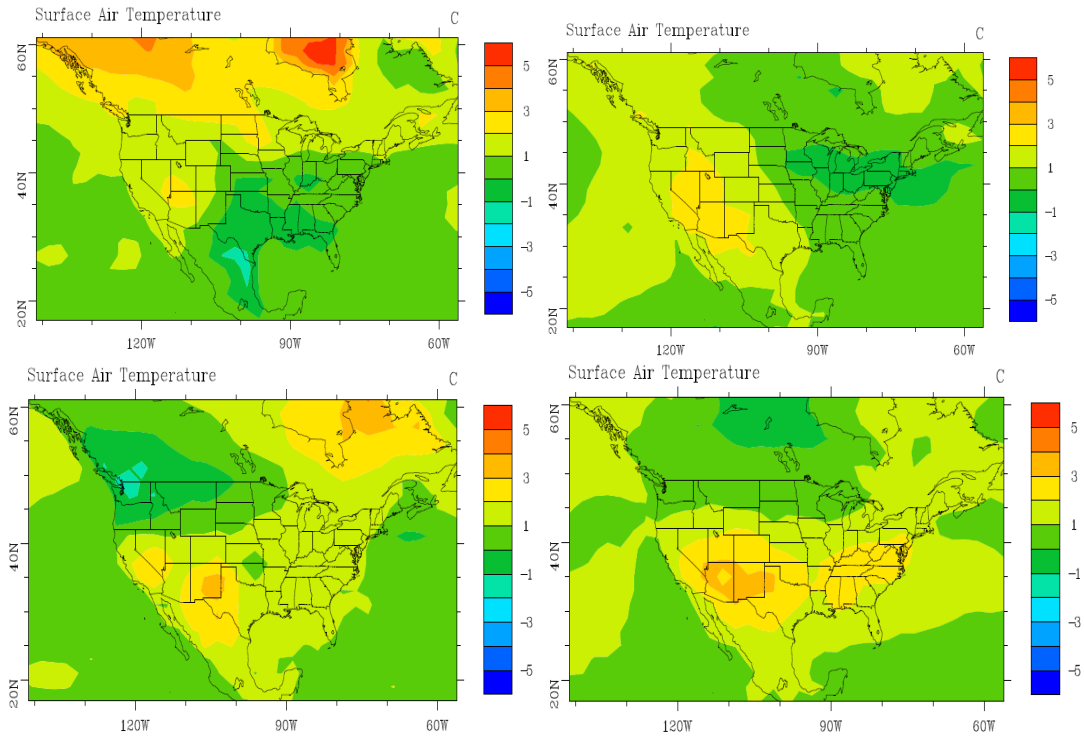

Figure A-1 Seasonal GISS GCM surface air temperature (SAT) difference: winter (top left), spring (top right), summer (bottom left), fall (bottom right).

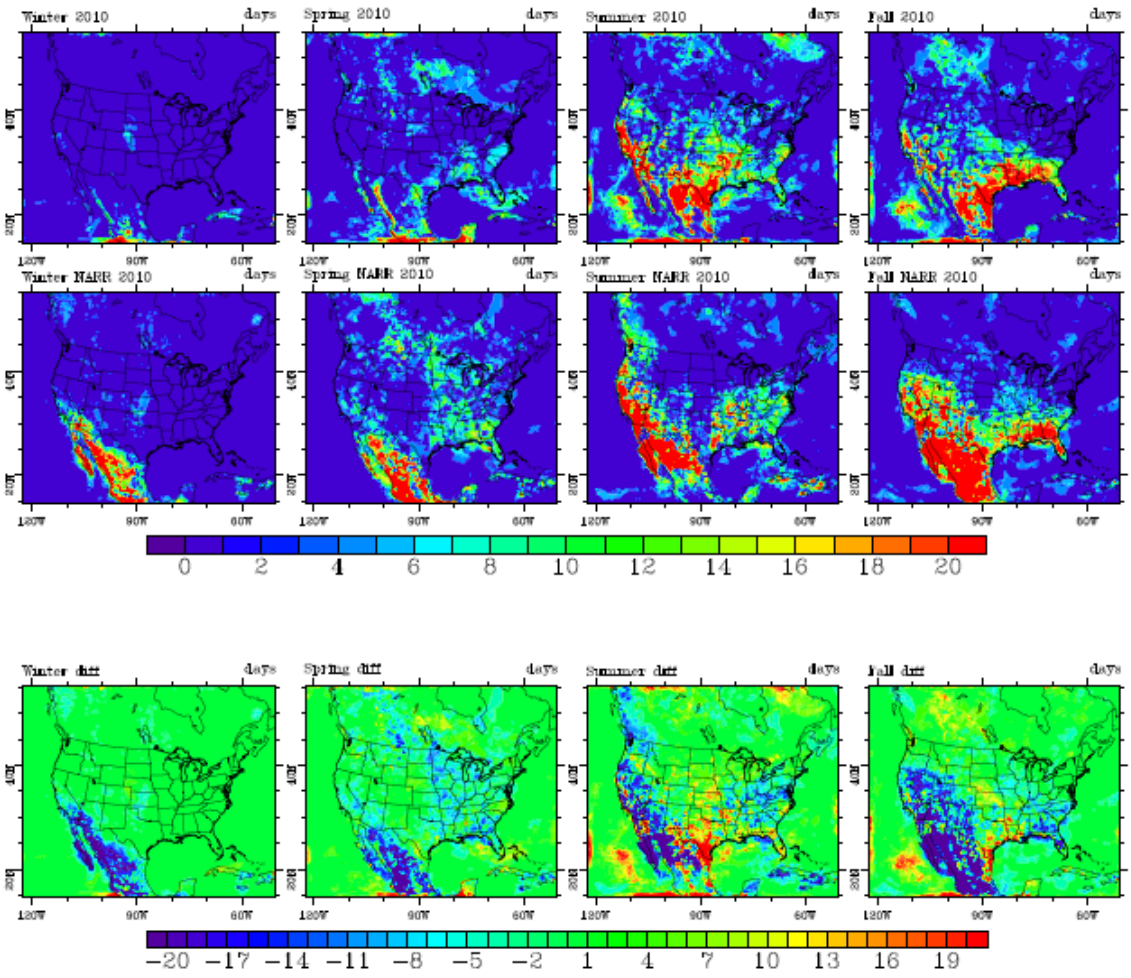

Figure A-2 Number of stagnation days per season for GISS model downscaled by WRF (top) and NCEP-NARR (middle) and the difference (GISS minus NCEP-NARR) (bottom)

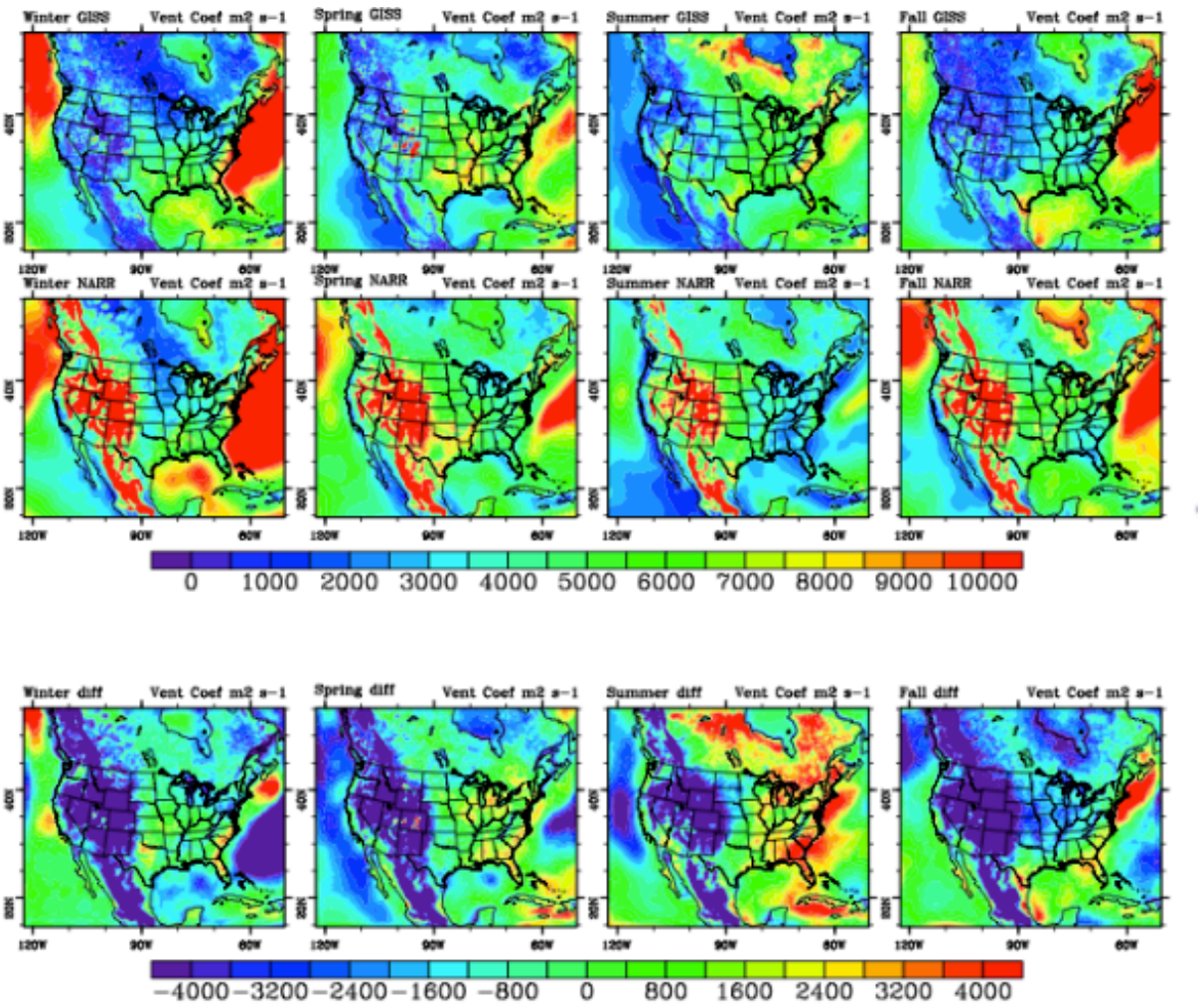

Figure A-3 Ventilation coefficient for GISS model downscaled by WRF (top) and NCEP-NARR (middle) and the difference (GISS minus NCEP-NARR) (bottom)

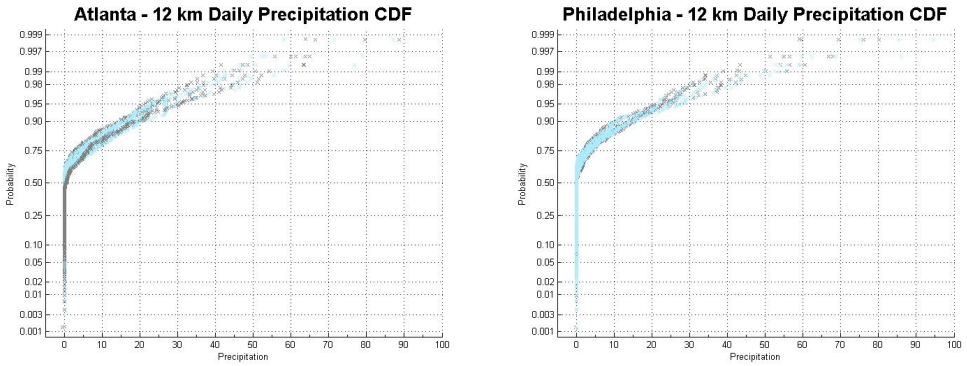

Figure A-4 Cumulative distribution of 12 km historic (dark) and future (light) daily precipitation in Atlanta (Left) and Philadelphia (Right).

APPENDIX B

SUPPLEMENTAL MATERIAL FOR CHAPTER 3

Table B-1 Seasonal performance of simulated O_3 for the year 2010. Simulated O_3 concentrations were compared with EPA_AQS O_3 data. The number of data points (number), mean observed concentration (MOC), mean bias (MB) and normalized mean bias (NMB) are shown for hourly O_3 (O3) and 8-hr average O_3 (8hrO3) without a cutoff and with a cutoff of 40 ppb and for maximum daily 1-hr and 8-hr average O_3 (M1hO3 and M8hO3).

Winter	O3	O3
cutoff	0.04	nocut
number	151630	1236573
MOC (ppm)	0.044	0.025
MB (ppm)	-0.009	0.006
NMB (%)	-19.27	23.83

Spring	O3	O3	8hrO3	8hrO3	M1hO3	M8hO3
cutoff	0.04	nocut	0.04	nocut	0	0
number	950849	2161826	878261	2180994	85424	89178
MOC (ppm)	0.050	0.036	0.049	0.036	0.052	0.049
MB (ppm)	-0.004	0.006	-0.003	0.006	0.001	0.005
NMB (%)	-7.40	17.26	-6.39	17.54	2.64	9.18

Summer	O3	O3	8hrO3	8hrO3	M1hO3	M8hO3
cutoff	0.04	nocut	0.04	nocut	0	0
number	873064	2497692	800324	2522862	101486	103378
MOC (ppm)	0.052	0.033	0.051	0.033	0.053	0.048
MB (ppm)	0.000	0.012	0.001	0.012	0.007	0.012
NMB (%)	0.17	35.83	1.08	36.17	13.05	25.00

Fall	O3	O3	8hrO3	8hrO3	M1hO3	M8hO3
cutoff	0.04	nocut	0.04	nocut	0	0
number	472568	1966896	397712	1987567	78085	81453
MOC (ppm)	0.050	0.028	0.049	0.028	0.046	0.042
MB (ppm)	-0.006	0.008	-0.005	0.009	0.002	0.006
NMB (%)	-11.00	29.82	-10.48	30.27	4.10	15.28

Table B-2 Seasonal performance of simulated $PM_{2.5}$ for the year 2010. Simulated $PM_{2.5}$ concentrations were compared with EPA_AQS $PM_{2.5}$ data. The number of data points (number), mean observed concentration (MOC), mean bias (MB) and normalized mean bias (NMB) are shown for hourly $PM_{2.5}$

PM2.5	Winter	Spring	Summer	Fall
number	28126	31064	29680	29965
MOC (ug m^{-3})	11.43	9.10	10.94	8.83
MB (ug m^{-3})	-2.46	-2.13	-4.33	-0.09
NMB (%)	-21.48	-23.40	-39.55	-1.02

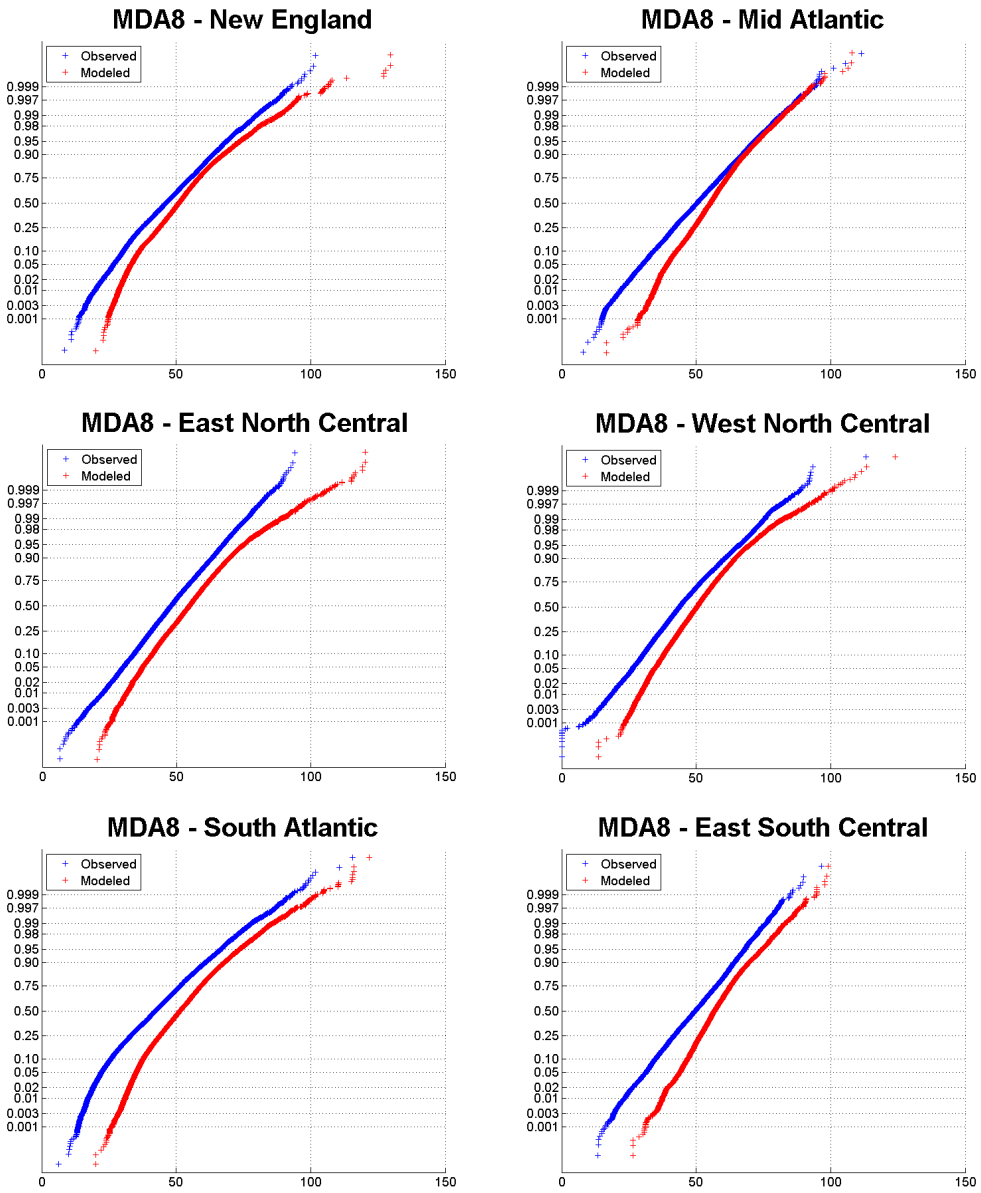

Figure B-1 (continued on next page) Cumulative distribution functions (CDFs) of observed (blue) and modeled (red) maximum daily 8-hr average (MDA8) ozone mixing ratios (ppb) for the nine U.S. census regions during 1May, 2010 to 30 September, 2010. Observed MDA8 mixing ratios were retrieved from the EPA-AQS data.

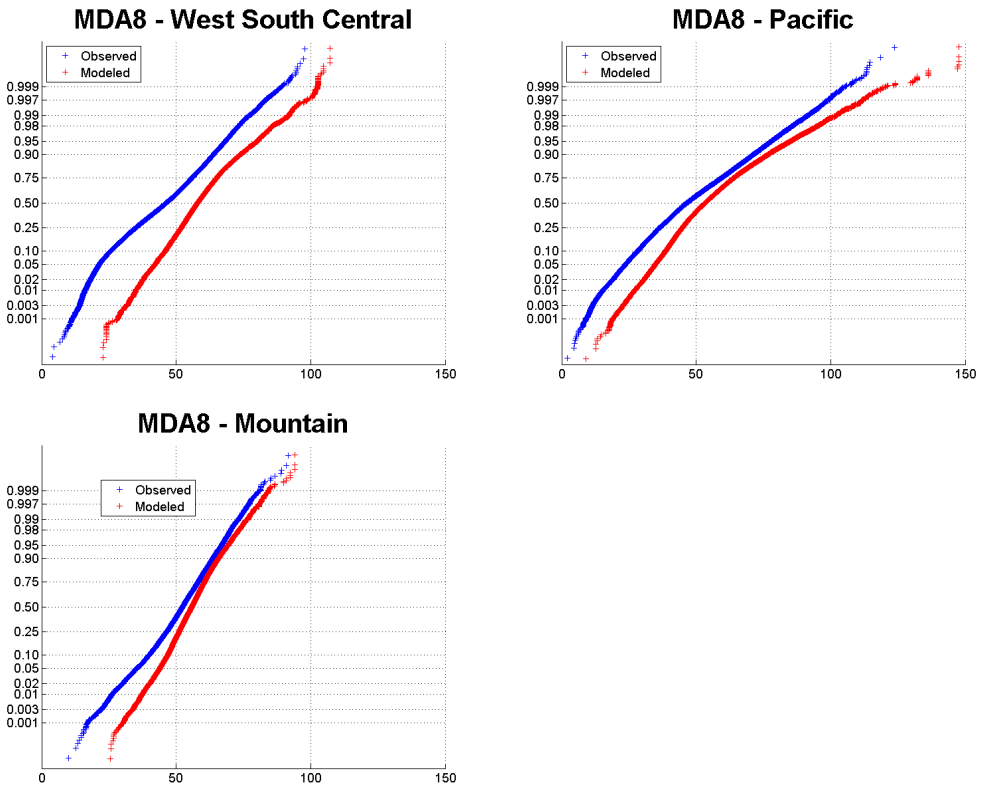

Figure B-1 (continued) Cumulative distribution functions (CDFs) of observed (blue) and modeled (red) maximum daily 8-hr average (MDA8) ozone mixing ratios (ppb) for the nine U.S. census regions during 1May, 2010 to 30 September, 2010. Observed MDA8 mixing ratios were retrieved from the EPA-AQS data.

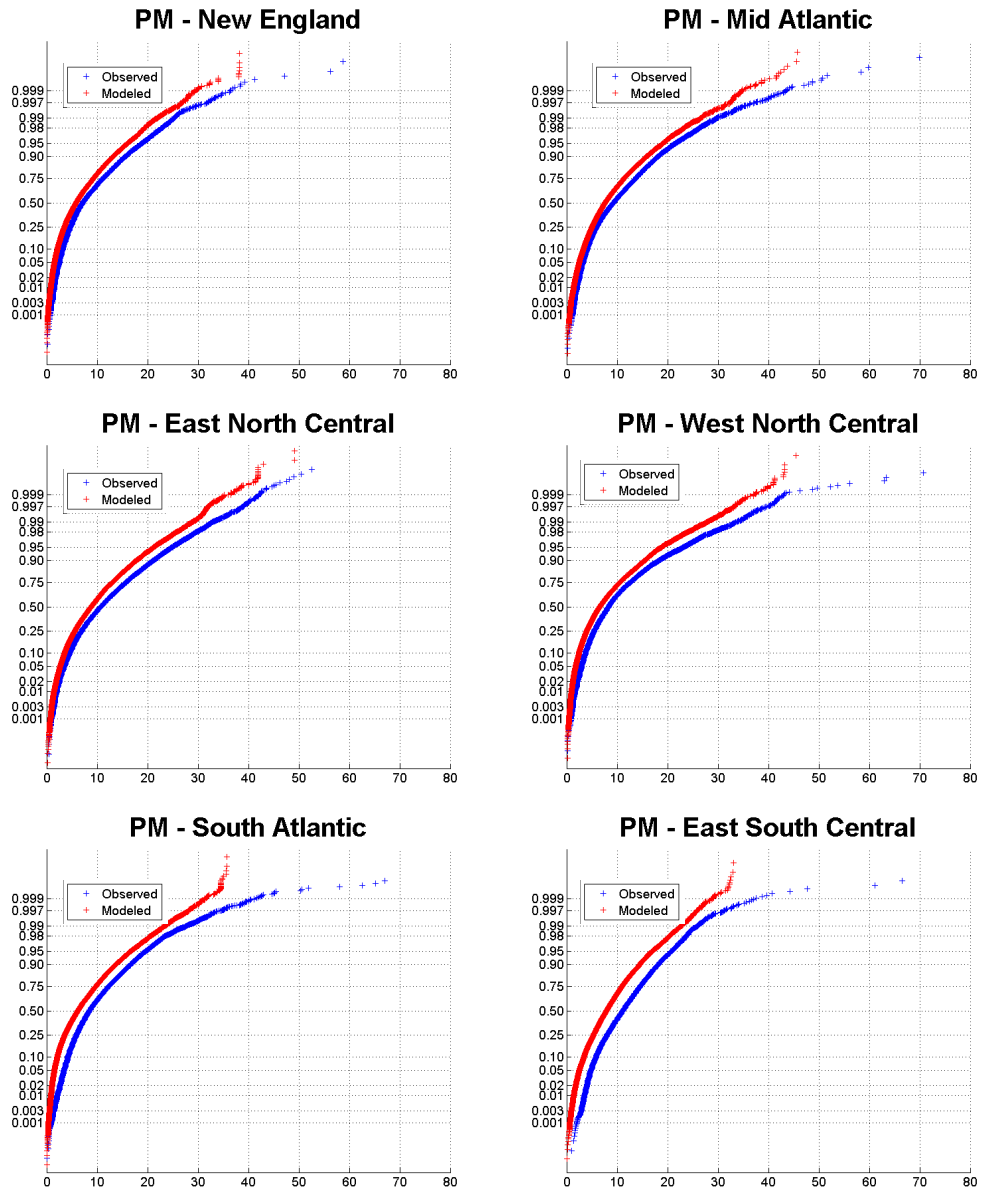

Figure B-2 (continued on next page) Cumulative distribution functions (CDFs) of observed (blue) and modeled (red) daily 24-hr average $PM_{2.5}$ concentrations (µg m^{-3}) for the nine U.S. census regions during the year 2010. Observed $PM_{2.5}$ concentrations were retrieved from the EPA-AQS data.

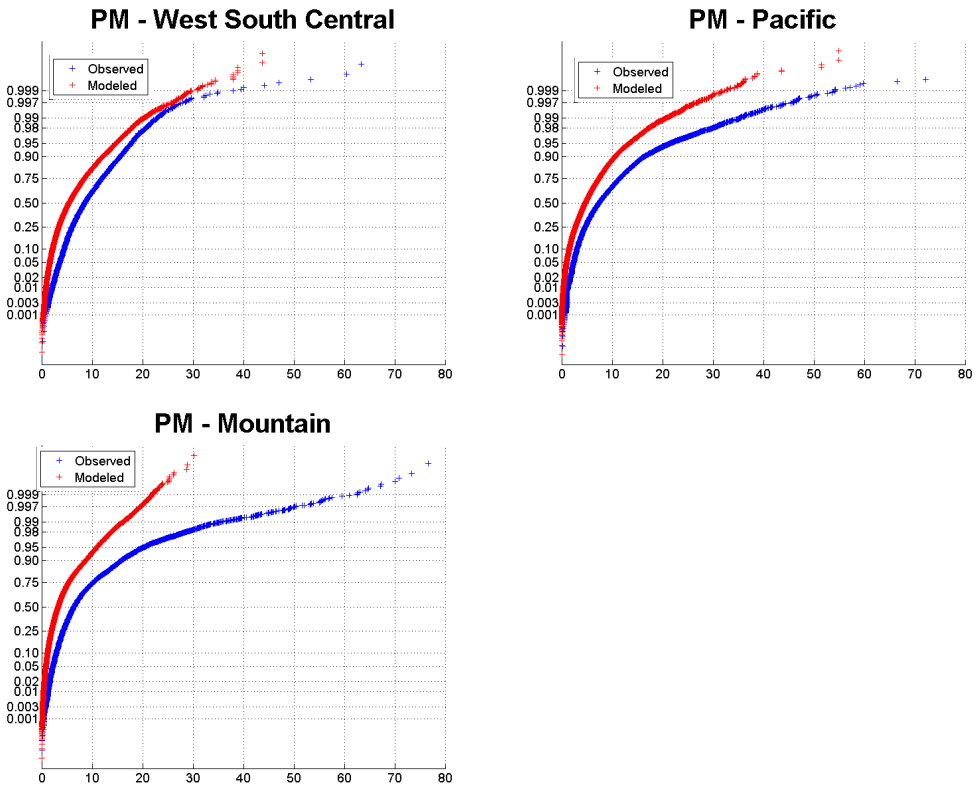

Figure B-2 (continued) Cumulative distribution functions (CDFs) of observed (blue) and modeled (red) daily 24-hr average $PM_{2.5}$ concentrations ($\mu g\ m^{-3}$) for the nine U.S. census regions during the year 2010. Observed $PM_{2.5}$ concentrations were retrieved from the EPA-AQS data.

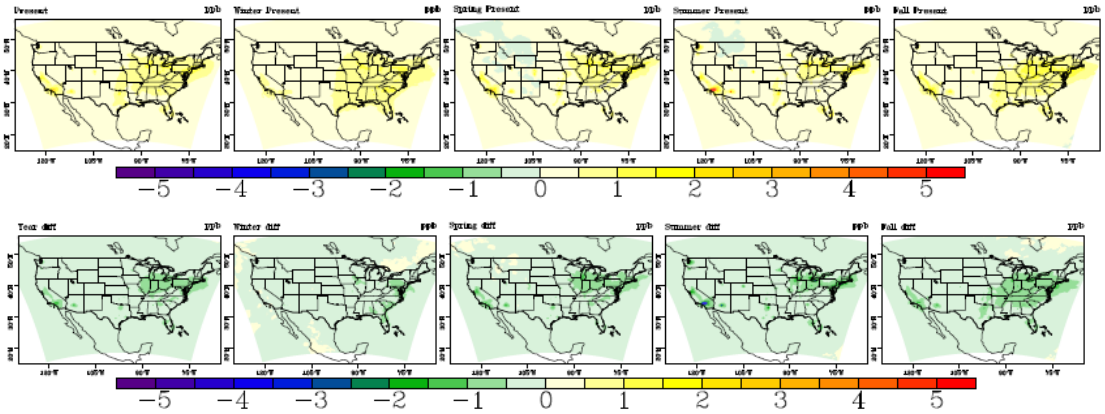

Figure B-3 Average present SA-MDA8 sensitivity to mobile sector emissions of VOC (top) and difference between present and future (future minus present) (bottom)

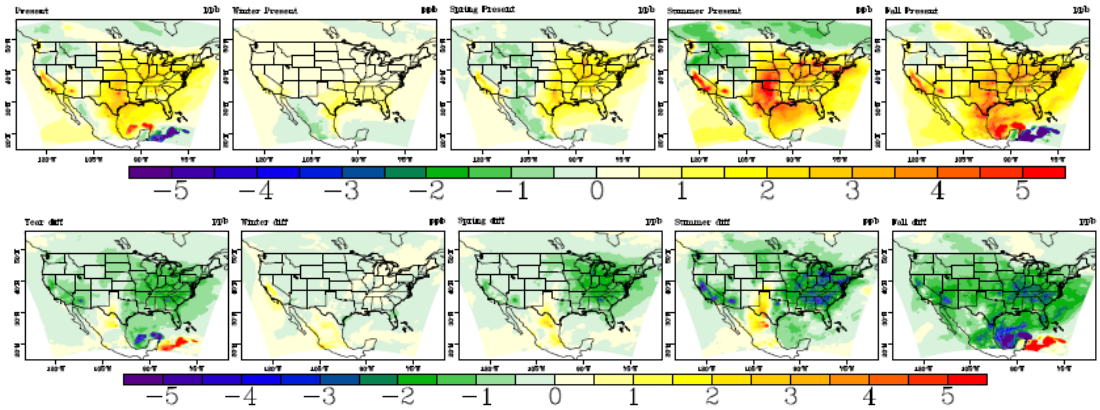

Figure B-4 Average present SA-MDA8 sensitivity to biogenic emissions of VOC (top) and difference between present and future (future minus present) (bottom)

(a)

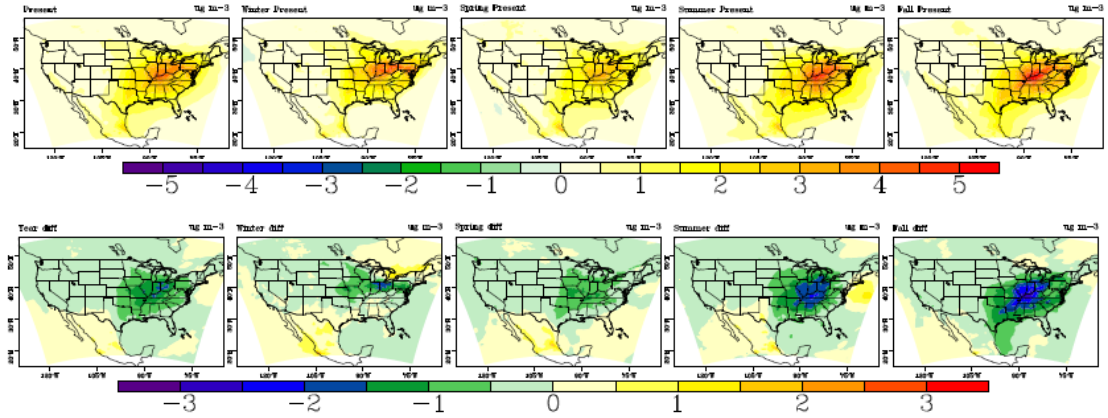

(b)

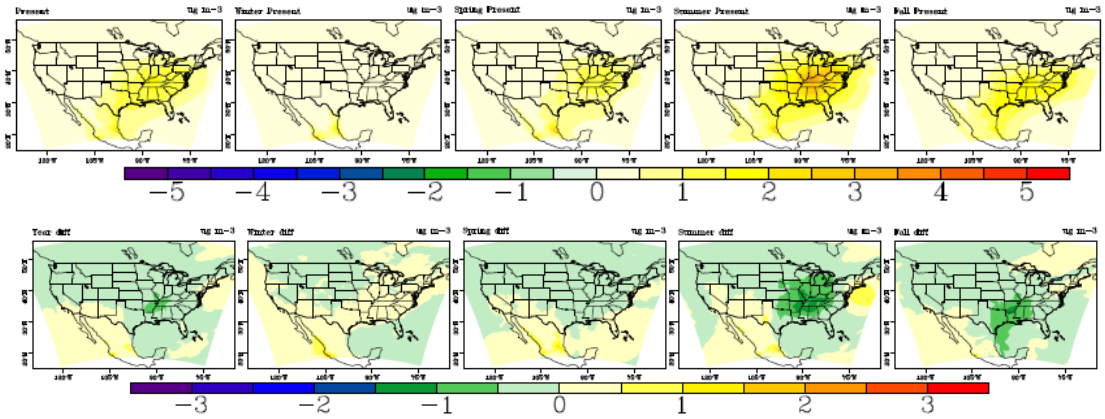

Figure B-5 Average present $PM_{2.5}$ sensitivity to total SO_X emissions (top) and difference (bottom) (a) and Average present $PM_{2.5}$ sensitivity to point SO_X (top) and difference (bottom) (b)

(a)

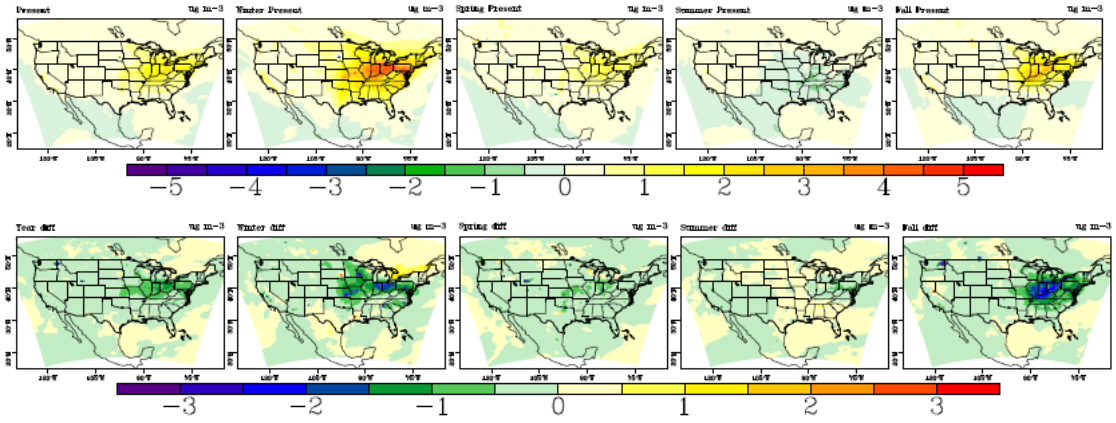

(b)

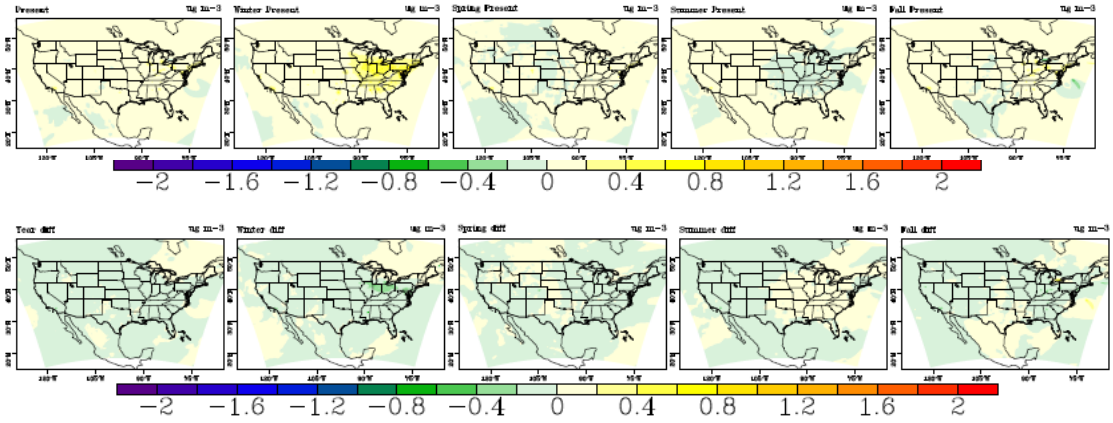

(c)

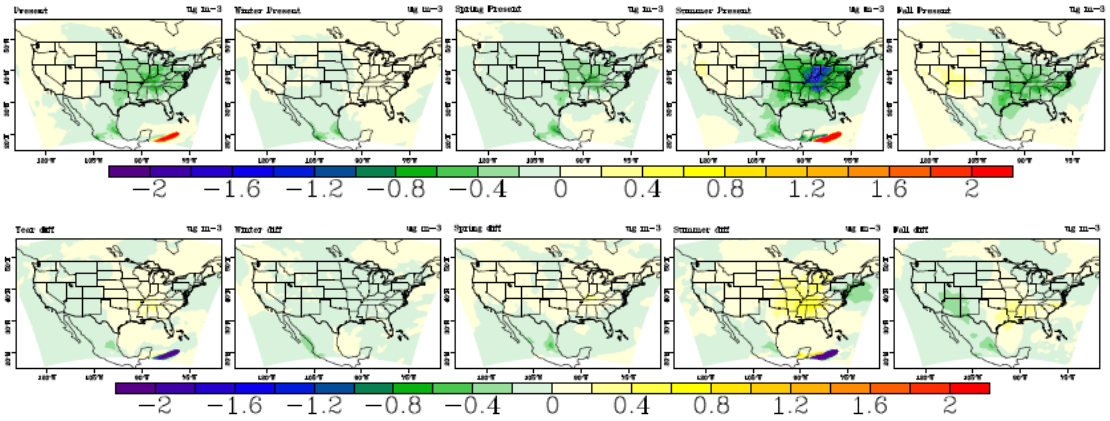

Figure B-6 Average present $PM_{2.5}$ sensitivity to total VOC (top) and future change (bottom) (a), average present $PM_{2.5}$ sensitivity to mobile VOC (top) and future change (bottom) (b) and average present $PM_{2.5}$ sensitivity to biogenic VOC (top) and future change (bottom) (c)

APPENDIX C

SUPPLEMENTAL MATERIAL FOR CHAPTER 4

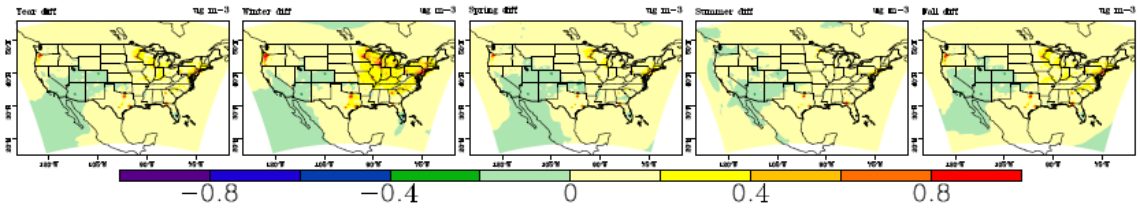

Figure C-1 Annual and seasonal average change in OM aerosol concentrations (µg m-3) for the TE scenario (scenario minus reference 2050)

APPENDIX D

SUPPLEMENTAL MATERIAL FOR CHAPTER 5

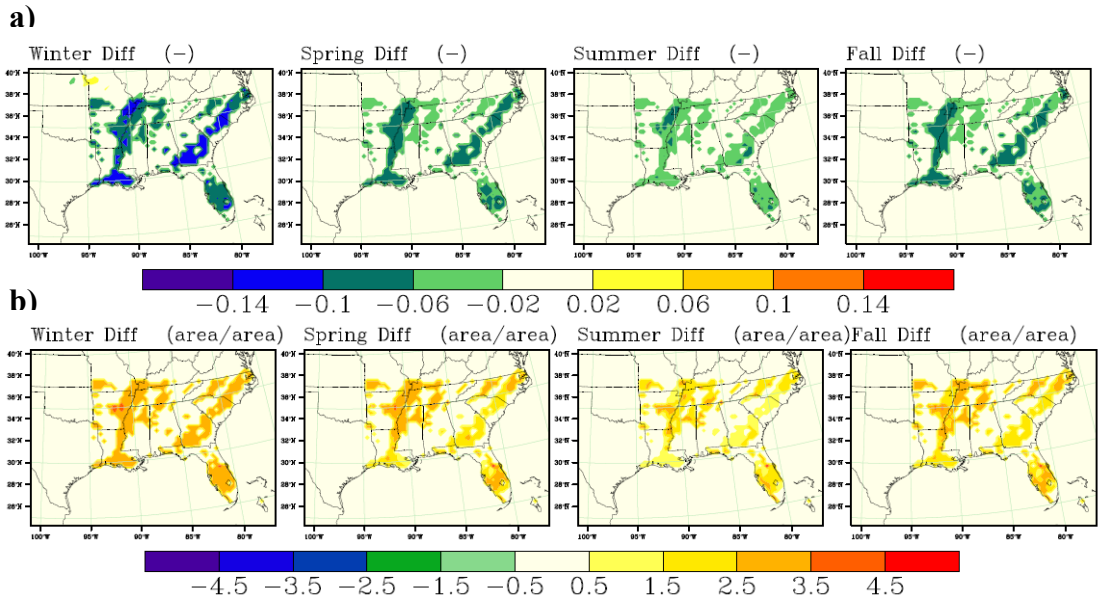

Figure D-1 Simulated albedo (a) and LAI (b) change of SE_for minus SE_norm scenario during the four seasons of the year 2050.

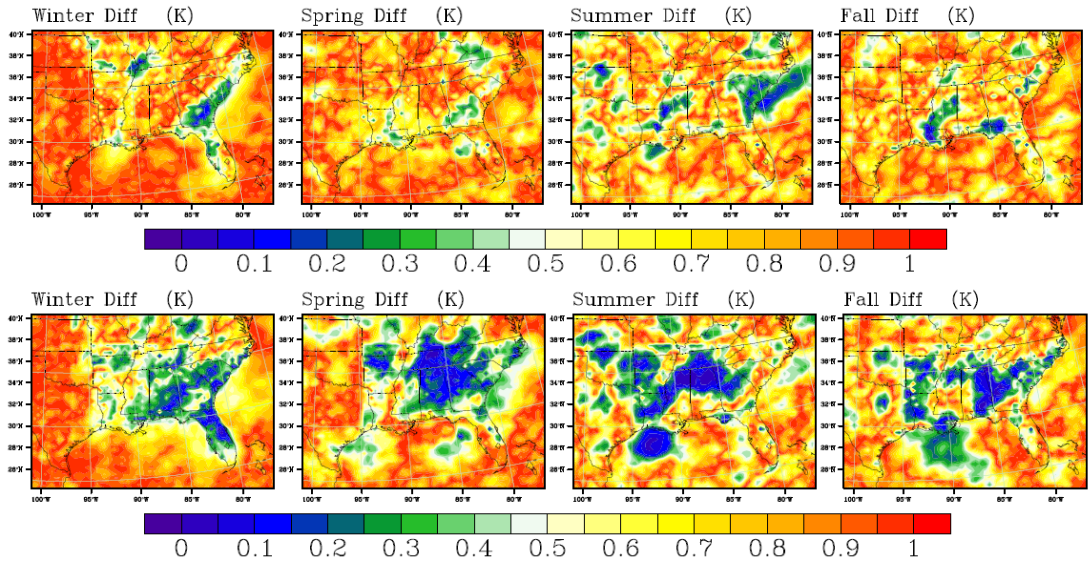

Figure D-2 Seasonal p-values resulting from a paired t-test of the surface temperature differences for the SE_for case (top) and SE_crop (bottom) case.

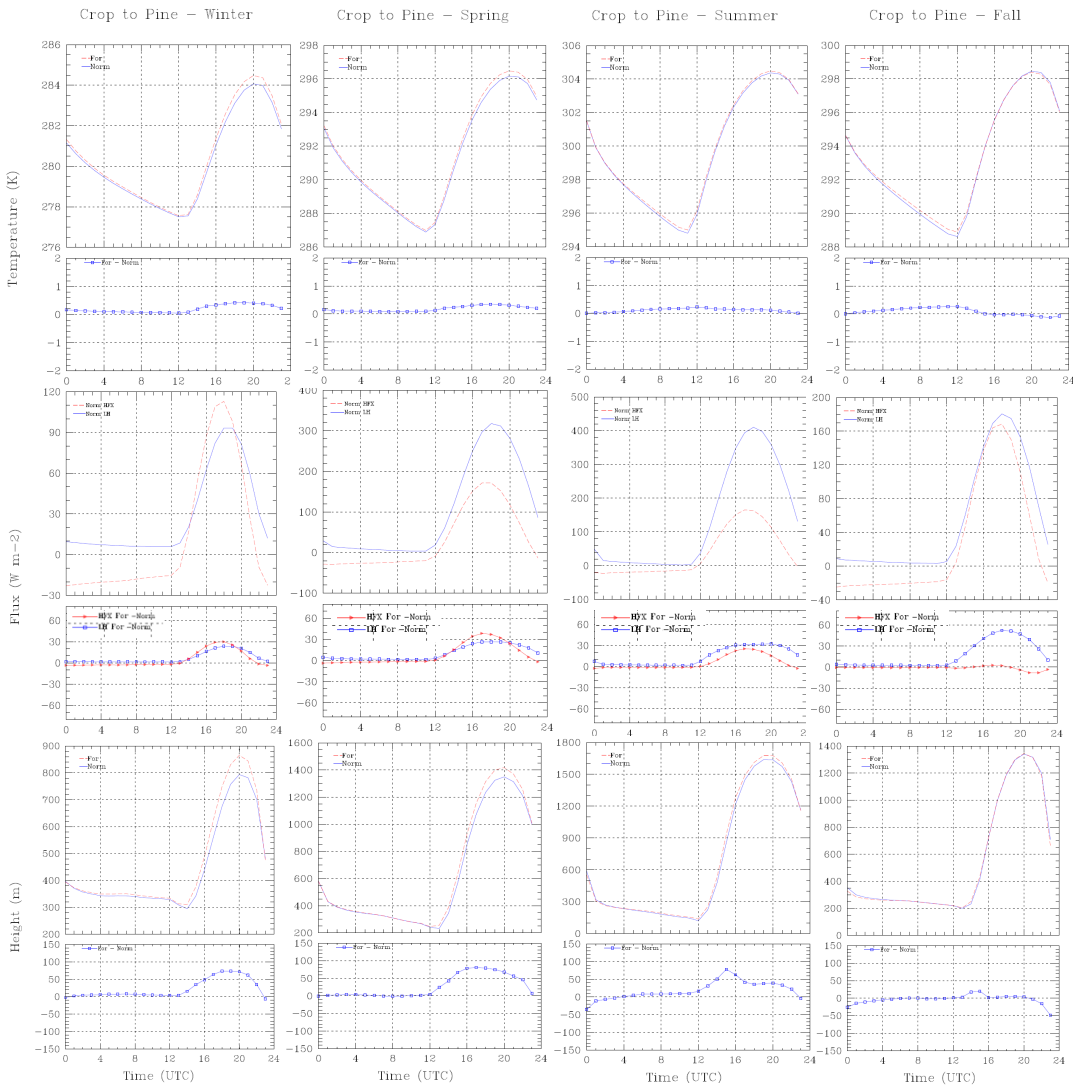

Figure D-3 Seasonal averages of the changes in diurnal surface temperature (top), heat flux partitioning (middle), and planetary boundary height (bottom) in grids where crop is converted to pine.

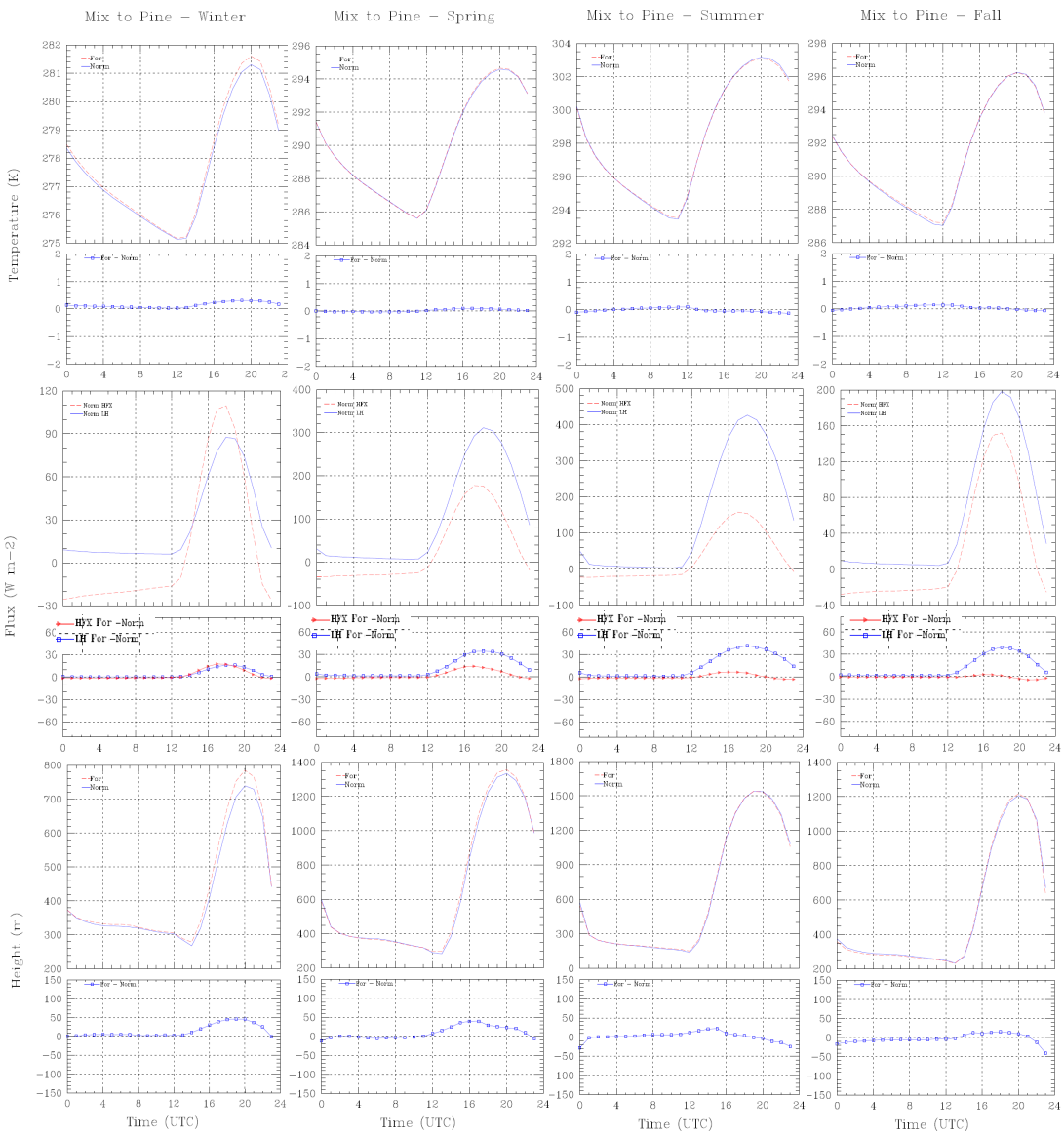

Figure D-4 Seasonal averages of the changes in diurnal surface temperature (top), heat flux partitioning (middle), and planetary boundary height (bottom) in grids where mixed cropland/woodland is converted to pine.

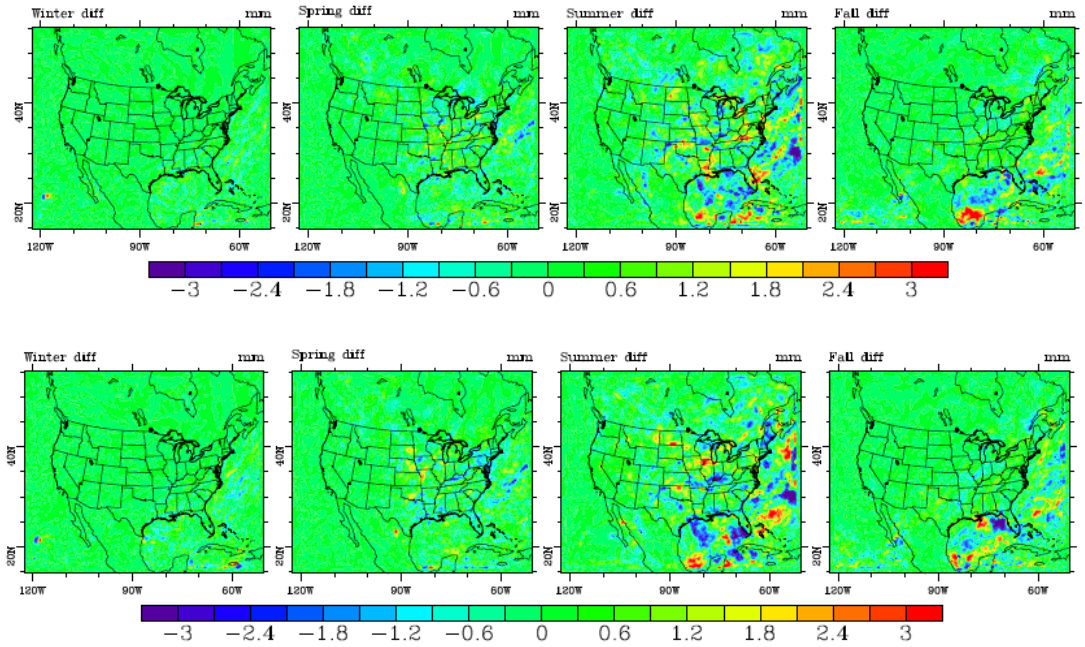

Figure D-5 Seasonal average precipitation difference for the SE_for (top) and SE_crop (bottom) scenarios

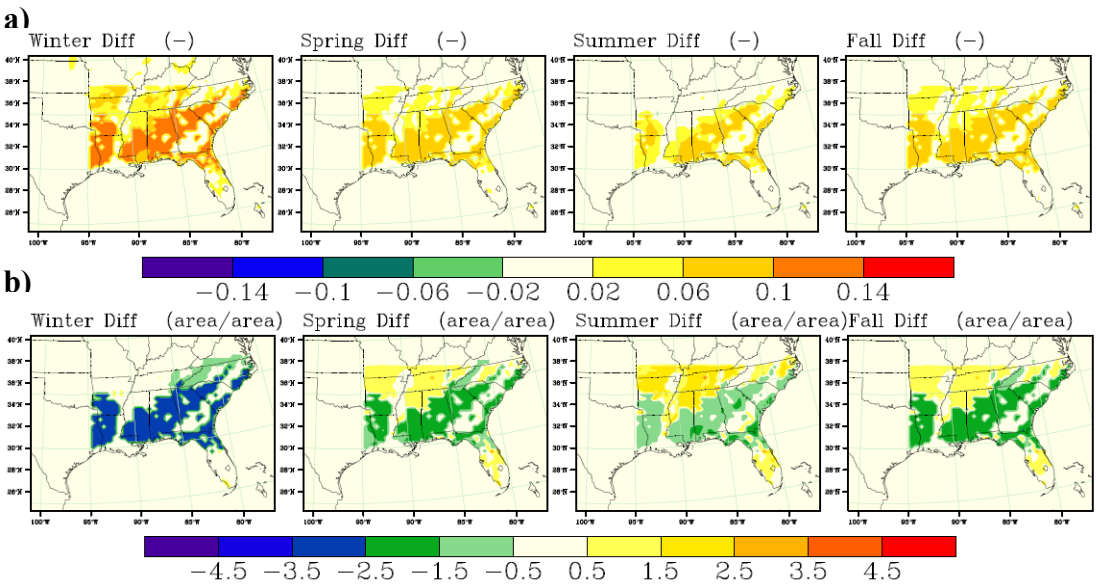

Figure D-6 Simulated albedo (a) and LAI (b) change of SE_crop minus SE_norm scenario during the four seasons of the year 2050.

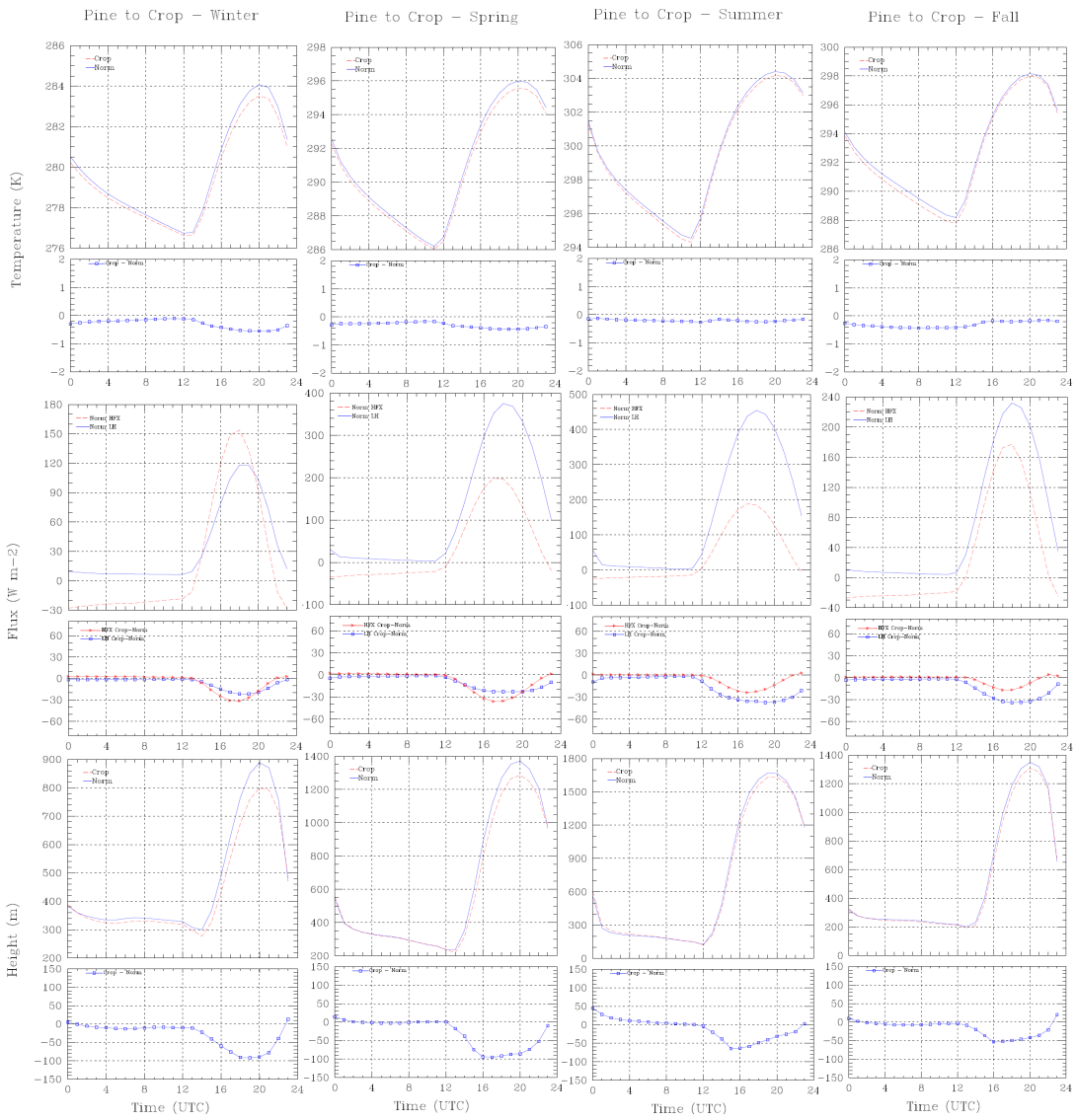

Figure D-7 Seasonal averages of the changes in diurnal surface temperature (top), heat flux partitioning (middle), and planetary boundary height (bottom) in grids where pine is converted to crop

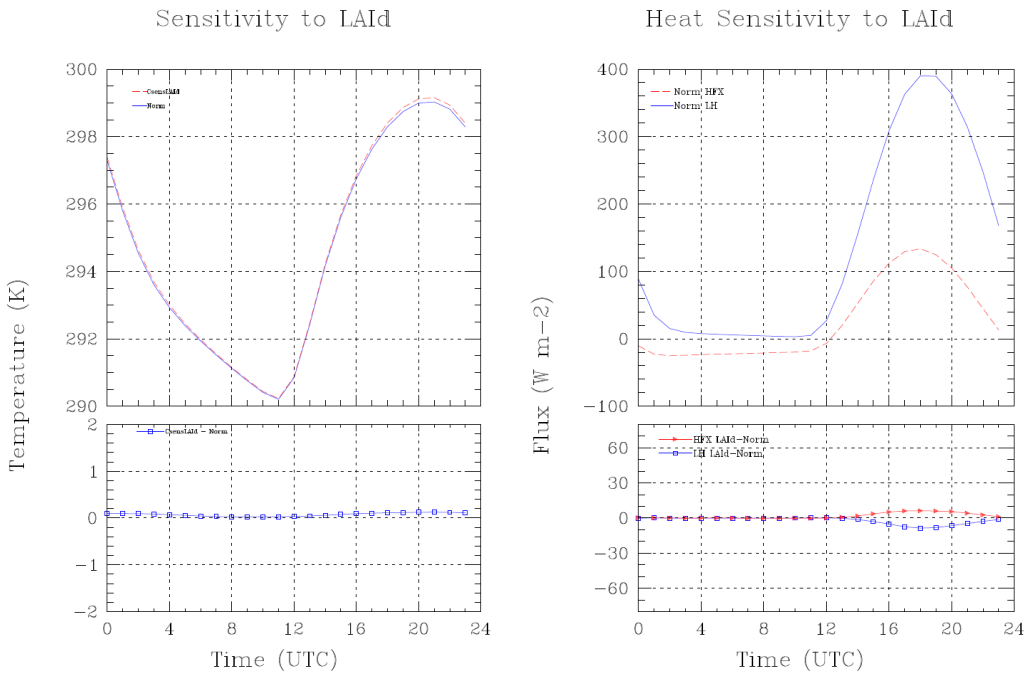

Figure D-8 Sensitivity of diurnal surface temperature (left) and heat flux partitioning (right) to LAI of deciduous forest applied to dryland cropland

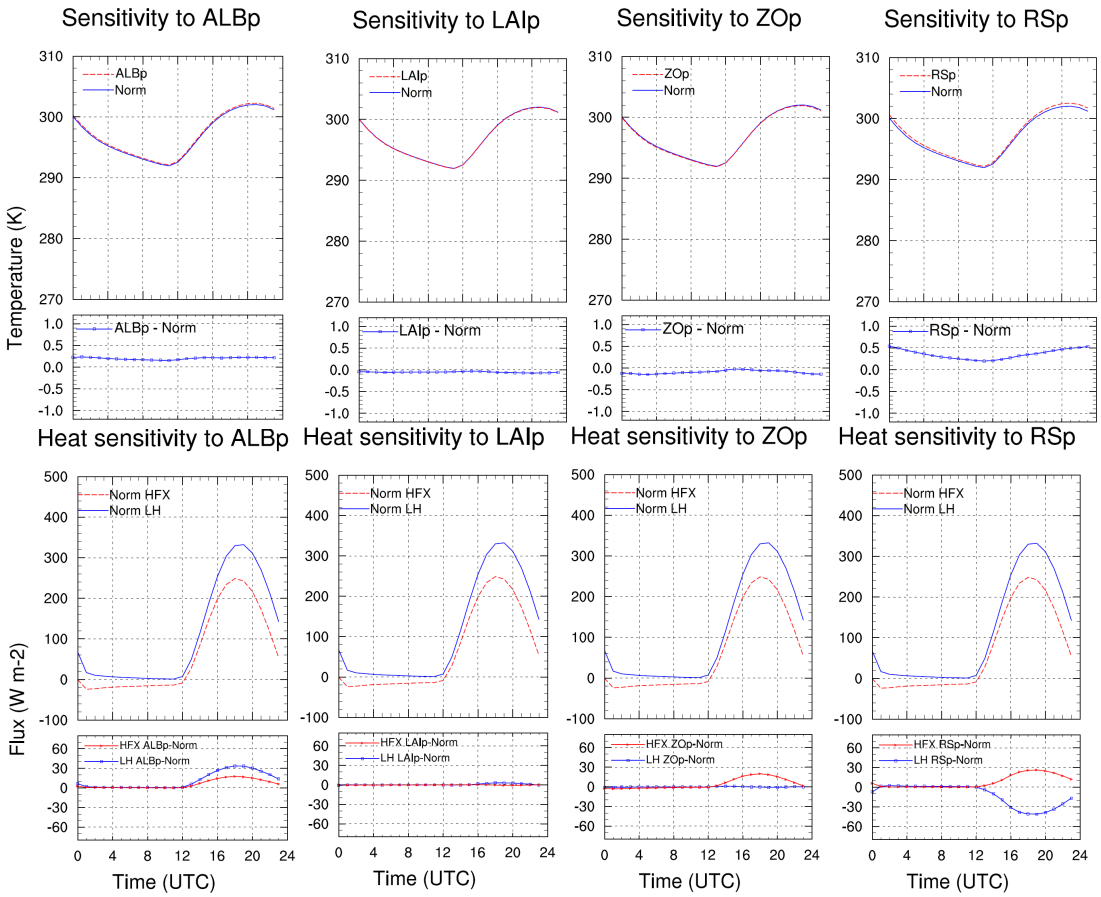

Figure D-9 Average diurnal temperature and heat flux trends and sensitivities to pine albedo (ALBp), leaf area index (LAI), surface roughness (Z^0p), and stomatal resistance (RSp) over the grid cells where the dominant landuse is crop during summer of the year 2050. These sensitivities were driven by NARR data as boundary and initial conditions with spectral nudging. Top row: average diurnal surface temperature of the base case (blue) and the perturbed parameter simulation (red). Second row: average diurnal surface temperature sensitivity (perturbed case minus base case). Third row: average diurnal sensible (red) and latent (blue) heat flux to the atmosphere for the base case. Bottom row: average diurnal sensible (red) and latent (blue) heat flux sensitivities (perturbed case minus base case).

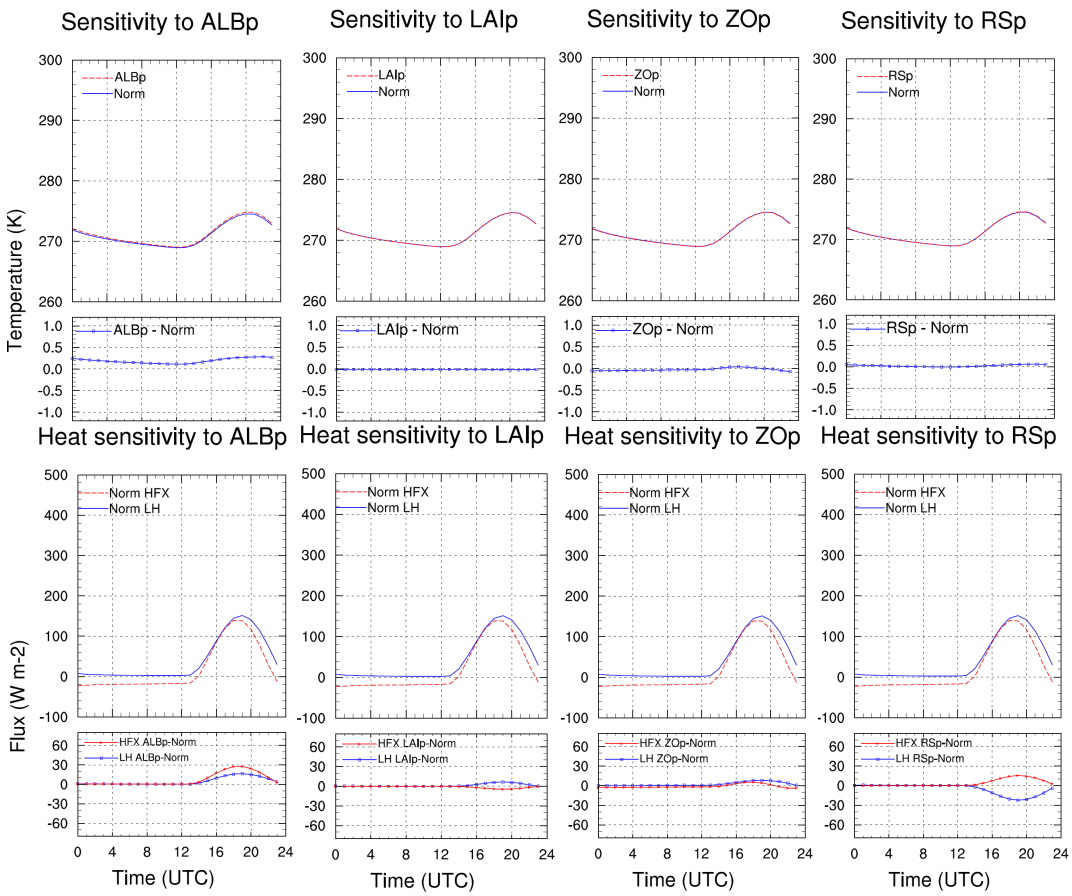

Figure D-10 Average diurnal temperature and heat flux trends and sensitivities to pine albedo (ALBp), leaf area index (LAI), surface roughness (Z^0p), and stomatal resistance (RSp) over the grid cells where the dominant landuse is crop during winter of the year 2050. These sensitivities were driven by NARR data as boundary and initial conditions with spectral nudging. Top row: average diurnal surface temperature of the base case (blue) and the perturbed parameter simulation (red). Second row: average diurnal surface temperature sensitivity (perturbed case minus base case). Third row: average diurnal sensible (red) and latent (blue) heat flux to the atmosphere for the base case. Bottom row: average diurnal sensible (red) and latent (blue) heat flux sensitivities (perturbed case minus base case).

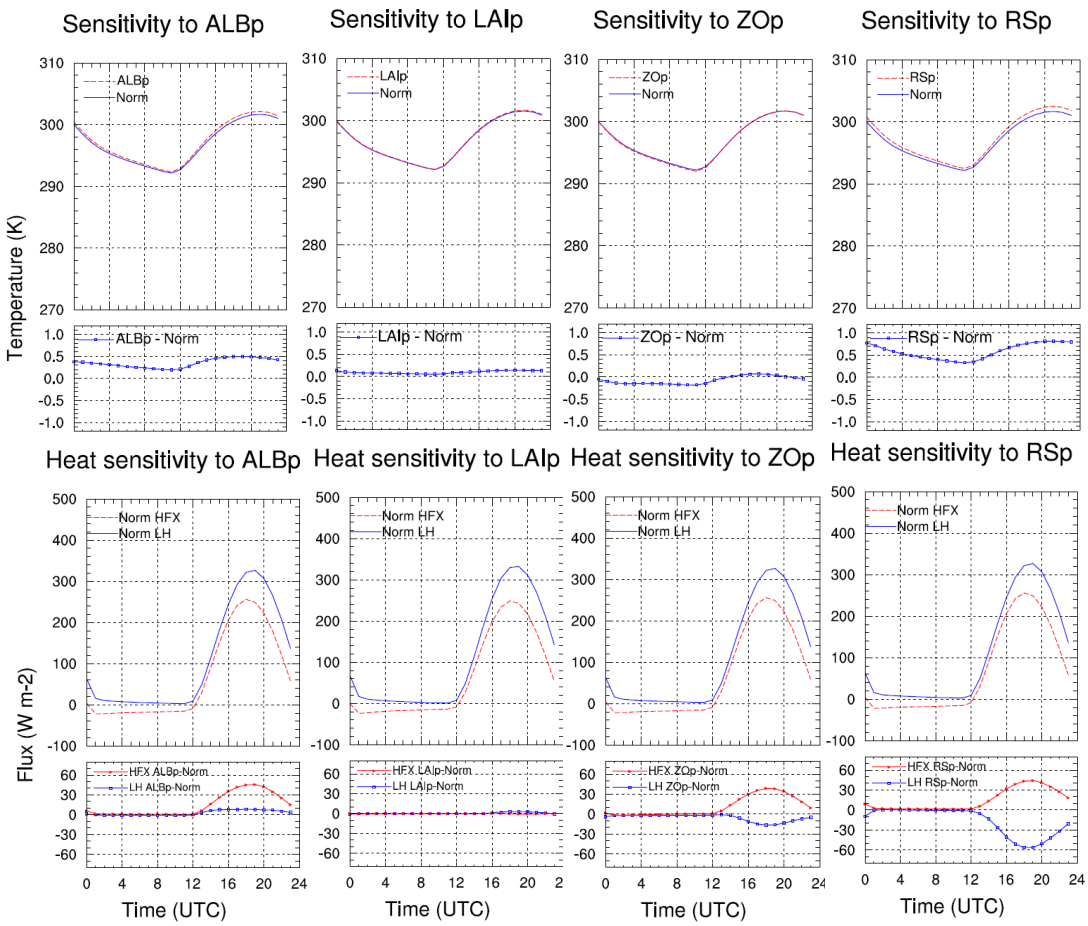

Figure D-11 Average diurnal temperature and heat flux trends and sensitivities to pine albedo (ALBp), leaf area index (LAI), surface roughness (Z^0p), and stomatal resistance (RSp) over the grid cells where the dominant landuse is crop during summer of the year 2050. These sensitivities were driven by NARR data as boundary and initial conditions with no nudging. Top row: average diurnal surface temperature of the base case (blue) and the perturbed parameter simulation (red). Second row: average diurnal surface temperature sensitivity (perturbed case minus base case). Third row: average diurnal sensible (red) and latent (blue) heat flux to the atmosphere for the base case. Bottom row: average diurnal sensible (red) and latent (blue) heat flux sensitivities (perturbed case minus base case).

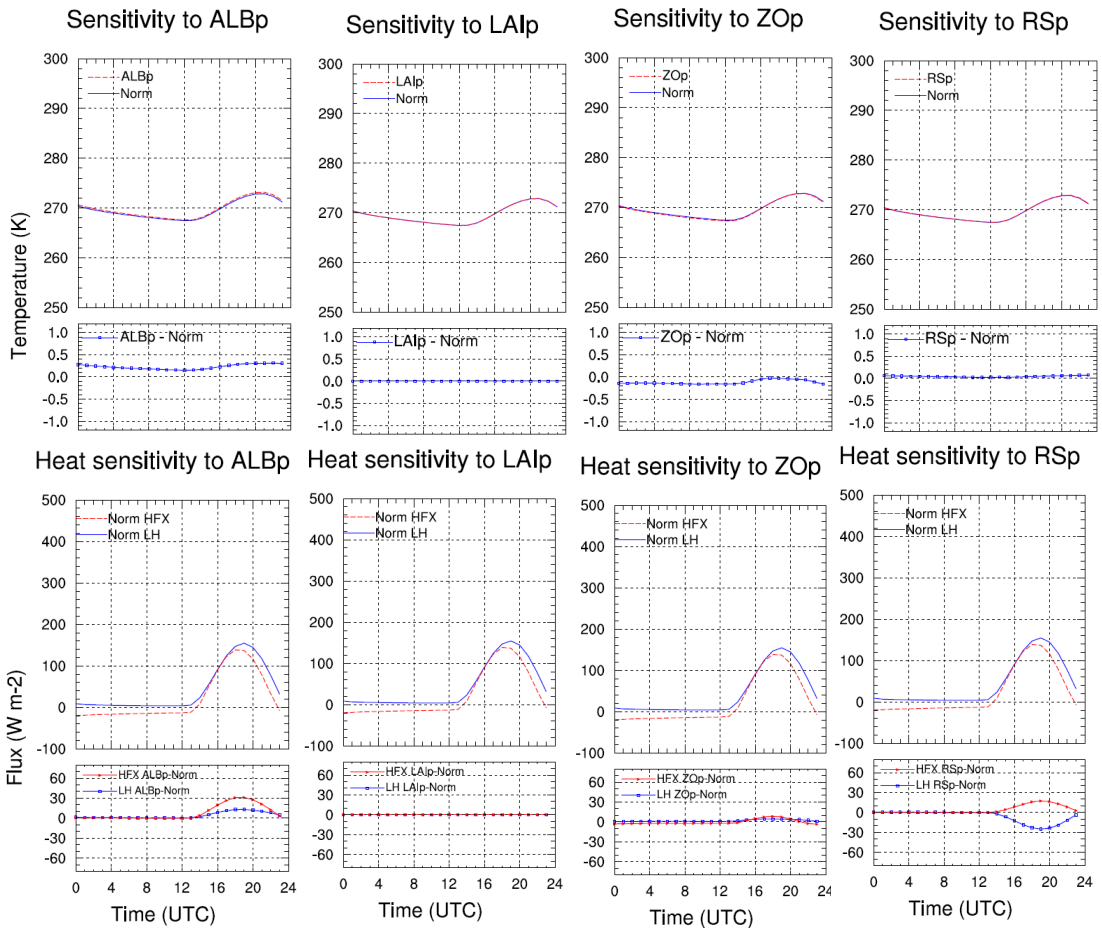

Figure D-12 Average diurnal temperature and heat flux trends and sensitivities to pine albedo (ALBp), leaf area index (LAI), surface roughness (Z^0p), and stomatal resistance (RSp) over the grid cells where the dominant landuse is crop during winter of the year 2050. These sensitivities were driven by NARR data as boundary and initial conditions with no nudging. Top row: average diurnal surface temperature of the base case (blue) and the perturbed parameter simulation (red). Second row: average diurnal surface temperature sensitivity (perturbed case minus base case). Third row: average diurnal sensible (red) and latent (blue) heat flux to the atmosphere for the base case. Bottom row: average diurnal sensible (red) and latent (blue) heat flux sensitivities (perturbed case minus base case).

References

Akhtar, F., et al. (2008), Beyond the standards: Designer Air Quality in 2050, *Bulletin of the American Meteorological Society*, *89*(1), 38-38

Alfarra, M. R., et al. (2007), Identification of the mass spectral signature of organic aerosols from wood burning emissions, *Environmental Science & Technology*, *41*(16), 5770-5777, doi:10.1021/es062289b.

Aneja, V. P., et al. (2012), Reactive nitrogen emissions from crop and livestock farming in India, *Atmospheric Environment*, *47*, 92-103, doi:10.1016/j.atmosenv.2011.11.026.

Bala, G., et al. (2005), Multiceutury changes to the global climate and carbon cycle: Results from a coupled climate and carbon cycle model, *Journal of Climate*, *18*(21), 4531-4544, doi:10.1175/jcli3542.1.

Bala, G., et al. (2007), Combined climate and carbon-cycle effects of large-scale deforestation, *Proc. Natl. Acad. Sci. U. S. A.*, *104*(16), 6550-6555, doi:10.1073/pnas.0608998104.

Beltran-Przekurat, A., et al. (2012), Modelling the effects of land-use/land-cover changes on the near-surface atmosphere in southern South America, *Int. J. Climatol.*, *32*(8), 1206-1225, doi:10.1002/joc.2346.

Betts, R. A. (2000), Offset of the potential carbon sink from boreal forestation by decreases in surface albedo, *Nature*, *408*(6809), 187-190, doi:10.1038/35041545.

Betts, R. A., et al. (2007), Biogeophysical effects of land use on climate: Model simulations of radiative forcing and large-scale temperature change, *Agric. For. Meteorol.*, *142*(2-4), 216-233, doi:10.1016/j.agrformet.2006.08.021.

Brown, K. E., et al. (2013), Accounting for Climate and Air Quality Damages in Future US Electricity Generation Scenarios, *Environmental Science & Technology*, *47*(7), 3065-3072, doi:10.1021/es304281g.

Bull, S. R. (1996), Renewable energy transportation technologies, *Renewable Energy*, *9*(1-4), 1019-1024

Byun, D., and K. Schere (2006), Review of the Governing Equations, Computational Algorithms, and Other Components of the Models-3 Community Multiscale Air Quality (CMAQ) Modeling System, *Applied Mechanics Reviews*, *59*(2), 51-77

Cai, M., and E. Kalnay (2004), Climate - Impact of land-use change on climate - Reply, *Nature*, *427*(6971), 214-214, doi:10.1038/427214a.

Carter, W. P. L. (2000), Documentation of the SAPRC-99 chemical mechanism for VOC reactivity assessment, University of California, Riverside, Riverside, CA.

Castro, C. L., et al. (2005), Dynamical downscaling: Assessment of value retained and added using the regional atmospheric modeling system (RAMS), *Journal of Geophysical Research-Atmospheres*, *110*(D5), 21, doi:D05108 10.1029/2004jd004721.

CEP (2003), Sparse Matrix Operator Kernel Emissions Modeling System (SMOKE) User Manual, edited, Chapel Hill, NC.

Chase, T. N., et al. (2000), Simulated impacts of historical land cover changes on global climate in northern winter, *Climate Dynamics*, *16*(2-3), 93-105, doi:10.1007/s003820050007.

Chen, C. C., and Y. T. Chen (2013), Energy recovery or material recovery for MSW treatments?, *Resour. Conserv. Recycl.*, *74*, 37-44, doi:10.1016/j.resconrec.2013.02.003.

Chen, C. H., et al. (2006a), Reductions in emissions of local air pollutants and co-benefits of Chinese energy policy: a Shanghai case study, *Energy Policy*, *34*(6), 754-762, doi:10.1016/j.enpol.2004.07.007.

Chen, H., et al. (2006b), Effect of land-cover change on terrestrial carbon dynamics in the southern United States, *J. Environ. Qual.*, *35*(4), 1533-1547, doi:10.2134/jeq2005.0198.

Christy, J. R., et al. (2006), Methodology and results of calculating central california surface temperature trends: Evidence of human-induced climate change?, *Journal of Climate*, *19*(4), 548-563, doi:10.1175/jcli3627.1.

Conner, R. C., and A. J. Hartsell (2002.), The Southern Forest Resource Assessment: Chapter 16, Forest Area and Conditions, Department of Agriculture, Forest Service, Southern Research Station,.

Davin, E. L., and N. de Noblet-Ducoudre (2010), Climatic Impact of Global-Scale Deforestation: Radiative versus Nonradiative Processes, *Journal of Climate*, *23*(1), 97-112, doi:10.1175/2009jcli3102.1.

Dawson, J. P., et al. (2008), Simulating present-day and future air quality as climate changes: Model evaluation, *Atmospheric Environment*, *42*(19), 4551-4566, doi:10.1016/j.atmosenv.2008.01.058.

Dholakia, H. H., et al. (2013), Impact of current policies on future air quality and health outcomes in Delhi, India, *Atmospheric Environment*, *75*, 241-248, doi:10.1016/j.atmosenv.2013.04.052.

Dudhia, J. (1989), Numerical study of convection observed during the winter monsoon experiment using a mesoscale two-dimensional model, *J. Atmos. Sci.*, *46*(20), 3077-3107

Dunker, A. M., et al. (2002), The decoupled direct method for sensitivity analysis in a three-dimensional air quality model - Implementation, accuracy, and efficiency, *Environmental Science & Technology*, *36*(13), 2965-2976

Ek, M. B., et al. (2003), Implementation of Noah land surface model advances in the National Centers for Environmental Prediction operational mesoscale Eta model, *Journal of Geophysical Research-Atmospheres*, *108*(D22), 16, doi:8851 10.1029/2002jd003296.

Elobeid, A., et al. (2013), Integration of agricultural and energy system models for biofuel assessment, *Environ. Modell. Softw.*, *48*, 1-16, doi:10.1016/j.envsoft.2013.05.007.

Emery, C., Edward Tai (2001), Meteorological Modeling and Performance Evaluation of hte September 13-20, 1999 Ozone Episode, in *Prepared for the Texas Near Non-Attainment Areas through the Alamo Area Council of Governments, by ENVIRON International Corp*, edited, Navato, CA.

EPA, U. S. (1989), The potential effects of global climate change on the United States, *EPA*, *EPA-230-05-89-050*, 457

Fall, S., et al. (2010a), Temperature and equivalent temperature over the United States (1979-2005), *Int. J. Climatol.*, *30*(13), 2045-2054, doi:10.1002/joc.2094.

Fall, S., et al. (2010b), Impacts of land use land cover on temperature trends over the continental United States: assessment using the North American Regional Reanalysis, *Int. J. Climatol.*, *30*(13), 1980-1993, doi:10.1002/joc.1996.
Fann, N., et al. (2013), The Recent and Future Health Burden of Air Pollution Apportioned Across US Sectors, *Environmental Science & Technology*, *47*(8), 3580-3589, doi:10.1021/es304831q.
Farooq, M. K., et al. (2013), Energy, environmental and economic effects of Renewable Portfolio Standards (RPS) in a Developing Country, *Energy Policy*, *62*, 989-1001, doi:10.1016/j.enpol.2013.07.098.
Fishbone, L. G., et al. (1980), MARKAL, a Multiperiod Linear-Programming Model for Energy-Systems Analysis Applied to the United-States, *Bulletin of the American Physical Society*, *25*(4), 494-495
Foley, K. M., et al. (2001), Incremental testing of the Community Multiscale Air Quality (CMAQ) modeling system version 4.7, *Geoscientific Model Development*, *3*(1), 205-226
Ganzeveld, L., and J. Lelieveld (2004), Impact of Amazonian deforestation on atmospheric chemistry, *Geophysical Research Letters*, *31*(6), 5, doi:L06105 10.1029/2003gl019205.
Geron, C., et al. (2006), Volatile organic compounds from vegetation in southern Yunnan Province, China: Emission rates and some potential regional implications, *Atmospheric Environment*, *40*(10), 1759-1773, doi:10.1016/j.atmosenv.2005.11.022.
Gielen, D., and C. H. Chen (2001), The CO2 emission reduction benefits of Chinese energy policies and environmental policies: A case study for Shanghai, period 1995-2020, *Ecol. Econ.*, *39*(2), 257-270, doi:10.1016/s0921-8009(01)00206-3.
Giorgi, F. (2006), Regional climate modeling: Status and perspectives, *J. Phys. IV*, *139*, 101-118, doi:10.1051/jp4:2006139008.
Grell, G. A., Dudhia, J., Stauffer, D. R. A (1994), A description of the fifth generation Penn State/NCAR mesoscale model (MM5), *National Center for Atmospheric Research: Boulder, CO*
Henze, D. K., et al. (2008), Global modeling of secondary organic aerosol formation from aromatic hydrocarbons: high- vs. low-yield pathways, *Atmospheric Chemistry and Physics*, *8*(9), 2405-2420
Hong, S. Y., et al. (2006), A new vertical diffusion package with an explicit treatment of entrainment processes, *Mon. Weather Rev.*, *134*(9), 2318-2341
Houweling, S., et al. (1998), The impact of nonmethane hydrocarbon compounds on tropospheric photochemistry, *Journal of Geophysical Research-Atmospheres*, *103*(D9), 10673-10696, doi:10.1029/97jd03582.
IPCC (2007), Climate Change 2007 IPCC Fourth Assessment Report: Synthesis Report, 184 pp, IPCC, Geneva, Switzerland.
Ito, K., et al. (2005), Associations between ozone and daily mortality - Analysis and meta-analysis, *Epidemiology*, *16*(4), 446-457, doi:10.1097/01.ede.0000165821.90114.7f.
Jacob, D. J., and D. A. Winner (2009), Effect of climate change on air quality, *Atmospheric Environment*, *43*(1), 51-63, doi:10.1016/j.atmosenv.2008.09.051.

Jiang, X. Y., et al. (2008), Predicted impacts of climate and land use change on surface ozone in the Houston, Texas, area, *Journal of Geophysical Research-Atmospheres*, *113*(D20), 16, doi:D20312 10.1029/2008jd009820.

Jihee, S., et al. (2008), The Impacts of Urbanization on Emissions and Air Quality: Comparison of Four Visions of Austin, Texas, *Environmental Science & Technology*, *42*(19), 7294-7300

Juang, J. Y., et al. (2007), Separating the effects of albedo from eco-physiological changes on surface temperature along a successional chronosequence in the southeastern United States, *Geophysical Research Letters*, *34*(21), 5, doi:L21408 10.1029/2007gl031296.

Kain J. S., F. J. M. (1993), Convective parameterization models: The Kain–Fritsch scheme. Cumulus Convection in Numerical Models, *American Meteorological Society*, *46*, 165-170

Kain, J. S., and J. M. Fritsch (1993), Convective parameterization models: The Kain–Fritsch scheme. Cumulus Convection in Numerical Models, *American Meteorological Society*, *46*, 165-170

Kalnay, E., and M. Cai (2003), Impact of urbanization and land-use change on climate, *Nature*, *423*(6939), 528-531, doi:10.1038/nature01675.

Korshover, J., and J. K. Angell (1982), A review of air-stagnation cases in the Eastern-United-States during 1981 - Annual summary, *Monthly Weather Review*, *110*(10), 1515-1518, doi:10.1175/1520-0493(1982)110<1515:aroasc>2.0.co;2.

Lamarque, J. F., et al. (2011), Global and regional evolution of short-lived radiatively-active gases and aerosols in the Representative Concentration Pathways, *Clim. Change*, *109*(1-2), 191-212, doi:10.1007/s10584-011-0155-0.

Lawrence, P. J., and T. N. Chase (2007), Representing a new MODIS consistent land surface in the Community Land Model (CLM 3.0), *J. Geophys. Res.-Biogeosci.*, *112*(G1), 17, doi:G01023 10.1029/2006jg000168.

Lawrence, P. J., and T. N. Chase (2010), Investigating the climate impacts of global land cover change in the community climate system model, *Int. J. Climatol.*, *30*(13), 2066-2087, doi:10.1002/joc.2061.

Leibensperger, E. M., et al. (2012a), Climatic effects of 1950-2050 changes in US anthropogenic aerosols - Part 1: Aerosol trends and radiative forcing, *Atmospheric Chemistry and Physics*, *12*(7), 3333-3348, doi:10.5194/acp-12-3333-2012.

Leibensperger, E. M., et al. (2012b), Climatic effects of 1950-2050 changes in US anthropogenic aerosols - Part 2: Climate response, *Atmospheric Chemistry and Physics*, *12*(7), 3349-3362, doi:10.5194/acp-12-3349-2012.

Leiby, P. N., and J. Rubin (2003), Transitions in light-duty vehicle transportation - Alternative-fuel and hybrid vehicles and learning, in *Energy, Air Quality, and Fuels 2003*, edited, pp. 127-134.

Leung, L. R., and W. I. Gustafson (2005), Potential regional climate change and implications to US air quality, *Geophysical Research Letters*, *32*(16), 4, doi:L16711 10.1029/2005gl022911.

Liao, H., et al. (2006a), Role of climate change in global predictions of future tropospheric ozone and aerosols, *Journal of Geophysical Research-Atmospheres*, *111*(D12), 18, doi:D12304 10.1029/2005jd006852.

Liao, H., et al. (2007a), Biogenic secondary organic aerosol over the United States: Comparison of climatological simulations with observations, *Journal of Geophysical Research-Atmospheres*, *112*(D6), 19, doi:D06201 10.1029/2006jd007813.

Liao, K. J., et al. (2006b), Impact of Climate Change on Sulfur and Nitrogen Deposition in the U.S, paper presented at 86th AMS Annual Meeting, Atlanta, GA.

Liao, K. J., et al. (2006c), Impact of Future Climate Change on Regional Air Quality in the U.S, paper presented at Environmental Science & Health Symposium, Atlanta, GA.

Liao, K. J., et al. (2007b), Sensitivities of ozone and fine particulate matter formation to emissions under the impact of potential future climate change, *Environmental Science & Technology*, *41*(24), 8355-8361, doi:10.1021/es070998z.

Likens, G. E., et al. (1996), Long-term effects of acid rain: Response and recovery of a forest ecosystem, *Science*, *272*(5259), 244-246, doi:10.1126/science.272.5259.244.

Lim, S. S., et al. (2012), A comparative risk assessment of burden of disease and injury attributable to 67 risk factors and risk factor clusters in 21 regions, 1990-2010: a systematic analysis for the Global Burden of Disease Study 2010 (vol 380, pg 2224, 2012), *Lancet*, *381*(9874), 1276-1276

Lin, Y. L., et al. (1983), Bulk parameterization of the snow field in a cloud model, *Journal of Climate and Applied Meteorology*, *22*(6), 1065-1092, doi:10.1175/1520-0450(1983)022<1065:bpotsf>2.0.co;2.

Liu, P., et al. (2012), Differences between downscaling with spectral and grid nudging using WRF, *Atmospheric Chemistry and Physics*, *12*(8), 3601-3610, doi:10.5194/acp-12-3601-2012.

Mahmood, R., et al. (2010), Impacts of land use/land cover change on climate and future research priorities, *Bulletin of the American Meteorological Society*, *91*(1), 37-+, doi:10.1175/2009bams2769.1.

Marti, O., and Coauthors (2005), The new IPSL climate system model: IPSL-CM4, *Note du Pole de Modelisation 26*, 86

Mauzerall, D. L., and X. P. Wang (2001), Protecting agricultural crops from the effects of tropospheric ozone exposure: Reconciling science and standard setting in the United States, Europe, and Asia, *Annu. Rev. Energ. Environ.*, *26*, 237-268, doi:10.1146/annurev.energy.26.1.237.

McCollum, D. L., et al. (2013), Climate policies can help resolve energy security and air pollution challenges, *Clim. Change*, *119*(2), 479-494, doi:10.1007/s10584-013-0710-y.

McMichael, A. J., et al. (2006), Climate change and human health: present and future risks, *Lancet*, *367*(9513), 859-869, doi:10.1016/s0140-6736(06)68079-3.

Mickley, L. J., et al. (2004), Effects of future climate change on regional air pollution episodes in the United States, *Geophysical Research Letters*, *31*(24), 4, doi:L24103 10.1029/2004gl021216.

Mickley, L. J. (2007), A future short of breath? Possible effects of climate change on smog, *Environment*, *49*(6), 34-43

Mlawer, E. J., et al. (1997), Radiative transfer for inhomogeneous atmospheres: RRTM, a validated correlated-k model for the longwave, *Journal of Geophysical Research-Atmospheres*, *102*(D14), 16663-16682, doi:10.1029/97jd00237.

Moss, R. H., et al. (2010), The next generation of scenarios for climate change research and assessment, *Nature*, *463*(7282), 747-756, doi:10.1038/nature08823.

Murphy, L. N., et al. (2012), Local and Remote Climate Impacts from Expansion of Woody Biomass for Bioenergy Feedstock in the Southeastern United States, *Journal of Climate*, *25*(21), 7643-7659, doi:10.1175/jcli-d-11-00535.1.

Murray, C. J. L., et al. (2013), Disability-adjusted life years (DALYs) for 291 diseases and injuries in 21 regions, 1990-2010: a systematic analysis for the Global Burden of Disease Study 2010, *Lancet*, *380*(9859), 2197-2223

Napelenok, S., et al. (2006), Implementation of the Decoupled Direct 3D Sensitivity Analysis Method for Particulate Matter and Analysis of Pollutant Responses in the Southeastern United States, *Atmospheric Environment*, *in press*

Nolte, C. G., et al. (2008), Linking global to regional models to assess future climate impacts on surface ozone levels in the United States, *Journal of Geophysical Research-Atmospheres*, *113*(D14), D14307, doi:10.1029/2007JD008497.

NRC (2005), Radiative Forcing of Climate Change: Expanding the Concept and Addressing Uncertainties, *National Research Council*, 208

Nunez, M. N., et al. (2008), Impact of land use and precipitation changes on surface temperature trends in Argentina, *Journal of Geophysical Research-Atmospheres*, *113*(D6), 11, doi:D06111 10.1029/2007jd008638.

Pacala, S. W., et al. (2001), Consistent land- and atmosphere-based US carbon sink estimates, *Science*, *292*(5525), 2316-2320, doi:10.1126/science.1057320.

Pielke, R. A., et al. (1991), A procedure to estimate worst-case air-quality in complex terrain, *Environ. Int.*, *17*(6), 559-574, doi:10.1016/0160-4120(91)90168-p.

Pielke, R. A., et al. (1998), Interactions between the atmosphere and terrestrial ecosystems: influence on weather and climate, *Glob. Change Biol.*, *4*(5), 461-475, doi:10.1046/j.1365-2486.1998.t01-1-00176.x.

Pielke, R. A., et al. (2011), Land use/land cover changes and climate: modeling analysis and observational evidence, *Wiley Interdiscip. Rev.-Clim. Chang.*, *2*(6), 828-850, doi:10.1002/wcc.144.

Pope, C. A., et al. (1995), Review of epidemiological evidence of health-effects of particulate air-pollution, *Inhal. Toxicol.*, *7*(1), 1-18, doi:10.3109/08958379509014267.

Prestemon, J. P., and R. C. Abt (2002), The Southern timber market to 2040, *Journal of Forestry*, *100*(7), 16-22

Racherla, P. N., and P. J. Adams (2006), Sensitivity of global tropospheric ozone and fine particulate matter concentrations to climate change, *Journal of Geophysical Research-Atmospheres*, *111*(D24), 11, doi:D24103 10.1029/2005jd006939.

Ramanathan, V., et al. (2001), Atmosphere - Aerosols, climate, and the hydrological cycle, *Science*, *294*(5549), 2119-2124, doi:10.1126/science.1064034.

Rind, D., and J. Lerner (1996), Use of on-line tracers as a diagnostic tool in general circulation model development .1. Horizontal and vertical transport in the troposphere, *Journal of Geophysical Research-Atmospheres*, *101*(D7), 12667-12683, doi:10.1029/96jd00551.

Rind, D., et al. (1999), Use of on-line tracers as a diagnostic tool in general circulation model development 2. Transport between the troposphere and stratosphere, *Journal of Geophysical Research-Atmospheres*, *104*(D8), 9151-9167, doi:10.1029/1999jd900006.

Rudokas, J. (2013), Regional Air Quality Management Aspects of Global Change:Impact of Climate Mitigation Options on Regional Air Emissions, In Review

Sarica, K., and W. E. Tyner (2013), Alternative policy impacts on US GHG emissions and energy security: A hybrid modeling approach, *Energy Econ.*, *40*, 40-50, doi:10.1016/j.eneco.2013.06.003.

Schmidt, G. A., et al. (2013), Configuration and assessment of the GISS ModelE2 contributions to the CMIP5 archive, *J. Adv. in Modeling Earth Systems, Submitted*

Schmidt, G. A., et al (2013), Configuration and assessment of the GISS ModelE2 contributions to the CMIP5 archive, *J. Adv. Modeling Earth Systems, in preparation*

Schwartz, J., et al. (1994), Accute effects of summer air-pollution on respiratory symptom reporting in children, *Am. J. Respir. Crit. Care Med.*, *150*(5), 1234-1242

Shindell, D., et al. (2012), Simultaneously Mitigating Near-Term Climate Change and Improving Human Health and Food Security, *Science*, *335*(6065), 183-189, doi:10.1126/science.1210026.

Shrestha, R. M., and S. Rajbhandari (2010), Energy and environmental implications of carbon emission reduction targets: Case of Kathmandu Valley, Nepal, *Energy Policy*, *38*(9), 4818-4827, doi:10.1016/j.enpol.2009.11.088.

Skamarock, W., et al. (2005), A Description of the Advanced Research WRF Version 2.

Skamarock, W. C., and J. B. Klemp (2008), A time-split nonhydrostatic atmospheric model for weather research and forecasting applications, *Journal of Computational Physics*, *227*(7), 3465-3485, doi:10.1016/j.jcp.2007.01.037.

Stauffer, D. R., and N. L. Seaman (1990), Use of a 4-dimensional data assimilation in a limeted-area mesoscale model .1. Experiments with synoptic-scale data, *Monthly Weather Review*, *118*(6), 1250-1277, doi:10.1175/1520-0493(1990)118<1250:uofdda>2.0.co;2.

Stevenson, D. S., et al. (2006), Multimodel ensemble simulations of present-day and near-future tropospheric ozone, *Journal of Geophysical Research-Atmospheres*, *111*(D8), D08301, doi:10.1029/2005JD006338

Steyaert, L. T., and R. G. Knox (2008), Reconstructed historical land cover and biophysical parameters for studies of land-atmosphere interactions within the eastern United States, *Journal of Geophysical Research-Atmospheres*, *113*(D2), 27, doi:D02101 10.1029/2006jd008277.

Stooksbury, D. (2008), A Primer on Drought History In Georgia, in *Georgia Climate and AIr Quality Summit*, edited, Atlanta, GA.

Tagaris, E., et al. (2007), Impacts of global climate change and emissions on regional ozone and fine particulate matter concentrations over the United States, *Journal of Geophysical Research-Atmospheres*, *112*(D14), D14312, doi:10.1029/2006JD008262.

Tagaris, E., et al. (2008), Potential impact of climate change on human health caused by changes in ozone and particulate matter concentrations, *submitted*

Thompson, S. L., et al. (2004), Quantifying the effects of CO2-fertilized vegetation on future global climate and carbon dynamics, *Geophysical Research Letters*, *31*(23), 4, doi:L23211 10.1029/2004gl021239.

Trail, M., Tsimpidi, A. P., Liu, P., Tsigaridis, K., Hu, Y., Nenes, A., and Russell, A. G. (2013), Downscaling a global climate model to simulate climate change impacts on US regional and urban air quality, *Geosci. Model Dev.*, *6*, 1429-1445, doi:10.5194/gmd-6-1429-2013.

Vithayasrichareon, P., and I. F. MacGill (2013), A Monte Carlo based decision-support tool for assessing generation portfolios in future carbon constrained electricity industries, *Energy Policy*, *41*, 374-392, doi:10.1016/j.enpol.2011.10.060.

Wang, Y. H., et al. (1998), Global simulation of tropospheric O-3-NOx-hydrocarbon chemistry 2. Model evaluation and global ozone budget, *Journal of Geophysical Research-Atmospheres*, *103*(D9), 10727-10755, doi:10.1029/98jd00157.

Wear, D. N., and J. G. Greis (2002), Southern Forest Resource Assessment - Summary of findings, *Journal of Forestry*, *100*(7), 6-14

Weaver, C. P., et al. (2009), A preliminary synthesis of modeled climate change impacts on US regional ozone concentrations, *Bulletin of the American Meteorological Society*, *90*(12), 1843-1863, doi:10.1175/2009bams2568.1.

Woo, J. H., et al. (2008), Development of North American Emission Inventories for Air Quality Modeling under Climate Change, *Journal of the Air & Waste Management Association*, *58*(11), 1483-1494, doi:10.3155/1047-3289.58.11.1483.

Wu, S. L., et al. (2008), Effects of 2000-2050 global change on ozone air quality in the United States, *Journal of Geophysical Research-Atmospheres*, *113*(D6)

Yang, Y. J., et al. (1997), Fast, direct sensitivity analysis of multidimensional photochemical models, *Environmental Science & Technology*, *31*(10), 2859-2868

Yu, S. C., et al. (2006), New unbiased symmetric metrics for evaluation of air quality models, *Atmos. Sci. Lett.*, *7*(1), 26-34, doi:10.1002/asl.125.

Zhou, J. A., et al. (2011), Time-Series Analysis of Mortality Effects of Fine Particulate Matter Components in Detroit and Seattle, *Environ. Health Perspect.*, *119*(4), 461-466, doi:10.1289/ehp.1002613.